SALMONELLA WITHIN MACROPHAGES—AN EXTREME HOST-PATHOGEN INTERFACE:

SMALL MOLECULE INHIBITORS OF BACTERIAL EFFLUX AND THE ROLES OF BACTERIAL LIPID METABOLISM AND MAMMALIAN CO-CULTURE DURING INFECTION

by

ABIGAIL L. REENS

S.B., Massachusetts Institute of Technology, 2012

A thesis submitted to the

Faculty of the Graduate School of the

University of Colorado in partial fulfillment

of the requirement for the degree of

Doctor of Philosophy

Department of Molecular, Cellular, & Developmental Biology

2019

This thesis entitled:

Salmonella within macrophages—an extreme host-pathogen interface:
small molecule inhibitors of bacterial efflux
and the roles of bacterial lipid metabolism
and mammalian co-culture during infection

written by Abigail L. Reens
has been approved for the Department of
Molecular, Cellular, & Developmental Biology

_____

Corrella Detweiler, Ph.D., Advisor

_____

Shelley Copley, Ph.D., Committee Chair

Date _____

The final copy of this thesis has been examined by the signatories,
and we find that both the content and the form meet
acceptable presentation standards of scholarly work
in the above mentioned discipline.

IACUC protocols # 1307.02, 2445

Reens, Abigail L. (Ph.D., Molecular, Cellular & Developmental Biology)

Salmonella within macrophages—an extreme host-pathogen interface: small molecule inhibitors of bacterial efflux and the roles of bacterial lipid metabolism and mammalian co-culture during infection

Thesis directed by Professor Corrella Detweiler

ABSTRACT

Pathogens withstand extreme host environments during infection. *Salmonella enterica* serovar Typhimurium survives within host macrophages, immune cells intended to phagocytose and destroy pathogens. Through decades of study, we know much about how *Salmonella* endures this challenging niche. I leveraged this host-pathogen interface to identify small molecules that disrupt *Salmonella* infection of macrophages. I developed a medium-throughput fluorescence microscopy-based screening assay and image analysis pipeline to quantify intracellular bacterial load. With this platform, I identified 300 small molecules that reduce *Salmonella* infection of macrophages. Of the top 60 hits, I characterized three compounds that inhibit bacterial efflux pumps and sensitize *Salmonella* to host antimicrobial peptides. This result highlights the importance of bacterial efflux pumps in defense against host antimicrobials, and validates efflux pumps as a therapeutic target to treat infection. I also characterized the antimicrobial activity of clomipramine, a clinically used tricyclic antidepressant. I found that anti-*Salmonella* activity was unrelated to clomipramine's canonical inhibition of the serotonin reuptake transporter, and that clomipramine may activate host autophagy to clear bacteria. However, clomipramine was ineffective against *Salmonella* infection *in vivo*, which limits the possibility of repurposing this drug as an antimicrobial. Together, these studies exemplify the

complexity of *Salmonella* infection of macrophages in how many possible pathways can be modulated by drugs to disrupt this host-pathogen interface.

Recent studies have established the roles that host and bacterial heterogeneity play in the progression and outcome of infection. I identified a unique macrophage phenotype that governs the use of lipids by *Salmonella*. Only within pro-inflammatory amino-acid-supplemented macrophages was lipid metabolism important for *Salmonella* infection. Further, only a subset of bacteria utilized lipids within these macrophages, highlighting that even in a specialized macrophage, individual *Salmonella* employ unique nutritional strategies. Finally, I investigated the effects of co-culturing leukocytes with infected macrophages on *Salmonella* infection. I found co-culturing erythrocytes or T cells altered activation, iron homeostasis, and nitric oxide levels, with the net effect of increasing *Salmonella* replication within macrophages. Thus, the macrophage niche is highly diverse and influenced by many factors. Together, my studies illustrate the complexity and uniqueness of the extreme *Salmonella*-macrophage host-pathogen interface.

DEDICATION

I dedicate this work to my parents,

Daniel and Shari Van Hook,

for kindling and fueling

the curiosity, thoroughness, and efficiency

that prompted me to begin this work

and the power to complete it.

ACKNOWLEDGEMENTS

I would like to thank my thesis advisor, Corrie Detweiler for the scientific home I've had while at CU Boulder. I appreciate the independence you allowed me, and your flexibility in our communication styles. I am grateful for your support throughout my graduate work, especially my time off to care for my sons. Thank you for the space you gave me to push through the frustrating aspects of research and writing over the years; I can truly say that my approach to writing has changed for the better.

I am grateful to the members of my thesis committee: Shelley Copley, Tin Tin Su, Amy Palmer, James Orth, and Lee Niswander. Thank you for your critical questions and for helping me to focus on finishing publications. I am also grateful to Natalie Ahn and the SCR Training Program for funding, camaraderie, and scientific development. I am also grateful to the professors with whom I rotated my first year: Norm Pace and James Orth. Both allowed me to develop skills and habits that endured throughout the rest of my graduate career and have shaped me as a scientist.

Thank you to the Detweiler lab members for discussions, ideas, and fun over the years. I am especially grateful to Toni Nagy for all of our conversations and for teaching me cloning and mouse infections, and to Amy Crooks for collaborations on screening and efflux pumps, as well as her sage and timely advice. I am thankful to Heidi Nick for many laughs in the midst of hard work, and for teaching me flow cytometry and qPCR. I thank M. Carolina Pilonieta for enforcing lunchtimes and the ensuing conversations, as well as teaching me bone marrow isolations. I am grateful to Maddie Edwards for her hard work and dedication on my projects. Thank you to our laboratory technicians for so many plates: Brenda Briggs, Jess Colmenero, Sarah Hillson, Olivia Bednarski, and Bekah Levy. I am thankful to Eugenia Silva-Herzog, Erin McDonald, Joe Villanueva, Jessy Podoll, Jamie Dombach, and Joaquin Quintana for good conversations and lab camaraderie over the years.

I am grateful for several department and university facilities. Yuming Han and the Flow Cytometry Facility for analysis and sorting. The Light Microscopy Core Facility, directed by Chris English, Jolien Tyler, and James Orth helped me obtain important data. Wei Wang and the HTS facility assisted with small molecule screening efforts. Theresa Nahreini of the JSCBB Cell Culture Facility loaned materials when supplies were on backorder. I am also grateful to the Transgenics Facility, especially Micah Stoltz and Toni Mufford, for training and maintenance.

I thank the administration of my department. In particular, I am grateful to Erik Hedl for computer management over the years. I thank Karen Brown, Sarah Morehead, and Kathy Lozier for managing academic and administrative aspects of my career. And I am especially grateful to Katie Lamb, Jean Balch, and Ken Krauter for helping me navigate the logistics of my maternity leaves. Thanks as well to Paul Muhlrad for reading manuscripts.

I am grateful to several individuals outside of CU Boulder who contributed important reagents or experiments: Laura Piddock of the University of Birmingham; Dirk Bumann of the University of Basel; Sophie Helaine and David Holden of the Imperial College London; Rajeev Misra of Arizona State University; Sarah Tasker and Paul Hergenrother of the University of Illinois; Chih-Chia Su and Edward Yu at Case Western Reserve University.

I thank my parents, Daniel and Shari Van Hook, for enabling me to pursue a PhD by their many years of support of my academic endeavors. I also thank my husband, Dave, who contributed in so many ways—materially, with coding assistance and company during late nights in the lab, emotionally, with a calm ear and a quiet heart to frustrations, and relationally, as my steadfast partner in graduate school. I also acknowledge my sons, Nathan and Sammy, who have brought joy and smiles, along with many logistical conundrums, to my life.

Finally, I acknowledge God—the creator of all that we see. I am privileged and grateful to be able to study our world as God's wonderful creation, and to work toward justice and peace.

GLOSSARY OF ABBREVIATIONS

5HT	5-hydroxytryptamine (serotonin)
AMP	antimicrobial peptide; ampicllin
ANOVA	analysis of variance
ara	arabinose
ARP	amitriptyline
BFP	blue fluorescent protein
BMDM	bone marrow-derived macrophage
bp	basepairs
BSA	bovine serum albumin
C	cecum
CCCP	carbonyl cyanide m-chlorophenylhydrazone
CFP	cyan fluorescent protein
CFU	colony-forming units
CM	chloramphenicol
CHX	cycloheximide
CMP	clomipramine
CPZ	chlorpromazine
C_T	cycle threshold
cytoD	cytochalasin D
DFX	deferasirox
DMSO	dimethyl sulfoxide
dNO	diethylenetriamine NONOate
deaNO	diethylamine-NONOate
DRB	5,6-Dichlorobenzimidazole 1-β-D-ribofuranoside

DSP	desipramine
DXP	doxepin
E. coli	*Escherichia coli*
EC_{50}	half maximal effective concentration
EP	efflux pump
EPM	efflux pump modulator
FACS	fluorescence-activated cell sorting
FBS	fetal bovine serum
FD	fluorescence dilution
FDA	Food and Drug Administration
FXM	fluvoxamine
FXT	fluoxetine
GFP	green fluorescent protein
Hb	hemoglobin
h.p.i.	hours post infection
hr	hour
IC_{50}	half maximal inhibitory concentration
IFN-γ	interferon-gamma
IL-4	interleukin-4
IL-10	interleukin-10
IL-13	interleukin-13
IMP	imimpramine
iNos	inducible nitric oxide synthase
IMP	imipramine
IP	intraperitoneal
KAN	kanamycin

L	liver
LB	lysogeny broth
LFP	lofepramine
M1	pro-inflammatory macrophage phenotype
M1	anti-inflammatory macrophage phenotype
M-CSF	macrophage colony-stimulating factor
MDR	multidrug resistance
MFI	median fluorescence intensity
MgMES	MES-buffered medium containing magnesium
MHC	major histocompatibility complex
MHB	Mueller Hinton broth
MIC	minimal inhibitory concentration
MN	mesenteric lymph nodes
NEAA	non-essential amino acids
NET	norepinephrine reuptake transporter
NFκB	nuclear factor kappa B
NMS	normal mouse serum
NO	nitric oxide
NRP	nortriptyline
OA	oleic acid
OD_{600}	Optical Density 600 nm
PAβN	Phe-Arg β-naphthylamide
PAMP	pathogen-associated molecular pattern
PaseK	proteinase K
PB	polymyxin B
PBS	phosphate buffered saline

p.i.	post-infection
PMZ	promethazine
PP	Peyer's patches
PRP	protriptyline
PRR	pattern recognition receptor
PS	phosphatidylserine
PS-RBC	phosphatidylserine erythrocyte (senescent)
PTIO	2-Phenyl-4,4,5,5-tetramethylimidazoline-1-oxyl 3-oxide
qHTS	quantitative high-throughput screening
qPCR	quantitative PCR
RBC	red blood cell (erythrocyte)
Rif	rifampicin
RFP	red fluorescent protein
RFU	relative fluorescence units
RND	resistance-nodulation-cell division
RNS	reactive nitrogen species
ROS	reactive oxygen species
S	spleen
SAFIRE	screen for anti-infectives using fluorescence microscopy of intracellular *Enterobactericeae*
SCV	*Salmonella*-containing vesicle
SD	standard deviation
SEM	standard error of the mean
SERT	serotonin reuptake transporter
shRNA	short hairpin RNA
Sif	*Salmonella*-induced filament

SPI-1	*Salmonella* pathogenicity island I
SPI-2	*Salmonella* pathogenicity island II
SSRI	selective serotonin reuptake inhibitor
*S.*tm	*Salmonella enterica* serovar Typhimurium
STR	streptomycin
T3SS	type III secretion system
TCA	tricyclic antidepressant; tricarboxylic acid cycle
TDZ	thioridazine
TET	tetracycline
TGF-β	transforming growth factor beta
Th1	T-helper 1
Th2	T-helper 2
TMRM	tetramethylrhodamine methyl ester
TNF-α	tumor necrosis factor alpha
WT	wild-type
Z’	Z’ statistical effect size factor

CONTENTS

LIST OF TABLES

LIST OF FIGURES

CHAPTER 1. INTRODUCTION

A. APPROACHES TO ANTIMICROBIAL DISCOVERY

New antibiotics are urgently needed, particularly against hard-to-treat and multidrug resistant pathogens. Historically, broth- and target-based screening platforms have been extensively used for antibiotic discovery, but these approaches are respectively limited to growth-related factors and curated enzyme targets. In contrast, empirical (or phenotypic) screens broaden the available target space and have the capacity to identify inhibitors of diverse infection-related processes. Recently, empirical assays have been employed to screen for antimicrobial compounds and probe host-pathogen interactions. From in-host-cell screens against intracellular pathogens to assays of host-directed toxicity, these studies highlight how creativity in assay design and downstream target identification are critical to harness the power of empirical screens.

I. The Need for New Antibiotics

Over the last century antibiotic use has transformed medical practice, animal husbandry, and microbial evolution. Most human infectious diseases are treatable with a short course of antibiotics, but there is a need for new antibiotics to address difficult-to-treat and multidrug resistant pathogens. Gram-negative bacteria not sensitive to many antibiotics due to a double-membrane cell envelope which restricts penetration of amphipathic and hydrophilic substances, including many drugs (Denyer and Maillard, 2002; Lewis, 2013; Silver, 2011; Tulkens, 1991). Similarly, intracellular pathogens that survive within the host cytosol or vesicular compartments are difficult to target because antibiotics may not accumulate to high concentrations or may be degraded (Carlier et al., 1990; Carryn et al., 2003; Labro, 1996; Seral et al., 2003; Tulkens, 1991). Chronic infections are typically uncurable, as a dormant reservoir of cells cannot be eradicated by traditional antibiotics that target growth processes in replicating microbes (Grant and Hung, 2013; Monack et al., 2004).

Finally, some pathogens have also become resistant to our current arsenal of clinical antibiotics. Resistance to clinical antibiotics has expanded over the last 20 years. More pathogens are resistant to antibiotics, and some pathogens are resistant to multiple antibiotics. The emergence of multidrug resistance (MDR) can be attributed to general adaptations which confer resistance to multiple toxic agents (Nikaido, 2009; Pages et al., 2008; Webber, 2003), such as altered cellular permeability or enhanced efflux. MDR pathogens may also acquire and maintain independent resistance mechanisms to multiple antibiotics; strong selection for antibiotic resistance compensates for the fitness cost of maintaining multiple resistance mechanisms (Nikaido, 2009).

II. Historical Strategies for Antibiotic Discovery

Diverse approaches in the hunt for anti-infectives have led to discovery of drugs with unique sources, pathogen targets, and molecular mechanisms of action (Aminov, 2010; Gould, 2016). Each approach has benefits and limitations that impact screening throughput, compound breadth of activity, usefulness, and the development of resistance. In the early 1900s, Paul Ehrlich and Sahachiro Hata systematically tested synthetic derivatives of arsanilic acid as a treatment for syphilis in rabbits—the first instance of medicinal chemistry to improve the therapeutic use of a small molecule (Ehrlich, 1910). Screening in an animal infection model was slow but ensured hit compounds were potent and nontoxic.

In 1928, the serendipitous discovery of penicillin from *Penicillium* fungi by Alexander Fleming (Fleming, 1929) launched the “golden age of antibiotic discovery.” Over the next several decades soil extracts and cultured microbes were tested to identify naturally occurring antibiotics optimized by nature, and thus extremely active. Samples were tested for the ability to inhibit growth of pathogenic bacteria in broth or on plates. This empirical platform enabled rapid screening and led to identification of the major classes of antibiotics in use today. However, growth-based screens are biased for antibiotics that target essential replication processes,

which leads to rediscovery of known inhibitors and a strong selective pressure for resistance (Lewis, 2013).

With the advent of genomics and the concurrent identification of microbial virulence factors, pharmaceutical companies invested in high-throughput screening of synthetic chemical libraries for inhibitory activity against biochemical targets. Over the last 30 years, these target-based approaches have yielded zero antibiotics for systemic use, due to a combination of meager hit identification from screens and a widespread lack of antibacterial activity even in molecules with potent biochemical inhibition (Payne et al., 2007). Indeed, chemical libraries biased for mammalian bioavailability are likely biased against intracellular microbial accumulation (Silver, 2011). Target-based screening using biochemical (Hurt et al., 2010; Scharf et al., 2016) or reporter assays in whole cells (Hung et al., 2005; Yep et al., 2014) disregard penetration into microbial or host cells, which can be difficult to engineer into lead compounds (Fischbach and Walsh, 2009; Lipinski, 2000; Payne et al., 2007). As a result, recent efforts to identify novel antibacterials have yielded few therapeutics (Payne et al., 2007).

III. Empirical Screening For Anti-infectives

Empirical or phenotypic screening approaches offer several critical advantages for identifying novel anti-infectives. Empirical screens are performed in the context of infection. This approach inherently allows for identification of inhibitors that target infection-relevant processes, expanding the potential target space to include compounds that might affect pathogen growth processes, maintenance of a chronic state, or virulence factors (Fischbach and Walsh, 2009; Moore and Rees, 2001). Hit compounds may also modulate the host response to infection (Anuforom et al., 2016; Bode et al., 2014; Mazzilli and Zecconi, 2010; Pasquale and Tan, 2005; Stanley et al., 2014) or be modified by host cells (1, 27–29). Targeting virulence may slow the spread of resistance, thus minimizing the threat of antibiotic resistance (Allen et al., 2014; Cegelski et al., 2008; Clatworthy et al., 2007; Hung et al., 2005; Rasko et al., 2008). Finally,

because they employ whole cells, empirical screens enable early evaluation of a compound's penetration through host and pathogen membranes and host toxicity in parallel with its anti-infective activity. Thus, empirical screens for antimicrobials in a whole host-pathogen system allow discovery of hit compounds capable of surmounting many of the barriers disregarded by typical antibiotic screens, and may enrich for inhibitors of infection-relevant targets.

The use of a complex whole host-pathogen system also presents a critical challenge in empirical screening: Biological variability must be adequately controlled in order to confidently identify hits. Reproducibility in a screening assay is described using the statistical effect size Z'-factor, calculated from the means and standard deviations of positive and negative controls (Zhang et al., 1999). Z' values from 0.5 – 1 are considered sufficient for screening, while values below 0.5 are marginal and may result in false positives and negatives. Maximizing the Z' is equivalent to improving the confidence of the assay. Few studies report how screening assays were optimized, but common approaches include modifying the assay conditions to increase signal, reducing throughput, employing robots, and using identical reagents for each assay run. Even with these modifications, cell-based assays typically present Z' ranging from 0.2-0.9. However, expanded analysis of the screening results can partially mitigate marginal a marginal Z'. Statistical approaches such as increasing the number of replicates, normalizing to controls (Z-scores), or accounting for variation using mathematical models (B-scores) can increase a screen's power (Brideau et al., 2003; Dragiev et al., 2011; Malo et al., 2006). After the screen is complete, hits must first be validated in the primary assay; we recommend also confirming activity in an orthogonal assay, which may be lower-throughput. Together, these approaches increase the confidence in the hits and improve the likelihood that they are worth pursuing.

An additional drawback to empirical screens is the difficulty of identifying the target for downstream optimization (Moore and Rees, 2001; Schenone et al., 2013). A common approach to antibiotic target identification is to evolve mutants resistant to the drug and sequence the genome. Although this method has the capacity to be highly successful, it may be technically

challenging to evolve resistant mutants resistant to drugs that act within host cells. A second strategy is to match phenotypic signatures of drug-treated cells with those of known inhibitors or mutants. These signatures can include flux through biosynthetic pathways (Ling et al., 2015), transcriptomics (Freiberg et al., 2005), cytological profiling (Nonejuie et al., 2013), and metabolomics (Birkenstock et al., 2012; Kwon et al., 2008). A third approach is chemical proteomics, which enables target identification by labeling proteins that physically interact with a small molecule (Evans et al., 2005; Rix and Superti-Furga, 2009; Wright and Sieber, 2016). This approach combines drug affinity chromatography with high-resolution mass spectrometry and has been successfully used to identify targets of natural-product-derived antibiotics (Nodwell et al., 2012; Peng et al., 2016). A fourth strategy is to use secondary screens to test for inhibition of core virulence systems. Many groups are identifying virulence-associated pathways which could be targeted in an empirical screen: toxin production, adhesins, secretion systems, quorum sensing, and virulence regulation (Clatworthy et al., 2007; Rasko and Sperandio, 2010). With luck, this approach may quickly identify the target process, which can enable candidate-based identification of the molecular target (Reens et al., 2018). A final bypass to the issue of target identification is to screen a library of molecules with known activities. However, the possibility exists that a molecule's anti-infective activity is distinct from any annotated activity. Even with these diverse strategies, there is no guarantee of successful target identification after empirical screening.

IV. Empirical Screening Complements Other Innovations

Many of the empirical screens described in this review also exploit other innovative approaches which merit a brief summary of recent developments. Current enthusiasm for host-directed therapeutics represents a paradigm shift in the search for anti-infectives. Several studies apply an empirical screen to identify anti-infective drugs that target the host rather than the microbe (Czyz et al., 2014; Korbee et al., 2018; Zumla et al., 2016). By inhibiting a host

factor required for intracellular infections, host-directed therapeutics could act as a sole therapy. For sepsis or chronic infections, host-directed therapeutics could modulate the immune response or support host health, and thus are more likely to serve as an adjunct treatment. Additionally, targeting the host has the advantage of avoiding direct selection for resistance to the drug. Thus, development of host-directed therapeutics could catalyze a new strategy of treating infectious disease.

Alternatives to the traditional small molecule synthetic screening library are becoming more prevalent. Many groups have performed repurposing screens of FDA-approved drugs. Screening libraries of known compounds has the potential to bypass time-consuming optimization of pharmacokinetics, phamacodynamics, and safety, thus accelerating entry of new anti-infectives into the clinic. In many cases, a repurposed drug has the same target for its known and anti-infective activities, and a focused screen could be performed based on known pathways involved in infection (Korbee et al., 2018). It is also possible that a drug targets a different molecule when functioning as an anti-infective; in this case, empirical screens have the greatest capacity to identify alternative functions of known compounds. The drug would still require optimization to better disrupt the novel target using medicinal chemistry, but this process may be expedited by existing structure-activity analyses performed during development of the parent compound (Stanley et al., 2014; Sundaramurthy et al., 2013). Repurposing screens are especially useful for identifying host-directed therapeutics (Andersson et al., 2016; Czyz et al., 2014; Korbee et al., 2018; Kouznetsova et al., 2014), as the majority of FDA-approved drugs already target host pathways.

Other groups have also screened natural products, which are re-emerging as a source of possible anti-infectives (Donia and Hamann, 2003; Ling et al., 2015). Historically, natural products have been more successful than synthetic compounds as anti-infectives (Payne et al., 2007), possibly due to environmental selection for bioactivity. Renewed interest in exploring natural products as antibacterials has led to technological developments to mine soil and ocean

biomass for drugs (Clardy et al., 2006; Donia and Hamann, 2003; Imhoff et al., 2011; Lewis, 2017; Ling et al., 2015), as well as novel chemistry methods to purify and derivatize natural products, which often present challenging chemistries (Harvey et al., 2015; Huigens III et al., 2013).

Finally, *in silico* approaches leverage biological data and computing power to predict the anti-infective activity of compounds or identify potential biological targets of a hit compound. As a result, fewer resources are required for initial stages of screening or target identification. Data from *in silico* studies can then be used to focus experimental efforts on the most likely compounds or targets. Several *in silico* approaches are increasing in popularity. Docking algorithms use structural data to predict association of small molecules and a target of interest, and can be used to identify virtual ligands that bind a desired target, or predict targets that could be bound by a particular small molecule of interest. Repurposing efforts can also benefit from *in silico* approaches. Available "interactome" data on the off-target activities of known small molecules could supply an immediate drug for a novel target of interest (Luo et al., 2011). Experimental data on a subset of compounds can be extrapolated to larger collections of small molecules which may have more favorable activities (Korbee et al., 2018). As computational biologists expand available datasets and develop novel ideas, additional *in silico* approaches will likely transform, accelerate, and cheapen drug discovery.

V. Concluding Remarks

Empirical screens represent a powerful approach to antimicrobial discovery, as they can identify diverse compounds that disrupt a host-pathogen system. However, it is important to recognize that assay constraints still do restrict the possible activities that can be identified and the power of the assay to identify active compounds. Thus, deliberate assay design is crucial to set the foundation for identification of diverse and worthwhile hits. Similarly, creativity is essential for downstream characterization and target identification, and care must be taken to

distinguish between antimicrobial and off-target activities of hit compounds from an empirical screen. However, together with other developments in drug discovery, empirical screening has the potential to transform antimicrobial discovery and contribute to the treatment of developing infections.

B. MACROPHAGE IMMUNE RESPONSES, METABOLISM, AND CELL-CELL INTERACTIONS IN THE CONTEXT OF MACROPHAGE POLARIZATION

Macrophages are key players in innate immunity and also contribute to the development of adaptive immunity, wound healing, and blood homeostasis. Macrophages are myeloid leukocytes derived from monocytes, which are produced via asymmetric division of bone marrow stem cells during hematopoiesis. After release from the bone marrow, monocytes circulate in the blood before entering tissues and differentiating into macrophages or dendritic cells. Macrophage differentiation is driven by macrophage colony-stimulating factor (M-CSF), but additional environmental cues influence the phenotypic polarization during infection or tissue damage (Mosser and Edwards, 2008).

Macrophages detect microbial or danger signals via pattern recognition receptors (PRRs), which bind specific ligands and activate microbiocidal or wound-healing functions (Aderem and Ulevitch, 2000; Krutzik et al., 2005; Martinez et al., 2008; Medzhitov, 2007). Stimulation of PRRs also alters survival / apoptosis pathways (Seimon et al., 2006), cytokine production (Mosser and Edwards, 2008), interaction with other cell types such as erythrocytes, T-cells, and natural killer cells (Bellora et al., 2010; Biswas and Mantovani, 2010; Grom and Mellins, 2010; McDonald et al., 2016; Milner et al., 2010), and the macrophage nutritional state (Biswas and Mantovani, 2012; Eisele et al., 2013; Kazemi et al., 2005; Miller et al., 2009; Recalcati et al., 2010). In addition to stimulation of specific PRRs, the underlying cytokine milieu drives macrophage polarization. Interferon-gamma (IFN-γ) and tumor necrosis factor alpha (TNF-α) polarize macrophages toward a pro-inflammatory, microbiocidal phenotype denoted as “M1” (Mosser

and Edwards, 2008; Nathan et al., 1983), while interleukin-4 (IL-4), interleukin-10 (IL-10), or interleukin-13 (IL-13) shift macrophages toward the “M2” anti-inflammatory wound healing phenotype (Bogdan and Nathan, 1993; Huang et al., 1999; Stein et al., 1992a). It is important to note that most macrophages *in vivo* exist along a spectrum between M1 and M2; these discrete classifications do not reflect the large heterogeneity.

M1 macrophages exhibit a strong pro-inflammatory response to infection. PRR detection of pathogen-associated molecular patterns (PAMPs) during acute infection typically induces microbiocidal activities within macrophages. M1 macrophages display high rates of phagocytosis to engulf infectious pathogens (Flannagan et al., 2009). To target and eliminate intracellular bacteria, mouse macrophages activate several antimicrobial effectors. Upon PAMP stimulation, pre-synthesized NADPH oxidase subunits rapidly assemble and produce the oxygen radical superoxide, which can also be converted into other reactive oxygen species (ROS) (Panday et al., 2015). ROS are thought to have multiple bacteriostatic and bactericidal effects on bacteria, including damaging DNA and disrupting iron-sulfur clusters, thus inactivating various microbial respiratory enzymes (Fang, 2011; Slauch, 2011). PAMPs also induce expression of inducible nitric oxidase synthase (iNos), which synthesizes nitric oxide (NO), a bacteriostatic antimicrobial thought to reversibly disrupt respiration and DNA replication (Fang, 2004a). NO can be converted to several other reactive nitrogen species (RNS) with similar targets. Additionally, macrophages express antimicrobial peptides (AMPs), as do many other host cell types; AMPs disrupt bacterial membranes and directly kill pathogens (Nguyen et al., 2011). Along with these molecular weapons against pathogens, macrophages route phagocytosed bacteria to the lysosome for degradation (Flannagan et al., 2009).

In contrast to M1 macrophages, M2 macrophages are not commonly observed in acute infections. M2 macrophages secrete factors that promote wound-healing and tissue regeneration rather than microbiocidal factors, and are involved in resolution of infection by reducing inflammation (Benoit et al., 2008). However, M2 macrophages may play a key role in

parasitic or chronic infections to control tissue damage; some pathogens may specifically induce M2 polarization to evade the M1 microbiocidal response (Fairweather and Cihakova, 2009; Kahnert et al., 2006; Kreider et al., 2007).

M1 and M2 macrophages also differ in their metabolism (Galván-Peña and O'Neill, 2014; Jha et al., 2015). A key driver of the functional differences is the metabolism of arginine, which in M1 macrophages is a precursor for the antimicrobial effector nitric oxide, but in M2 macrophages is converted by arginase-1 into wound-healing effectors. Energy generation is also different between the two kinds of macrophages. M1 macrophages primarily metabolize glucose through lactate fermentation; by not employing respiration, M1 macrophages are not damaged by the ROS produced to target microbes. In contrast, M2 macrophages increase oxidative phosphorylation and degradation of fatty acids. Strikingly, metabolism is tightly bound to activity, as blocking or forcing oxidative metabolism has been shown to override the cytokine environment and drive macrophages into M1 or M2 polarizations, respectively (Rodriguez-Prados et al., 2010; Vats et al., 2006). Polarization also likely influences availability of essential bacterial micronutrients. M1 macrophages have been shown to tightly sequester iron by upregulating the iron-storage protein ferritin and downregulating the iron exporter ferroportin, a phenomenon deemed nutritional immunity (Cairo et al., 2011; Corna et al., 2010). In contrast, M2 macrophages express iron-related proteins to recycle iron and aid tissue repair, including ferroportin, CD163, a scavenger receptor for hemoglobin from damaged erythrocytes, and heme oxygenase, which releases iron from heme (Corna et al., 2010).

Finally, during infection and homeostasis macrophages interact with many other host cell types including T cells and erythrocytes. Classically activated M1 macrophages express MHCII and co-stimulatory molecules. These surface molecules interact with binding partners on the surface of antigen-specific T cells to form an immunological synapse, leading to activation and proliferation of the T cell. Whether M2 macrophages directly play a role in activating T cells is unclear. M2 macrophages stimulated with IL-10 do not express MHCII, but those activated with

IL-4 or IL-13 do (Gordon, 2003; Stein et al., 1992b). Although alternatively activated macrophages are important in controlling the destructive T cell response to parasitic infections (Herbert et al., 2004), it is unclear whether M2 macrophages directly interact with T cells to exert this effect (Arnold et al., 2015; Edwards et al., 2006; Gordon, 2003).

A key homeostatic function of macrophages is to phagocytose and degrade aged or damaged circulating erythrocytes, a process known as erythrophagocytosis. Senescent erythrocytes alter the conformation of CD47, switching it from a “don’t eat me” to an “eat me” signal for its receptor SIRPα, which triggers phagocytosis (Burger et al., 2012; Gottlieb et al., 2012; Oldenborg et al., 2000). Damaged erythrocytes expose phosphatidylserine, which is bound by several macrophage receptors and triggers uptake of the erythrocyte (Lee et al., 2011; Mandal et al., 2002; Ohyagi et al., 2013). Although variable expression levels of SIRPα and the phosphatidylserine receptors has been shown for distinctly polarized macrophages (Canton et al., 2013; Thornley et al., 2014), little is known about how polarization affects erythrophagocytosis of damaged or senescent erythrocytes. However, immune hyperactivation due to immunological deficiencies or chronic infection has been shown to induce hemophagocytosis, which is engulfment of healthy, nonsenescent erythrocytes and leukocytes by macrophages and other phagocytes. The mechanisms of hemophagocytosis are not well understood. Some evidence suggests hemophagocytic macrophages may be M2 polarized (McCoy et al., 2012), but hemophagocytosis can be experimentally induced *in vivo* using both M1- and M2-polarizing cytokines as well as PRR ligands (Behrens et al., 2011; McDonald et al., 2016; Milner et al., 2010; Pilonieta et al.; Zoller et al., 2011). Although hemophagocytes are known to contribute to pathological anemia, whether or how they alter the course of hyperinflammation or chronic infection is unclear (Brown et al., 2010; Grom and Mellins, 2010; Nix et al., 2007; Ohyagi et al., 2013; Zoller et al., 2011).

C. *SALMONELLA* PATHOGENESIS

Salmonella is a Gram-negative pathogen and is acquired through contaminated food or water. *Salmonellae* are classified into two categories, depending on the type of infection in humans. Nontyphoidal strains cause gastroenteritis and invade intestinal epithelial and submucosal lymphoid cells (Majowicz et al., 2010). In contrast, typhoidal *Salmonella enterica* serovars Typhi and Paratyphi spread systemically and can cause fever, bacteremia, and death (Crump et al., 2004; Ohl and Miller, 2001). Typhoidal *Salmonella* colonizes macrophages and dendritic cells, and can persist in a chronic infection for decades in human hosts (Gunn et al., 2014; Levine et al.). In immunocompetent mice, a typhoid-fever-like disease is caused by *Salmonella enterica* serovar Typhimurium (*Salmonella*). Approximately 1 week post infection, mice develop signs of acute illness, which resolves into a chronic infection that can persist for the life of the animal (Monack, 2004).

Salmonella is an intracellular pathogen, and colonizes epithelial cells and phagocytes. To survive and replicate within host cells, *Salmonella* employs two Type III secretion systems (T3SS), encoded within 2 large genomic regions denote *Salmonella* pathogenicity islands 1 and 2 (SPI-1, SPI-2). The T3SS comprises a needle-like apparatus that crosses the bacterial membranes and the host membrane(s) to inject effector proteins which modulate host physiology. Some effectors are encoded in the SPI-1 and SPI-2, while others are distributed around the bacterial genome. SPI-1 and its secreted effectors primarily facilitate host cell invasion, while SPI-2 enables intracellular survival and replication (Haraga et al., 2008; Waterman and Holden, 2003). Expression of the SPIs and effectors are triggered by exposure to a host-like environment. For SPI-1, numerous environmental cues are thought to be integrated to activate the master regulator HilA (Ellermeier and Slauch, 2007). Expression of SPI-2 is activated by exposure to acidic pH, low magnesium, and low phosphate, mimicking the phagosomal environment; these triggers activate the two-component sensor PhoPQ (Bijlsma and Groisman, 2005; Deiwick et al., 1999; Hensel, 2000).

During systemic infection of macrophages, *Salmonella* employs diverse secreted effectors to overcome multiple host antimicrobial defenses. A key strategy is the formation of a specialized vesicle derived from the host phagosome, termed the *Salmonella*-containing vesicle (SCV). Although the SCV has components of normal phagolysosomes such as LAMP-1, *Salmonella* prevents delivery of mannose-6-phosphate receptor, lysosomal cathepsins, NADPH oxidase, and iNos to the SCV, thereby avoiding destruction by these host antimicrobial mediators (Brumell and Grinstein, 2004; Buchmeier and Heffron, 1991; Chakravortty et al., 2002; Garvis et al., 2001; McGourty et al., 2012; Vazquez-Torres et al., 2000a). *Salmonella* also detoxifies host antimicrobials by upregulating the oxidative and nitrosative stress responses, the acid tolerance response, and efflux pumps (Bogomolnaya et al., 2013; Buckley et al., 2006; Eriksson et al., 2003; Nishino et al., 2006a). In addition, *Salmonella* can disrupt host immune signaling and cellular trafficking (Boucrot, 2005; Haraga et al., 2008; Kuhle et al., 2004; Miao et al., 2003). During infection, *Salmonella* effectors also lead to the construction of *Salmonella*-induced filaments (Sifs), which are microtubule-associated endosomal tubules that contribute to *Salmonella* replication (Brumell et al., 2002; Liss et al., 2017; Rajashekar et al., 2008). Sifs appear to serve as a reservoir for nutrients within the endolysosomal system (Liss et al., 2017), and *Salmonella* may also gain access to autophagic vesicles rich with host-derived macromolecules (Singh et al., 2017). The molecular mechanisms enabling *Salmonella* acquisition of nutrients within host cells are not fully understood. A broad overview of the literature indicates that *Salmonella* is capable of utilizing diverse nutrients depending on its specific microenvironment during infection (Bumann and Schothorst, 2017; Dandekar et al., 2014; Eisenreich et al., 2015). Many studies indicate that glucose is a key nutrient source during systemic infection (Bowden et al., 2009; Diacovich et al., 2016; Eisele et al., 2013; Eriksson et al., 2003; Tchawa Yimga et al., 2006a), although peptides and lipids also have been shown to play a role (Fang et al., 2005; Gotz et al., 2010; Singh et al., 2017).

D. SYNOPSIS OF RESULTS

In this work, I explore several research topics relevant for our understanding of the *Salmonella* microenvironment during infection. Using a cell culture model of *Salmonella* infection of macrophages, I developed an empirical screen to identify novel small molecules that reduce intracellular bacterial load (Reens et al, 2018). I created an image analysis pipeline to quantify high-throughput microscopy images. Using this platform, we screened 14,400 small molecules and identified 309 that reduced bacterial load. Excitingly, few of the top hits inhibited *Salmonella* grown in broth, suggesting the screen may have enriched for compounds that target bacterial virulence or host processes relevant for infection. These non-antibiotic compounds may be less likely to select for drug resistance, and thus may address the current problems of antibiotic resistance and few therapeutic antibacterials. Similar empirical screens may represent a powerful approach to identifying novel antibacterial compounds (Cegelski et al., 2008; Lewis, 2013, 2017; Rybniker et al., 2014; Samantaray et al., 2016).

Some of the compounds from the primary screen were identified by a secondary screen as potential inhibitors of bacterial efflux pumps, which contribute to virulence and to antimicrobial resistance (Bogomolnaya et al., 2013; Buckley et al., 2006; Nishino et al., 2006a). We further characterized these three small molecules (Reens et al, 2018) and found that they do not nonspecifically disrupt bacterial membranes or proton motive force. The three drugs sensitize *Salmonella* to membrane permeabilization by antimicrobial peptides, suggesting they may synergize with host antimicrobials during infection. I also tested the activity of the three drugs against intracellular *Salmonella* mutants lacking specific efflux pumps, and found that the drugs still inhibited the mutants. This result suggests that the drugs may target multiple pumps, as deletion of one pump typically leads to upregulation of other pumps (Wang-Kan et al., 2017), or that the three drugs may have additional targets.

I also explored the antibacterial mechanism of action of clomipramine, which was the top hit from my screen. Clomipramine canonically inhibits the host serotonin reuptake transporter,

thereby increasing serotonin signaling. I found that clomipramine and related compounds were all highly active against intracellular *Salmonella* but had no activity against bacteria grown in broth. Although macrophages express the serotonin reuptake transporter and serotonin signaling has been shown to alter macrophage physiology (de las Casas-Engel et al., 2013; Li et al., 2011; Malubay, 2008; Maneglier et al., 2008; Rudd et al., 2005), I found that clomipramine activity was likely independent of serotonin reuptake. Clomipramine or related compounds have also been suggested to modulate host calmodulin signaling (Asano, 1989; Plenge-Tellechea et al., 1999; Prozialeck and Weiss, 1982a, 1982b), protozoal glutathione redutase (Benson et al., 1992; Chan et al., 1998; Richardson et al., 2009), bacterial efflux (Gunics et al., 2000; Rodrigues et al., 2008), and autophagy (Rossi et al., 2009, 2014). Work by Toni Nagy suggested that clomipramine antibacterial activity is mediated by altering autophagic flux. Finally, clomipramine had no antibacterial activity *in vivo* during acute or chronic models of *Salmonella* infection.

Next, I investigated the role of *Salmonella* lipid metabolism during infection using a series of deletion mutants lacking genes essential for lipid utilization. I found that *Salmonella* utilizes lipids in M1 pro-inflammatory macrophages but not M2 anti-inflammatory macrophages. In particular, the data suggested that a consistent subpopulation of bacteria relied primarily on lipids, suggesting lipid use may be tied to the subcellular microenvironment or colonization of different macrophages within the same culture dish. I also found that lipid metabolism genes were important for infection of immunocompetent mice. Mutants lacking single lipid import or glyoxylate shunt genes were defective in mice; however, loss of both cognate enzymes from the two fatty acid beta-oxidation pathways was required to reduce bacterial load. Together, these data indicate that lipids play an important role for *Salmonella* during infection.

Finally, in the process of investigating the role of *Salmonella* lipid metabolism for infection of hemophagocytic macrophages, I began studies to characterize the phenomenon that co-culture of healthy or senescent erythrocytes or T cells with macrophages increased growth of

Salmonella. I found that healthy erythrocytes scavenge nitric oxide from macrophages, leading to reduced nitric oxide stress and enhanced *Salmonella* replication independent of hemophagocytosis. I also found that T cells and senescent erythrocytes shift the macrophage toward a more anti-inflammatory activation state and increase iron access for *Salmonella*. Senescent erythrocytes also appear to decrease nitric oxide exposure through an unknown mechanism. T cells require uptake to influence macrophages, while healthy and senescent erythrocytes do not. These studies illustrate that cellular interactions have a strong influence on the interaction between macrophage and *Salmonella*.

Together, my work demonstrates that many factors converge to generate an extreme macrophage microenvironment. By defining these factors and how *Salmonella* responds to the challenges of its infectious environment, we can expand our understanding of *Salmonella* host-pathogen interactions and steer future antibacterial development toward therapeutics that render bacteria unable to survive during infection.

CHAPTER 2. SAFIRE, A HOST-PATHOGEN SCREEN FOR ANTI-INFECTIVES

A. INTRODUCTION

Whole-cell screens for small molecules that modulate infection represent a powerful approach to understanding host-pathogen interactions and developing fresh approaches to treating infection. In contrast to broth- or target-based screening approaches, empirical whole-cell assays are performed in the context of infection. This approach allows for identification of modulators that disrupt infection-dependent processes in both pathogen and host cell, including virulence factors, host signaling and trafficking, and protein-protein interactions. Therapeutics that target infection rather than growth may reduce selective pressure for resistance, thus minimizing the threat of antibiotic resistance (Allen et al., 2014; Cegelski et al., 2008). Cell-based assays also inherently enable identification of modulators that penetrate both pathogen and host cells, which enhances utility both as a probe for infection studies and as a potential therapeutic. Thus, empirical screens for anti-infectives in a whole host-pathogen system enriches for discovery of hit compounds with drug-like qualities and infection-relevant targets.

However, such phenotypic whole-cell assays involve significant technical challenges which must be surmounted to enable a successful high-throughput screen. Several groups have recently performed chemical screens for modulators of intracellular infection. Lieberman and Higgins identified several FDA-approved drugs with known mammalian targets that inhibited *Listeria monocytogenes* infection of primary macrophages using a fluroescence-microscopy based screening platform (Lieberman and Higgins, 2009). Other groups have performed similar fluorescence-based screens using compounds with known targets to probe host and bacterial factors involved in *Mycobacterium tuberculosis* and *Cryptococcus neoformans* infection of macrophages (Samantaray et al., 2016; Stanley et al., 2014). There have also been studies using unbiased chemical libraries, which may generate probes for processes beyond those targeted by known compounds, although this approach presents the challenge of identifying the target of novel probes (Schenone et al., 2013). Several groups have performed fluorescence-

based screens with unbiased chemical libraries for compounds that modulate virulence processes and identified an unconventional myosin in *Toxoplasma gondii* required for invasion of host cells (Carey et al., 2004; Heaslip et al., 2010; Leung et al., 2014) and a *M. tuberculosis* histidine kinase involved in regulation of virulence protein secretion within cells (Rybniker et al., 2014). Thus, cell-based screens of known or unbiased small molecule libraries can contribute to our understanding of host-pathogen interactions.

Inspired by these cell-based screens for modulators of intracellular infection, I developed SAFIRE, a Screen for Anti-infectives using Fluorescence microscopy of IntracellulaR *Enterobacteriacea*, to identify modulators of *Salmonella* infection of macrophages (Reens et al, 2018). I incorporated the principal achievements of previous work into the design of SAFIRE. To enable high-throughput screening, we employed GFP-expressing *Salmonella*, an immortalized macrophage cell line, and automated fluorescence microscopy. We developed a versatile MATLAB®-based image analysis pipeline that uses a mitochondrial vital dye for simultaneous image segmentation based on host cells and evaluation of host cell toxicity. This platform enabled us to screen a larger library than has been previously reported for an infection-based screen. We screened the 14,400-compound Maybridge Hitfinder™ Collection v11, a synthetic library of diverse drug-like chemical structures. We identified 309 hits that decreased bacterial infection (Reens et al, 2018); despite frequent use of this library, the majority of our hits have not been previously identified as antibacterial compounds. Similarly, very few hits possess antibiotic activity against bacteria grown in standard microbiological media, suggesting that our hits target virulence-associated processes or host factors that mediate infection. Our screen represents a powerful approach to identify modulators of intracellular infection, and potentially therapeutic antibacterials, within existing libraries by directly assaying bacterial infection of host cells.

B. SAFIRE, A SCREEN FOR ANTI-INFECTIVES USING FLUORESCENCE MICROSCOPY OF INTRACELLULAR *ENTEROBACTERIACEAE*

I designed a high-content fluorescence microscopy-based screening platform to assay *Salmonella* load within host cells (**Figure 2-1A, Appendix A**). To increase throughput and reproducibility, I employed a cell line, RAW 264.7, a murine macrophage-like cell line widely used for bacterial infection studies (Berghaus et al., 2010; Carey et al., 2004; Stanley et al., 2014). RAW 264.7 cells are permissive for *Salmonella* replication largely due to lack of the phagosomal Nramp1 cation transporter (Fritsche et al., 2012; Nairz et al., 2009); this high

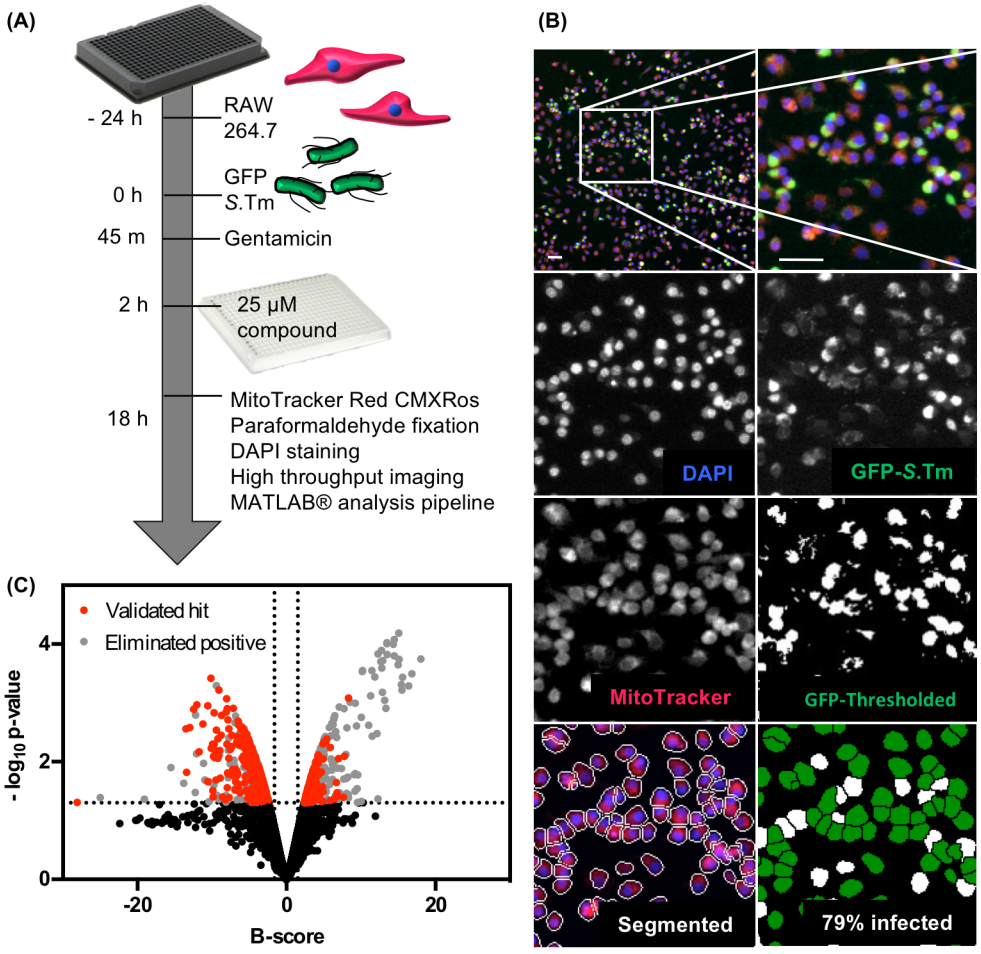

Figure 2-1. SAFIRE, Screen for Anti-infectives using Fluorescence microscopy of IntracellulaR Enterobacteriaceae. (A) Schematic of screening methodology. **(B)** Representative microscopy analysis of DMSO-treated wells. Upper left is a single field with 522 macrophages; remaining images are the indicated channels zoomed in the boxed region. Scale bars are 50 µm. **(C)** Distribution of B-scores and *p*-values for 14,400 compounds from the Maybridge HitFinder™ v11 library.

replication enables a large dynamic range for screening. RAW 264.7 macrophages were infected with GFP-expressing *Salmonella* (ALR#109; DET#1021) in a standard gentamicin protection assay (Nagy et al., 2013). Bacteria expressed GFP from the *Salmonella sifB* promoter, which is induced within macrophages (Rollenhagen et al., 2004). Infected macrophages were incubated with test compound beginning at 2 hours post-infection. This methodology better models a treatment scenario, as compounds are added after infection is established. At 18 hours post-infection, cells were stained with MitoTracker Red CMXRos as a marker of macrophage vitality, fixed, and stained with DAPI for identification of macrophages.

C. MATLAB® PIPELINE FOR IMAGE ANALYSIS

Together with David Reens, I developed a MATLAB®-based algorithm to quantify infection (**Figure 2-1B, Appendix B**). Initially, the algorithm identifies macrophage boundaries using MitoTracker and DAPI signals. Next, it thresholds the GFP channel using untreated and uninfected controls. Finally, the algorithm quantifies infection. I compared two measures of infection: First, percentage of infected cells was determined by counting the proportion of macrophages within a field with at least 2 GFP+ pixels (threshold optimized based on infected and uninfected controls); second, infection area was calculated by normalizing the number of GFP+ pixels within a cell to the total area of that cell, then averaging across all cells in the field. To evaluate the two measures of infection, I tested 2 μg/ml rifampicin in 96-well and 384-well plates in three independent replicates. I calculated the Z'-factor as a measure of assay reproducibility; numbers close to 1 indicate high reproducibility (Zhang et al., 1999). For percentage of infected macrophages, the Z'-factor was 0.59 and 0.48 in 96-well and 384-well plates, respectively, compared with 0.66 and 0.38 for infection area. The optimal Z'-factor threshold for high-throughput screening is 0.5; however, values above 0 are considered feasible, particularly for complicated cell-based screens (Zhang et al., 1999). Indeed, a sampling of several successful infection-based screens yielded Z'-factors of 0.2, 0.37, and 0.55 (Brodin et

al., 2010; Rybniker et al., 2014; Samantaray et al., 2016). I therefore proceeded with high-throughput screening using the percentage of infected macrophages statistic.

D. SCREEN OF 14,400 COMPOUNDS FROM MAYBRIDGE HITFINDER V11

Along with Amy Crooks, I screened the 14,400 compound library Maybridge HitFinder™ v11, a "drug-like" library optimized for mammalian cell penetration. This library has also been extensively screened against mammalian and microbial targets (Cremades et al., 2009; Durk et al., 2010; Johnson et al., 2016; Mathew et al., 2016). We screened the library in duplicate at 25 μM in 384-well plates. To compensate for the fairly low Z'-factor of our screen, I addressed well-to-well variability (Dragiev et al., 2011) using B-score normalization, a more rigorous approach than the standard Z-score-based normalization (Brideau et al., 2003; Malo et al., 2006). To minimize false negatives, I employed a relaxed hit selection threshold. Typically, a hit selection threshold is 2-3 standard deviations away from the mean (Brodin et al., 2010; Rybniker et al., 2014; Samantaray et al., 2016). I opted for an activity threshold of at least 1 standard deviation from the mean B-score. However, I also used *p*-value as a second threshold for reproducibility. I calculated significance of B-scores using a modified t-test assuming an inverse gamma distribution of variances (Malo et al., 2006; Wright and Simon, 2003). Compounds with a *p*-value less than 0.05 were considered reproducible. This approach identified 907 compounds (6.3%) that significantly altered the percentage of infected macrophages; of these, 461 decreased percentage of infected macrophages (**Figure 2-1C**). Next, I manually reviewed microscopy images to eliminate host-toxic and autofluorescent compounds, and retested the remaining positives using SAFIRE in 96-well plates (**Figure 2-2A,B**). I considered compounds validated hits if they altered infection by at least 75% in 96-well plates. I found 309 compounds (2.1%) that decreased infection and 137 (0.95%) that increased infection. This frequency is higher than reported in other cell-based drug screens, which range from 0.2-1.6% (Carey et al., 2004; Hung et al., 2005; Rybniker et al., 2014; Samantaray et al., 2016). However, my goal at this stage was

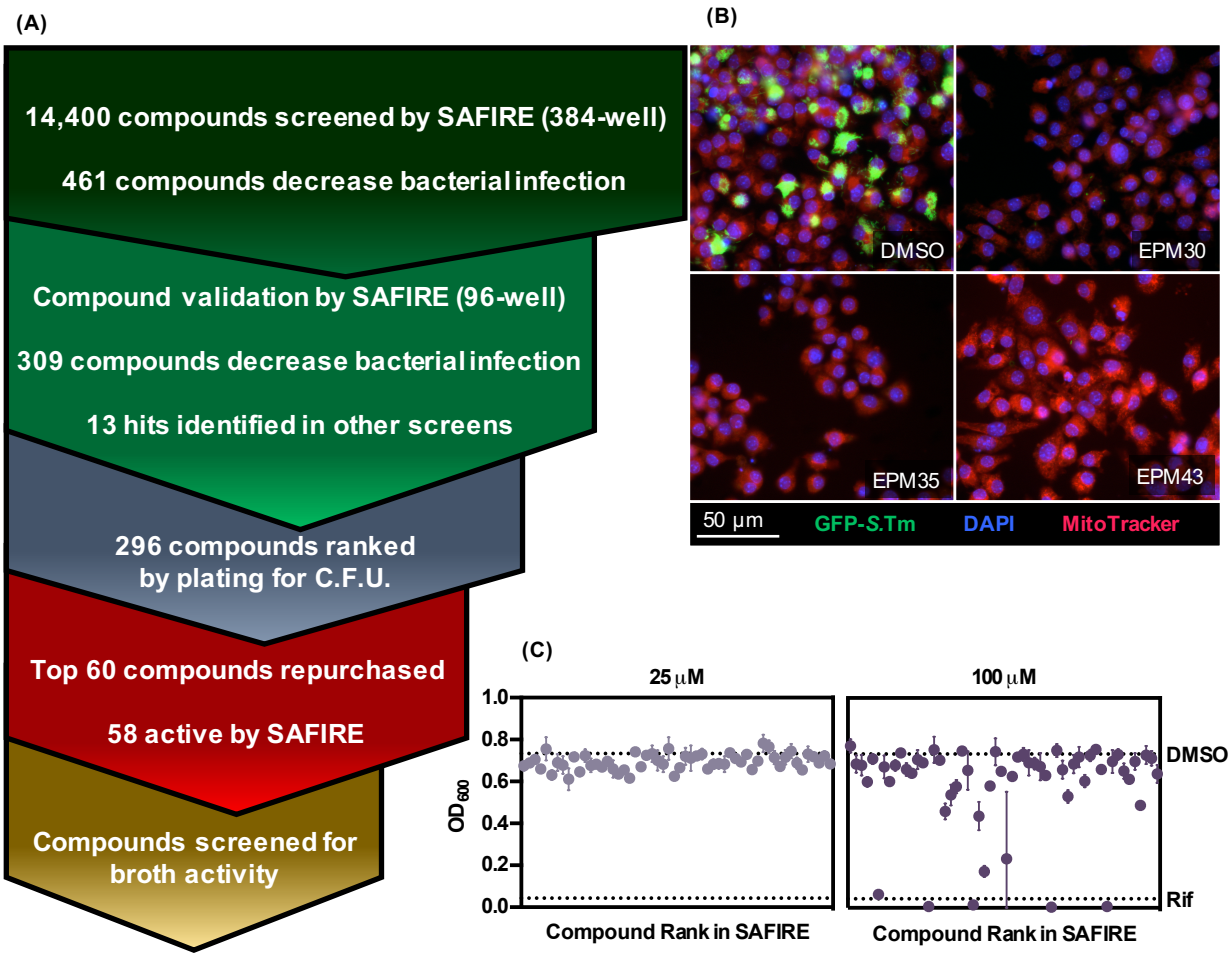

Figure 2-2. Identification and characterization of antimicrobials. (A) Screening workflow. **(B)** Representative microscopy of RAW 264.7 macrophages in 96-well plates infected with GFP-*S.*Tm and treated with 25 µM of the indicated compounds. **(C)** OD_{600} measurements for *S.*Tm grown for 16 hours in MHB with the indicated concentrations of each of the top 58 repurchased hits or rifampicin. Dotted lines indicate OD_{600} of wells treated with DMSO or rifampicin. Data shown are mean + SD of 2 independent biological replicates.

to preserve compounds with moderate activity but that are likely cell permeable; it may be more straightforward to improve inhibitory activity than to engineer cell permeability into an existing structural backbone (Fischbach and Walsh, 2009; Lipinski, 2000; Payne et al., 2007).

Of the 309 compounds that decreased the percentage of infected macrophages, 13 have been previously identified to have antimicrobial activity according to the PubChem BioAssay database (**Table 2-1**) (Kim et al., 2016; Wang et al., 2014). Identifying these built-in controls

serves as internal validation for our screening approach. In particular, we found chloramphenicol, a known antibiotic, and 9-aminoacridine, a topical antiseptic. We also identified a putative inhibitor of PhoP, a *Salmonella* virulence determinant required for infection of mice and macrophages (Miller et al., 1989a). Another hit is thought to inhibit MbtI, a bifunctional siderophore biosynthesis enzyme in *Mycobacterium tuberculosis* (Vasan et al., 2010); this same hit may target EntC, a related enzyme in *Salmonella* that is essential for infection (Crouch et al., 2008; Lamb, 2011). Several other compounds have been found in high-

Table 2-1. Selected hits previously identified in PubChem BioAssays

Compound ID	Assay ID	BioAssay
2741258	1864	A small molecule screen for inhibitors of the PhoP regulon in *Salmonella typhi*
6364829	493033	A Screen For Compounds That Inhibit The Bacterial Siderophore Biosynthetic Enzyme MbtI
2810137	651820	qHTS Assay for Inhibitors of Hepatitis C Virus (HCV)
2728899	751942	Antiviral activity against Influenza A virus (A/Aichi/2/1968(H3N2))
2802120	449704	NOVARTIS: Inhibition of Plasmodium falciparum W2 (drug-resistant) proliferationin erythrocyte-based infection assay
2738961	1968	Broad Institute MLPCN T. Cruzi Inhibition Project
2795980	588855	qHTS for Inhibitors of TGF-β
6845675	US2006194819	Activation specific inhibitors of NFκB and method of treating inflammatory processes in cardio-vascular diseases
632099	1792	Luminescence-based primary cell-based high throughput screening assay to identify inhibitors of NADPH oxidase 1 (Nox1): Maybridge Library
305310	624267	Fluorescence-based cell-based primary high throughput screening assay to identify inhibitors of the interaction of nucleotide-binding oligomerization domain containing 2 (NOD2) and the receptor-interacting serine-threonine kinase 2 (RIPK2)
2741794	489005	Inhibitors of T-Type Calcium Channel
2806019	1065399	Inhibition of human telomerase activity by TRAP assay

throughput screens against microbes including hepatitis C, influenza, malaria, and trypanosomes. Sixty-one hits have known activities against mammalian cells (**Table 2-1**). Some of these compounds target immune processes with defined roles in infection, including modulators of the immunoregulatory cytokines TGF-β and NFκB and inhibitors of NADPH oxidase and the inflammasome receptor NOD2. We also identified compounds that target other mammalian processes, including inhibitors of T-type calcium channels, telomerase, and neurotransmitter transporters (**Table 2-1**); whether these processes have roles in infection remains to be seen. Together, the presence of known bioactive chemicals in our hits suggests our work has the potential to identify novel probes for host-pathogen studies following the paradigm of chemical genetics.

To estimate the frequency of false negatives in our screen, Jessica Podoll cataloged known drugs and substances in the Maybridge HitFinder™ v11 library using the Chemical Structure Lookup Service from the CADD Group Chemoinformatics Tools and User Services (Nicklaus and Sitzmann, 2016) (**Table 2-2**). The library contains two compounds with established antibiotic activity that we did not identify in our screen. The first, 6-aminopenicillinate, is a synthetic beta-lactam precursor (Perron et al., 1960). We eliminated this compound because it had a *p*-value (0.056) just above the threshold (0.05), although it displayed significant anti-*Salmonella* activity (B-score of -2.29, compared to threshold of -2.17). The second false negative, nalidixic acid, is a synthetic quinolone. It had substantial activity in the first replicate of the screen (B-score -4.41), but was inactive in the second replicate (B-score 0.70). I subsequently cherry-picked and retested the compound from the original screening plate, which again

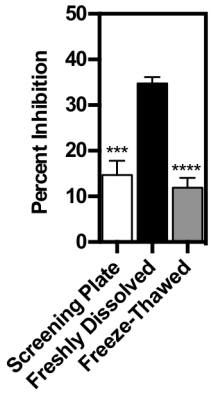

Figure 2-3. Nalidixic acid dissolved in DMSO is sensitive to freeze-thawing. SAFIRE was used to quantify infection of macrophages treated with 25 μM nalidixic acid that was cherry-picked from the plates used to perform the screen (n=2), freshly dissolved in DMSO (n=3), or freshly dissolved and freeze thawed 20 times (n=3). Data are mean + SEM; *** $p < 0.001$; **** $p < 0.0001$ compared to freshly dissolved by one-way ANOVA with Tukey's post-test.

Table 2-2. Known substances in the Maybridge Hitfinder™ v11 chemical library.

Name	Known Activity	Code	Maybridge Location (96-well)
Santowax M	Heat Transfer Fluid	BTB10963	002_E05
Naproxen	Anti-inflammatory	SB01071	003_F08
Heteroauxin	Hormone	RH01882	004_D02
Clomipramine [1]	Antidepressant	RJC01223	007_F04
Kinetin	Hormone	RJC03303	008_D02
Mycanodin	Antifungal	JFD01904	008_H09
Tolzamide	Hypoglycemic agent	JFD01580	013_D07
Pyrithyldione	Sedative	JFD03934	018_H07
Lipoamide	Metabolite	JFD01918	023_G11
Chloramphenicol [1]	Antibiotic	JFD01781	028_F05
Diphencyprone	Immunostimulant	BTB10303	042_G05
Glyburide	Antihypoglycemic agent	RJC01668	048_H11
Arecoline	Cholinergic agonist	SB01660	049_D02
Tolfenamic acid	Anti-inflammatory	JFD01579	069_E08
9-aminoacridine [1]	Antiseptic	NRB04719	095_D11
Tolnaftate	Antifungal	BTB13928	096_D04
Xylitol	Artificial sweetener	NRB05167	117_B03
Menadione	Synthetic vitamin	SB01122	124_F03
Indoramin [1]	Antihypertensive	RH01633	140_B11
Carboxin	Antifungal	XBX00001	140_E03
Phenylbiguanide	Serotonin receptor agonist	RJF01059	142_H09
Coumarin 4	Anticoagulant	BTB10013	146_B04
6-aminopenicillinate [2]	Metabolite	SB01619	146_E07
Nithiamide	Antiprotozoan	JFD03897	157_C10
Nalidixic acid [2]	Antimicrobial	RJC03974	162_E02
Hydroflumethiazide	Diuretic	SB01887	164_F08
Phenytoin	Anticonvulsant	BTB14870	170_C02

[1] Compounds identified as hits in SAFIRE screen.
[2] Substances with known antibacterial activity not identified as hits in SAFIRE screen; 6-aminopenicillinate was just below the hit threshold and nalidixic acid was inactive in one replicate.

showed minimal activity; further experiments suggested that nalidixic acid is sensitive to freeze-thawing when dissolved in DMSO (**Figure 2-3**). Overall, these results suggest the use of a dual screening threshold increased selectivity for highly active and reproducible compounds.

To further categorize our hit compounds, we retested 296 of the hits for anti-*Salmonella* activity using gentamicin protection assays and plating for colony forming units (CFUs). This

approach quantifies viable bacteria, allowing us to distinguish bactericidal from bacteriostatic compounds. Macrophages were infected as described above in 96-well plates and treated with 25 μM compound. At 18 hours post-infection, macrophages were lysed to release intracellular bacteria and lysates were diluted and plated to determine CFUs. Although known antibiotics such as rifampicin, ampicillin, and ciprofloxacin show similar activity in both assays (CFU and SAFIRE) only half of the hits displayed substantial (> 25%) reductions in bacteria by CFU plating (**Figure 2-4**). The remainder may partially inhibit bacterial replication but not cause extensive bacterial killing. However, 64 of the top 75 compounds as ranked by SAFIRE exhibited significant activity by the CFU assay, suggesting that the most highly active compounds are robust in both assays. Thus, the most potent compounds indeed reduce *Salmonella* replication and/or survival within macrophages. We repurchased 60 of our top hits and confirmed activity by SAFIRE. Fifty-eight repurchased compounds (97%) were active with IC50s ranging from 0.5-10.5 μM (data not shown).

Figure 2-4. Compound activity at 25 μM in CFU assays versus compound activity in SAFIRE. The top 75 compounds by SAFIRE (96-well validation) are represented with red dots.

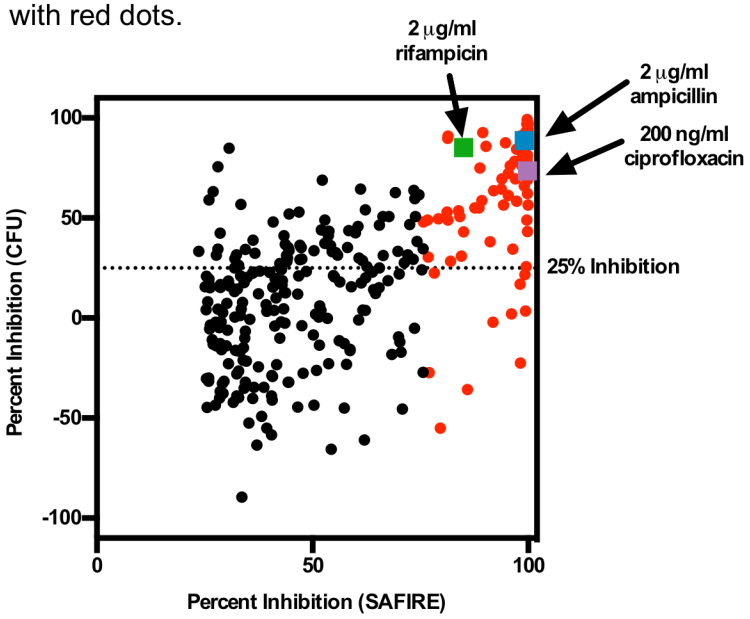

E. TOP HITS DO NOT INHIBIT BACTERIAL GROWTH IN BROTH

Compounds may disrupt infection by targeting essential bacterial processes, virulence-associated bacterial processes (Anuforom et al., 2016; Bode et al., 2014; Carey et al., 2004; Rybniker et al., 2014; Samantaray et al., 2016), or the host (Mura et al., 2011; Sisson et al., 2002; Stanley et al., 2014). To determine whether the top hits target essential bacterial

processes independent of the host cell environment, we tested for antibiotic activity against *Salmonella* in broth. Madeline Edwards screened the top 58 repurchased hits for activity against *Salmonella* grown in MHB broth (**Figure 2-2C**). At our screening concentration of 25 μM, none of the compounds altered *Salmonella* growth kinetics (data not shown) or final OD_{600}. Even at 100 μM, only a few of the hits inhibited or reduced growth. Thus, the majority of top hits do not appear to act as conventional antibiotics or as pan-assay interference compounds (M Nissink and Blackburn, 2014); instead, they likely target bacterial virulence or the host and would not have been identified in a broth-based screen.

F. DISCUSSION

As antibiotic resistance becomes more prevalent, empirical cell-based screens represent a promising strategy to identify novel antimicrobials. We performed a screen for antimicrobials that reduce intracellular load of *Salmonella* within macrophages. I hypothesized that this platform would enable identification of cell-permeable antibiotics capable of penetrating both host and bacterial cells. Surprisingly, we found minimal broth inhibition by the top repurchased 58 compounds, which were a subset of the best hits from the screen. Subsequent work in our lab showed that about half of these compounds could function as antibiotics in the presence of agents that permeabilize the bacterial membrane, or against Gram-positive bacteria, which lack an outer membrane. We propose that these compounds were identified in my screen because the macrophage intracellular environment disrupts *Salmonella* outer membrane permeability. Antimicrobial peptides (AMPs) are thought to be the major driver of intracellular *Salmonella* membrane disruption, as specific *Salmonella* AMP resistance genes and induced and contribute to infection of macrophages (Ernst et al., 2001; Faucher et al., 2006; Groisman et al., 1992; Parra-Lopez et al., 1993, 1994). This explanation of our data suggests that few compounds in the screening library we used are independently permeable to Gram-negative membranes. Indeed, other groups have speculated that drug-like screening libraries, like the Maybridge

HitFinder employed in our screen, are inherently biased *against* entry into Gram-negatives, by virtue of being biased *for* mammalian permeability (Livermore et al., 2011; Payne et al., 2007; Silver, 2011). However, these compounds may be useful for treating intracellular Gram-negative infections, since they are host-cell-permeable and may synergize with host antimicrobials that permeabilize the membrane during infection.

I anticipated that the non-antibiotic hits would likely target infection-specific processes such as bacterial virulence or host immune function; successive work expands on this hypothesis. In **Chapter 3**, I characterize three compounds that appear to inhibit bacterial efflux pumps. In **Chapter 4**, I explore the antibacterial mechanism of clomipramine, a known drug that inhibits the serotonin reuptake transporter. Other work in the lab has identified a compounds that modulate host autophagy (T. Nagy, unpublished data) and disrupt bacterial membranes (J. Dombach, unpublished data). Together, these results indicate that infection-based screens have the capacity to identify compounds that target host-pathogen interactions and that would not have been identified in traditional broth-based screens. Recently, other groups have employed similar infection-based approaches to identify antimicrobials or probe host-pathogen interactions. Several studies have developed cell-based infection assays to screen libraries of FDA-approved drugs for anti-infective activity (Andersson et al., 2016; Kouznetsova et al., 2014; Stanley et al., 2014), and others have used unbiased synthetic libraries as I did (Rybniker et al., 2014; Samantaray et al., 2016). The key challenge with this approach to antibacterial discovery is identifying the mechanism of the drug, which requires a combination of intelligent secondary screening and good fortune.

In conclusion, this work demonstrates that empirical in-cell screens have the capacity to identify novel antibacterials that would not be identified in traditional broth-based screens. We found that few hits targeted bacteria grown in broth, indicating that these compounds do not function as cell-permeable antibiotics. However, they may enter bacteria in the context of host antimicrobials, inhibit bacterial virulence mechanisms, or activate host immune responses. As

resistance to traditional antibiotics increases, these alternative strategies may represent an effective approach to treating infections.

G. MATERIALS AND METHODS

Bacterial strains. *Salmonella enterica* serovar Typhimurium strain SL1344 expressing GFP from the *sifB* promoter (Rollenhagen et al., 2004) (ALR#109; DET#1021) was used for screening and validation experiments. Saturated overnight cultures grown in LB with 30 µg/ml streptomycin and 30 µg/ml kanamycin were diluted to an OD of 0.001 and frozen in 100 µL aliquots at -80 °C with a final concentration of 20% glycerol. Prior to infection, aliquots were thawed into 5 mL cultures of LB with 30 µg/ml streptomycin and 30 µg/ml kanamycin and grown for 18 hours at 37 °C with aeration.

Cell culture. Murine macrophage-like RAW 264.7 were grown in DMEM high glucose (Sigma) supplemented with 10% fetal bovine serum, 2 mM L-glutamine, 1 mM sodium pyruvate, 10 mM HEPES, and 50 µM β-mercaptoethanol, and maintained in a 5% CO_2 humidified atmosphere at 37 °C. For screening and validation, frozen aliquots of RAW 264.7 were thawed and allowed to expand for 3 days prior to scraping and reseeding.

Bacterial infections for SAFIRE and CFU plating. For high-throughput screening and validation, 7 x 10^3 macrophages in 40 µL or 5 x 10^4 macrophages in 100 µL were seeded in 384- or 96-well black-walled, glass-bottomed plates (Brooks Automation). Twenty-four hours post-seeding, bacteria in 20 or 50 µL PBS were added to a final concentration of 1 x 10^7 cfu / mL; we determined that these conditions resulted in infection of approximately 70% of macrophages at 18 hours post-infection with minimal macrophage toxicity (**Appendix A**). Forty-five minutes after bacterial addition, 20 or 50 µL gentamicin was added to a final concentration of 40 µg / mL; this concentration did not affect intracellular infection but was sufficient to inhibit replication of extracellular bacteria (**Appendix A**). At 2 hours post-infection, 200 or 500 nL

compound was added using a pin tool (CyBio) to yield a final concentration of 25 μM. Each assay plate included rifampicin and DMSO controls. At 17.5 hours post-infection, PBS containing MitoTracker Red CMXRos (Life Technologies) was added to yield a final concentration of 300 nM (384-well) or 100 nM (96-well). Thirty minutes later, 16% paraformaldehyde was added to a final concentration of 1-2% and incubated at room temperature for 15 minutes. Wells were washed twice with PBS and stained for 20 minutes with 1 μM DAPI; wells were washed twice and stored in 90% glycerol in PBS until imaging. Infections to determine *Salmonella* CFUs were performed as described above, except cells were seeded in 96-well tissue culture coated plates (Greiner). At 18 hours post-infection, wells were washed three times in PBS, lysed with 30 μL 0.1% Triton X-100, diluted and plated to determine colony-forming units.

Image acquisition, MATLAB®-based screening analysis, and hit selection. High magnification images were acquired on an Olympus IX81 inverted widefield microscope. For screening imaging, three-color images were acquired at 10X or 20X on a Cellomics ArrayScan VTI (Thermo) and exported to DIB files. At least two fields were imaged per well for all experiments. I developed an automated MATLAB® script (**Appendix B**) to quantify intracellular bacterial load; scripting packages have been deposited on MATLAB® File Exchange (https://www.mathworks.com/matlabcentral/fileexchange/), deposited as “SAFIRE_ArrayScan” and “SAFIRE_OlympusIX81.” Briefly, the algorithm identifies macrophage borders via watershed segmentation using DAPI and MitoTracker signal. In order to identify bacteria, the user supplies an empirically determined GFP threshold that maximizes signal to noise based on uninfected and untreated controls. Within each macrophage, the number of pixels above the GFP threshold is counted. If more than 2 pixels are above the GFP intensity threshold, the macrophage is labeled infected. The script calculates the percentage of macrophages infected in the image. To determine infection area for each cell, the number of GFP+ positive pixels is divided by the number of total pixels in the cell. Average infection area is determined by

averaging across all cells within the image. Raw data for at least 2 images from the same well are averaged to yield one value for each well. Raw screening data was subjected to B-score normalization because I identified significant row and column effects by the method described in (Dragiev et al., 2011). To determine significance of screening data, I employed the modified one-sample t-test (Malo et al., 2006) by fitting the variances of replicates to an inverse gamma distribution (Wright and Simon, 2003). Assay positives were defined as having a *p*-value less than 0.05 and a B-score outside one standard deviation from the mean.

Broth activity assays. Overnight *Salmonella* cultures were washed 3 times in PBS and diluted to an OD of 0.01 in Mueller Hinton Broth in 96-well flat-bottom plates. Compound was added using a pin tool (CyBio) or manually, yielding a final concentration of no more than 1% DMSO. Plates were grown at 37 °C shaking and OD_{600} was monitored using a BioTek Eon incubator shaker microplate absorbance reader.

CHAPTER 3. EFFLUX PUMP INHIBITORS THAT REDUCE BACTERIAL LOAD

A. INTRODUCTION

Bacterial efflux pumps (EPs) represent a key pathogen virulence strategy (Baucheron et al., 2004; Bogomolnaya et al., 2013; Buckley et al., 2006; Nishino et al., 2006a). EPs utilize active transport to export chemicals, small molecules, and peptides. Bacterial EPs are naturally important for defense against host-derived antimicrobials such as antimicrobial peptides and reactive oxygen species (Piddock, 2006; Bogomolnaya et al., 2013; Buckley et al., 2006; Nishino et al., 2006a; Chan and Chua, 2005; Lin et al., 2003; Lacroix et al., 1996; Martinez et al., 2009; Shafer et al., 1998; Padilla et al., 2010). EPs also contribute to antibiotic resistance in many multidrug resistant (MDR) pathogens by excluding antibiotics from the bacterial cell (Abouzeed et al., 2008; Alonso and Martinez, 2001; Baucheron et al., 2004; Jiang et al., 2008; Ziha-Zarifi et al., 1999). *Salmonella* encodes nine EPs (**Figure 3-1, adapted from (Andersen et al., 2015)**) which contribute to antibiotic efflux and also are required for virulence *in vivo* (Baucheron et al., 2004; Bogomolnaya et al., 2013; Buckley et al., 2006; Nishino et al., 2006a). In particular, the EPs encoded by the *acrAB* and *macAB* operons are both required for infection of macrophages and mice (Bogomolnaya et al., 2013; Buckley et al., 2006; Nishino et al., 2006a).

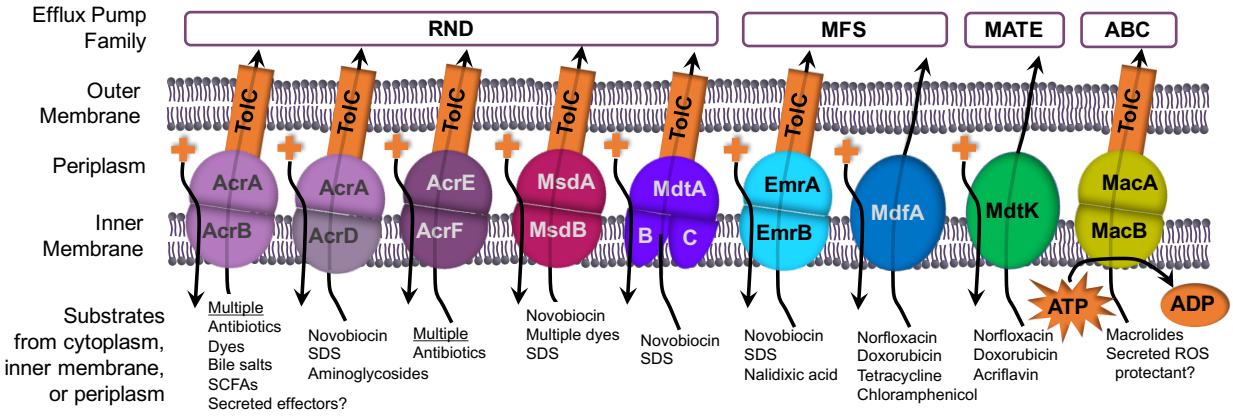

Figure 3-1. *Salmonella* encodes nine efflux pumps which export diverse substrates.

Efflux pump modulators (EPMs) have potential as therapeutics for ordinary and MDR infections by sensitizing pathogens to host defenses as well as clinical antibiotics. Diverse small molecules have been identified as having EPM activity, including synthetic compounds, natural structures, and non-antibacterial drugs (Venter et al., 2015). Three synthetic compounds with activity against Gram-negative bacteria have been extensively characterized. The naphthyl peptidomimetic Phe-Arg β-naphthylamide (PAβN) was identified in a screen for compounds that potentiated the effluxed antibiotic levofloxacin against *Pseudomonas aeruginosa* (Lomovskaya et al., 2001; Renau et al., 1999). A second series of pyridopyrimidine compounds identified in the same screen has undergone significant medicinal chemistry; the lead compound D13-9001 demonstrated efficacy against *Pseudomonas aeruginosa* infection of rats (Nakayama et al., 2003; Yoshida et al., 2007). Finally, a screen for small molecules that synergize with ciprofloxacin identified the pyranopyridine MBX2319, which potentiated the activity of multiple antibiotics against multiple *Enterobactericeae* (Nguyen et al., 2015; Opperman et al., 2014; Sjuts et al., 2016; Vargiu et al., 2014). All three of these compounds, and the majority of known EPMs, were identified through assays of antibiotic potentiation, and were later shown to inhibit efflux. Many EPMs have proved troublesome for drug development due to host toxicity (Lomovskaya and Bostian, 2006; Venter et al., 2015).

We recently performed a screen to identify inhibitors of intracellular *Salmonella* infection (**Chapter 2**, Reens et al, 2018). We hypothesized that EPMs might have been identified by our screen. In this chapter, we identify and characterize three putative EPMs from our top 58 repurchased hits. We found that the three compounds prevent efflux of fluroescent dyes but do not nonspecifically disrupt *Salmonella*'s outer membrane or proton motive force. The EPMs potentiated the activity of antimicrobial peptides (AMPs) against bacteria *in vitro*, suggesting that they may synergize with host AMPs within macrophages. The EPMs also potentiated the activity of effluxed antibiotics against wild-type and multidrug resistant *Salmonella in vitro* and within macrophages. To establish the specific EP targeted by the drugs, I tested in-macrophage drug

susceptibility of *Salmonella* mutants lacking candidate EPs; the results suggest the compounds target multiple EPs or additional infection-relevant processes.

B. IDENTIFICATION OF NOVEL EFFLUX PUMP INHIBITORS THAT PREVENT EFFLUX OF FLUORESCENT DYES

To identify possible EPMs within our collection of hits from SAFIRE, Amy Crooks screened the 58 repurchased compounds identified in our SAFIRE screen (**Chapter 2**) in a Hoechst accumulation assay (Coldham et al., 2010). Bacteria were incubated with Hoechst 33342, an EP substrate that fluoresces when bound to DNA. Heat-killed bacteria exhibited very high fluorescence immediately after exposure to the dye, as these cells are unable to efflux the dye **(Figure 3-2)**. After 60 minutes of exposure, wild-type *Salmonella* exhibited low fluorescence, likely because Hoechst is effluxed before it binds DNA. As expected, Hoechst accumulation was higher in a strain lacking the AcrAB efflux pump and in wild-type bacteria incubated with the known EPM PAβN (Coldham et al., 2010). Three of the top 58 compounds also increased

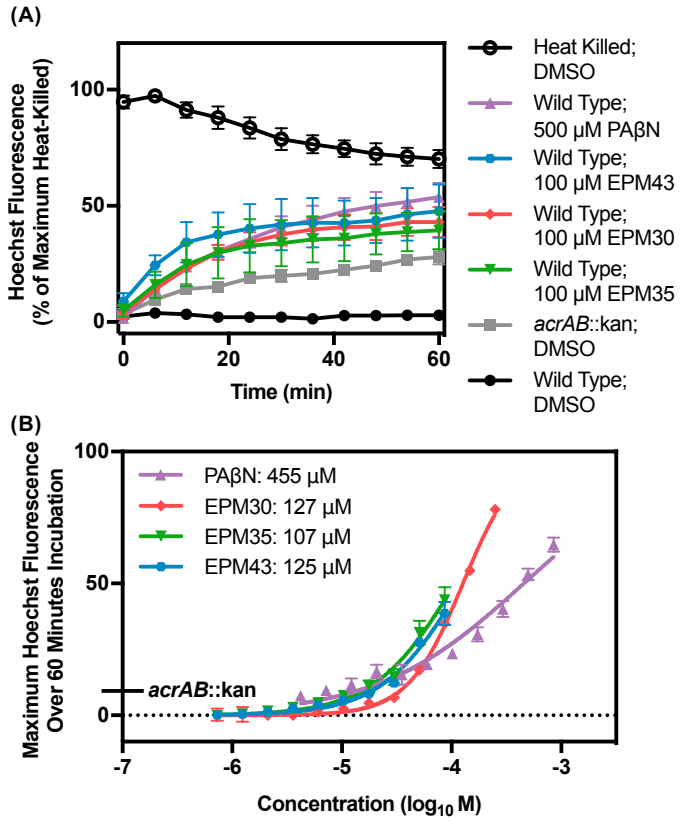

Figure 3-2. EPMs increase Hoechst accumulation. (A) Timecourse plots of Hoechst fluorescence of *S*.Tm incubated in Hoechst 33342 and the indicated EPMs. Data shown are mean + SEM of 3 independent biological replicates. **(B)** Quantification of maximum Hoechst fluorescence over 60 minutes of incubation. Data shown are mean + SEM of 3 independent biological replicates, each performed in duplicate. EC_{50}s are noted in the legend were established using a nonlinear four-parameter fit (GraphPad Prism).

Salmonella accumulation of Hoechst 33342 in a dose-dependent manner, with EC50s lower than that of PAβN. We named these three compounds EPM30, EPM35, and EPM43; all three exhibited potent inhibition of intracellular *Salmonella* during SAFIRE screening and validation (**Figure 2-2B, Figure 3-3**).

I next tested the ability of the three compounds to inhibit efflux of nitrocefin, a chromogenic beta-lactam and known substrate of the AcrAB efflux pump (Misra et al., 2015; Opperman et al., 2014). Nitrocefin is hydrolyzed by beta-lactamase and results in a color change. I measured nitrocefin accumulation in *E. coli* strain RAM121, which has increased influx due to a mutated porin and encodes the periplasmic AmpC beta-lactamase (Misra and Benson, 1988). DMSO-treated bacteria exhibited a low rate of nitrocefin hydrolysis, as the dye is effluxed (**Figure 3-4**).

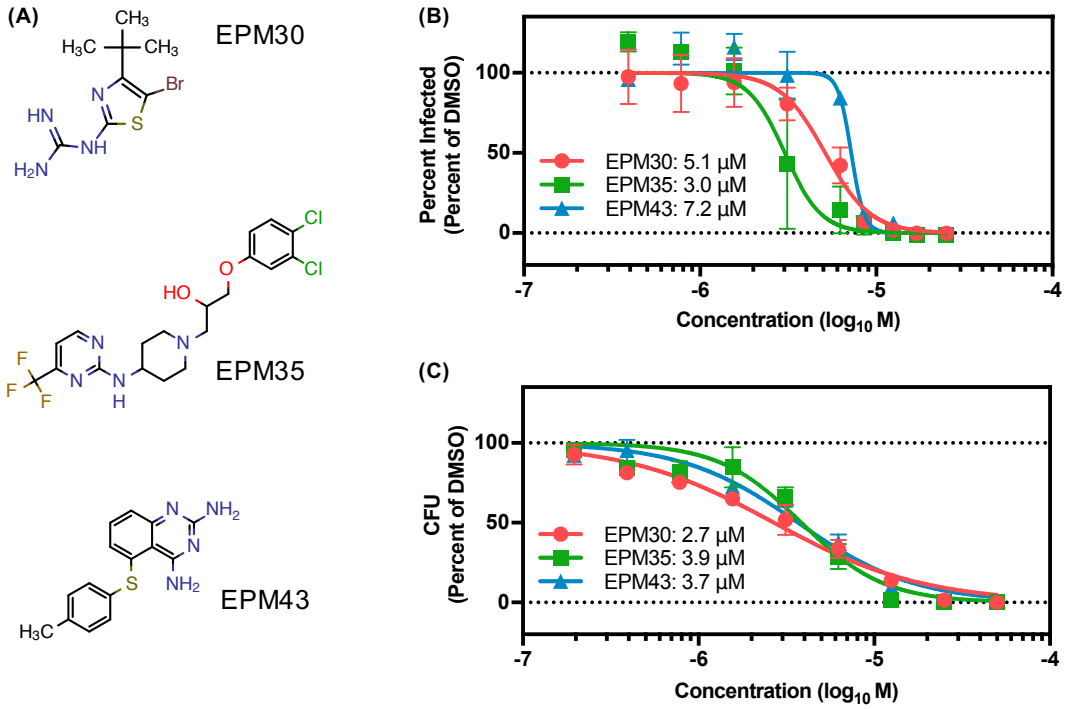

Figure 3-3. EPMs inhibit intracellular *Salmonella* within macrophages. Two hours after infection cells were treated with the indicated compound [25 µM] for 16 hours. (B) Dose response curve for SAFIRE and (C) CFU; keys includes IC_{50}values. Mean and SEM from three independent biological replicates. The nonlinear curve fitting is constrained using uninfected cells as the minimum and DMSO-treated cells as the maximum.

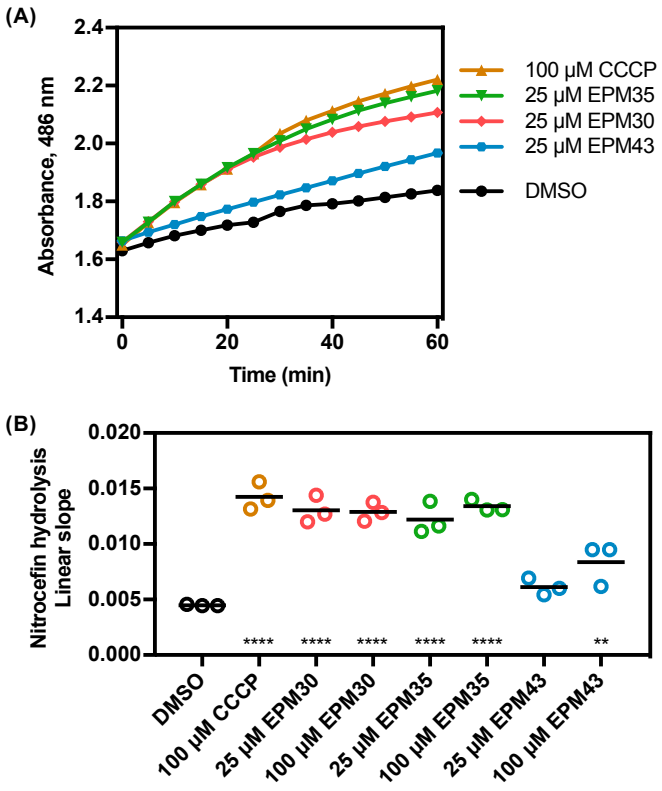

Figure 3-4. EPMs increase nitrocefin accumulation. (A) Timecourse plots of absorbance of RAM121 *E. coli* incubated with nitrocefin and the indicated EPMs. Data shown are representative of 3 independent biological replicates. **(B)** Slope of the linear region of the A_{486} plot from at least three experiments. ** $p < 0.001$, **** $p < 0.0001$ by one-way ANOVA with Dunnett's post-test.

Carbonyl cyanide m-chlorophenylhydrazone (CCCP) is a protonophore that disrupts efflux pumps; CCCP treatment increased nitrocefin hydrolysis. Treatment with EPM30 or EPM35 yielded a similar result to CCCP treatment, whereas treatment with EPM43 only modestly increased hydrolysis. Together, these data suggest that the EPMs reduce efflux.

The Hoechst and nitrocefin assays measure accumulation of an effluxed dye. To more directly measure efflux, we next assayed loss of a preloaded lipophilic membrane-partitioning dye, Nile Red (Lomovskaya et al., 2001; Misra et al., 2015). Nile Red is efficiently loaded into cells in the absence of glucose to reduce efflux pump activity, enabling measurement of bacterial efflux upon addition of glucose (Bohnert et al., 2010; Ivnitski-Steele et al., 2009; Misra et al., 2015). We preloaded *Salmonella* with Nile Red and measured loss of Nile Red fluorescence (**Figure 3-5**). Upon addition of glucose, bacteria rapidly effluxed Nile Red and fluorescence returned to baseline levels. Treatment with PAβN inhibited glucose-activated efflux in a dose-dependent manner. We next tested whether the EPMs inhibit glucose-activated efflux

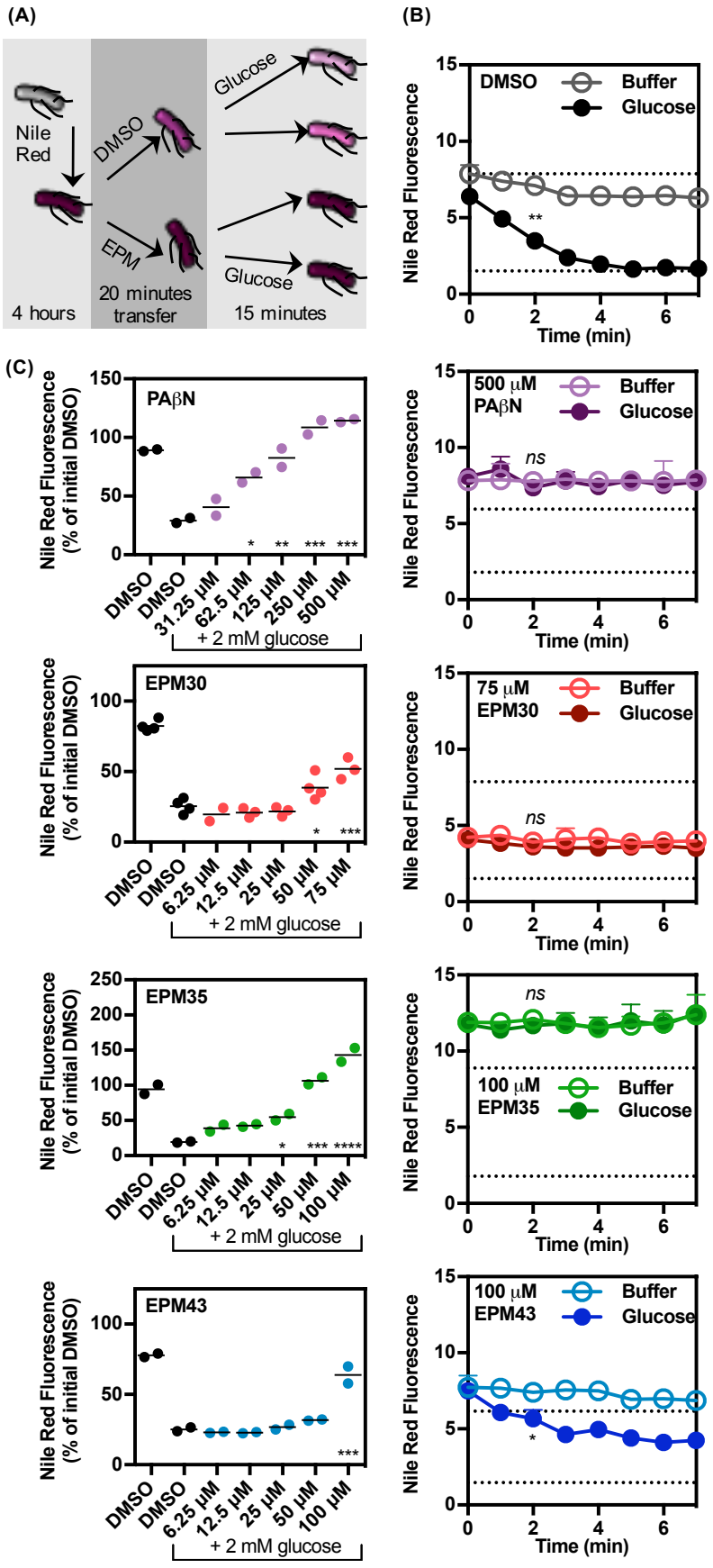

Figure 3-5. EPMs block efflux of Nile Red. (A) Wild-type *S.Tm* were loaded with Nile Red, a fluorescent dye that associates with the outer membrane and is exported by EPs upon addition of glucose. Relative Nile Red fluorescence is indicated by the color of the bacterium in the schematic. Nile Red-loaded cells were incubated with the indicated concentrations of drugs. Glucose or buffer was added and Nile Red fluorescence was monitored. **(B)** Representative timecourse plots from 2 independent biological replicates; dotted lines represent initial Nile Red fluorescence in the same experiment for DMSO-treated cells in the absence of glucose and endpoint fluorescence for DMSO-treated cells in the presence of glucose. Error bars represent standard deviation of technical duplicates. **(C)** Endpoint data (7 minutes) for each treatment condition were normalized to the initial Nile Red fluorescence for DMSO-treated cells in the absence of glucose. Data shown are mean and SEM of 2 biological replicates. * $p < 0.05$; ** $p < 0.01$; *** $p < 0.001$; **** $p < 0.0001$ as determined by (B) t-test of slopes calculated from linear fit of 0-2 minutes relative to buffer, or (C) comparison to DMSO + glucose with a one-way ANOVA and Dunnett's multiple comparison post-test.

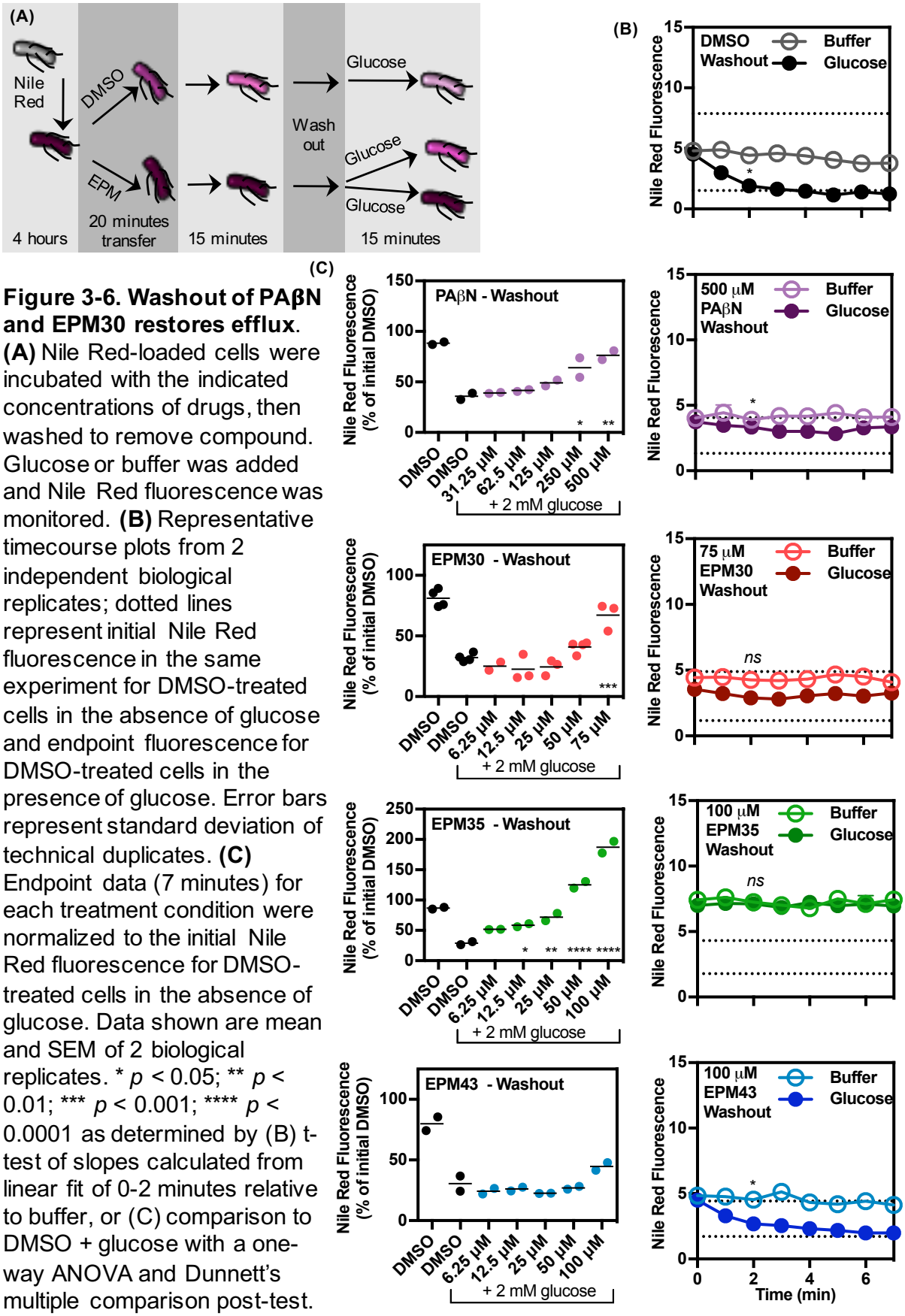

Figure 3-6. Washout of PAβN and EPM30 restores efflux. **(A)** Nile Red-loaded cells were incubated with the indicated concentrations of drugs, then washed to remove compound. Glucose or buffer was added and Nile Red fluorescence was monitored. **(B)** Representative timecourse plots from 2 independent biological replicates; dotted lines represent initial Nile Red fluorescence in the same experiment for DMSO-treated cells in the absence of glucose and endpoint fluorescence for DMSO-treated cells in the presence of glucose. Error bars represent standard deviation of technical duplicates. **(C)** Endpoint data (7 minutes) for each treatment condition were normalized to the initial Nile Red fluorescence for DMSO-treated cells in the absence of glucose. Data shown are mean and SEM of 2 biological replicates. * $p < 0.05$; ** $p < 0.01$; *** $p < 0.001$; **** $p < 0.0001$ as determined by (B) t-test of slopes calculated from linear fit of 0-2 minutes relative to buffer, or (C) comparison to DMSO + glucose with a one-way ANOVA and Dunnett's multiple comparison post-test.

of Nile Red. Treatment with all three EPMs inhibited Nile Red efflux in a dose-dependent manner. At the highest concentrations tested, EPM30 (75 μM) and EPM35 (100 μM) fully inhibited efflux, but EPM43 (100 μM, limited by solubility) only partially inhibited efflux, suggesting that EPM30 and EPM35 may be more potent.

Next, we determined whether efflux pump activity was restored after removal of compound. Bacteria were incubated with compound for 15 minutes, pelleted, and resuspended in buffer lacking compound, and then stimulated with glucose. PAβN washout partially restored Nile Red efflux upon glucose addition (**Figure 3-6**), which is consistent with PAβN specifically binding to efflux pumps during short incubations (Lomovskaya et al., 2001; Misra et al., 2015). EPM30 washout partially restored efflux, suggesting EPM30 may reversibly bind efflux pump components. In contrast, EPM43 washout did not increase efflux, suggesting its effect is maintained in the absence of drug. Similarly, cells treated with EPM35 remained unable to efflux even after removal of the drug, implying that this compound may interact with its target tightly or

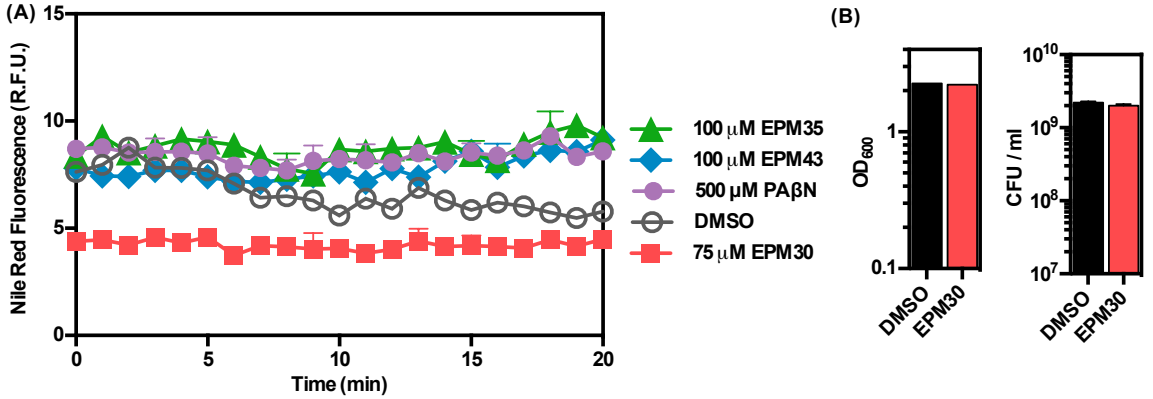

Figure 3-7. DMSO-treated cells efflux Nile Red in the absence of glucose. (A) Nile Red-loaded bacteria were washed, combined with the indicated concentrations of compounds and fluorescence was immediately measured. Data shown are mean + SD. These data suggest that the discrepancy in starting fluorescences in **Figures 3-5, 3-6** are due to the time between compound addition and the beginning of measurement (15-20 minutes). As indicated here, during this timeframe DMSO-treated cells efflux the dye even in the absence of glucose. Thus, EPM35, EPM43, and PAβN inhibit basal loss of Nile Red. However, treatment with EPM30 led to an immediate reduction in fluorescence. **(B)** Bacteria remain intact and viable after 20 minutes incubation in 75 μM EPM30, indicating the immediate reduction in fluorescence in (**A**) is not due to death of the bacteria. It is possible that EPM30 reduces Nile Red fluorescence by quenching or by altering membrane properties, as Nile Red's fluorescent properties are highly dependent on membrane polarity, content, and dynamics.

irreversibly. Overall, these data suggest the EPMs we identified may employ distinct modes of efflux inhibition and/or target distinct biochemical pathways.

Of note, EPM treatment during sample preparation prior to measurement of Nile Red fluorescence (**Figure 3-7**) led to higher initial and final measurements compared to DMSO-treated cells (**Figure 3-5, 3-6**).

C. EFFLUX PUMP INHIBITORS DO NOT DISRUPT THE PROTON MOTIVE FORCE

Efflux pumps translocate substrates using either the proton motive force or ATP (**Figure 3-1**). Thus, efflux can be inhibited by disrupting the proton gradient, which is directly or indirectly (via ATP synthase) required for substrate translocation. To establish whether the EPMs alter the proton gradient, I observed their effect on incorporation of the voltage-sensitive dye tetramethylrhodamine methyl ester (TMRM). After 30 minutes of exposure to the ionophore CCCP, TMRM levels in *Salmonella* were approximately 50-fold lower than upon treat ment with DMSO, but treatment with the three EPMs did not alter TMRM signal (**Figure 3-8**). These observations suggest that membrane potential remains intact in the presence of EPMs.

To establish whether a longer incubation with EPMs may compromise membrane integrity,

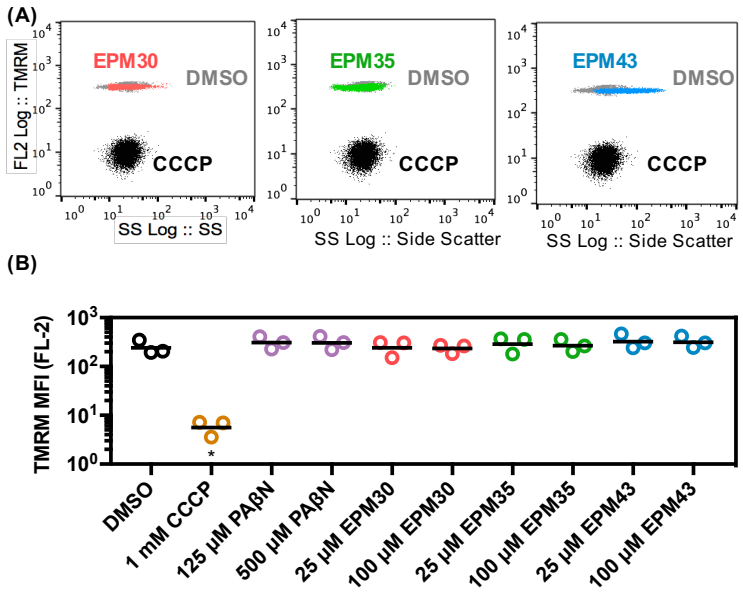

Figure 3-8. EPMs do not disrupt TMRM accumulation. Bacteria treated with DMSO or EPMs [100 µM] but not CCCP [1 mM] acquire TMRM staining within 30 minutes. **(A)** Representative data from one of three independent experiments. **(B)** Median fluorescence intensity from three experiments normalized to unstained control (0). * $p < 0.05$, *** $p < 0.001$, **** $p < 0.0001$ by one-way ANOVA with Dunnett's post-test.

Amy Crooks and I monitored the effect of the EPMs on the ability of *Salmonella* to swim in soft agar plates, which requires an intact membrane potential (Yep et al., 2014). We injected bacteria into the center of the plates and pipetted 10 µl of compound onto paper disks on the periphery; compound diffusion through the agar led to formation of a halo where swimming was inhibited. As expected, we observed a halo around filters spotted with the protonophore CCCP

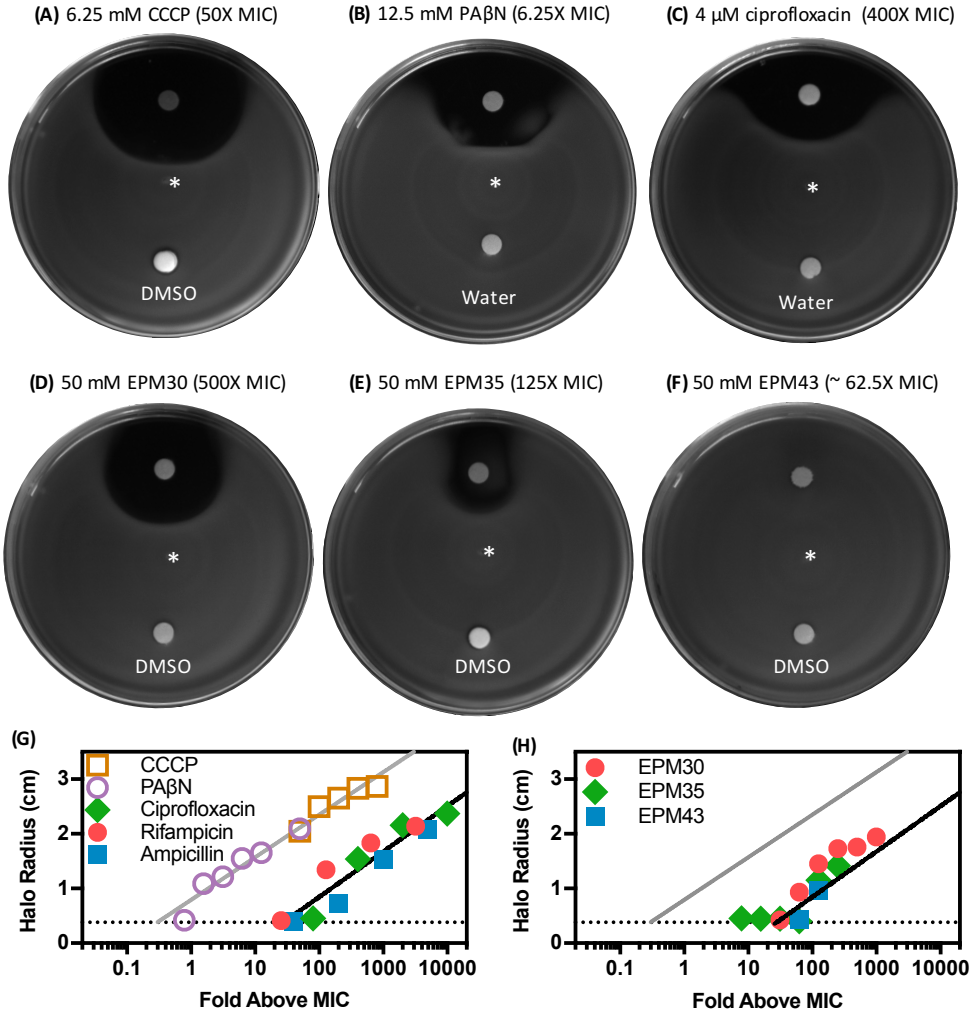

Figure 3-9. Novel EPMs do not disrupt overnight swimming. Bacteria were injected into the center of the plate (indicated with *); 10 µl of the indicated compound or vehicle was spotted onto filter paper disks. Fifteen hours later, plates were imaged. **(A-F)** Representative images. **(G,H)** The distance from the center of the disk to the edge of the halo was measured using ImageJ. Dotted line is the disk radius and limit of measurable halo. Black line is the semilog fit for the combined data set of ampicillin, ciprofloxacin, and rifampicin; gray line is the semilog fit for the combined data set of CCCP and PAβN. Data shown are the average of two measurements from each image captured, and are from a single experiment. Each compound was tested at a range of concentrations in at least two independent experiments and yielded similar trends.

at 50X the MIC (6.25 mM) (**Figure 3-9A**). PAβN is also thought to disrupt membranes over long (> 30 minutes) exposures, at high concentrations, or in efflux-deficient bacteria (Lamers et al., 2013; Matsumoto et al., 2011), although other studies contradict this observation (Lomovskaya et al., 2001; Misra et al., 2015). We found that filters containing PAβN at only 6.25X its MIC (12.5 mM) produced a large halo (**Figure 3-9B**), suggesting that PAβN does have the ability to disrupt membrane potential. Since swimming overnight requires not only an intact proton gradient but also bacterial growth, we tested whether filters containing bacteriostatic antibiotics not known to disrupt the proton motive force created halos. *Salmonella* treated with ciprofloxacin at 400X the MIC (4 μM) formed a halo similar in size to that of CCCP-treated bacteria (**Figure 3-9C**). Plotting halo radius versus concentration as fold MIC for a range of concentrations revealed that the ciprofloxacin, ampicillin, and rifampicin-treated samples converged along one line, whereas those treated with CCCP and PAβN converged along a second, left-shifted line (**Figure 3-9G**). Thus, membrane disruptors form considerably larger radii at similar MIC-adjusted concentrations than antibiotics. None of the three EPMs at 50 mM (500X, 125X, and 62.5X MIC, respectively) formed halos as large as CCCP (50X its MIC) or PAβN (6.25X its MIC) (**Figure 3-9**). Moreover, the halo radii formed by the three EPMs converged along the antibiotic line (**Figure 3-9H**). These data indicate that the inhibition of swimming by the EPMs in this assay likely reflects growth perturbation rather than non-specific disruption of membranes or energy generation.

We confirmed that the EPMs do not permeabilize bacterial membranes using a nitrocefin hydrolysis assay of membrane integrity (Misra et al., 2015). Beta-lactamase-expressing *Salmonella* were exposed to low concentrations of nitrocefin, a chromogenic beta-lactamase substrate which is excluded from cells with intact membranes; disruption of the outer membrane increases beta-lactamase access to nitrocefin resulting in increased hydrolysis. Treatment of beta-lactamase-expressing bacteria with polymyxin B, a pore-forming antimicrobial peptide, led to rapid nitrocefin hydrolysis compared to DMSO (**Figure 3-10**). Treatment with PAβN led to a

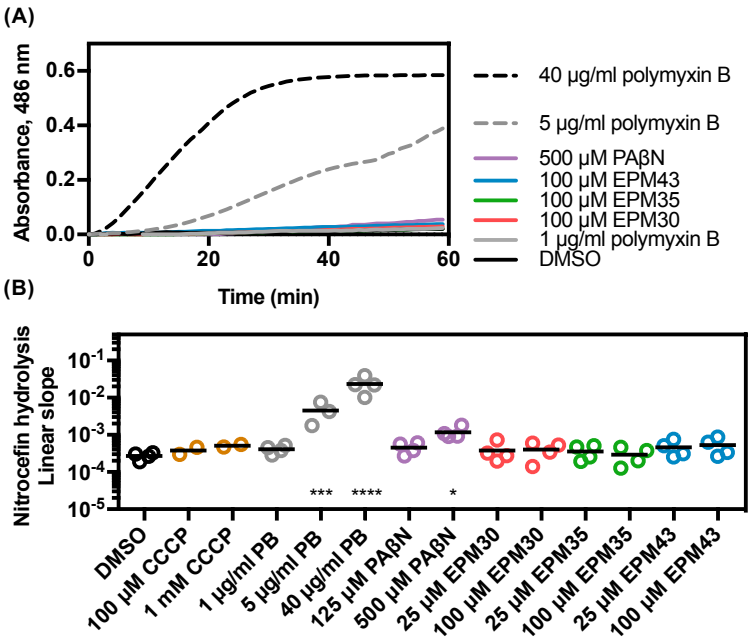

Figure 3-10. Novel EPMs do not permeabilize membranes. Nitrocefin access to the periplasm as monitored by nitrocefin [100 µM] hydrolysis in the presence of the indicated concentrations of compounds. **(A)** Absorbance 486 nm of *bla*+ *Salmonella* normalized to *bla*- *Salmonella.* Data is representative of 3-4 independent biological replicates. **(B)** Slope of the linear region of the A486 plot from at least three experiments. Data is normalized to A486/minute. * $p < 0.05$, *** $p < 0.001$, **** $p < 0.0001$ by one-way ANOVA with Dunnett's post-test.

small increase in nitrocefin hydrolysis after long exposure, as expected, but treatment with the three EPMs did not alter nitrocefin hydrolysis. Together, these data confirm that the EPMs do not disrupt membrane integrity and likely do not disrupt efflux by altering membrane potential.

D. EFFLUX PUMP INHIBITORS SENSITIZE *SALMONELLA* TO HOST ANTIMICROBIAL PEPTIDES

Inactivation of efflux pumps by genetic knockout or chemical inhibitor does not prevent bacterial growth in rich broth (Nishino et al., 2006a). To identify the mechanism of killing by EPMs, I first verified that treatment of *Salmonella* with the three EPMs did not independently eliminate growth in broth (**Figure 3-11**), as expected. I therefore hypothesized that EPMs increase *Salmonella* exposure to effluxed host antimicrobials. The AcrAB efflux pump has been shown to export macrophage antimicrobial peptides, and the MacAB efflux pump protects against reactive oxygen species (ROS) (Bogomolnaya et al., 2013; Buckley et al., 2006; Nishino et al., 2006a; Padilla et al., 2010; Shafer et al., 1998). We found that deletion of either AcrAB or MacAB compromised *Salmonella* infection of macrophages (**Figure 3-12**), suggesting the EPMs could facilitate macrophage killing by increasing exposure to these AMPs or ROS.

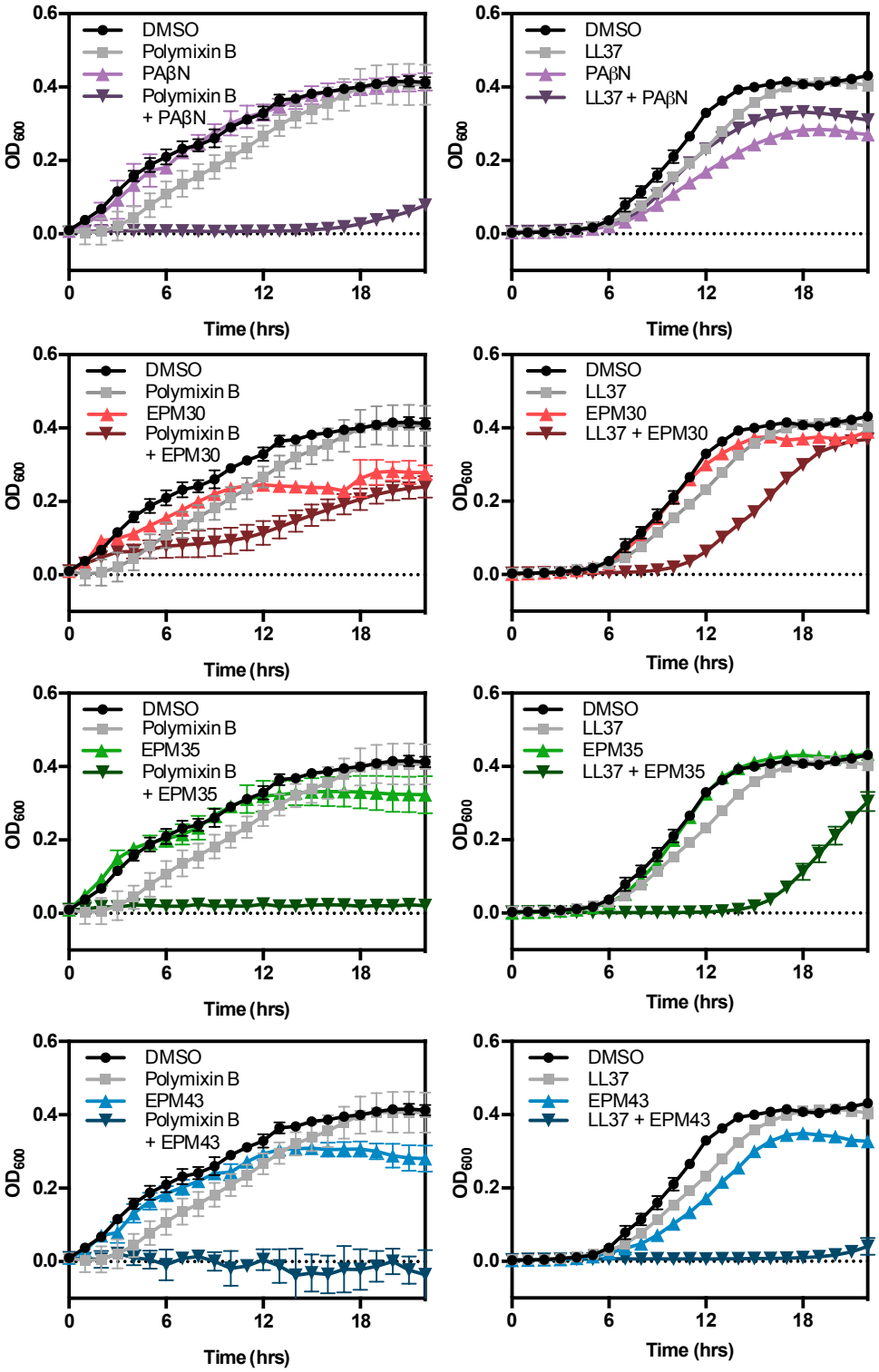

Figure 3-11. EPMs synergize with antimicrobial peptides in broth. *Salmonella* was grown in M9-based defined media in the presence of polymyxin B (5 µg/ml; 1/8 MIC) or LL37 (5 µg/ml; 1/8 MIC) and EPMs (PAβN, 500 µM; EPMs, 25 µM). Mean and SD of triplicate samples from one representative experiment of three independent biological replicates. DMSO, polymyxin B and LL37 curves repeat across graphs.

Next, I established whether EPMs potentiated AMPs or ROS in broth. I modeled AMP stress using polymyxin B, a microbial AMP, and LL-37, the human ortholog of cathelicidin, which is the major AMP produced by mammalian macrophages. Bacteria treated with 5 μg/ml AMP (1/8 MIC) or 25 μM EPM exhibited mild to no growth inhibition. However, combination treatment significantly inhibited growth; similar results were obtained with 500 μM PAβN **(Figure 3-11**). In contrast, the EPMs had no effect on bacterial growth in 0.2 mM H_2O_2, suggesting they do not synergize with reactive oxygen species (**Figure 3-13**).

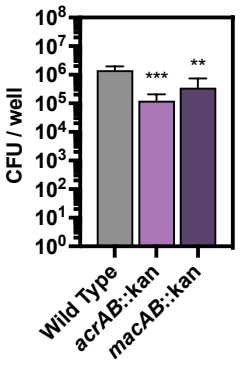

Figure 3-12. Efflux pumps contribute to *Salmonella* infection of macrophages. Monitoring of bacterial load by CFU in RAW 264.7 cells infected with the indicated strains for 18 hours, followed by macrophages lysis and plating for CFU. ** $p < 0.01$; *** $p < 0.001$ by one-way ANOVA with Dunnett's post-test.

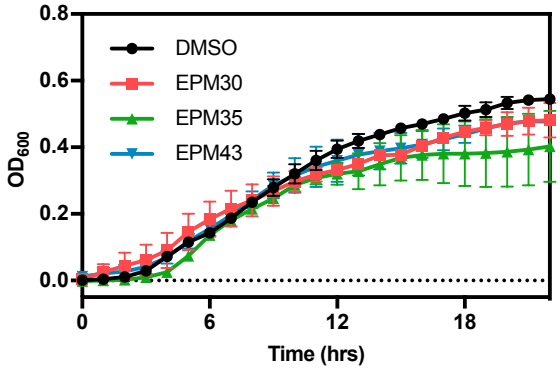

Figure 3-13. EPMs do not potentiate ROS in broth. Wild-type *S.*Tm were grown in the presence of 0.2 mM H_2O_2 and 25 μM of the indicated EPMs. Data shown are mean + SEM from two independent biological replicates.

To further establish whether EPMs potentiate AMP membrane-permeabilizing activity, I tested w hether 1 μg/ml polymyxin B, which does not independently allow nitrocefin access to the periplasm (**Figure 3-10B**) increased the rate of nitrocefin hydrolysis in a beta-lactamase-expressing *Salmonella* strain when EPMs where present (**Figure 3-14**). Treatment with PAβN or the EPMs significantly increased nitrocefin hydrolysis by polymyxin B, indicating that the EPMs

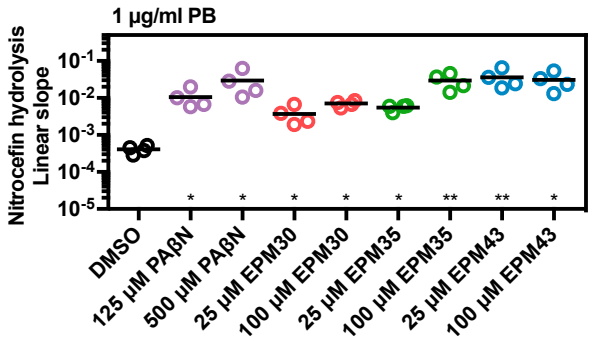

Fig 3-14. EPMs sensitize bacteria to outer membrane permeabilization by antimicrobial peptides. Nitrocefin access to the periplasm in the presence of a non-permeabilizing concentration of polymyxin B [1 μg/ml] and the indicated concentrations of EPMs, quantitated as in **Figure 3-10**. * $p < 0.05$, ** $p < 0.01$ by one-way ANOVA with Dunnett's post-test.

facilitate membrane permeabilization. To rule out the possibility that polymixin B potentiated EPM activity, I next determined that bacterial exposure to 5 µg/ml polymixin B, which allows nitrocefin access to the periplasm (**Figure 3-10B**), did not enhance the ability of the EPMs to increase Hoechst accumulation or Nile Red retention compared to polymyxin B or EPMs alone (**Figure 3-15, 3-16**). Therefore, EPMs may increase the effective concentration of AMPs and have indirect antibacterial activity in the context of the host.

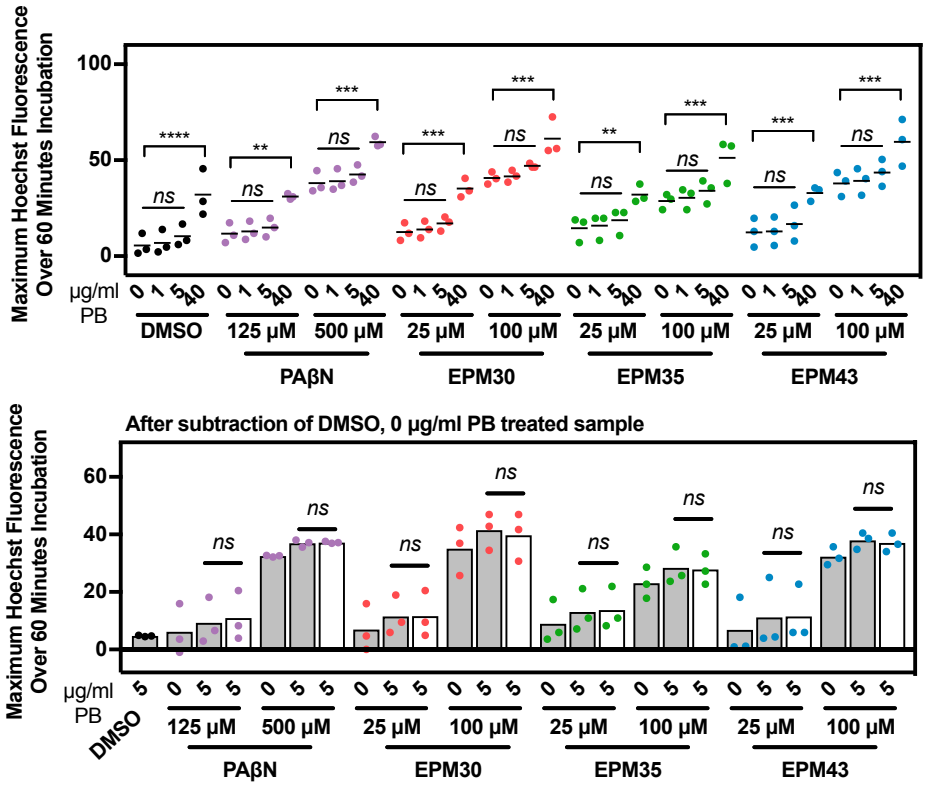

Figure 3-15. Polymyxin B [5 µg/mL] did not increase Hoechst accumulation in the presence of EPMs. (A) Hoechst accumulation assay, quantitated as in Figure 3-2A. **(B)** The DMSO, no-polymyxin B-treated samples were subtracted from treated samples (gray bars). Assuming additivity as the null hypothesis, the sum of the 5 µg/ml polymyxin B sample and each EPM sample was calculated (white bars). No significant differences were identified between observed and calculated data, suggesting that EPMs and polymyxin B do not synergize in this assay of efflux inhibition. * $p < 0.05$, ** $p < 0.01$, *** $p < 0.001$, **** $p < 0.0001$ calculated using one-way ANOVA with Dunnett's post-test.

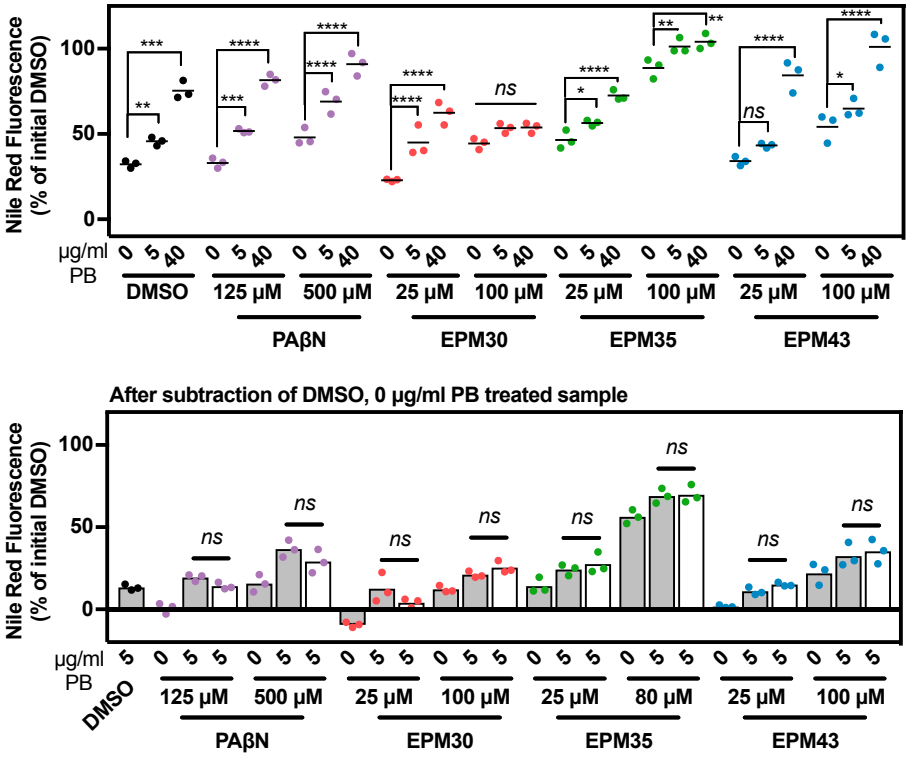

Figure 3-16. Polymyxin B [5 μg/mL] did not increase Nile Red retention in the presence of EPMs. (A) Nile Red efflux assay, quantitated as in Figure 3-5. **(B)** The DMSO, no-polymyxin B-treated samples were subtracted from treated samples (gray bars). Assuming additivity as the null hypothesis, the sum of the 5 μg/ml polymyxin B sample and each EPM sample was calculated (white bars). No significant differences were identified between observed and calculated data, suggesting that EPMs and polymyxin B do not synergize in this assay of efflux inhibition. * $p < 0.05$, ** $p < 0.01$, *** $p < 0.001$, **** $p < 0.0001$ calculated using one-way ANOVA with Dunnett's post-test.

E. EFFLUX PUMP INHIBITORS COOPERATE WITH THE INTRINSIC IMMUNE RESPONSE

Some AMPs are constitutively expressed and stored (Bals et al., 1998; Hooper et al., 2003); others are upregulated in response to infection (Ogushi et al., 2001; O'Neil et al., 1999). Key responses to *Salmonella* are not induced until 4 hours post-infection (Shi et al., 2009). Along with Toni Nagy, I therefore asked whether host transcription or translation of AMPs or other factors are required for EPM antibacterial activity. We performed SAFIRE in the presence of the transcription inhibitor DRB or the translation inhibitor cycloheximide (CHX) **(Figure 3-17)**.

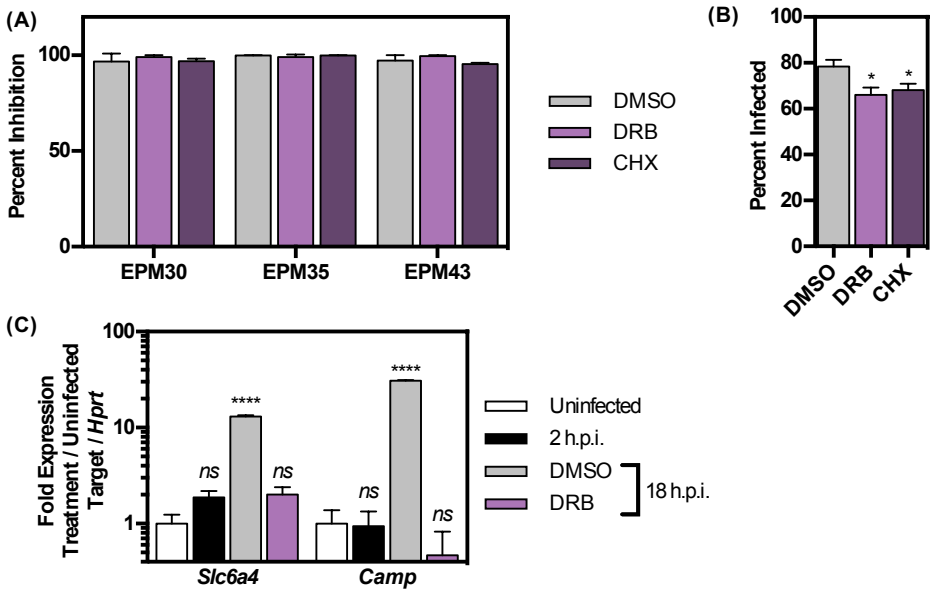

Figure 3-17. EPMs do not require transcription or translation for antibacterial activity. (A) RAWs were infected and treated with 25 μM of the indicated EPMs at 2 hours post infection using SAFIRE. From 2-18 hours post infection, cells were treated with DMSO, 100 μM DRB, or 1 μM cycloheximide (CHX). Data for each inhibitor (DRB, CHX) treatment are normalized to cells not treated with EPMs, as differences in basal infection were observed with DRB and CHX treatment **(B)**. Data are mean + SEM of three independent biological replicates, each performed in triplicate. **(B)** RAWs were seeded in 6-well dishes and treated as in (A). RNA was extracted at the indicated timepoints, reverse transcribed, and expression of the indicated genes was determined using qPCR. Data shown are mean + SEM of four separate wells from one replicate, and were performed in parallel with one replicate of (A). **** $p < 0.0001$ compared to uninfected by two-way ANOVA with Dunnett's post-test.

Since exposure to inhibitors prior to infection greatly diminished macrophage viability, we added DRB or CHX at 2 hours post-infection, concurrent with EPMs. This procedure prevents production of late-induced host defense genes (Shi et al., 2009). We did not observe infection-induced macrophage expression of *Slc6a4* and *Camp* after DRB treatment. While treatment with DRB or CHX decreased infection, antibacterial activity of the EPMs did not change in the presence of inhibitors. These data suggest that transcripts made after 2 hours of infection do not contribute to EPM antibacterial activity. Instead, the EPMs may synergize with host antibacterial effectors that are induced early (Shi et al., 2009) or are part of the intrinsic immune response.

Next, we hypothesized that EPMs might inhibit *Salmonella* growth in non-immune cells, which can express AMPs and other components of the intrinsic immune response (Bals et al., 1998; Hooper et al., 2003; Ogushi et al., 2001; O'Neil et al., 1999). Thus, we tested whether EPMs inhibit *Salmonella* growth in HeLa cells, a model of epithelial cell infection; HeLa cells express AMPs but not ROS (Mineshiba et al., 2005; Park et al., 2011). We first tested whether EPs are required for infection of HeLa cells. Deletion of *acrAB* but not *macAB* reduced bacterial colonization (**Figure 3-18A**). Next, we infected HeLa cells with *Salmonella* expressing GFP from the constitutive *rpsM* locus (Vazquez-Torres et al., 1999) and monitored bacterial infection with SAFIRE after treatment with the three EPMs (**Figure 3-18B,C**). Treatment with EPM30 and EPM35 appeared to decrease MitoTracker signal in HeLa cells, which agrees with SAFIRE in RAWs (**Figure 2-2B**). However, all three EPMs decreased bacterial load in HeLa cells at 25 μM,

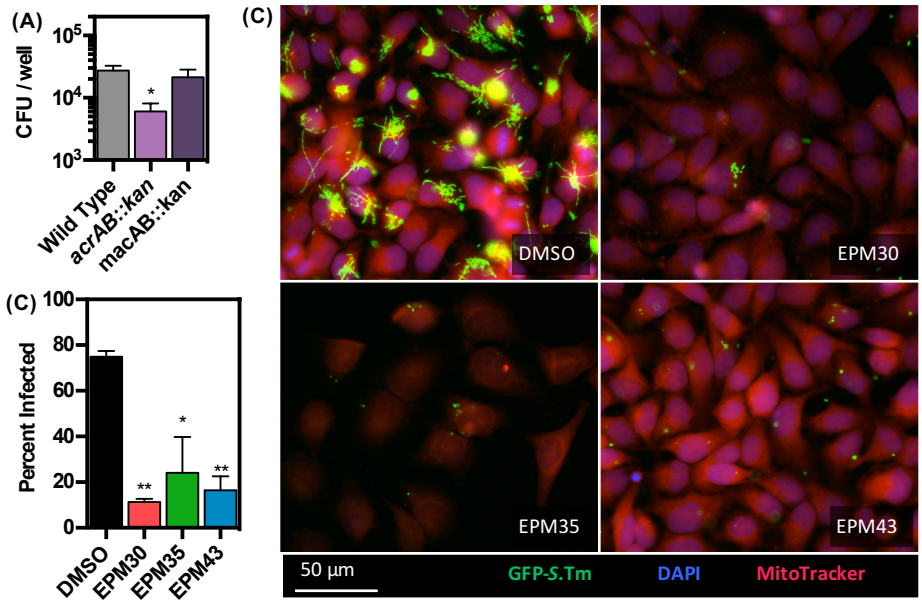

Figure 3-18. EPMs are active against *Salmonella* in HeLa cells. **(A)** HeLa cells were infected with the indicated strains; at 18 hours post infection cells were lysed and plated to enumerate CFUs. **(B,C)** HeLa cells were infected with *rpsM*::*GFP S.*Tm and treated with 25 μM compound for 16 hours according to the SAFIRE protocol. **(B)** Mean + SEM of three independent biological replicates. **(C)** Representative microscopy from one experiment. * $p < 0.05$; ** $p < 0.01$ compared to DMSO by one-way ANOVA with Tukey's post-test.

although we observed isolated intact bacteria. In contrast, treatment of infected RAWs led to very few observable bacteria (**Figure 2-2B**). It is likely that the EPMs are predominantly bacteriostatic, as HeLa cells do not kill replication-deficient *Salmonella* (Garcia-del Portillo et al., 1993; Malik-Kale et al., 2012; Steele-Mortimer et al., 2002). We conclude that EPMs synergize with intrinsic immune responses to reduce *Salmonella* infection in both RAW and HeLa cells.

F. EFFLUX PUMP INHIBITORS LIKELY TARGET RND-FAMILY EFFLUX PUMPS

Salmonella encodes nine efflux pumps which export different substrates (Nishino et al., 2006a). I and others have shown that the AcrAB and MacAB pumps are important for infection of macrophages (Bogomolnaya et al., 2013; Buckley et al., 2006), (**Figure 3-12**). Both pumps also utilize the TolC outer membrane export channel. I next evaluated whether the pumps or TolC were required for EPM activity against intracellular *Salmonella* (**Figure 3-19**). Treatment of macrophages with any of the three compounds reduced load of wild-type bacteria below those observed in DMSO-treated cells infected with the *acrAB*, *macAB*, or *tolC* mutant strains. Compound treatment of the mutant strains further reducd the levels of bacteria. These data indicate that the AcrAB and MacAB pumps are not required for EPM activity, indicating that these are not the sole target of the EPMs, and that other pumps or virulence determinants could be inhibited by the EPMs.

Since all three EPMs reduced *Salmonella* efflux of Nile Red, a well-studied substrate of the AcrAB-TolC efflux pump (Bohnert et al., 2010), we established whether any of the compounds bind *E. coli* AcrB. We collaborated with another group, who employed isothermal titration calorimetry and demonstrated that all three EPMs are capable of binding AcrB (Reens et al., 2018). Although binding does not necessarily entail inhibition of AcrB by EPMs, together with our previous data this result suggests that the EPMs may inhibit AcrAB.

Salmonella encodes 4 pumps in the same structural family as AcrAB that are upregulated and may contribute to *Salmonella* survival in the absence of *acrAB* (Nishino et al., 2009; Wang-

Kan et al., 2017; Zhang et al., 2017) (**Figure 3-1**). Thus, together these data suggest that the three EPMs target multiple RND-family efflux pumps.

G. EFFLUX PUMP INHIBITORS POTENTIATE ANTIBIOTICS AND TARGET ANTIBIOTIC-RESISTANT BACTERIA IN BROTH, MACROPHAGES, AND MICE

Efflux pumps are upregulated in some multidrug resistant (MDR) strains. I found that a clinical MDR *Salmonella* isolate (S10801) was recovered from EPM-treated macrophages at levels 1000-fold lower than from DMSO-treated macrophages (**Figure 3-19**). These results indicate that the three compounds inhibit not only SL1344 but also an MDR clinical isolate during infection of cells.

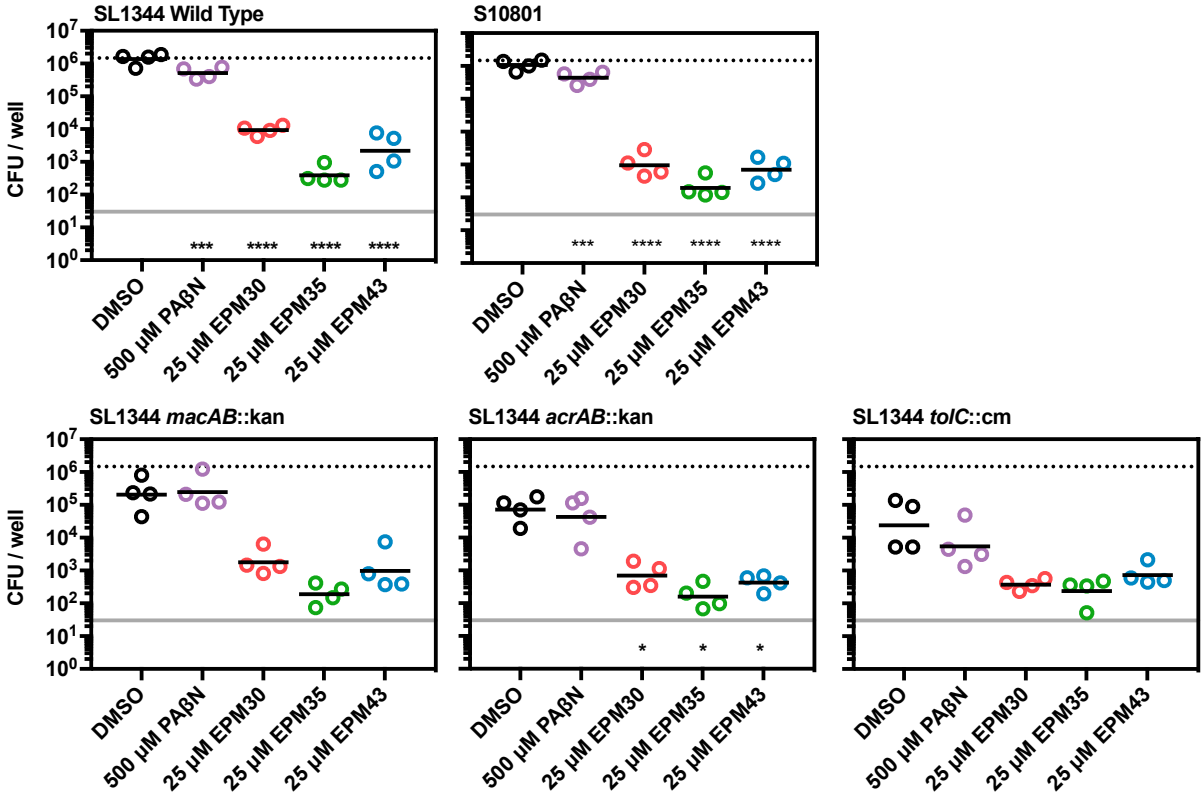

Figure 3-19. EPMs are active against *Salmonella* lacking efflux pumps and multidrug resistant *Salmonella*. Monitoring of bacterial load by CFU in RAW264.7 cells infected for two hours with the strain of *Salmonella* shown and then treated with the indicated compound for 16 hours, followed by macrophage lysis and plating for CFU. DMSO data is replotted from **Figure 3-12**. Geometric mean of four biological replicates. Upper lines, mean CFU/well of wild-type SL1344 with DMSO treatment; lower lines, limit of detection. * $p < 0.05$, ** $p < 0.01$; *** $p < 0.001$, **** $p < 0.0001$ relative to DMSO, one-way ANOVA with Dunnett's post-test.

Efflux pumps export antibiotics and play a role in multidrug resistance. I next investigated whether EPMs increase *Salmonella* sensitivity to antibiotics exported by efflux pumps. I found that co-incubation with EPMs reduced the MIC of established AcrB substrates in wild-type SL1344 and S10801. Exposure to EPM35 or EPM43 decreased by four-fold the MIC of chloramphenicol for one or both strains (**Table 3-1**). EPM35 also potentiated tetracycline and erythromycin. Similar effects were observed in the SL1344-derived *macAB* mutant strain but not in the *acrAB* or *tolC* mutant strains. These data support the idea that the AcrAB-TolC efflux pump may be a relevant target for EPM35 and EPM43 with regard to antibiotic potentiation, and more importantly, that these EPMs appear to reduce the effective dose in broth of some clinical antibiotics.

Table 3-1. MICs (μg/ml) of AcrAB substrates in combination with EPMs**.**

		SL1344	S10801	*macAB*::kan	*acrAB*::kan	*tolC*::cm
Tetracycline	DMSO	2	128	2	0.5	0.5
	25 μM EPM30	2	128	2	0.5	0.5
	25 μM EPM35	0.5	64	0.5	0.5	0.5
	25 μM EPM43	1	64	1	0.5	0.5
Chloramphenicol	DMSO	4	256	4	2	
	25 μM EPM30	2	256	2	2	
	25 μM EPM35	1	64	1	1	
	25 μM EPM43	1	128	1	1	
Ciprofloxacin	DMSO	0.004	0.016	0.004	0.002	0.002
	25 μM EPM30	0.002	0.008	0.002	0.002	0.002
	25 μM EPM35	0.002	0.008	0.002	0.002	0.002
	25 μM EPM43	0.002	0.008	0.002	0.002	0.002
Novobiocin	DMSO	512	512	512	256	256
	25 μM EPM30	256	256	256	256	256
	25 μM EPM35	256	256	256	256	256
	25 μM EPM43	256	256	256	256	256
Erythromycin	DMSO	128	64	128	32	32
	25 μM EPM30	64	64	64	32	32
	25 μM EPM35	32	32	32	32	32
	25 μM EPM43	64	32	64	32	32
Crystal Violet	DMSO	16	16	16	8	8
	25 μM EPM30	16	16	16	8	8
	25 μM EPM35	8	8	8	8	8
	25 μM EPM43	8	8	8	8	8

Since intracellular conditions are distinct from microbiological media, I tested whether the EPMs also synergize with AcrAB-exported antibiotics for bacterial killing in macrophages. RAW264.7 macrophages were infected with wild type *Salmonella* followed two hours later by treatment with antibiotic over a dose range with or without an EPM [6.25 μM]. SAFIRE analysis revealed that both erythromycin and ciprofloxacin were potentiated by the EPMs, as indicated by a difference between the co-treatment data and calculated additivity curves (**Figure 3-20**).

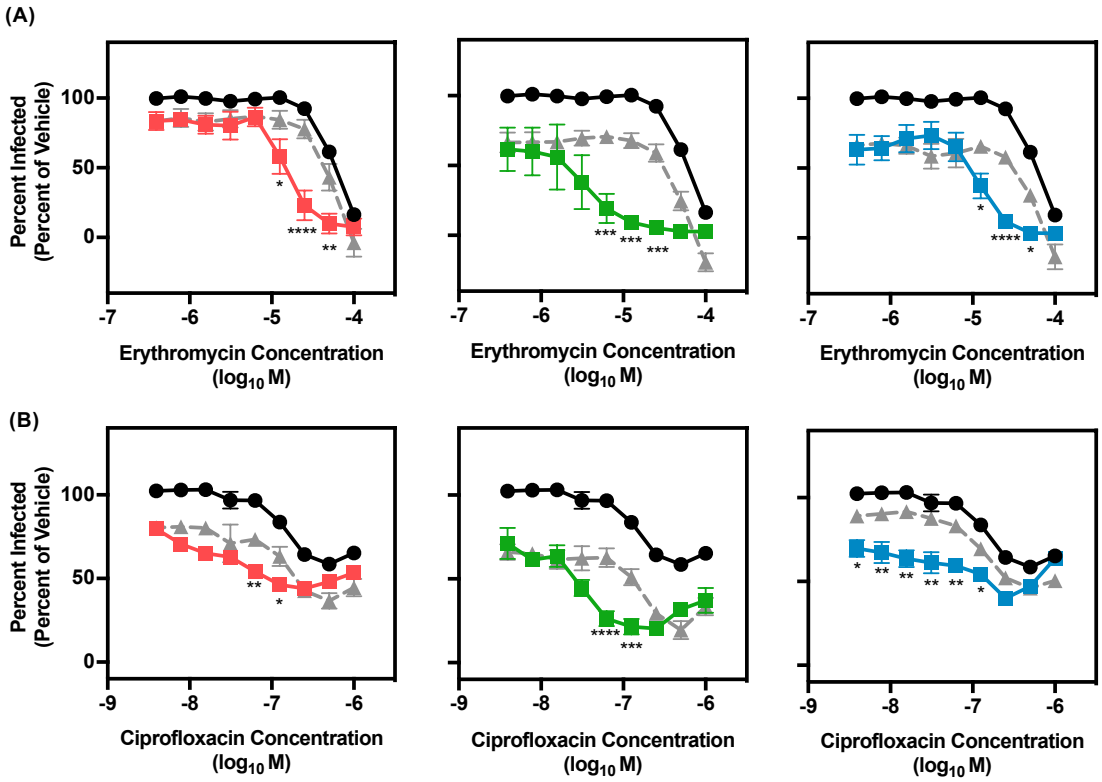

Figure 3-20. EPMs enhance activity of erythromycin and ciprofloxacin against *Salmonella* in macrophages. RAW 264.7 macrophages were infected with *Salmonella* and treated with a dose range of (A) erythromycin or (B) ciprofloxacin and with DMSO or the indicated concentration of an EPM. At 18 hours post infection samples were processed for fluorescence microscopy as described. Data were normalized to treatment with DMSO and antibiotic vehicle (100%). Key: black, DMSO; red, EPM30; green, EPM35; blue, EPM43; gray, calculated additivity of the antibiotic and the corresponding EPM using the formula (100 –([percent inhibition EPM] + [percent inhibition antibiotic])), where percent inhibition is calculated as 100 –[percent of DMSO]. Data are mean + SEM of three biological replicates. * $p < 0.05$; ** $p < 0.01$; *** $p < 0.001$; **** $p < 0.0001$ of EPM treatment versus calculated additivity by one-way ANOVA with Sidak's multiple comparison test.

Thus, the EPMs may reduce the effective dose of erythromycin and ciprofloxacin in macrophages.

Finally, I tested whether EPM35 increased sensitivity of S10801 and wild-type *Salmonella* to tetracycline *in vivo*. I intraperitoneally infected 7 week old C57BL/6 mice with $1x10^4$ bacteria. At 30 minutes and 24 hours post-infection, we intraperitoneally injected 25 mg/kg tetracycline and 50 mg/kg EPM35. We observed more severe signs of distress in mice treated with EPM35 compared to DMSO-treated mice, including squinty eyes and hunching posture, as well as neurological abnormalities in one mouse (loss of coordination, tail stiffening). Thus, we ended the experiment at 30 hours post-infection; I harvested spleen and liver and plated to determine bacterial CFU. S10801-infected mice treated with tetracycline alone had lower levels of bacteria, but co-treatment with EPM35 further reduced bacterial CFU (**Figure 3-21**), suggesting this combinatorial effect may be useful for treatment of MDR infections. We did not observe a similar

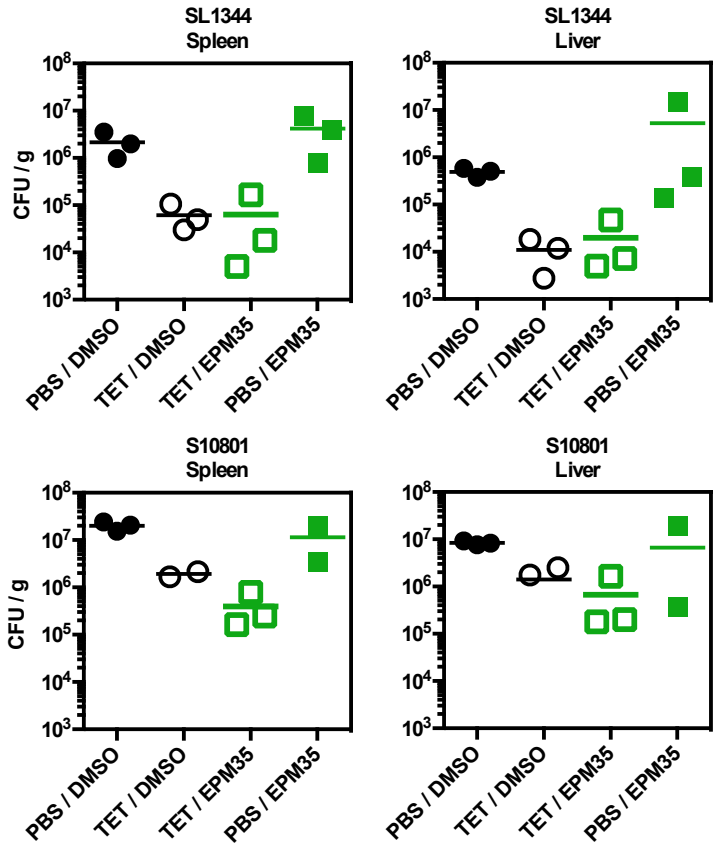

Figure 3-21. EPMs may increase sensitivity of MDR *Salmonella* to tetracycline *in vivo*. C57/Bl6 mice were infected with 10^4 *S*.Tm intraperitoneally. At 30 minutes and 24 hours post infection, mice received 25 mg/kg tetracycline, 50 mg/kg EPM35, or both. Six hours after the second injection, tissues were harvested and plated to enumerate CFUs.

pattern in mice infected with wild-type bacteria, suggesting efflux inhibition *in vivo* does not sensitize *Salmonella* to macrophage antimicrobials as potently as *in vitro*. Due to the signs of distress observed in mice treated with EPM35, we did not repeat the experiment. Overall, the data indicate that future efforts to separate EPM35 activity from toxicity may be of value.

H. DISCUSSION

Pathogens require efflux pump activity to survive in host tissues, suggesting modulators of bacterial efflux may be identified with in-cell screens for pathogen survival (Bogomolnaya et al., 2013; Wang-Kan et al., 2017). *Salmonella* encodes nine efflux pumps (Andersen et al., 2015). The two demonstrated to be required for bacterial survival in cells and in mice are AcrAB and MacAB (Bogomolnaya et al., 2013; Buckley et al., 2006; Lacroix et al., 1996; Nishino et al., 2006b, 2009). The first hint that several of the hit compounds may modulate bacterial efflux was the observation that treatment of wild-type *Salmonella* with PAβN or with any of the three EPMs allowed Hoechst to accumulate to higher levels than in vehicle-treated bacteria. We speculate that treatment with PAβN or the EPMs was more effective at raising Hoechst levels than was deletion of the *acrAB*::kan locus because the compounds may target other efflux pumps. We also note that EPMs are not expected to function as clinical antibiotics: EPMs have high MICs in standard broth-based assays (Venter et al., 2015). However, EPMs are of interest because of their potential to enhance the activity of existing antibiotics and/or host antimicrobials. These properties further underscore the biology of efflux pumps and highlight the importance of looking beyond MIC assays to identify chemicals with antimicrobial activity under conditions that approximate infection.

All three of our hit compounds bind the efflux pump subunit AcrB, a subunit of the most thoroughly studied RND efflux pump. AcrB integrates into cellular membranes and captures substrates from the outer leaflet of the cytoplasmic membrane or the periplasm (Murakami et al., 2002, 2006; Nakashima et al., 2013). The identified compounds bind AcrB (EPM30 K_D: 1.79

+/- 0.37 μM; EPM35 K_D: 0.29 +/- 0.03 μM; EPM43 K_D: 0.56 +/- 0.06 μM) more tightly than several known AcrB substrates, such as ethidium (K_D of 8.7 +/- 1.9 μM), proflavin (K_D of 14.5 +/- 1.1 μM), and ciprofloxacin (K_D of 74.1 +/- 2.6 μM) (Su and Yu, 2007; Reens et al., 2018). The chemical structures of the three compounds have some resemblance to known efflux pump inhibitors (**Figure 3-3**). EPM30 is a small compound with an aminothiazole core, and several aminothiazole compounds have been identified that inhibit efflux (Costa et al., 2016; Nakayama et al., 2003). EPM35 is a trifluoro-pyrimidine linked to a piperidine. A very similar compound was suggested to bind the AcrB substrate-binding pocket in an *in silico* screen (Velmurugan, 2015). EPM43 is a small quinazoline, a planar moiety which is a common drug pharmacophore. Other quinazolines have been identified as inhibitors of bacterial and fungal efflux pumps (Chevalier et al., 2010; Lemoine et al., 2004). EPM43 itself has been identified as an inhibitor of fungal dihydrofolate reductase (DHFR), but is not known to inhibit bacterial or human DHFR (Chan et al., 1995; Whitlow et al., 2001). Where on the AcrB protein the EPMs bind remains unknown. EPM35 and EPM43 potentiate multiple AcrB substrates, suggesting they bind in the hydrophobic trap (Sjuts et al., 2016). Alternatively, the EPMs may bind outside of the substrate pocket and, for instance, disrupt AcrB folding, localization or interactions with AcrA. It is notable that the three EPMs do not behave identically in broth assays that monitor export of AcrB substrates, potentiation of antibiotics, or activity against other Gram-negative pathogens, emphasizing that they may not interact identically with AcrB and/or any other molecules they may target.

Why the three EPMs are more potent as antibacterials in mammalian cells than they are as efflux pump inhibitors in broth is not completely clear. A simple model supported by existing data is that the EPMs increase bacterial sensitivity to host AMPs by binding efflux pump subunits, thereby reducing AMP export (Shafer et al., 1998) and decreasing the effective concentration of AMPs. During infection of a whole animal, endogenous AMPs, which are ubiquitous in body fluids, may synergize with EPMs, even in severely immunocompromised

patients for whom innate immunity typically remains intact (Lin et al., 2015; Sakoulas et al., 2017). While *Salmonella* RND efflux pumps have not been demonstrated to export AMPs, it is nevertheless encouraging that two of the EPMs inhibit efflux in other major MDR bacterial pathogens, suggesting they may have utility beyond *Salmonella*. Another possible explanation for higher potency during infection than in broth is that the EPMs could accumulate in the SCV, thereby increasing the concentration of compound experienced by the bacterium within host cells. An EPM could also target the host cell and, for instance, increase production of antimicrobial mediators. Alternatively, or in addition, EPMs may interfere with other bacterial processes and/or bind targets that are not present or accessible under the broth conditions tested. To facilitate our understanding of how the EPMs function, it may be useful to identify more potent, less toxic chemical derivatives. Desirable derivatives would have efficacy in SAFIRE, potency in efflux assays, and, most importantly, resensitize MDR pathogens to clinical antibiotics by reducing the antibiotic dosage needed to treat an infection.

I. MATERIALS AND METHODS

Bacterial strains. *Salmonella enterica* serovar Typhimurium strains were routinely grown at 37 °C with aeration in LB medium with appropriate antibiotics: 30 μg/ml streptomycin, 30 μg/ml kanamycin, 50 μg/ml ampicillin, 34 μg/ml chloramphenicol, 10 μg/ml tetracycline. Wild-type strain SL1344 (ALR#001; DET#0001) was used for validation experiments. Fluorescent strains for microscopy expressed GFP from the *sifB* promoter (AL4 #109; DET#1270) (Rollenhagen et al., 2004) or from the *rpsM* promoter (AL4#218; DET#0222) (Vazquez-Torres et al., 1999). For flow cytometry, wild-type *Salmonella* were transformed with a plasmid encoding blue fluorescent protein (BFP) driven by the *rpsM* promoter (AL4#234; DET#1271) (McQuate et al., 2017). The *acrAB*::*kan* (ALR#411; DET#1257), *macAB*::*kan* (ALR#400; DET#1258), and *tolC*::*cm* (AL4#401; DET#1269) strains were constructed as described (Kim et al., 2014). Strain

S10801 (ALR#393; DET#1248) was obtained through BEI Resources, NIAID, NIH: *Salmonella enterica* subsp. *enterica* Strain S10801 (Serovar Typhimurium), NR-22067. S10801 is a multidrug resistant isolate and was grown in 30 μg/ml streptomycin, 50 μg/ml ampicillin, 10 μg/ml tetraycycline; this strain was originally isolated from a calf with sepsis (Daniels et al., 2009). *E. coli* strain RAM121 (ALR#522; DET#1258) was a gift from R. Misra (Misra and Benson, 1988).

Cell culture. Murine macrophage-like RAW 264.7 and HeLa human epithelial cells were grown in DMEM high glucose (Sigma) supplemented with 10% fetal bovine serum, 2 mM L-glutamine, 1 mM sodium pyruvate, 10 mM HEPES, and 50 μM β-mercaptoethanol. All cell lines were maintained in a 5% CO_2 humidified atmosphere at 37 °C. Assays were performed with cultures between passages 4 and 20.

Bacterial infections for SAFIRE and CFU plating. For microscopy experiments 5 x 10^4 macrophages in 100 μL were seeded in 96-well black-walled, glass-bottomed plates (Brooks Automation). Twenty-four hours post-seeding, bacteria in 20 or 50 μL PBS were added to a final concentration of 1 x 10^7 cfu / mL; we determined that these conditions resulted in infection of approximately 70% of macrophages at 18 hours post-infection with minimal macrophage toxicity. Forty-five minutes after bacterial addition, 50 μL gentamicin was added to a final concentration of 40 μg / mL; this concentration did not affect intracellular infection but was sufficient to inhibit replication of extracellular bacteria. At 2 hours post-infection, medium was removed and replaced with fresh medium containing 40 μg / mL gentamicin and the indicated concentrations of drugs. At 17.5 hours post-infection, PBS containing MitoTracker Red CMXRos (Life Technologies) was added to yield a final concentration of 300 nM (384-well) or 100 nM (96-well). Thirty minutes later, 16% paraformaldehyde was added to a final concentration of 1-2% and incubated at room temperature for 15 minutes. Wells were washed twice with PBS and

stained for 20 minutes with 1 μM DAPI; wells were washed twice and stored in 90% glycerol in PBS until imaging.

Infections of HeLa cells with *Salmonella* were performed as above in 96-well plates, except 1 x 10^4 cells were seeded, cells were infected with *Salmonella* constitutively expressing GFP from the *rpsM* locus because *sifB* is poorly expressed in HeLa cells, and plates were spun for 5 minutes at 500 x *g* after addition of bacteria to enhance infection.

Infections to determine *Salmonella* CFUs were performed as described above, except cells were seeded in 96-well tissue culture coated plates (Greiner). At 18 hours post-infection, wells were washed three times in PBS, lysed with 30 μL 0.1% Triton X-100, diluted and plated to determine colony-forming units.

Image acquisition and MATLAB®-based microscopy analysis. High magnification images were acquired on an Olympus IX81 inverted widefield microscope. For screening imaging, three-color images were acquired at 10X or 20X on a Cellomics ArrayScan VTI (Thermo) and exported to DIB files. At least two fields were imaged per well for all experiments. We developed an automated MATLAB® script to quantify intracellular bacterial load; scripting packages have been deposited on MATLAB® File Exchange (https://www.mathworks.com/matlabcentral/fileexchange/), deposited as “SAFIRE_ArrayScan” and “SAFIRE_OlympusIX81.” Briefly, the algorithm identifies macrophage borders via watershed segmentation using DAPI and MitoTracker signal. In order to identify bacteria, the user supplies an empirically determined GFP threshold that maximizes signal to noise based on uninfected and untreated controls. Within each macrophage, the number of pixels above the GFP threshold is counted. If more than 2 pixels are above the GFP threshold, the macrophage is labeled infected. The script calculates the percentage of macrophages infected in the image.

Broth antibacterial activity assays. Overnight *Salmonella* cultures were washed three times in PBS and diluted to an OD_{600} of 0.01 in MHB in 96-well flat-bottom plates. Compound was added using a pin tool (CyBio) or manually, yielding a final concentration of no more than

1% DMSO. Plates were grown at 37°C shaking and OD_{600} was monitored using a BioTek Eon or Synergy H1 incubator shaker microplate absorbance reader. For experiments with polymyxin B, bacteria were grown in M9 minimal medium supplemented with 100 mM Tris pH 7.4, 0.35% glycerol, 0.002% histidine, 10 mM $MgCl_2$, and 0.1% casamino acids and 5 μg/mL polymyxin B. For experiments with LL37, bacteria were grown in M9 minimal medium supplemented with 0.4% dextrose, 0.004% histidine, 1 mM $MgSO_4$, and 5 μg/ml LL37.

Hoechst accumulation assays. Hoechst accumulation assays were performed essentially as described (Coldham et al., 2010). Briefly, overnight *Salmonella* cultures were washed three times in PBS and diluted to an OD_{600} of 0.1 in PBS with 2.5 μM Hoechst 33342 in the presence of the indicated concentrations of compounds. Fluorescence was monitored on a Biotek Synergy 2 with a 360/40 nm excitation filter and 460/40 nm emission filter. The maximum Hoechst fluorescence over 60 minutes of incubation was normalized to the signal from the equivalent number of heat-killed bacteria, after subtraction of autofluorescence signal determined from compound incubated in the absence of bacteria. EC50s were determined using a 4-parameter nonlinear fit constrained using DMSO-treated Wild-Type as the minimum and Heat Killed as the maximum (GraphPad Prism). Concentrations of PAβN used in all assays were determined by titration with the *Salmonella* wild-type strain in the corresponding assay.

Nile Red efflux assays. Nile red assays were adapted from an established protocol (Bohnert et al., 2010). Briefly, overnight *Salmonella* LB cultures were washed in PBS with 1 mM $MgCl_2$ and resuspended at an OD_{600} of 2.0. Cells were incubated in 10 μM Nile red for three hours at 37°C in glass tubes on a roller drum and then at room temperature standing for one hour. Cells were pelleted at 2,050 x *g*, resuspended in PBS with 1 mM $MgCl_2$, and 200 μl was added to 96-well black walled plates (Greiner) with compound at the indicated concentrations. In washout experiments, after 35 minutes of incubation with compound, cells were centrifuged at 16,000 x *g*, resuspended in PBS with 1mM $MgCl_2$ without compound and aliquoted into 96-well black walled plates (Greiner). During loading into plates (~ 20 minutes), bacteria effluxed some

Nile red even in the absence of glucose (**Figure 3-7**). Samples were read using a Varioskan Flash Multimode Reader at 540 nm (excitation) and 625 nm (emission) or a Biotek Synergy H1 at 560 nm and 655 nm. To activate efflux, glucose was added to a final concentration of 2 mM.

Nitrocefin efflux and permeability assays. Bacteria were subcultured to mid-log phase, washed, and combined with 100 μM nitrocefin and the indicated concentrations of drugs in 96-well plates in 200 μL (Misra et al., 2015). Washes and incubations were performed in 20 mM KPO_4, pH 7.0, 1 mM $MgCl_2$. Absorbance (486 nm) was measured on a BioTek Eon or Synergy H1 spectrophotometer every 60 seconds for one hour. To observe efflux inhibition, *E. coli* RAM121 (Misra and Benson, 1988) were added to plates at a final OD_{600} of 10. This strain produces an OmpC variant with a larger pore size to allow increased influx of nitrocefin and other bulky molecules, and nitrocefin is hydrolyzed by the endogenous AmpC beta-lactamase. To measure outer membrane permeability, wild-type *Salmonella* harboring beta-lactamase *(bla)*-expressing pACYC177-mTagBFP2 (McQuate et al., 2017) were added to plates at a final OD_{600} of 0.1.

Tetramyethylrhodamine methyl ester (TMRM) potential assays. Wild-type *Salmonella* harboring pACYC177-mTagBFP2 (McQuate et al., 2017) were subcultured to mid-log phase, diluted to 1 x 10^6 CFU/ml in PBS, aliquoted into flow cytometry tubes, and treated with the indicated concentrations of compounds. TMRM was immediately added to a final concentration of 100 nM. After incubation for 30 minutes at 37°C, samples were analyzed on a CyAn ADP (Beckman Coulter) in channels FL6 and FL2. Data were analyzed using FlowJo; bacteria were gated based on side scatter and BFP signal in the FL6 channel, and the FL2 median fluorescence intensity (MFI) was calculated.

Bacterial swimming membrane potential assays. Saturated overnight cultures were diluted to an OD_{600} of 0.01 in LB, and 1 μL was injected into the center of low (0.25%) agar LB plates. Ten microliters of the indicated compounds up to concentrations of 100 mM were added to sterilized Whatman paper disks (diameter 0.7 cm) placed equidistant from the plate center;

solubility issues arose at concentrations above 100 mM. Plates were incubated face up at 37 °C overnight; no change in halo size was observed between 14–24 hours incubation. Plates were imaged using a Gel Logic 200 imaging system, and halo radius (distance from center of disk to outermost edge of halo) was measured using ImageJ.

Real-time reverse transcription PCR. Infections were performed as described above, except that 8 x 10^4 RAW 264.7 macrophages were seeded in 6-well dishes and volumes were scaled for the larger culture volume. At indicated timepoints, wells were washed twice with PBS and RNA was extracted using the RNeasy mini kit (Qiagen) including Qiashredder homogenization and on-column DNase treatment. RNA yields ranged from 5-40 ng. First-strand cDNA was synthesized from 250 ng of total RNA using the iScript cDNA synthesis kit (BioRad) and diluted 10-fold. Quantitative PCR (qPCR) for the indicated genes was performed using the following primers: *Hprt* (GCGTTGGGCTTACCTCACT, ATCGCTAATCACGACGCTGG); *Sert* (TTGGATAGTACGTTCGCAGGC, ACCACGATGAGCACAAACCA); *Camp* (CAGCTGTAACGAGCCTGGTG, CACCTTTGCGGAGAAGTCCA). *Hprt* was selected as the reference gene based on validation experiments. The qPCR reactions were performed in technical duplicates and contained 8 µL diluted cDNA, 200 nM of each primer, and 10 µL 2X Power SYBR Green (Applied Biosystems) in 20 µL total volume. Reactions were run on an Eppendorf Realplex^2 MasterCycler with the following cycling conditions: 10 minutes at 95 °C, then 40 cycles at 95 °C for 15 sceondary and 60 °C for 60 seconds. Melting curve analysis of the PCR reaction showed a single amplicon for each target. No-template and no-reverse-transcriptase controls showed no product. Amplification results were baseline corrected, followed by manual determination of the threshold for each gene. The resulting C_T values were analyzed as follows: *(i)* The mean C_T of qPCR technical duplicates was determined for each sample. *(ii) Slc6a4* and *Camp* expression for each sample was normalized to that of *Hprt*, resulting in the ΔC_T. *(iii)* Each sample was normalized to the mean of the uninfected samples for that experiment, resulting in the $\Delta\Delta C_T$ for that sample. *(iv)* The mean of sample replicates from

the same experiment was calculated. *(v)* Fold expression and error were calculated using the $2^{-\Delta\Delta CT}$ equation.

Mouse infections. Bacteria were grown overnight in LB, then diluted in PBS. Seven week old C57/Bl6 female mice were intraperitoneally injected with 1 x 10^4 *Salmonella* in 100 µL. Thirty minutes later, mice received two intraperitoneal injections: 25 mg/kg tetracycline in 150 µL PBS or PBS alone, and 50 mg/kg EPM35 in 100 µL DMSO or DMSO alone. Drug injections were repeated at 24 hours post-infection. At 30 hours post-infection, mice were humanely euthanized using carbon dioxide asphyxiation followed by cervical dislocation. Spleens and livers were harvested, homogenized, diluted in PBS, and plated to enumerate *Salmonella* CFUs.

CHAPTER 4. CLOMIPRAMINE AND RELATED ANTIDEPRESSANTS TARGET *SALMONELLA* WITHIN CULTURED MACROPHAGES

A. INTRODUCTION

Increases in antibiotic resistant infections demonstrate the need for novel antimicrobials, but recent efforts to identify and develop novel therapies have been unsuccessful (Fischbach and Walsh, 2009; Lipinski, 2000; Payne et al., 2007). A key limitation in drug development is optimization of pharmacokinetic and toxicity profiles of novel compounds. To bypass this bottleneck and accelerate entry of novel antimicrobials into clinical use, several groups have suggested repurposing existing FDA-approved drugs as antibacterials (Ashburn and Thor, 2004; Law et al., 2013). Clinical drugs typically have already been well-characterized and the structure-activity relationship defining bioavailbility and toxicity is known. Thus, any drugs with antibacterial activity could be fast-tracked into clinical use as an antibiotic. Recent studies have investigated repurposing FDA-approved small molecules as therapies against Ebola virus, *Borrelia burgdoferi*, *Coxiella burnetti*, *Legionella pneumophila*, and *Yersinia pestis* (Andersson et al., 2016; Czyz et al., 2014; Feng et al., 2014; Kouznetsova et al., 2014; Zumla et al., 2015). These studies demonstrate that some compounds can reduce pathogen load or toxicity by modulating their canonical host target, as diverse host processes are involved in infection. In this situation, the drug may be immediately ready for use in treating infections. Alternatively, some compounds may reduce infection by disrupting a new target. In this case, a drug may require additional optimization to improve activity against this secondary target while reducing activity against the canonical target; however, such efforts would be greatly accelerated by previous studies on analogs of the clinical compound.

We previously carried out a high-throughput cell-based screen for antimicrobials that reduce *Salmonella* infection of macrophages (**Chapter 2**). Jessy Podoll cataloged known substances within the screening library using the Chemical Structure Lookup Service from the CADD Group Chemoinformatics Tools and User Services (Nicklaus and Sitzmann, 2016) (**Table**

2-2). One hit compound was clomipramine (CMP), a tricyclic antidepressant clinically used to treat depression, obsessive compulsive disorder, and chronic pain (Dell'Osso et al., 2006). CMP preferentially inhibits the serotonin reuptake transporter SERT but also inhibits the norepinephrine transporter NET (Takano et al., 2011). CMP was the most potent hit from our screen. Thus, I aimed to define the antibacterial activity and mechanism of action of CMP, in order to evaluate the feasibility of repurposing CMP as an antibacterial. My experiments indicate that CMP does not exert its antibacterial effect through its canonical target SERT, and it remains unclear how CMP leads to bacterial clearance within macrophages. Currently the data suggest that CMP may modulate host autophagy, but further work is required to test this possibility. However, CMP does not show activity against *Salmonella in vivo*, so it is not a likely candidate for repurposing.

B. CLOMIPRAMINE ACTIVITY IS INDEPENDENT OF SEROTONIN REUPTAKE

Previous work identified clomipramine as a potent inhibitor of intracellular *Salmonella* infection (**Chapter 2**). Treatment of infected macrophages with 20-25 μM CMP led to significant reductions in bacteria by SAFIRE and by CFU plating (**Figure 4-1**). CMP canonically inhibits mammalian SERT, which takes up extracellular serotonin to halt signaling through serotonin receptors. The role of serotonin signaling and SERT in macrophages during infection is unclear: SERT is induced during the immune response (Malubay, 2008; Rudd et al., 2005), and serotonin signaling may alter macrophage activation state during infection and inflammation (de las Casas-Engel et al., 2013; Ghia et al., 2009; Li et al., 2011; Maneglier et al., 2008). Thus, CMP's antibacterial activity could be mediated by inhibition of SERT and subsequent alterations in macrophage serotonin signaling. To test this hypothesis, I first investigated the requirement for extracellular serotonin for clomipramine activity. Macrophages do not synthesize serotonin, but it is typically present in serum added to cell culture media. I cultured macrophages in the absence of serum for 24 hours to eliminate extracellular serotonin; this protocol has been used

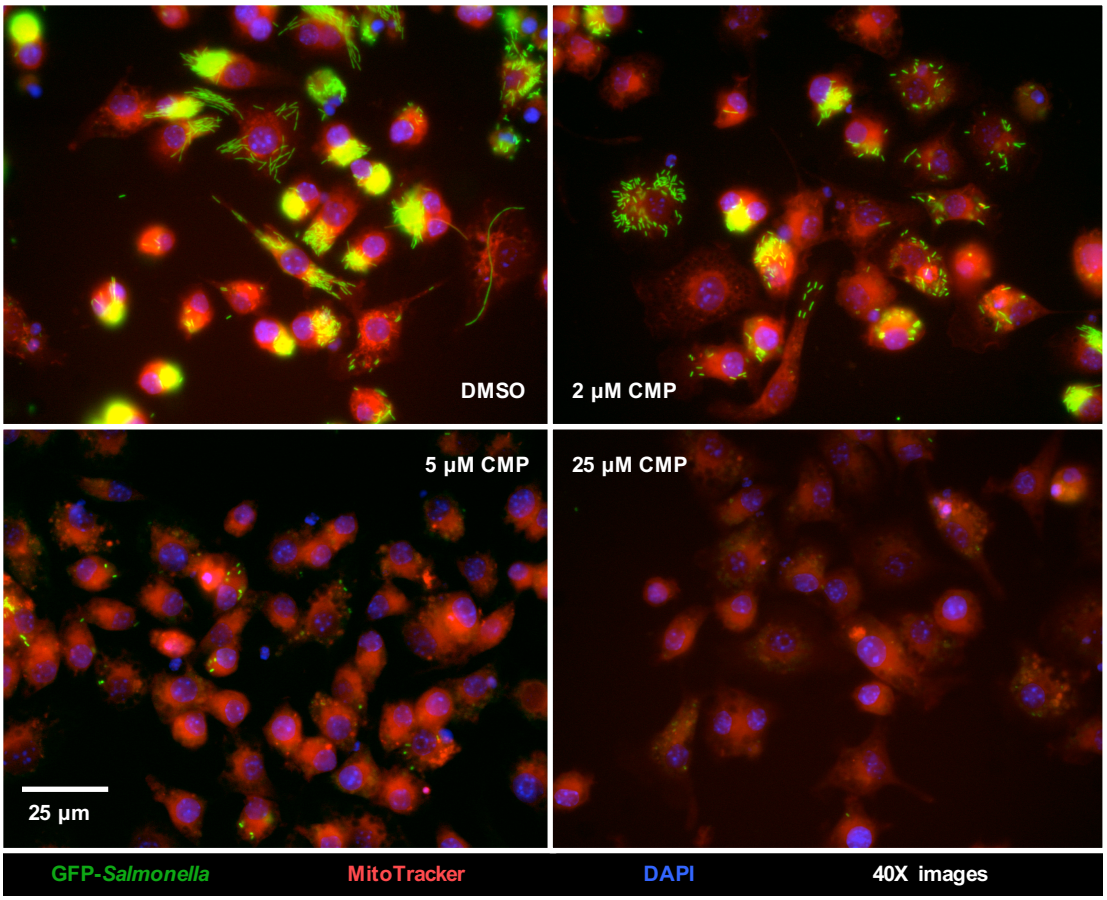

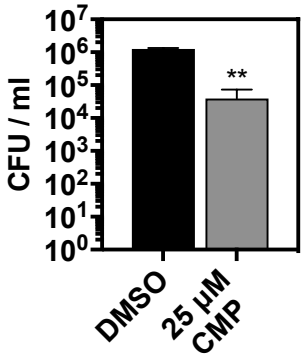

Figure 4-1. Clomipramine reduces bacterial load in macrophages. RAW 264.7 macrophages were infected in 96-well plates as described in Chapter 2 and treated with the indicated concentrations of CMP from 2-18 hours, then processed and imaged at 40X, or lysed and plated for CFU. Data are representative of 2 independent biological replicates. ** $p < 0.01$ by t test.

by others to study serotonin signaling (de las Casas-Engel et al., 2013). I then infected macrophages and treated with CMP as previously described. Removal of serum did not affect CMP activity, nor did supplementation of serum-free medium with serotonin during infection (**Figure 4-2A**). Additionally, removal of serum only modestly affected infection, indicating serotonin or other serum components have minimal impact on infection (**Figure 4-2B**). These data suggest that serotonin signaling is not required for CMP antibacterial activity.

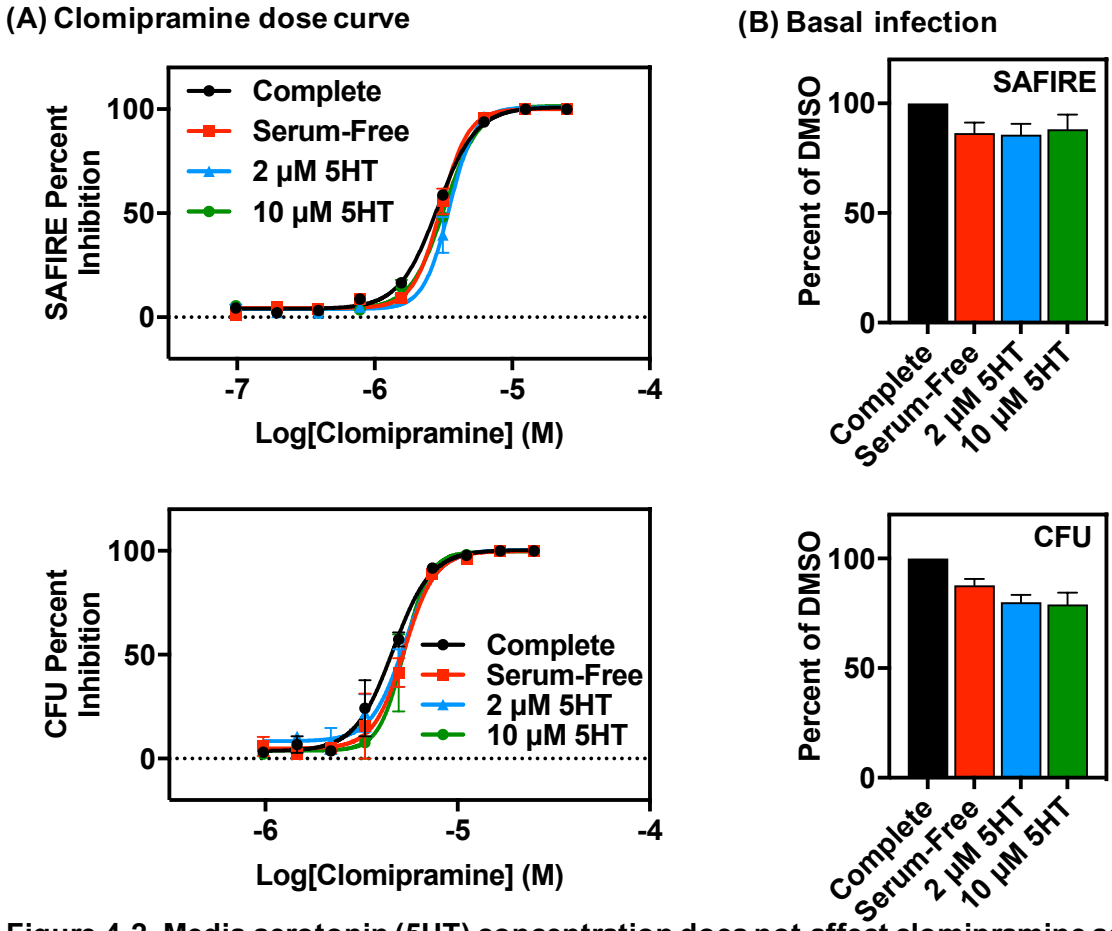

Figure 4-2. Media serotonin (5HT) concentration does not affect clomipramine activity. Beginning 24 hours prior to infection, macrophage were incubated in serum-free medium. Macrophages were infected and treated with different concentrations of clomipramine from 2-18 h.p.i. Beginning at 2 h.p.i., macrophages were incubated in complete medium containing serum, serum-free medium, or serum-free medium supplemented with the indicated concentrations of serotonin (5HT). At 18 h.p.i. macrophages were processed for SAFIRE and CFU as described previously. Right: infection of cells for each media condition not treated with clomipramine. Data shown are mean + SEM of three independent biological replicates.

Next, I tested whether SERT is required for CMP antibacterial activity. I constructed macrophage lines stably expressing shRNAs targeting SERT. I observed no difference in the activity of CMP in the *sert* knockdown cell lines compared to cells expressing a control shRNA (**Figure 4-3A**). Further, there was no difference in infection between macrophages treated with control and *sert* shRNAs, indicating SERT does not contribute to infection (**Figure 4-3B**). qPCR analysis of LPS-stimulated macrophages confirmed knockdown of *sert* mRNA (**Figure 4-3C**).

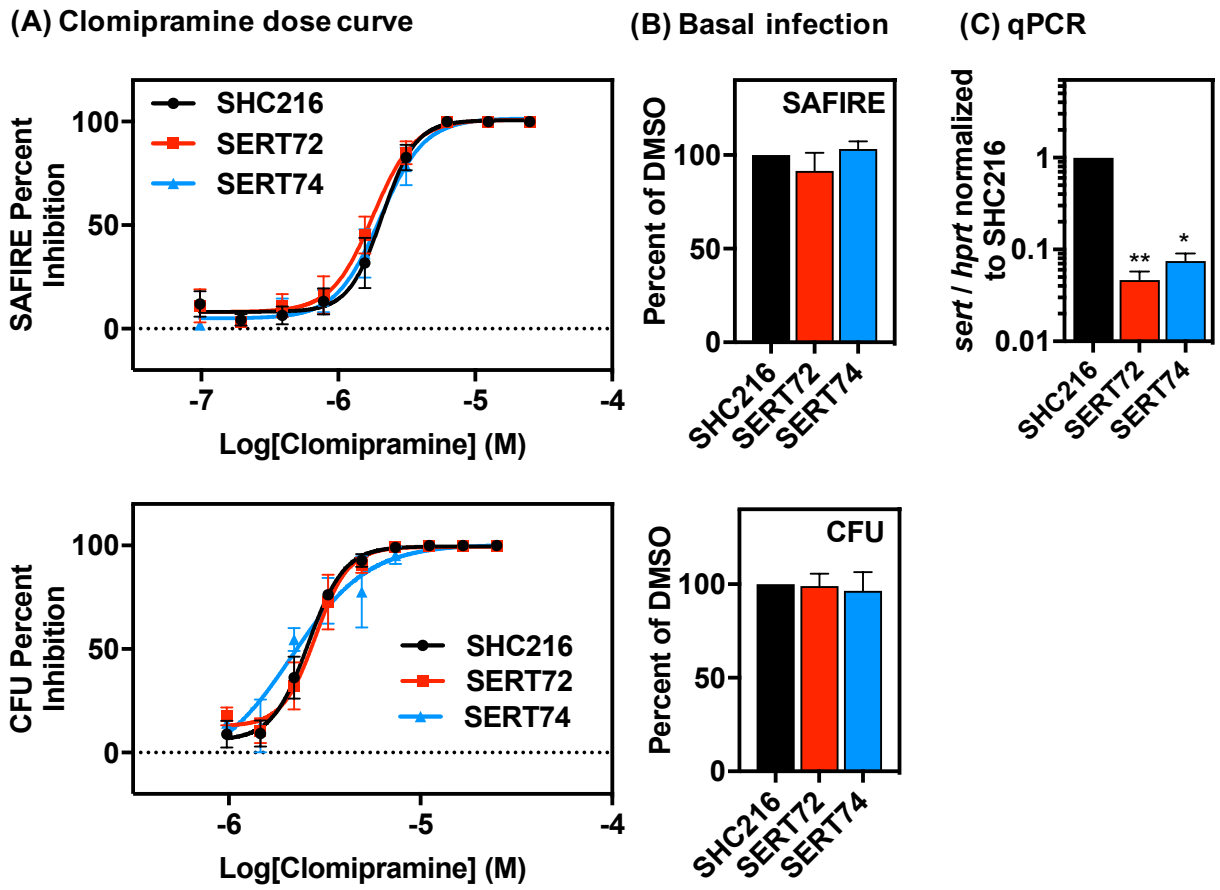

Figure 4-3. The serotonin reuptake transporter (SERT) is not required for clomipramine activity. RAW 264.7 stably expressing shRNAs targeting SERT (SERT72, SERT74) or a control shRNA (SHC216) were infected and treated with different concentrations of clomipramine from 2-18 h.p.i. At 18 h.p.i. macrophages were processed for SAFIRE and CFU as described previously. Center: infection of cells for each media condition not treated with clomipramine. Data shown are mean + SEM of three independent biological replicates. Right: quantitative reverse-transcription PCR of *sert* expression in shRNA-expressing cell lines treated with 20 ng/ml LPS for 18 hours. Data shown are mean + SD of duplicate samples from one experiment. * $p < 0.05$; ** $p < 0.01$ by one-sample t test.

C. RELATED COMPOUNDS ARE HIGHLY ACTIVE AGAINST INTRACELLULAR *SALMONELLA*

CMP belongs to the class of tricyclic antidepressants (TCAs), which typically target SERT and/or the norepinephrine transporter NET (British Medical Association et al., 2006; Takano et al., 2011). I next asked whether other commercially available TCAs are also able to inhibit intracellular *Salmonella* infection (**Figure 4-4**). Imipramine (IMP) is the original parent molecule

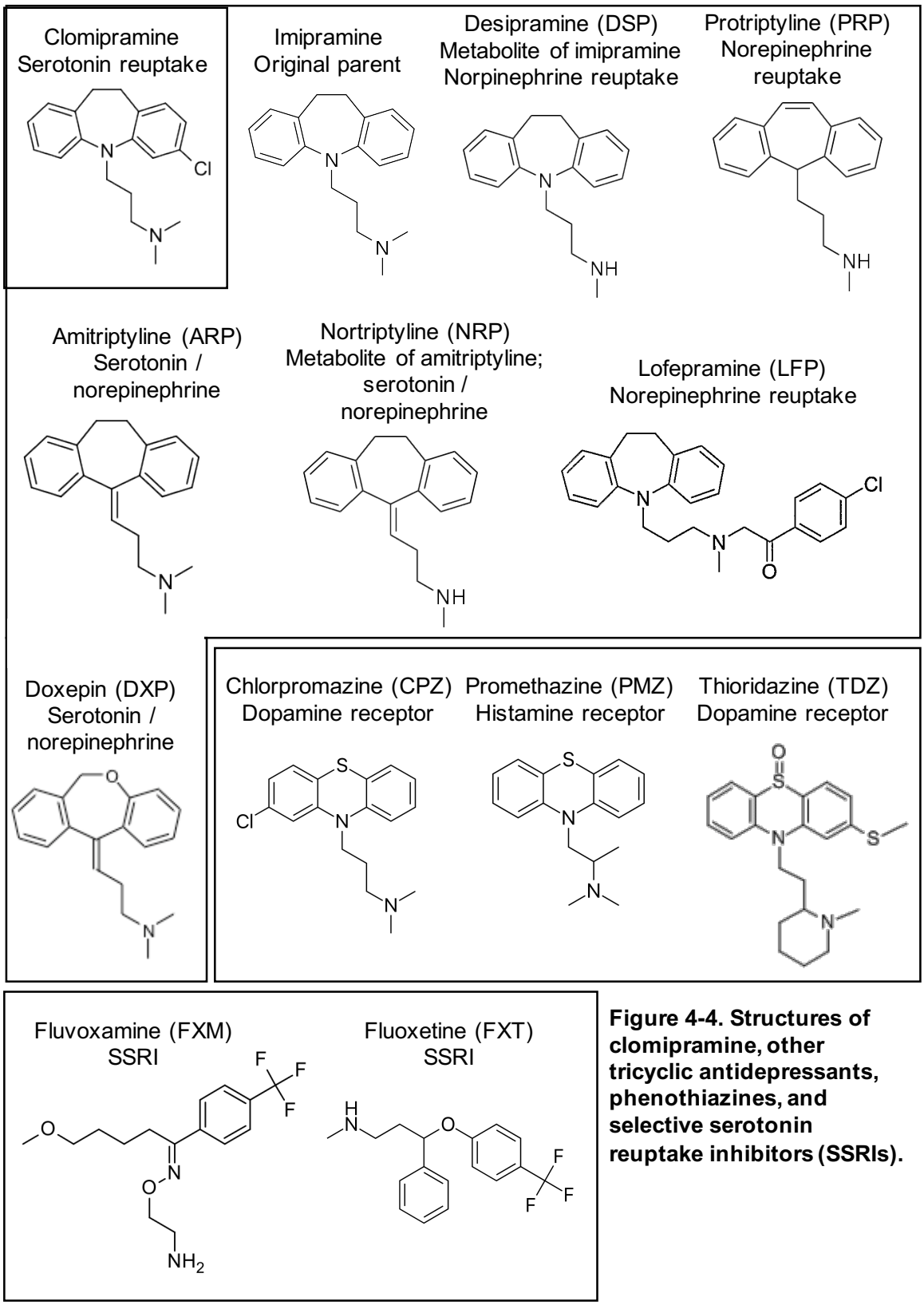

Figure 4-4. Structures of clomipramine, other tricyclic antidepressants, phenothiazines, and selective serotonin reuptake inhibitors (SSRIs).

of CMP and similarly targets SERT. IMP is metabolized *in vivo* into desipramine (DSP), which primarily targets NET. The TCAs protriptyline (PRP) and lofepramine (LFP) also preferentially inhibit NET. Several TCAs target both SERT and NET: doxepin (DXP) and the highly similar amitriptyline (ARP) as well as ARP's metabolite nortriptyline (NRP). I tested a range of concentrations for each drug using SAFIRE and CFU plating (**Figure 4-5**). Regardless of whether the drug canonically targets SERT or NET, all the TCAs demonstrated similar inhibition of intracellular *Salmonella*, with IC_{50}s in the single-digit micromolar range.

TCAs are highly related to another class of neuromodulatory drugs called phenothiazines, which contain a tricyclic structure with a functionalized side chain similar to that of the TCAs. Phenothiazines target a variety of neurotransmitter receptors including dopamine, histamine, muscarinic, and adrenergic receptors. Several phenothiazines have been shown to have antibacterial activity (AMARAL et al., 1992; Ordway et al., 2003). I next tested the activity of chlorpromazine (CPZ), promethazine (PMZ), and thioridazine (TDZ) against intracellular *Salmonella*. As was observed for the TCAs, all three phenothiazines displayed highly potent activity by SAFIRE and CFU plating (**Figure 4-5**).

The original hit CMP targets SERT, but does have activity against other neurotransmitter receptors. Many of the TCAs and phenothiazines have activity against multiple targets, one of which could mediate the antibacterial activity of these drugs. I next tested the antibacterial activity of two selective serotonin reuptake inhibitors (SSRIs)—fluvoxamine (FXM) and fluoxetine (FXT). These molecules are structurally distinct from TCAs and phenothiazines, and are highly specific for SERT. Both SSRIs exhibited potent inhibition of intracellular *Salmonella* (**Figure 4-5**). As a comparison, I also determined the activity of rifampicin, a known antibiotic, against intracellular *Salmonella*. By SAFIRE and CFU, rifampicin was more potent than CMP and related compounds.

It is unclear why this collection of antidepressants display similar activity against intracellular bacteria, given they canonically target different neurotransmitter transporters and

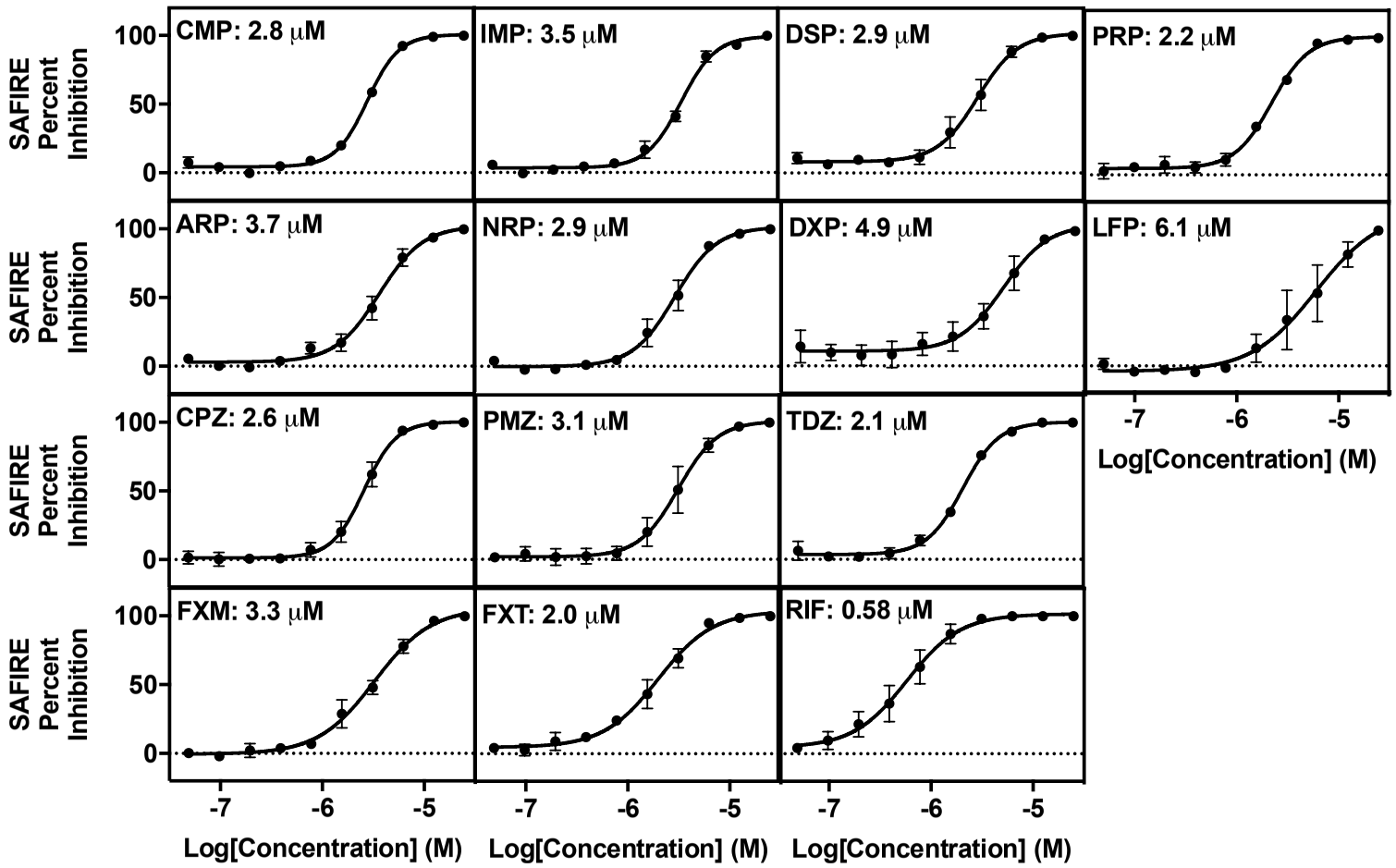

Figure 4-5. TCAs, phenothiazines, and SSRIs have similar potencies against intracellular *Salmonella*. Infected macrophages were treated with drug from 2-18 h.p.i. and processed for SAFIRE and flow cytometry as described previously. Data are mean + SEM of three independent biological replicates, and nonlinear fits. IC50 values are given for each compound. SAFIRE data are on this page; CFU data are on the following page.

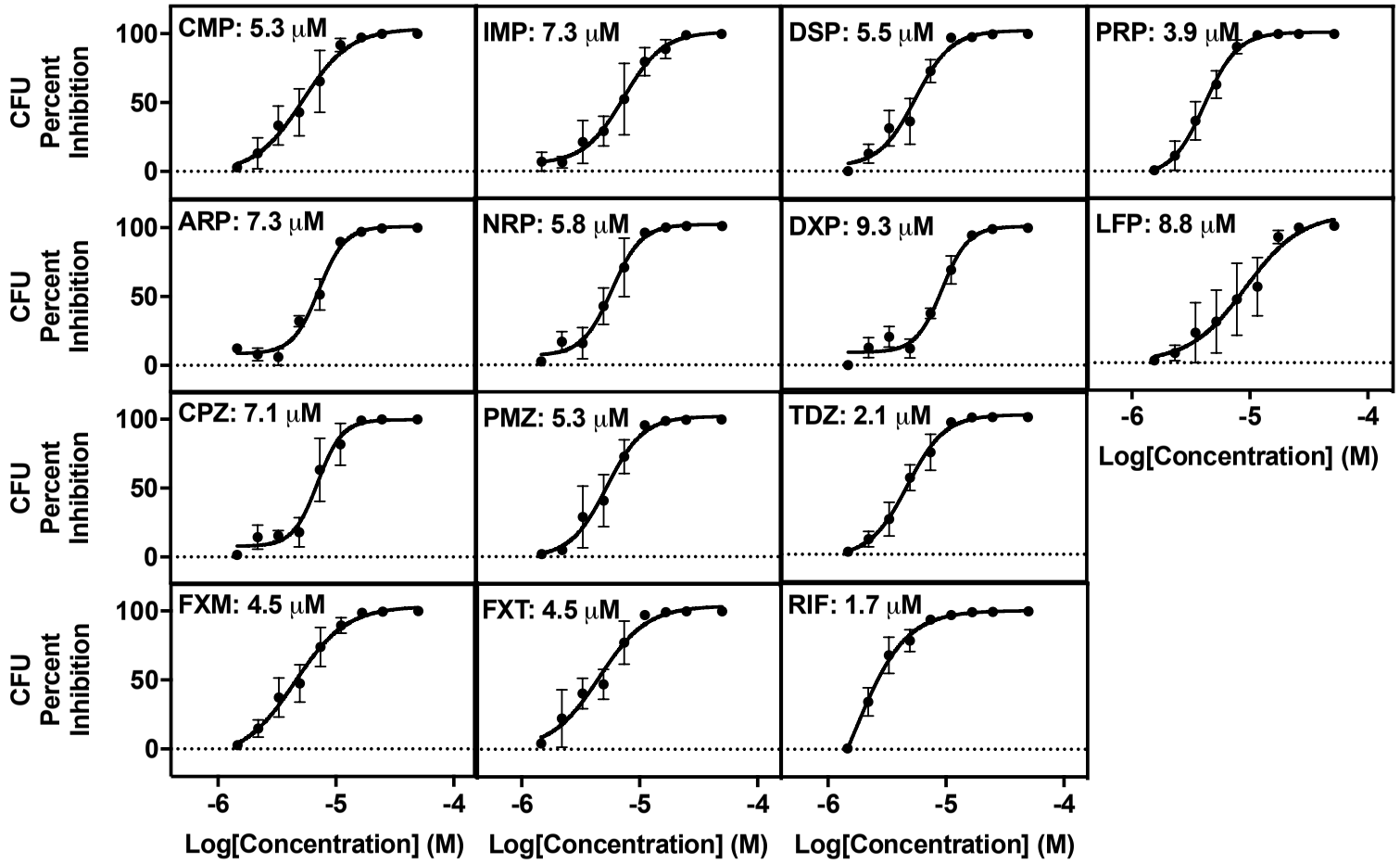

Figure 4-5 (continued). TCAs, phenothiazines, and SSRIs have similar potencies against intracellular *Salmonella*. Infected macrophages were treated with drug from 2-18 h.p.i. and processed for SAFIRE and flow cytometry as described previously. Data are mean + SEM of three independent biological replicates, and nonlinear fits. IC50 values are given for each compound. CFU data are on this page; SAFIRE data are on the preceding page.

comprise different structural classes. One possibility is that all of the canonical targets of these drugs play a role in *Salmonella* infection of macrophages, although this seems unlikely given that only certain transporters are expressed in macrophages. Alternatively, structurally similar compounds (TCAs and phenothiazines) could share secondary targets that lead to their antibacterial activity. Why then do the SSRIs, which are structurally distinct, display similar antibacterial activity? One explanation is that the secondary target(s) contains a similar drug-binding surface to that present in the canonical targets of these drugs; this is plausible as all of the drugs target membrane transporters, which are ancient backbones present in many organisms. Thus, further defining of the antibacterial targets of this collection of drugs is needed to fully understand the similarities and differences between their antibacterial activities.

D. CLOMIPRAMINE AND RELATED COMPOUNDS ARE POORLY ACTIVE AGAINST *SALMONELLA* GROWN IN BROTH

I next explored whether the compounds directly target *Salmonella*. Traditional antibiotics target bacterial processes required for growth such as DNA replication, transcription, translation, or cell wall production. I first examined whether CMP inhibits *Salmonella* growth in broth. I found that high concentrations of CMP (>500 μM) were required to completely inhibit growth in MHB, and the IC50 was in the hundreds of micromolars (**Figure 4-6**). In comparison, I had observed potent inhibition of infection at 20-25 μM and IC50s in the single-digit micromolar for CMP against intracellular *Salmonella*. Next, I tested the activity of the TCAs, phenothiazines, and SSRIs against *Salmonella* grown in broth. Similar to CMP, all the related compounds demonstrated poor inhibition of *Salmonella* growth.

E. ONLY CLOMIPRAMINE, THIORIDAZINE, AND CHLORPROMAZINE INHIBIT BACTERIAL EFFLUX

CMP, TDZ, and CPZ have been suggested to inhibit bacterial efflux which could contribute to clearance within macrophages (AMARAL et al., 1992; Gunics et al., 2000; Rodrigues et al.,

2008). I tested the ability of these three and the other compounds to increase *Salmonella* accumulation of Hoechst 33342, a fluorescent dye which is exported by efflux pumps (Coldham et al., 2010). Live bacteria are able to efflux the dye, and exhibit low fluorescence, but heat-killed bacteria exhibit high fluorescence. I measured the Hoechst accumulation over 1 hour of incubation with a range of compound, and normalized the maximum fluorescence to that of DMSO-treated (0% Hoechst signal) or heat-killed bacteria (100% Hoechst signal). The known efflux pump inhibitor phe-arg β-napthylamide (PAβN) significantly increased Hoechst signal, with an EC50 of 712 μM, but rifampicin, an antibiotic which targets RNA polymerase, had no activity, as expected (**Figure 4-7**). CMP, TDZ, and CPZ increased Hoechst signal, with EC50s of 997, 450, and 575 μM, respectively, indicating that these drugs modestly inhibit efflux pumps in *Salmonella*. However, the other TCAs, phenothiazines, and SSRIs demonstrated minimal Hoechst activity, with EC50s above 4 mM.

Efflux pumps can export host antimicrobials; thus, inhibition of efflux pumps within macrophages may lead to increased exposure to toxic molecules including antimicrobial peptides and reactive oxygen species (Bogomolnaya et al., 2013; Buckley et al., 2006; Nishino et al., 2006a; Piddock, 2006). I next tested whether treatment with CMP and other compounds increased *Salmonella* sensitivity to polymixin B, an antimicrobial peptide. I found that 20 μM of TDZ, the most potent antidepressant in the Hoechst assay, significantly potentiated polymixin B. CMP also increased sensitivty to polymixin B. CPZ slightly increased sensitivity. The remaining compounds, which also showed minimal activity in the Hoechst assay, did not alter polymixin B sensitivity (**Figure 4-8**). Further work is required to determine whether efflux inhibition mediates bacterial clearance by CMP, TDZ, and CPZ within macrophages. However, together these data indicate that efflux inhibition is not an ability shared among the collection of TCAs, phenothiazines, and SSRIs.

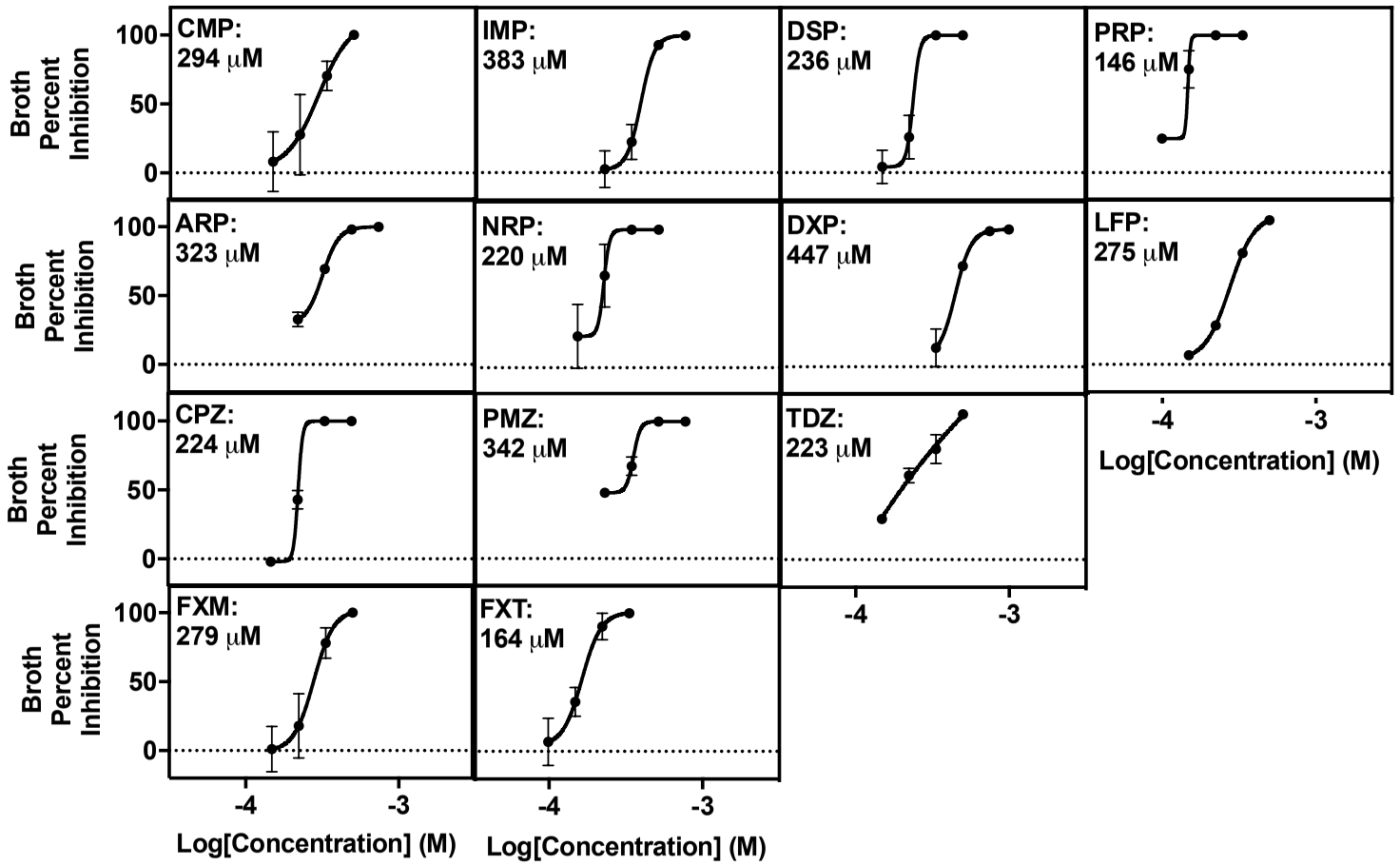

Figure 4-6. TCAs, phenothiazines, and SSRIs are inactive against Salmonella in broth. Bacteria were grown in MHB broth and treated with drug. The OD600 at 18 hours was measured and normalized to DMSO-treated wells. Data are mean + SEM of at least 2 independent biological replicates, and nonlinear fits. IC50 values are given for each compound..

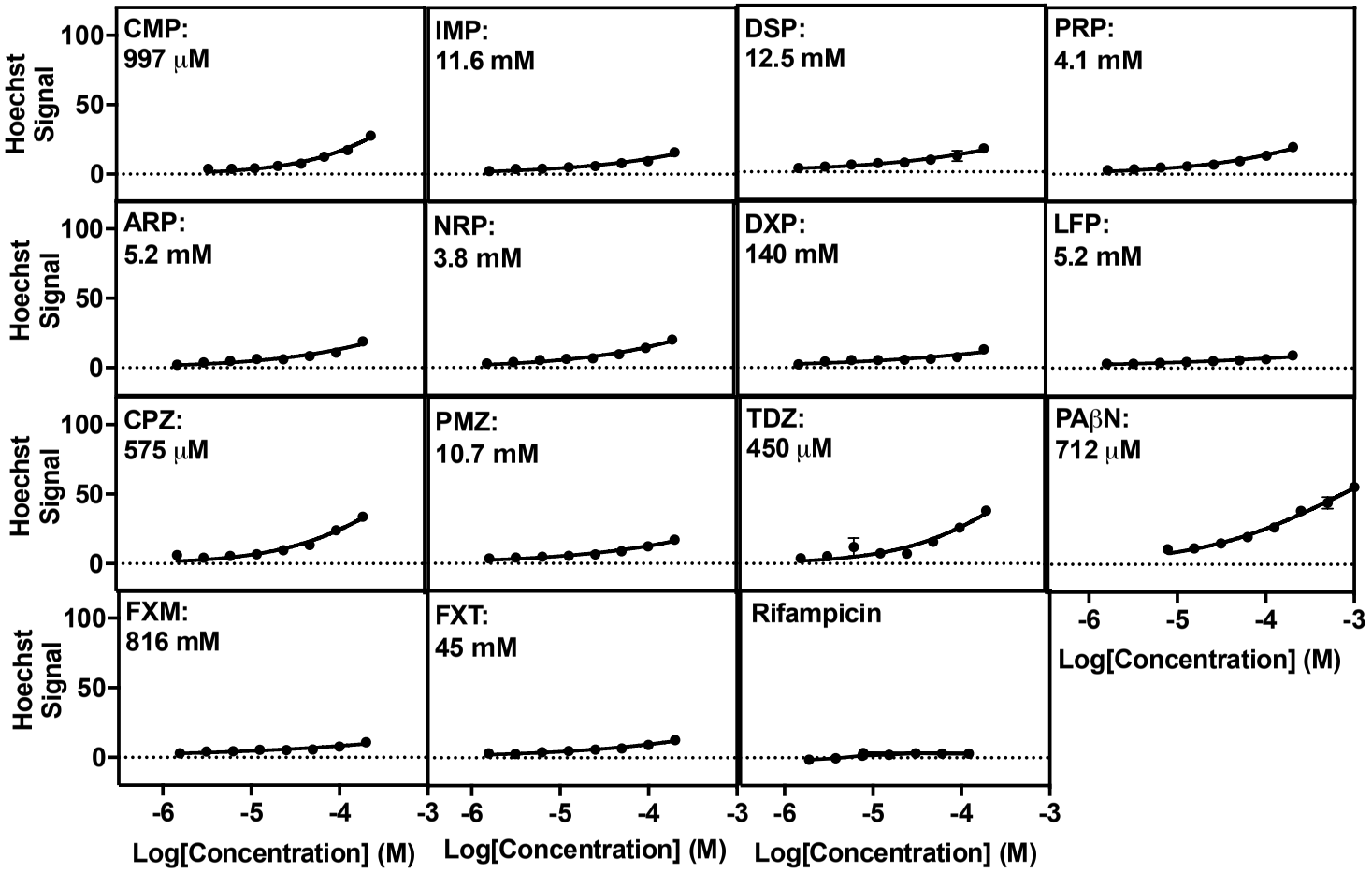

Figure 4-7. TCAs, phenothiazines, and SSRIs have inconsistent anti-efflux activity. Bacteria were incubated with 2.5 μM Hoechst 33342 and treated with drug. Intracellular accumulation of Hoechst was determined by measuring fluorescence (excitation = 354 nm; emission = 456 nm). The maximum Hoechst fluorescence over 60 minutes of incubation was normalized to vehicle-treated (0%) and heat-killed bacteria (100%). Data are mean + SEM of 2 independent biological replicates and nonlinear fits. EC50 values are given for each compound.

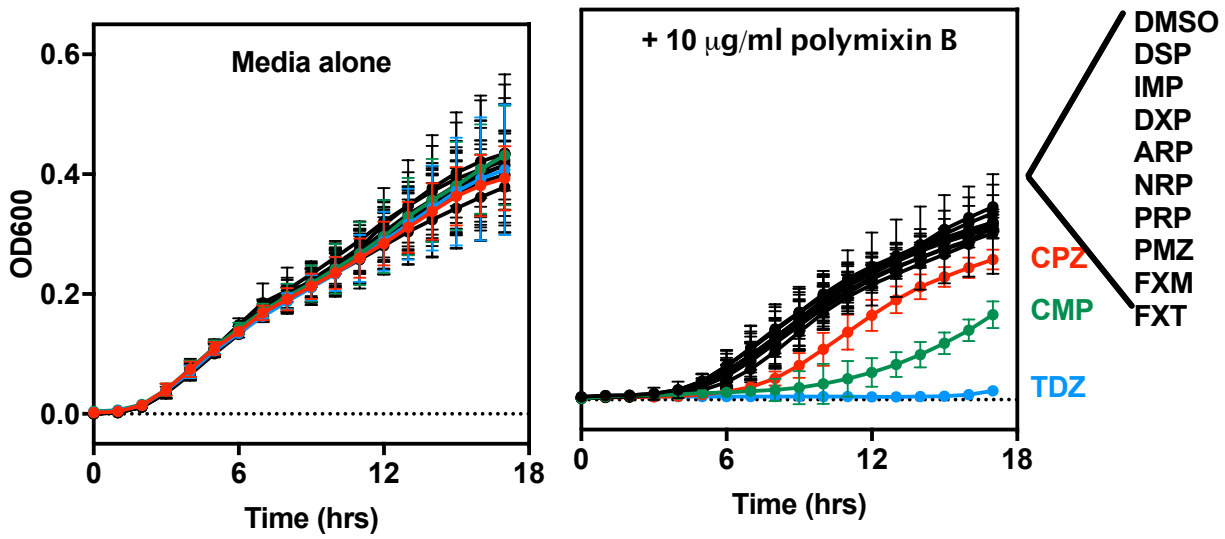

Figure 4-8. Clomipramine, thioridazine, and chlorpromazine potentiate an antimicrobial peptide. Bacteria were incubated in media (see methods) with and without polymixin B and 20 μM drugs.

F. CLOMIPRAMINE MAY ALTER MACROPHAGE PHYSIOLOGY

I next tested whether CMP targets the host cell to exert its antibacterial effect. To explore this possibility, I transiently treated macrophages and washed away drug for the remainder of the experiment. I found that pretreating macrophages with CMP prior to infection inhibited bacterial load, although with 10-fold reduced potency (**Figure 4-9**). Treating infected macrophages from 2-4 h.p.i. led to similar inhibition of bacterial load as treating from 2-18 h.p.i. These data suggest that treatment with CMP could induce long-lasting changes in the macrophage which lead to bacterial clearance.

Changes in the macrophage could be mediated by expression of additional factors such as antimicrobial effectors. I next tested whether host transcription or host translation were required for CMP activity. Infected macrophages were co-treated with CMP and either the transcription inhibitors DRB, triptolide (TPL), or the translation inhibitor cycloheximide (CHX). CMP activity was unchanged in the presence of the transcription or translation inhibitors (**Figure 4-10A**). However, treatment with DRB, TPL, and CHX did alter infection (**Figure 4-10B**), indicating that host transcription and translation alter the interaction between *Salmonella* and macrophage.

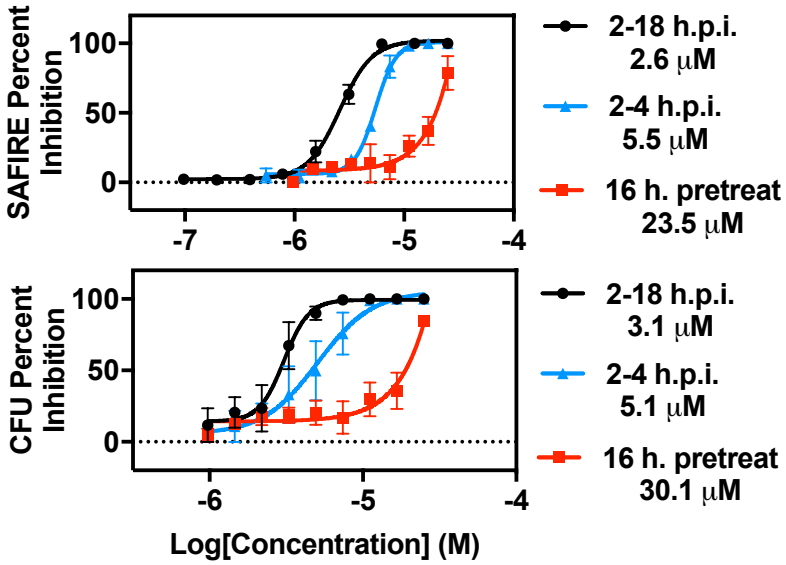

Figure 4-9. Pretreatment or transient early treatment with clomipramine inhibits *Salmonella* infection. Macrophages were infected and treated with different concentrations of clomipramine for the indicated durations. At 18 h.p.i. macrophages were processed for SAFIRE and CFU as described previously. IC50s values for each condition are given. Data shown are mean + SEM of three independent biological replicates.

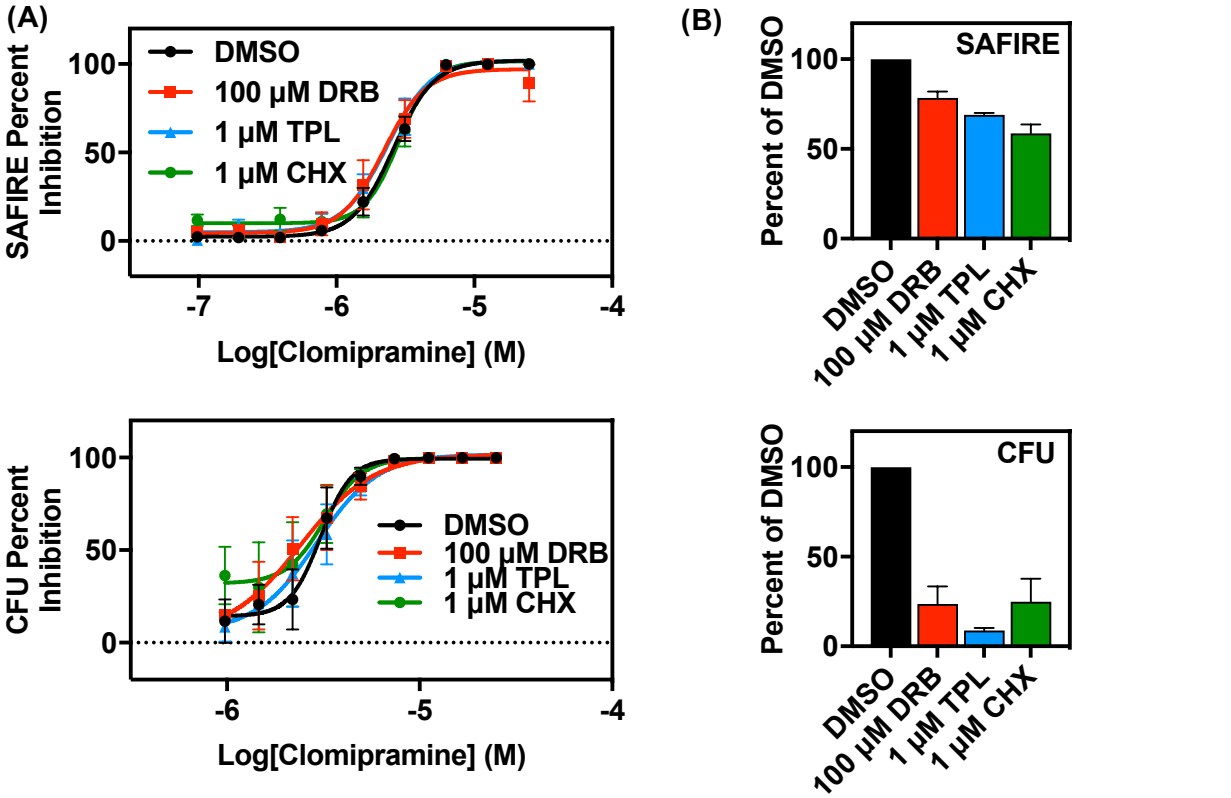

Figure 4-10. Inhibition of macrophage transcription or translation does not alter clomipramine activity. Macrophages were infected and treated with different concentrations of clomipramine from 2-18 h.p.i. in the presence of the transcription inhibitors DRB, triptolide (TPL), or the translation inhibitor cycloheximide (CHX). At 18 h.p.i. macrophages were processed for SAFIRE and CFU as described previously. Right: infection of cells for each inhibitor not treated with clomipramine. Data shown are mean + SEM of three independent biological replicates.

G. CLOMIPRAMINE ACTIVITY APPEARS UNRELATED TO CALMODULIN INHIBITION

Given that CMP did not require host transcription or translation for activity, we next hypothesized that it could directly affect macrophage cellular processes. Other tricyclic antidepressants have been shown to inhibit calmodulin (Asano, 1989; Plenge-Tellechea et al., 1999; Prozialeck and Weiss, 1982b)., a calcium-binding protein that regulates cellular processes including inflammatory responses (Racioppi et al., 2012). I tested whether CMP

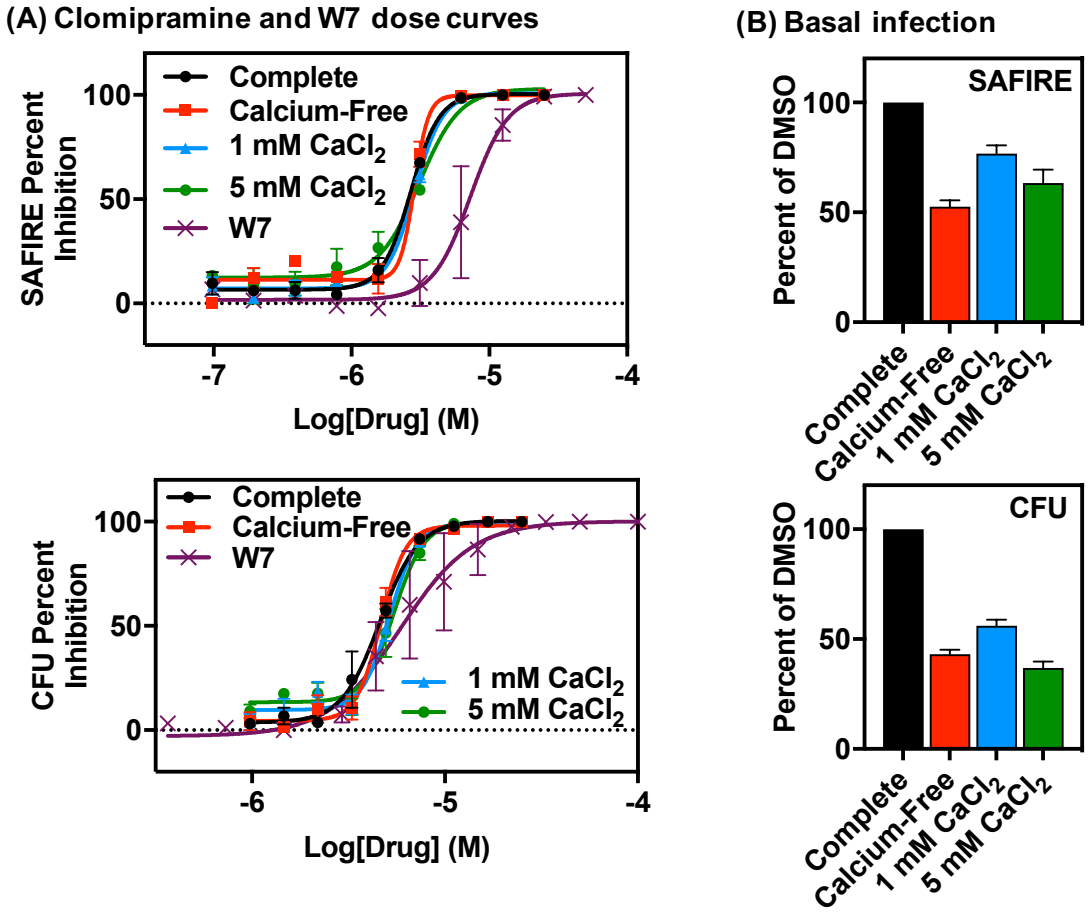

Figure 4-11. Media calcium concentrations do not affect clomipramine activity. Beginning 24 hours prior to infection, macrophages were incubated in calcium-free media. Macrophages were infected and treated with different concentrations of clomipramine from 2-18 h.p.i. Beginning at 2 h.p.i., macrophages were incubated in complete medium containing calcium and serum, calcium-free medium without serum, or calcium-free medium without serum supplemented with the indicated concentrations of calcium. At 18 h.p.i. macrophages were processed for SAFIRE and CFU as described previously. Right: infection of cells for each media condition not treated with clomipramine. Data shown are mean + SEM of three independent biological replicates.

antibacterial activity was modulated by calcium levels, which would suggest that the antibacterial mechanism could involve calmodulin. I cultured macrophages in calcium-free medium for 24 hours prior to infection with *Salmonella*, and then I treated with CMP. I did not see a change in CMP activity under these conditions, or when I added $CaCl_2$ into the calcium-free medium, although altering calcium levels did affect infection (**Figure 4-11**). Next, I found that the known calmodulin inhibitor W7 was active against intracellular *Salmonella*, but with distinct IC50s from CMP. These data support the idea that calcium levels contribute to infection, but suggest that CMP antibacterial activity is not mediated by calmodulin inhibition.

H. CLOMIPRAMINE ACTIVITY MAY BE MEDIATED BY AUTOPHAGY MODULATION

Autophagy can be regulated independently of transcription and translation, and likely plays a role in *Salmonella* infection (Hernandez et al., 2003; Mesquita et al., 2012; Wild et al., 2011) CMP and other tricyclic antidepressants have been shown to disrupt autophagic flux, that is, block clearance of autophagic compartments, which leads to an accumulation of autophagosomes (Guan et al., 2018; Rossi et al., 2009, 2014). Autophagy and other endolysosomal events play a key role in *Salmonella* virulence (Birmingham et al., 2006; Cirillo et al., 1998; Hernandez et al., 2003; Mesquita et al., 2012; Wild et al., 2011), and disruption of

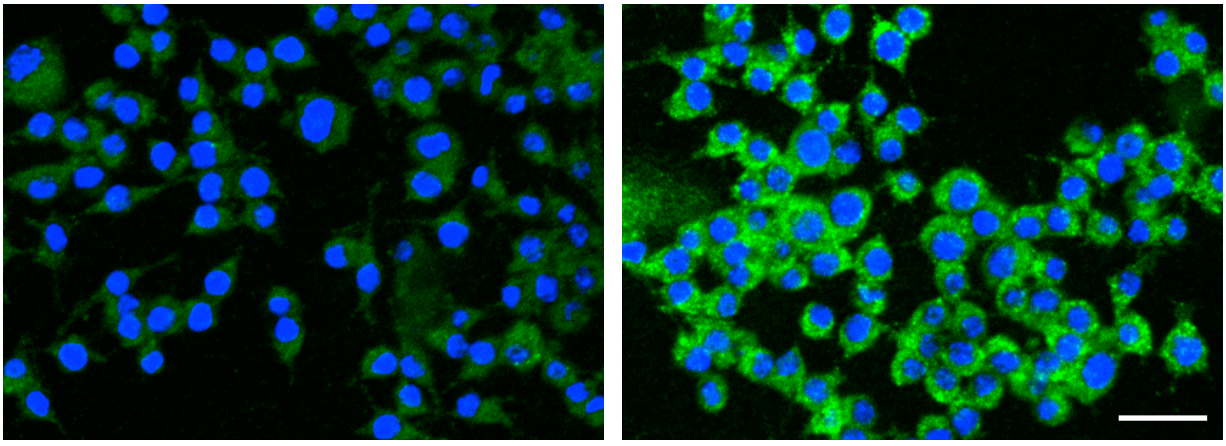

Figure 4-12. Clomipramine induces accumulation of LC3 in uninfected macrophages. Macrophages were treated with DMSO or 25 μM CMP for 18 hours, fixed, immunostained for LC3 (green), and stained with DAPI (blue). Scale bar is 50 μm.

autophagy could lead to bacterial clearance. To test whether CMP causes the accumulation of autophagosomes in macrophages, Toni Nagy treated uninfected macrophages with CMP and stained for LC3, a marker of autophagosomes. We found a significant increase in LC3 staining after CMP treatment (**Figure 4-12**). These data suggest that CMP may modulate autophagy in macrophages, which could mediate bacterial clearance by CMP.

I. CLOMIPRAMINE DOES NOT INHIBIT ACUTE OR CHRONIC *IN VIVO* INFECTION

Several reports have demonstrated that clomipramine and related compounds target microbes *in vivo* (Amaral and Viveiros, 2012; Rivarola et al., 2005). Because clomipramine is used clinically, it represents an attractive antibacterial therapeutic. I next tested whether clomipramine is effective against *Salmonella* in two models of infections. First, I employed an

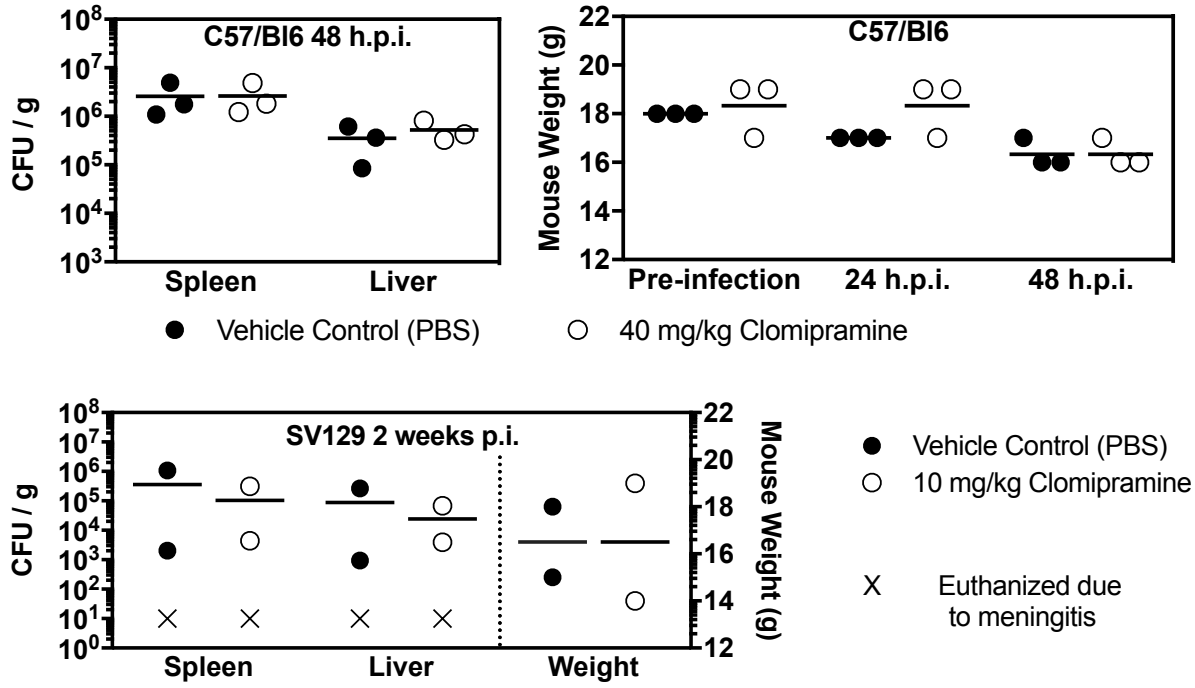

Figure 4-13. Clomipramine does not alter acute or chronic *Salmonella* infection in mice. C57/Bl6 mice were intraperitoneally infected with $1x10^4$ CFU *Salmonella* and treated at 30 minutes and 24 h.p.i. with 40 mg/kg intraperitoneal clomipramine. SV129 mice were orogastrically infected with $1x10^9$ CFU and treated daily with 10 mg/kg intraperitoneal clomipramine. At the indicated timepoints, animals were sacrificed and spleen and liver were harvested to enumerate CFUs.

acute model of *Salmonella* infection wherein C57/Bl6 mice are intraperiteonally infected; typically these mice succumb to infection within 3-5 days. I treated mice with 40 mg/kg CMP at 30 minutes and 24 h.p.i. At 48 h.p.i. I harvested tissues to enumerate bacterial load. I observed no differences between mice treated with CMP or with vehicle (**Figure 4-13**). In addition, I did not observe any improvements in weight loss during infection, suggesting CMP treatment did not reduce disease symptoms. Next, I tested CMP in a model of chronic *Salmonella* infection. I orograstrically infected SV129 mice with *Salmonella* and intraperitoneally treated with 10 mg/kg clomipramine daily. As with the acute model, I did not observe reductions in bacterial load or improvements in weight loss at 2 weeks p.i.

J. DISCUSSION

I found that CMP is a potent inhibitor of intracellular *Salmonella* infection. Other antidepressants also targeted intracellular *Salmonella* with similar potencies to CMP, despite having different canonical targets. Further, the drugs comprise three different structural classes, which suggests that any secondary targets are likely not shared between groups. Thus, it is unclear why all of these antidepressants are also antibacterial.

Many reports have also demonstrated antimicrobial activity of diverse psychoactive drugs (Benson et al., 1992; Chan et al., 1998; Fauro et al., 2013; Lieberman and Higgins, 2009, 2010; Rivarola et al., 2001, 2005; Salie et al., 2014; Stanley et al., 2014). Why so many psychotropic drugs possess antimicrobial activity, despite having unique targets and structures, is unclear. Although it is possible that the canonical targets of these drugs mediate their antimicrobial activity, some appear to have direct microbial targets (Chan et al., 1998; Richardson et al., 2009; Rodrigues et al., 2008). Alternatively, these drugs may be predisposed to disrupt players at the host-pathogen interface by virtue of targeting primitive membrane transporters that are shared across many organisms. It is also possible that it is simply coincidence, given how many antidepressants are in use, that so many possess antimicrobial activity. To better understand

this phenomenon, more work is needed to identify the antimicrobial mechanism of action for these drugs.

The mechanism of action for several psychotropic drugs has been established. TCAs and phenothiazines have been shown to inhibit trypanothione reductase, the analog of glutathione reductase in trypanosomes and *Leishmania* (Chan et al., 1998; Martyn et al., 2007; Richardson et al., 2009). Several TCAs have also been shown to disrupt bacterial efflux (Rodrigues et al., 2008). Psychotropic drugs are also known to have off-target effects on mammalian processes. Phenothioazines are also known to inhibit calmodulin activity (Asano, 1989; Plenge-Tellechea et al., 1999; Prozialeck and Weiss, 1982a, 1982b), though others have been shown this to be unrelated to antimicrobial activities (Lieberman and Higgins, 2009, 2010). TCAs and SSRIs have also been shown to alter autophagy (Guan et al., 2018; Rossi et al., 2009, 2014; Stanley et al., 2014). Thus, antidepressants appear to have many possible off-target effects and may target the microbe or the host to exert antimicrobial activity.

The mechanism of action of clomipramine and related TCAs, phenothiazines, and SSRIs against intracellular *Salmonella* remains unclear. CMP did not display a dependence on its canonical target SERT or serotonin levels, suggesting it has a different target in the macrophage. I also found that none of the drugs inhibited *Salmonella* growth in broth, and only CMP, TDZ, and CPZ modestly inhibited bacterial efflux, together suggesting that there is no essential bacterial target shared by these molecules. I next found that CMP activity persisted after washout of the drug, suggesting CMP made long-lasting changes to cellular processes such as calmodulin regulation or autophagy which are known secondary targets of TCAs. I found that disruptions in calcium levels did not alter CMP activity, suggesting calmodulin inhibition does not mediate CMP activity.

Next, I found that CMP strongly increased autophagosomes in the macrophage, suggesting CMP modulation of autophagy could mediate antibacterial activity. Our observation is consistent with CMP disrupting autophagic flux and preventing breakdown of autophagic vesicles (Guan et

al., 2018; Rossi et al., 2009, 2014). Further studies are needed to determine whether CMP is indeed disrupting flux in macrophages, and whether that is due to changes in vesicular acidifcation, degradation, or trafficking. Additionally, it is currently unclear how disruptions in autophagic flux could lead to bacterial clearance. If CMP is disrupting acidifcation across the entire endolysosomal compartment, it is possible that *Salmonella* does not activate expression of virulence genes in response to acidification which is required for infection (Cirillo et al., 1998). Alternatively, changes in autophagosome degradation could alter recycling of nutrients for *Salmonella* (Singh et al., 2017; Yu et al., 2014). Changes in cellular trafficking might alter delivery of important factors to the *Salmonella*-containing vesicle, thus disrupting the *Salmonella* niche (Garvis et al., 2001; McGourty et al., 2012; Uchiya et al., 1999; Vazquez-Torres et al., 2000a). These possibilities could advance our understanding of the role of autophagy in *Salmonella* infection, as many studies demonstrate that disrupting autophagy actually facilitates *Salmonella* infection (Birmingham et al., 2006; Mesquita et al., 2012; Spinnenhirn et al., 2014).

Antidepressants such as clomipramine represent an attractive source of possible drugs to repurpose as antimicrobials. Indeed, several phenothiazines are under development as putative anti-parasitics (Martyn et al., 2007; Richardson et al., 2009). However, CMP does not appear to be an effective *in vivo* therapeutic against *Salmonella*, as it demonstrated no activity against acute or chronic infection of mice. Though some studies have found efficacy for antidepressants against *in vivo* infection (Macedo et al., 2017; Mandal et al., 2010), others have suggested that the effective concentrations required for antimicrobial activity are too high to attain without disrupting neurological function (Cederlund and Mardh, 1993; Munoz-Bellido et al., 2000). Thus, *in vitro* antimicrobial activity of repurposed drugs may not translate to therapeutic potential.

K. MATERIALS AND METHODS

Cell culture. Murine macrophage-like RAW 264.7 cells were routinely grown in complete DMEM high glucose (Sigma) supplemented with 10% fetal bovine serum (Sigma), 2 mM L-

glutamine (Sigma), 1 mM sodium pyruvate (Sigma), 10 mM HEPES (Sigma), and 50 μM β-mercaptoethanol (Sigma). In some experiments, serum was not added to the medium. In some experiments, DMEM high-glucose no-calcium medium was used and supplemented with the above concentrations of L-glutamine, sodium pyruvate, HEPES, and β-mercaptoethanol but no serum. In all experiments, macrophages were maintained in a 5% CO_2 humidified atmosphere at 37 °C. Construction of shRNA-expressing cell lines was performed using spinfection of lentiviral particles (Functional Genomics Facility, University of Colorado) at 2500 x *g* for 1 hour at 33 °C in the presence of 10 μg/ml polybrene, followed by 16 hours incubation. Medium was replaced with fresh medium for 1 day prior to treatment with 6-10 μg/ml puromycin; mock-infected cells were eliminated between 4-5 days post addition of puromycin.

Bacterial strains. *Salmonella enterica* serovar Typhimurium strain SL1344 expressing GFP from the *sifB* promoter (ALR#109; DET#1270) (Rollenhagen et al., 2004) was used for macrophage infection experiments. Wild-type SL1344 (ALR#001; DET#0001) was used for broth and mouse infection experiments. Overnight cultures were routinely grown in LB with 30 μg/ml streptomycin and 30 μg/ml kanamycin (*sifB*::GFP) strain only) at 37 °C with aeration.

Broth activity assays. Overnight *Salmonella* cultures were washed 3 times in PBS and diluted to an OD of 0.01 in 96-well flat-bottom plates. Compound was added manually, yielding a final concentration of no more than 1% DMSO. Plates were grown at 37 °C shaking and OD_{600} was monitored using a BioTek Eon or Synergy 2 incubator shaker microplate absorbance reader. To determine broth IC50s, bacteria were grown in Mueller Hinton broth (MHB) and the OD_{600} at 18 hours was used to determine drug inhibtion. For experiments with polymixin B, bacteria were grown in M9 minimal medium supplemented with 100 mM Tris pH 7.4, 0.35% glycerol, 0.002% histidine, 10 mM $MgCl_2$, and 0.1% casamino acids.

Macrophage infections for SAFIRE and CFU plating. Fifty thousand macrophages in 100 μL were seeded in 96-well black-walled, glass-bottomed plates (Brooks Automation). Twenty-

four hours post-seeding, bacteria in 50 µL PBS were added to a final concentration of 1 x 10^7 cfu / mL; I determined that these conditions resulted in infection of approximately 70% of macrophages at 18 hours post-infection with minimal macrophage toxicity (**Appendix A**). Forty-five minutes after bacterial addition, 50 µL gentamicin was added to a final concentration of 100 µg / mL. At 2 h.p.i., medium was blotted and replaced with medium containing 10 µg / mL gentamicin. For SAFIRE analysis, PBS containing MitoTracker Red CMXRos (Life Technologies) was added at 17.5 h.p.i. to yield a final concentration of 100 nM. Thirty minutes later, 16% paraformaldehyde was added to a final concentration of 1-2% and incubated at room temperature for 15 minutes. Wells were washed twice with PBS and stained for 20 minutes with 1 µM DAPI; wells were washed twice and stored in 90% glycerol in PBS until imaging. Plates were imaged using an Olympus IX81 inverted widefield microscope at 10X and images were analyzed using the SAFIRE scripts (**Appendix B)**. High magnification images were taken at 40X.

Infections to determine *Salmonella* CFUs were performed as described above, except cells were seeded in 96-well tissue culture coated plates (Greiner). At 18 hours post-infection, wells were washed three times in PBS, lysed with 30 µL 0.1% Triton X-100, diluted and plated to determine colony-forming units.

Hoechst efflux assay. Hoechst accumulation assays were performed essentially as described (Coldham et al., 2010). Briefly, overnight *Salmonella* cultures were washed 3 times in PBS and diluted to an OD of 0.1 in PBS with 2.5 µM Hoechst 33342 in the presence of the indicated concentrations of compounds. Fluorescence was monitored on a Biotek Synergy H1 with excitation at 354 nm and emission at 456 nm. The maximum Hoechst fluorescence over 60 minutes of incubation was normalized to the signal from the equivalent number of heat-killed bacteria (100%) and from vehicle-treated bacteria (0%).

Mouse infections. Bacteria were grown overnight in LB, then diluted in PBS. Seven week old C57/Bl6 female mice were intraperitoneally injected with 1 x 10^4 *Salmonella* in 100 µL.

Seven-week old female SV129/SvEvTac mice were fasted 8-12 hours prior to oral gavage with 1 x 10^9 bacteria in 100 µL. Beginning thirty minutes after infection, mice daily received the indicated amount of drug or vehicle in 100 µL PBS by intraperitoneal injection. At the indicated timepoints, mice were humanely euthanized using carbon dioxide asphyxiation followed by cervical dislocation. Spleens and livers were harvested, homogenized, diluted in PBS, and plated to enumerate *Salmonella* CFUs.

Real-time reverse transcription PCR. One million RAW 264.7 macrophages expressing the indicated shRNAs were seeded in 6-well dishes and stimulated with 20 ng/ml lipopolysaccharide. After 18 hours, wells were washed twice with PBS and RNA was extracted using the RNeasy mini kit (Qiagen) including Qiashredder homogenization and on-column DNase treatment. RNA yields ranged from 5-40 ng. First-strand cDNA was synthesized from 250 ng of total RNA using the iScript cDNA synthesis kit (BioRad) and diluted 10-fold. Quantitative PCR (qPCR) for the indicated genes was performed using the following primers: *Hprt* (GCGTTGGGCTTACCTCACT, ATCGCTAATCACGACGCTGG); *Sert* (TTGGATAGTACGTTCGCAGGC, ACCACGATGAGCACAAACCA). *Hprt* was selected as the reference gene based on validation experiments. The qPCR reactions were performed in technical duplicates and contained 8 µL diluted cDNA, 200 nM of each primer, and 10 µL 2X Power SYBR Green (Applied Biosystems) in 20 µL total volume. Reactions were run on an Eppendorf Realplex^2 MasterCycler with the following cycling conditions: 10 minutes at 95 °C, then 40 cycles at 95 °C for 15 seconds and 60 °C for 60 seconds. Melting curve analysis of the PCR reaction showed a single amplicon for each target. No-template and no-reverse-transcriptase controls showed no product. Amplification results were baseline corrected, followed by manual determination of the threshold for each gene. The resulting C_T values were analyzed as follows: *(i)* The mean C_T of qPCR technical duplicates was determined for each sample. *(ii) Slc6a4* and *Camp* expression for each sample was normalized to that of *Hprt*, resulting in the ΔC_T. *(iii)* Each sample was normalized to the mean of the uninfected samples for

that experiment, resulting in the $\Delta\Delta C_T$ for that sample. *(iv)* The mean of sample replicates from the same experiment was calculated. *(v)* Fold expression and error were calculated using the $2^{-\Delta\Delta CT}$ equation.

Immunostaining for LC3. Macrophages were plated as described for SAFIRE imaging. After fixation in 100% methanol for 20 minutes at -20 ºC, plates were rinsed in PBS in incubated with 1.5% BSA/PBS containing 0.1% Triton X-100 for 1 hour at room temperature. Plates were immunostained with rabbit polyclonal anti-LC3 antibody (Cell Signaling Technology) at 1:200 in 1.5% BSA/PBS containing 0.1% Triton X-100 overnight at 4 ºC. Plates were washed and incubated with 1:1000 goat anti-rabbit AlexaFluor-488-conjugated antibody (Invitrogen) at a concentration for one hour at room termpature. Nuclei were stained with DAPI as described above, and wells were stored in 90% glycerol/PBS. Images were acquired at 20X using the Yokogawa CellVoyager™ CV1000 Confocal Scanner System.

Statistics. Curve fitting to determine IC50s and EC50s was performed using GraphPad Prism four-parameter nonlinear fit analysis. Statistical significances were determined using the indicated test in GraphPad Prism.

CHAPTER 5. LIPID DEGRADATION GENES CONTRIBUTE TO *SALMONELLA* INFECTION OF IMMUNOCOMPETENT MICE AND REPLICATION IN PRO-INFLAMMATORY MACROPHAGES

A. INTRODUCTION

Microbial pathogens must tailor their survival and replication strategy to specific host microenvironments. Many pathogens encounter diverse niches throughout infection (Bumann, 2015). Spatially, infection spreads to new tissues or cell types. Temporally, the innate immune response gives way to adaptive effectors, and infection may evolve into a chronic state. Within each unique niche, the availability of nutrients is influenced by factors such as the host metabolic state (Daniel et al., 2011; Garcia-Gutierrez et al., 2016; Liu et al., 2017), the host inflammatory state (Eisele et al., 2013; Muraille et al., 2014; Peyron et al., 2008; Saliba et al., 2016), interactions with other microbes (Faber et al., 2017; Hammer et al., 2014; Rivera-Chávez et al., 2016), and stochastic heterogeneity (Helaine et al., 2014; Manina et al., 2015; Sureka et al., 2008). Together, these factors define the nutritional microenvironment and influence pathogen replication, persistence, spread, and the outcome of infection.

Pathogenic *Salmonella* species occupy many microenvironments over the course of infection (Becker et al., 2006; Barat et al., 2012; Diacovich et al., 2016; Haraga et al., 2008). *Salmonella enterica* serovar Typhimurium infection of mice has been used to model the acute and chronic stages of human typhoid fever, which is caused by *Salmonella enterica* serovar Typhi and is responsible for 200,000 deaths globally each year (Crump et al., 2004). Initially, bacteria are acquired through contaminated food or water and reach the anaerobic small intestine, where they invade and traverse the intestinal epithelium (Jones et al., 1994). *Salmonella* are taken up by professional phagocytes and within these cells colonize gastrointestinal and systemic tissues including Peyer's patches, mesenteric lymph nodes, spleen, and liver (Vazquez-Torres et al., 1999). However, *Salmonella* likely encounter differentially polarized phagocytes, which present unique nutritional challenges. Macrophages polarized with pro-inflammatory cytokines such as interferon-γ (IFN-γ) present a microbiocidal

"M1" phenotype and metabolize glucose, while macrophages stimulated with anti-inflammatory cytokines such as interleukin-4 (IL-4) are termed "M2" and utilize oxidative phosphorylation of fatty acids (Eisele et al., 2013; Galván-Peña and O'Neill, 2014; Jha et al., 2015). Thus, polarization dictates macrophage metabolism and likely influences the assortment of nutrients available for *Salmonella*.

I hypothesized that lipids might provide carbon and energy during systemic infection, as *Salmonella* has been observed in lipid-rich macrophages that accumulate during typhoid fever (Nix et al., 2007; Brown et al., 2010; Fisman, 2000; Shin et al., 1994). However, data on the use of lipids during systemic *Salmonella* infection are mixed: some studies report no *in vivo* defect for mutants lacking key enzymes in lipid metabolism (Kim et al., 2006; Spector et al., 1999; Tchawa Yimga et al., 2006a), but others demonstrate attenuation (Fang et al., 2005; Steeb et al., 2013). While bulk expression profiling and proteomics do not point to significant induction of lipid metabolism genes during infection of macrophages or mice (Becker et al., 2006; Eriksson et al., 2003; Shi et al., 2006), recent single-cell work using fluorescent reporters suggests a subset of bacteria utilize lipids (Diacovich et al., 2016). It is possible that bacterial subpopulations employ different nutritional strategies within the same niche, suggesting that certain *Salmonella* could use lipids even in host environments where glucose is a key carbon and energy source (Bowden et al., 2009, 2010, 2014; Diacovich et al., 2016; Eisele et al., 2013; Eriksson et al., 2003; Mercado-Lubo et al., 2009; Tchawa Yimga et al., 2006a). *Salmonella* may also utilize lipids in unique host cell microenvironments that have not yet been studied (Becker et al., 2006; Barat et al., 2012; Diacovich et al., 2016). Thus, whether and where *Salmonella* utilizes lipids during infection is unclear.

To convert lipids into carbon and energy, *Salmonella* fatty acid degradation comprises several core steps (**Figure 5-1**) (Clark and Cronan, 2005; Heath et al., 2002; Iram and Cronan, 2006). Medium- and long-chain fatty acids are imported via an outer-membrane transporter and activated with the addition of coenzyme-A (**Figure 5-1A**). The resulting acyl-coA molecule is

serially β-oxidized to produce acetyl-coA (**Figure 5-1B**), which is subsequently oxidized via the TCA cycle to produce energy. TCA cycle intermediates are also routed to biosynthetic pathways to incorporate carbon into the cell, and must be replenished to comprise a complete TCA cycle. When glycolytic carbon sources are available, these intermediates can be directly synthesized. However, during growth on lipids as a sole carbon source, acetyl-coA derived from lipids must instead be converted into TCA intermediates by the glyoxylate shunt, which bypasses a portion of the TCA cycle to preserve carbon (**Figure 5-1C**). I found that inactivation of *Salmonella* lipid metabolism genes compromised systemic colonization of mice and replication in M1 pro-inflammatory macrophages, indicating that lipids are a nutrient source for *Salmonella* during infection of specific host environments.

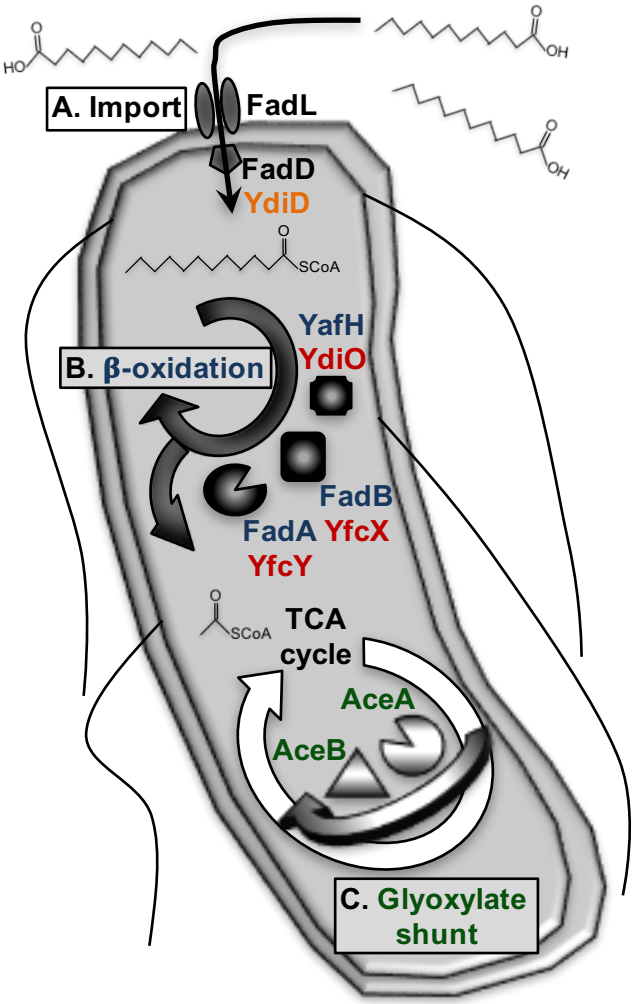

Figure 5-1. Schematic of lipid metabolism in *Salmonella*. (A) Long-chain free fatty acids are imported via FadL (outer membrane translocase) and activated by FadD or YdiD (acyl-coA synthetases). Canonical import genes are black; putative secondary import genes are orange. **(B)** Resulting acyl-thioesters are serially **β**-oxidized via YafH or YdiO (acyl-CoA dehydrogenases), FadB or YfcX (3-hydroxyacyl-CoA dehydrogenases), and FadA or YfcY (3-ketoacyl-CoA thiolases), producing acetyl-CoA, which is metabolized via the TCA cycle. Canonical **β**-oxidation genes are blue; putative secondary **β**-oxidation genes are red. **(C)** The gyoxylate shunt (green) consists of AceA (isocitrate lyase) and AceB (malate synthase), and bridges the TCA cycle to preserve carbon and cofactors during growth in the absence of glycolytic energy sources.

B. DELETION OF *SALMONELLA* LIPID METABOLISM GENES ABROGATES GROWTH ON FATTY ACIDS

To probe the relevance of lipids as a *Salmonella* nutrient source during infection, I first verified the requirement for *Salmonella* lipid degradation genes during growth on lipids (**Figure 5-1**). Import genes *fadL* and *fadD* respectively encode a long-chain fatty acid transporter and acyl-CoA synthetase, which primes fatty acids for degradation (Heath et al., 2002). Deletion of *fadL* or *fadD* eliminated growth on oleic acid as a sole carbon source, but did not affect growth

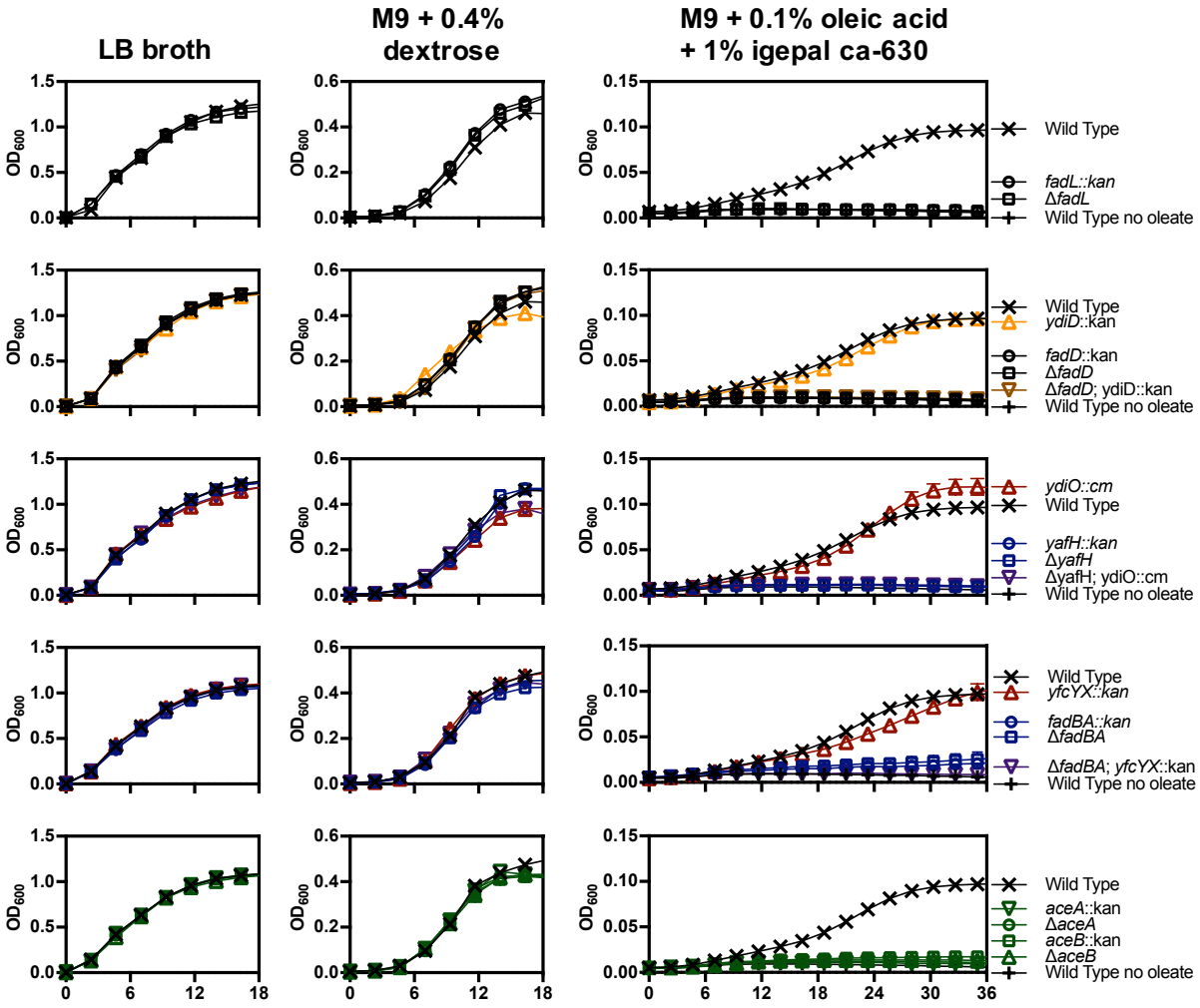

Figure 5-2. Lipid metabolism mutants do not grow on oleate. Bacteria were grown in the indicated media and optical density was measured over 18-36 hours. Data shown are mean + standard deviation of triplicate samples, representative of 3 independent experiments. Oleate was solubilized with igepal; no growth was observed in the igepal, no oleate condition (+). Import mutants are black (canonical), orange (secondary), or brown (canonical/secondary double mutant); β-oxidation mutants are blue (canonical), red (secondary), or purple (canonical/secondary double mutant); glyoxylate shunt mutants are green.

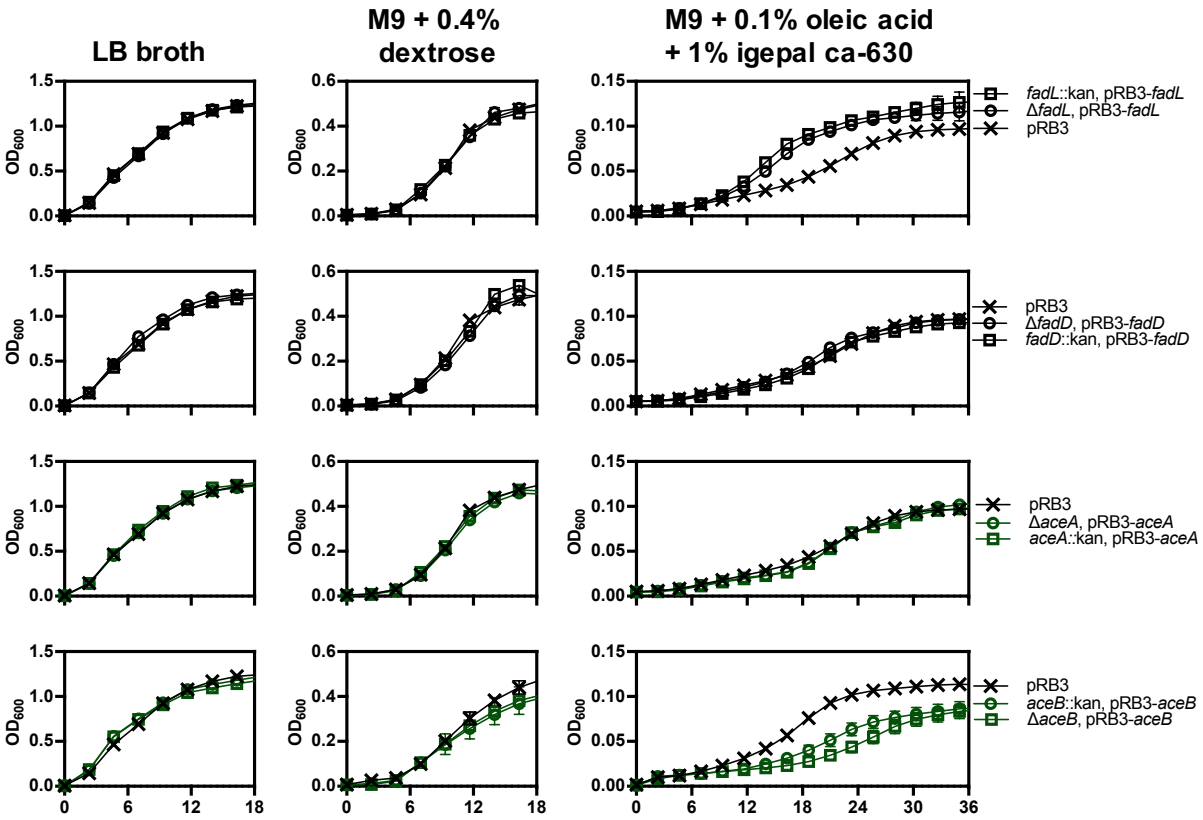

Figure 5-3. Complementation of oleate growth phenotypes as in Figure 5-2.

in rich broth or on glucose, as expected; complementation of these mutants with the gene on a plasmid restored growth (**Figure 5-2, 5-3, Table 5-1**). *Salmonella* also encodes a paralog of *fadD*, denoted *ydiD*, which did not affect growth on lipids. Since the *ydiD* ortholog in *Escherichia coli* plays a role in anaerobic growth (Morgan-Kiss and Cronan, 2004), I next tested whether this was the case in *Salmonella*. I found that *fadL* and *fadD*, but not *ydiD*, were required for anaerobic growth on lipids (**Table 5-1**).

β-oxidation of lipids is performed by enzymes encoded by *yafH*/*fadE*/*fadF*, *fadB*, and *fadA*. These enzymes serially liberate acetyl-coA from acyl chains for incorporation via the TCA cycle (Campbell and Cronan, 2002; Iram and Cronan, 2006). I also identified a secondary pathway encoded by *ydiO*, *yfcX*, and *yfcY*; the *E. coli* orthologs are required for anaerobic growth on lipids (Campbell et al., 2003; Dellomonaco et al., 2011). A strain lacking *yafH* was unable to grow aerobically on oleic acid, and a strain lacking *ydiO* was unable to grow anaerobically,

Table 5-1. Growth of lipid metabolism mutants on plates with the indicated carbon sources.

Genotype	Aerobic [1]				Anaerobic + 25 mM nitrate [2]			
	Glu	C18:1	C10	C8	Glu	C18:1	C10	C8
WT WT, pRB-273c	1 [3]	2	- [4]	-	3	6	8	10
Δ*fadR* [5]	1	2	4	6	3	6	8	10
Δ*fadL* *fadL*::kan	1	-	-	-	3	-	-	-
Δ*fadL*, pRB3-*fadL* *fadL*::kan, pRB3-*fadL*	1	1-2	-	-	3	6	8	10
Δ*fadD* *fadD*::kan	1	-	-	-	3	-	-	-
Δ*fadD*, pRB3-*fadD* *fadD*::kan, pRB3-*fadD*	1	2	-	-	3	6	8	10
ydiD::kan	1	2	-	-	3	6	8	10
Δ*fadD; ydiD*::kan	1	-	-	-	3	-	-	-
Δ*yafH* *yafH*::kan	1	-	-	-	3	6	8	10
ydiO::cm	1	2	-	-	3	-	-	-
Δ*yafH*; *ydiO*::cm	1	-	-	-	3	-	-	-
Δ*fadBA* *fadBA*::kan	1	3-4 [6]	-	-	3	6	8	10
yfcYX::kan	1	2	-	-	3	14	-	-
Δ*fadBA*; *yfcYX*::kan	1	-	-	-	3	-	-	-
Δ*aceA* *aceA*::kan	1	-	-	-	3	-	-	-
Δ*aceA*, pRB3-*aceA* *aceA*::kan, pRB3-*aceA*	1	2	-	-	3	6	8	10
Δ*aceB* *aceB*::cm	1	-	-	-	3	-	-	-
Δ*aceB*, pRB3-*aceB* *aceB*::cm, pRB3-*aceB*	1	2	-	-	3	6	8	10

[1] Bacteria were grown on M9 minimal plates containing the indicated carbon sources solubilized using 1% igepal CA-630; other supplements are listed in the methods. No growth was observed on plates lacking a carbon source. Import mutants are black (canonical) or orange (secondary) or brown (canonical/secondary double mutant); β-oxidation mutants are blue (canonical) or red (secondary) or purple (canonical/secondary double mutant); glyoxylate shunt mutants are green.

[2] Nitrate was added as an alternative electron acceptor; no anaerobic growth was observed on plates lacking nitrate.

[3] Growth is recorded as the day on which colonies were discernible by eye; data are from 2 independent biological replicates.

[4] No colonies were discernible for up to two weeks.

[5] *fadR* encodes a regulator which represses transcription of canonical lipid metabolism genes in the absence of long-chain acyl-CoA molecules, preventing aerobic growth on medium-chain fatty acids.

[6] Strains lacking *fadBA* grow oleate, albeit slowly, due to compensation by *yfcYX*; see **Figure 5-4**

indicating that these cognate enzymes play distinct roles and do not compensate for each other *in vitro* (**Table 5-1, Figure 5-2**). I next found that deletion of the canonical *fadBA* operon significantly but not entirely compromised aerobic growth on oleic acid; the residual growth was dependent on *yfcYX* as the double mutant was unable to grow aerobically on oleic acid (**Table 5-1, Figure 5-2, 5-4**). The roles of these operons were reversed during anaerobic growth, as loss of *yfcYX* drastically reduced but did not eliminate growth on oleic acid; the residual anaerobic growth was dependent on *fadBA*. These results indicate that the *fadBA* and *yfcYX* operons primarily function during aerobic and anaerobic growth respectively, but can partially compensate for each other.

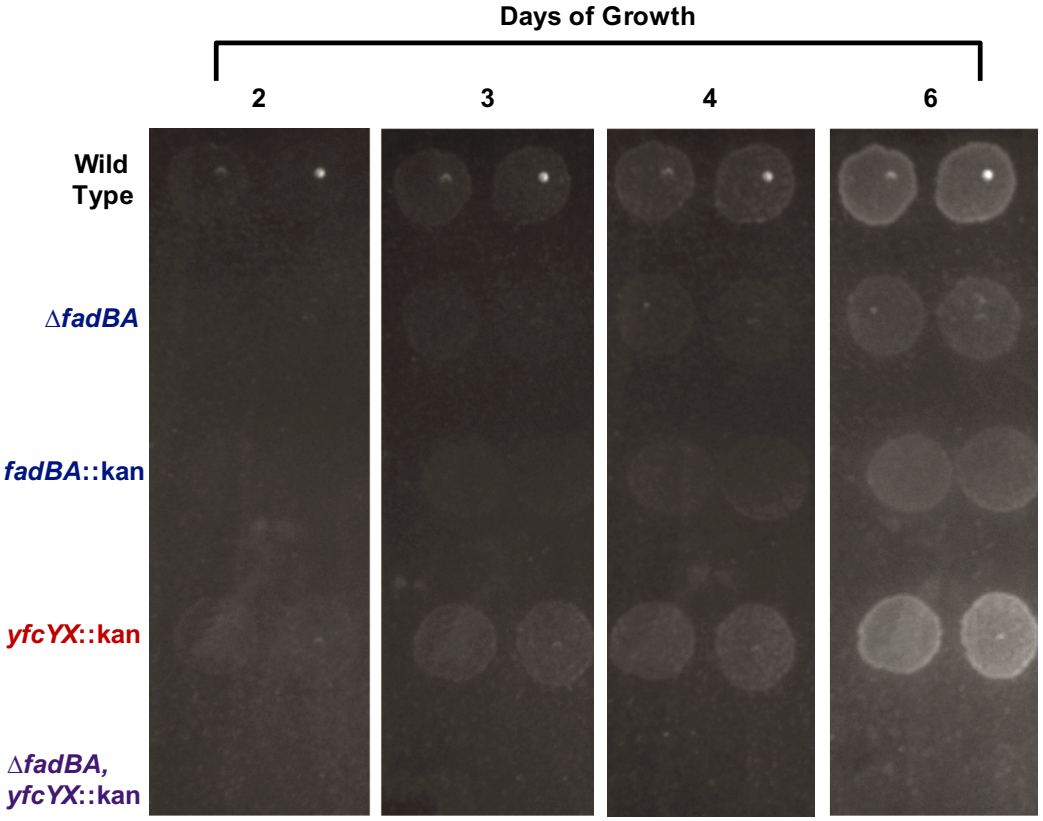

Figure 5-4. *Salmonella* lacking *fadBA* grow aerobically on oleate. Bacteria were prepared as in **Table 5-1**. Representative image of duplicate spots on the same plate over multiple days of incubation from one experiment. Wild-type and *yfcYX*::kan bacteria displayed visible growth after 2 days; mutants lacking *fadBA* grew after 3 days and this growth was dependent on *yfcYX*.

The glyoxylate shunt replenishes metabolic intermediates in the absence of glycolytic carbon sources and comprises two enzymes located in an operon: isocitrate lyase, encoded by *aceA*, and malate synthase, encoded by *aceB* (Wilson and Maloy, 1987). Nonpolar deletions of either *aceA* or *aceB* eliminated aerobic and anaerobic growth on oleic acid as a sole carbon source, and these defects were complemented by a plasmid containing the target gene (**Figure 5-2, Figure 5-3, Table 5-1**).

C. *SALMONELLA* REQUIRES LIPID DEGRADATION GENES FOR OROGASTRIC OR INTRAPERITONEAL INFECTION OF 129SV MICE

Several groups have found differing requirements for *Salmonella* lipid metabolism during infection, though these studies were primarily conducted in immunocompromised mice that develop acute lethal infection (Fang et al., 2005; Kim et al., 2006; Spector et al., 1999; Steeb et al., 2013; Tchawa Yimga et al., 2006b). I performed mixed-infection experiments in immunocompetent 129S6/SvEvTac mice, which become chronically infected with *Salmonella* (Monack, 2004). Fasted male and female mice were orogastrically infected with equal numbers of wild-type and mutant bacteria and euthanized at two weeks post infection, when bacteria have disseminated systemically within macrophages and begin shifting into a chronic infectious state (Brown et al., 2010; Eisele et al., 2013; Monack, 2004). Tissues were harvested to enumerate CFUs, and the competitive index was calculated as the ratio of recovered wild-type to mutant CFUs, normalized to the ratio in the inoculum. I observed no differences in infection of male or female mice.

Strains lacking canonical import genes *fadL* or *fadD* were attenuated in competition with wild type, indicating that fatty acid transport and activation are needed for tissue colonization in mice (**Figure 5-5**). Complementation of each of these strains with a plasmid containing the target gene rescued colonization to wild type levels. A strain lacking *ydiD*, the secondary paralog of *fadD*, competed equivalently with wild type, suggesting *ydiD* does not contribute to

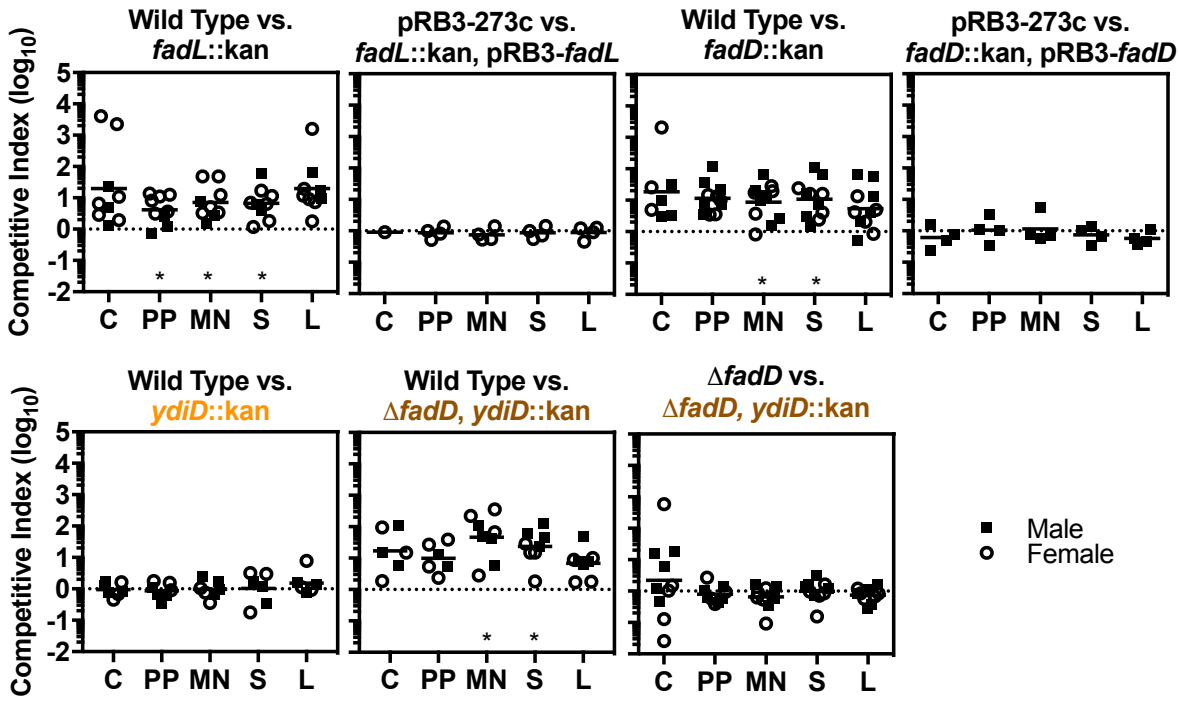

Figure 5-5. Loss of lipid import genes compromises *Salmonella* infection of mice. Mice were orogastrically inoculated with 1 x 10^9 or 2 x 10^9 (Δ*fadD* vs. Δ*fadD*, *ydiD*::kan experiment only) CFUs of the indicated strains. At 2 weeks post infection tissues were harvested to enumerate CFUs: cecum (C), Peyer's patches (PP), mesenteric lymph nodes (MN), spleen (S), and liver (L). The ratio of the indicated strains at harvest was normalized to that in the inoculum to calculate the competitive index. Each symbol represents one mouse. * $p < 0.05$ by one-sample t test.

infection. Loss of *ydiD* did not further attenuate a *fadD* mutant, and the double mutant competed equivalently with the Δ*fadD* strain. Together, these data indicate *ydiD* is dispensable, but that the canonical fatty acid import genes *fadL* and *fadD* contribute to infection of mice.

Next, I examined the role of the canonical and secondary β-oxidation pathways (*yafH-fadB-fadA* and *ydiO-yfcX-yfcY* respectively). Strains lacking a gene or operon from a single pathway competed equivalently to wild type (**Figure 5-6**). However, strains lacking genes encoding both cognate enzymes were attenuated. Thus, the canonical and secondary **β**-oxidation pathways are redundant with one another during infection, and **β**-oxidation of lipids is necessary for infection.

The glyoxylate shunt replenishes TCA cycle intermediates in the absence of glucose and is required for growth on lipids as a sole carbon source. Mutant strains lacking either *aceB* or *aceA*

were outcompeted by wild type, and these defects were complemented by the corresponding gene on a plasmid (**Figure 5-7**). These data suggest in some situations lipids may be the only carbon source available to *Salmonella* during infection.

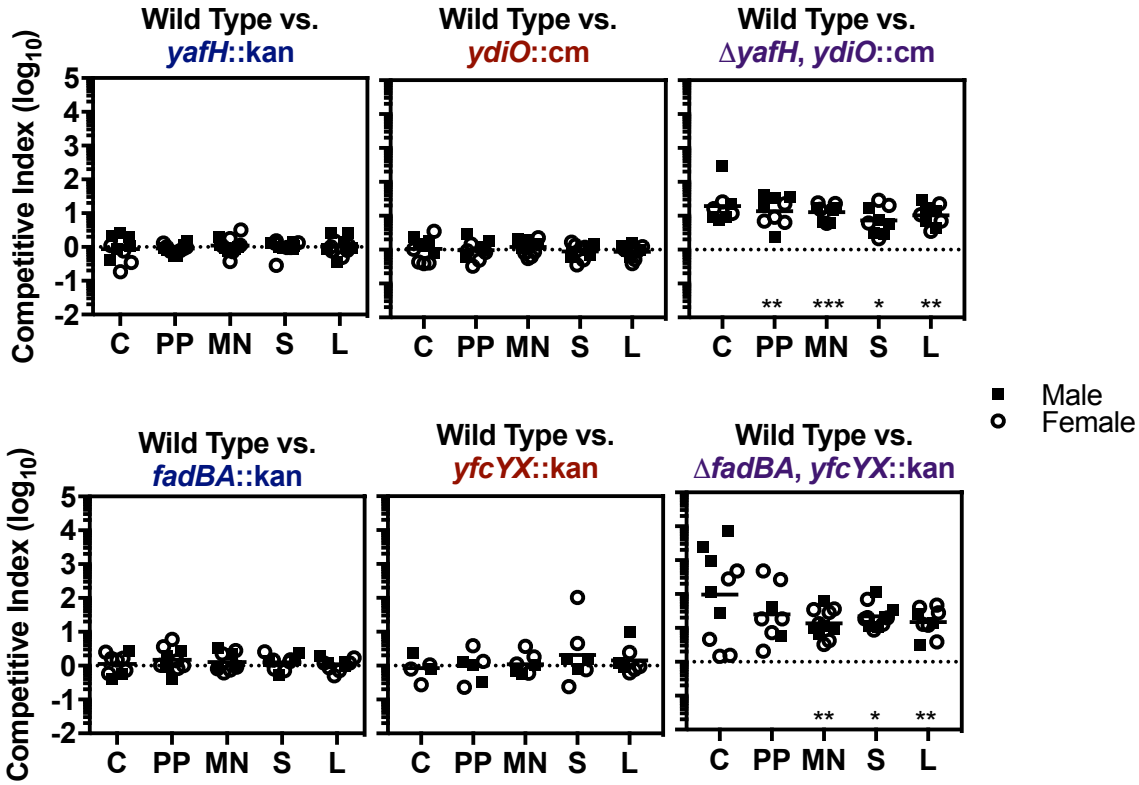

Figure 5-6. Loss of β-oxidation genes compromises *Salmonella* infection of mice as in Figure 5-5. * $p < 0.05$; ** $p < 0.01$; *** $p < 0.001$ by one-sample t test.

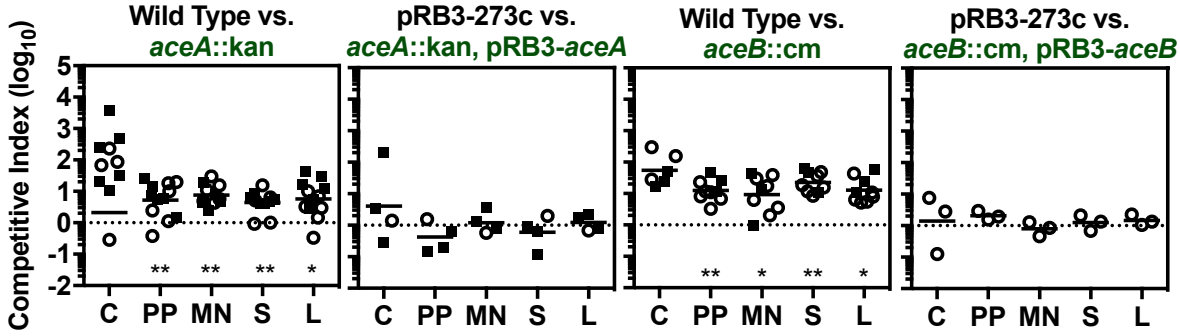

Figure 5-7. Loss of the glyoxylate shunt compromises *Salmonella* infection of mice as in Figure 5-5. * $p < 0.05$; ** $p < 0.01$ by one-sample t test.

To disseminate to the spleen and liver during orogastric infection, *Salmonella* must first colonize and traverse the gut. Intestinal fatty acids could represent a nutrient source for replication within the intestine. Intestinal fatty acids also regulate *Salmonella* virulence gene expression in the intestine, and mutants lacking lipid metabolism genes have altered intestinal invasion during early infection (Golubeva et al., 2016; Lawhon et al., 2002; Lucas et al., 2000; Viarengo et al., 2013). Although my experiments were conducted in fasting mice which show a minimal effect of fatty-acid-mediated virulence regulation (Golubeva et al., 2016), I verified the phenotypes were not due to initial defects in the intestine. I performed mixed infections using an intraperitoneal infection model, in which bacteria bypass the gastrointestinal tract and are rapidly phagocytosed by resident peritoneal macrophages and disseminate systemically (Vazquez-Torres et al., 1999). Equivalent numbers of wild-type and *fadD*::*kan* or *aceA*::*kan* bacteria were injected into the intraperitoneal cavity. Animals were euthanized two weeks post-infection and tissues were processed as described above. Mutant strains lacking *fadD* or *aceA* were again defective, indicating these genes play a role in systemic tissue colonization, independent of any roles in the gastrointestinal tract (**Figure 5-8**).

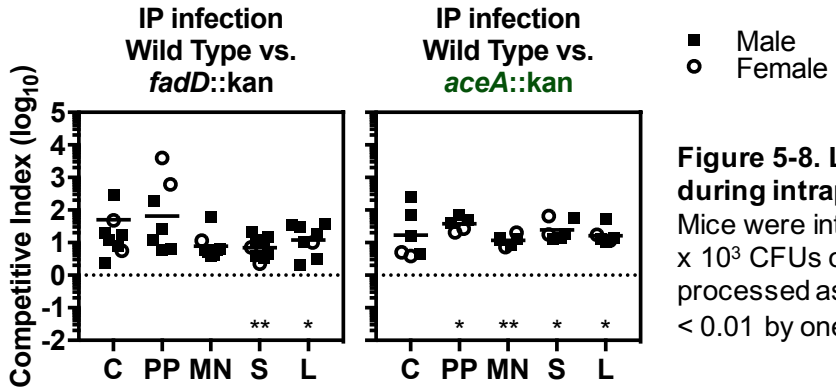

Figure 5-8. Lipid mutants are defective during intraperitoneal infection of mice. Mice were intraperitoneally infected with 1 x 10^3 CFUs of the indicated strains and processed as in **Figure 5-5**. * $p < 0.05$; ** $p < 0.01$ by one-sample t test.

D. LIPID UPTAKE AND β-OXIDATION GENES CONTRIBUTE TO *SALMONELLA* GROWTH IN PRO-INFLAMMATORY MACROPHAGES, SPECIFICALLY DURING AMINO ACID SUPPLEMENTATION

Since *Salmonella* survives within macrophages during systemic infection, the *in vivo* data suggested lipids could be a nutrient source in the macrophage niche. Thus, I tested whether lipid metabolism genes contribute to colonization of primary bone-marrow-derived macrophages (BMDMs). I activated macrophages with interferon-gamma (IFN-γ), which polarizes toward a classical M1 pro-inflammatory state and glycolytic metabolism. BMDMs were infected with wild-type or mutant bacteria, and I determined CFUs at 2 and 18 hours post infection. Surprisingly, loss of lipid metabolism genes did not decrease *Salmonella* growth between 2 and 18 hours (**Figure 5-9A, left**).

BMDMs efficiently kill bacteria, and killing could mask any replication defects of the lipid mutants. I next directly quantified fold replication of the entire bacterial population using fluorescence dilution and flow cytometry (Helaine et al., 2010) **(Figure 5-10**). *Salmonella* replicated approximately 2-fold in BMDMs (**Figure 5-11, left**). As in the CFU growth assays, I found the lipid metabolism mutants replicated similarly to wild-type bacteria (**Figure 5-9B, left**). I also quantified the percentage of bacteria that replicated and found no differences between wild-type and mutant strains (**Figure 5-9C, left**).

Primary cultured macrophages limit bacterial replication, but increased replication could reveal a requirement for lipid metabolism due to depletion or other carbon and energy sources. Indeed, a recent study reported phenotypes for lipid metabolism mutants within less stringent immortalized macrophages (Diacovich et al., 2016). Thus, I next tested whether lipid metabolism genes contribute to growth in RAW 264.7 macrophages, an immortalized mouse monocyte cell line which is more permissive for *Salmonella* replication (Helaine et al., 2010). As expected, wild-type *Salmonella* displayed increased growth and replication (4-fold) in RAW 264.7 cells (**Figure 5-11A,B, right**); however, lipid metabolism mutants grew and replicated similarly to wild-type (**Figure 5-9D-F, left**).

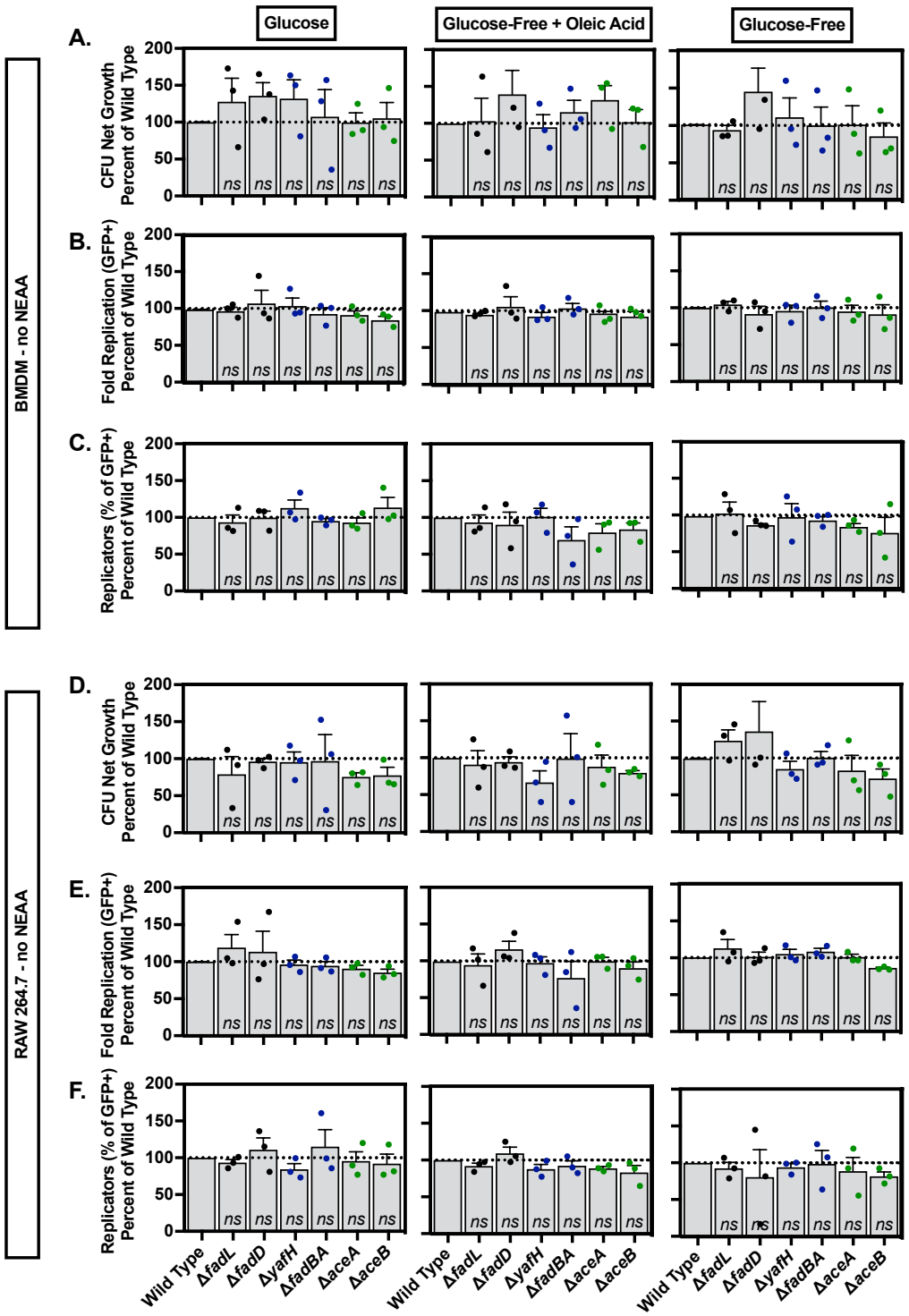

Figure 5-9. Lipid metabolism genes are not required for growth or replication in macrophages in the absence of non-essential amino acids. BMDMs **(A,B)** or RAW 264.7 **(C,D)** cells were transferred into defined medium with the indicated carbon source in the absence of non-essential amino acids and activated with interferon-γ for 18-24 hours prior to infection with the indicated strains. **(A,C)** Net growth was calculated as CFU at 18 hours divided by CFU at 2 hours post infection. **(B,D)** Fold replication was calculated using fluorescence dilution for the GFP+ population. Data were normalized to wild type (100%). Average of triplicate samples from each of 3 independent biological replicates (circles) is superimposed on mean and SEM. There were no significant differences by one-way ANOVA.

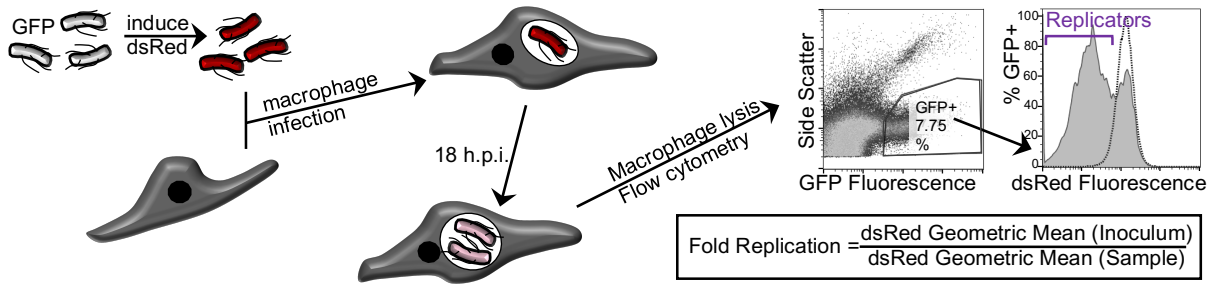

Figure 5-10. Schematic of fluorescence dilution methodology. GFP-expressing *Salmonella* are induced prior to infection to express dsRed. Macrophage lysates are subjected to flow cytometry to identify GFP+ bacteria. The GFP+ population is further gated for low dsRed fluorescence to identify bacteria that have replicated. Fold replication is calculated using the dilution of dsRed relative to the fluorescence in the inoculum.

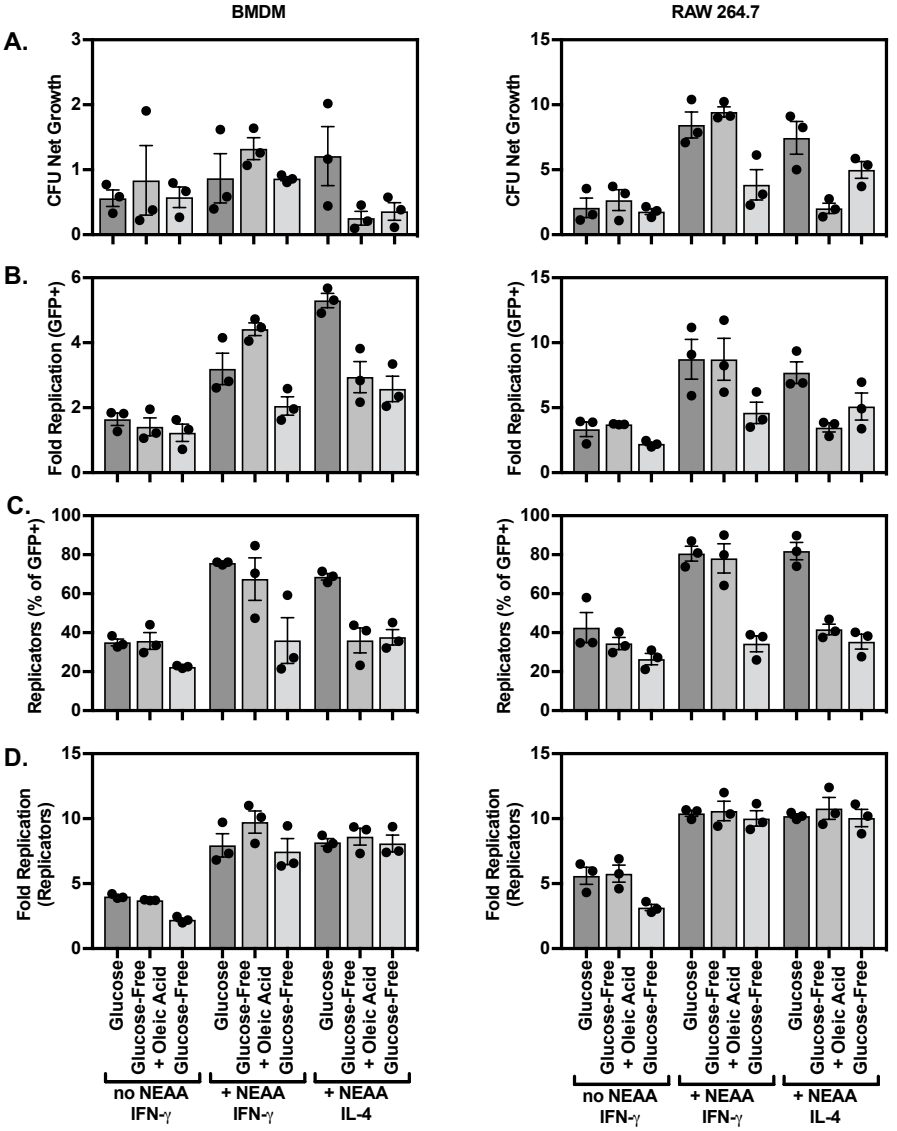

Figure 5-11. Wild type growth and replication in the absence and presence of non-essential amino acids and different macrophage activations. BMDMs or RAW 264.7 cells were transferred into defined medium with the indicated carbon source, without or with non-essential amino acids and activated with interferon-γ or interleukin-4 for 18-24 hours prior to infection with wild type *Salmonella*. **(A)** Net growth was calculated as CFU at 18 hours divided by CFU at 2 hours post infection. Fold replication was calculated using fluorescence dilution for the GFP+ population **(B)** and for the replicators **(D)**. Data were normalized to wild type (100%). **(C)** Percentage of bacteria that replicated were gated as GFP-low based on the fluorescence of the inoculum. Average of triplicate samples from each of 3 independent biological replicates (circles) is superimposed on mean and SEM.

Bacterial access to carbon and energy sources is likely influenced by the availability of nutrients within macrophages, which in turn can be influenced by the culture medium (Diacovich et al., 2016). Our standard cell culture medium lacks lipids, so cultured macrophages may not contain high levels of lipids for *Salmonella* to acquire and metabolize. *Salmonella* has been observed in lipid-rich macrophages during infection (Brown et al., 2010), indicating fatty macrophages are a relevant niche and worth investigating. Additionally, standard medium contains high levels of glucose, and *Salmonella* has been shown to catabolize glucose within macrophages (Bowden et al., 2009; Eisele et al., 2013). In macrophages with reduced glucose or excess lipids, lipids may play a more significant role as a carbon and energy source for *Salmonella*. I therefore tested whether lipid metabolism genes contribute to colonization of macrophages cultured in glucose-free medium with oleic acid, which results in the accumulation of lipid droplets (**Figure 5-12**), or glucose-free medium alone. Compared to glucose-containing medium, I found that wild-type *Salmonella* replicated similarly within macrophages in glucose-

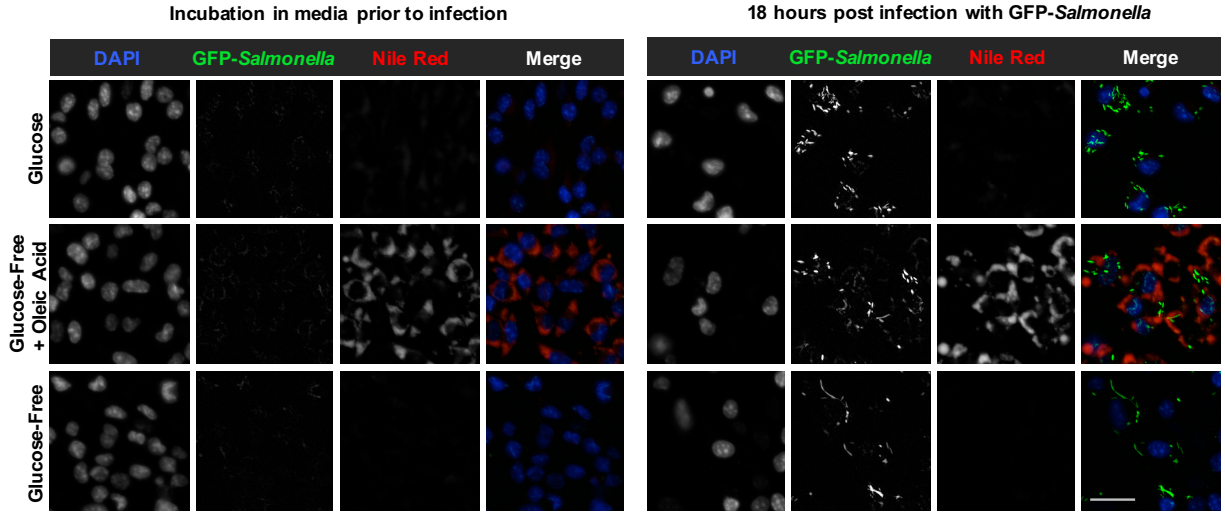

Figure 5-12. Culturing macrophages in glucose-free medium with oleic acid leads to lipid droplet accumulation. Cells were seeded onto glass coverslips, and transferred into defined medium containing NEAA with the indicated carbon source and activated with interferon-γ for 18-24 hours and fixed. Parallel samples were infected with GFP-expressing wild-type bacteria and fixed after 18 hours. Coverslips were stained with 1 μM DAPI and 1 μg/ml Nile Red, and imaged on a widefield fluorescence microscope using a 40X objective. Similar results were observed for RAW 264.7 macrophages or for macrophages cultured in the absence of NEAA. Scale bar is 20 μm.

free medium with oleic acid, and replicated slightly less in glucose-free medium **(Figure 5-11**). However, loss of lipid metabolism genes conferred no change in growth or replication compared to wild-type bacteria (**Figure 5-9A-D, center, right**).

Levels of diverse macromolecules could affect the aggregate host cell nutritional environment and transform *Salmonella*'s replicative strategy. A previous study reported defects in lipid metabolism mutants when macrophages were cultured in the presence of non-essential amino acids (NEAA), including alanine, asparagine, aspartic acid, glycine, serine, proline, and glutamic acid (Diacovich et al., 2016). I found that culturing BMDMs or RAW 264.7 cells in medium supplemented with NEAA led to increased replication of wild-type *Salmonella* (**Figure 5-11**). Further, mutants lacking import or β-oxidation genes grew only 45% (CFU) and 62% (fluorescence dilution) as well as wild type (**Figure 5-13A,B left; Figure 5-14A,B left**),

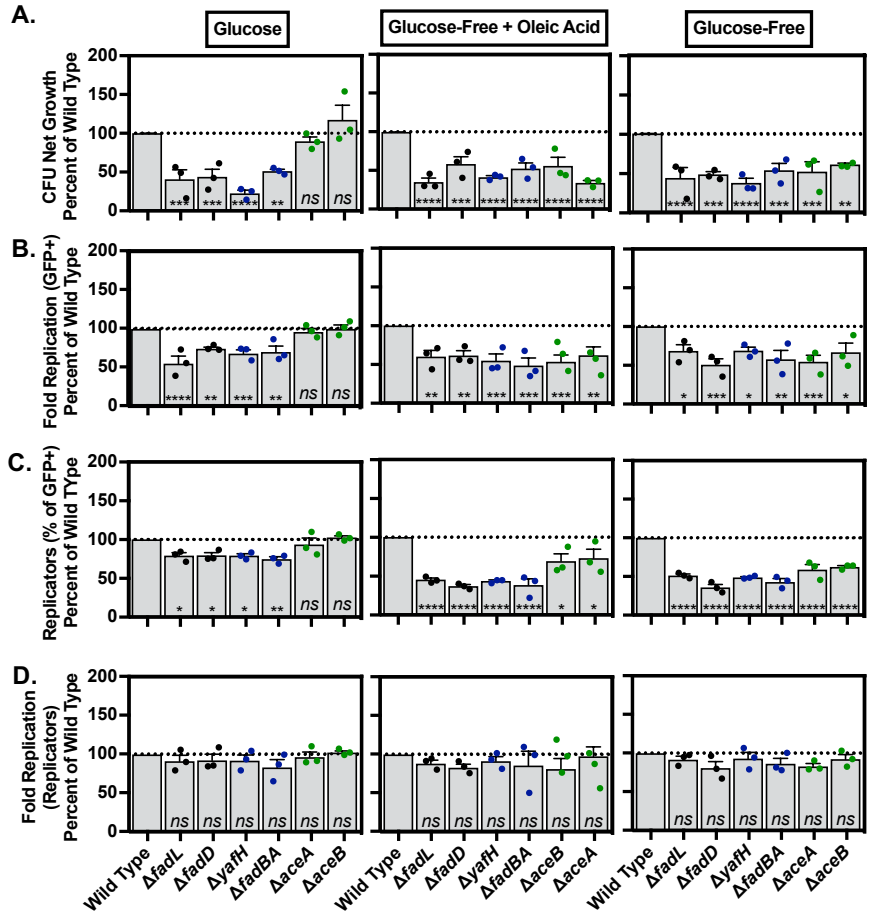

Figure 5-13. Fewer *Salmonella* replicate in IFN-γ -activated BMDMs upon loss of lipid metabolism genes. BMDMs were transferred into defined medium with the indicated carbon source and activated with interferon-γ for 18-24 hours prior to infection with the indicated strains. **(A)** Net growth was calculated as CFU at 18 hours divided by CFU at 2 hours post infection. Fold replication was calculated using fluorescence dilution for the GFP+ population **(B)** and for the replicators **(D)**. Data were normalized to wild type (100%). **(C)** Percentage of bacteria that replicated were gated as GFP-low based on the fluorescence of the inoculum. Average of triplicate samples from each of 3 independent biological replicates (circles) is superimposed on mean and SEM. * $p < 0.05$; ** $p < 0.01$; *** $p < 0.001$; **** $p < 0.0001$ by one-way ANOVA.

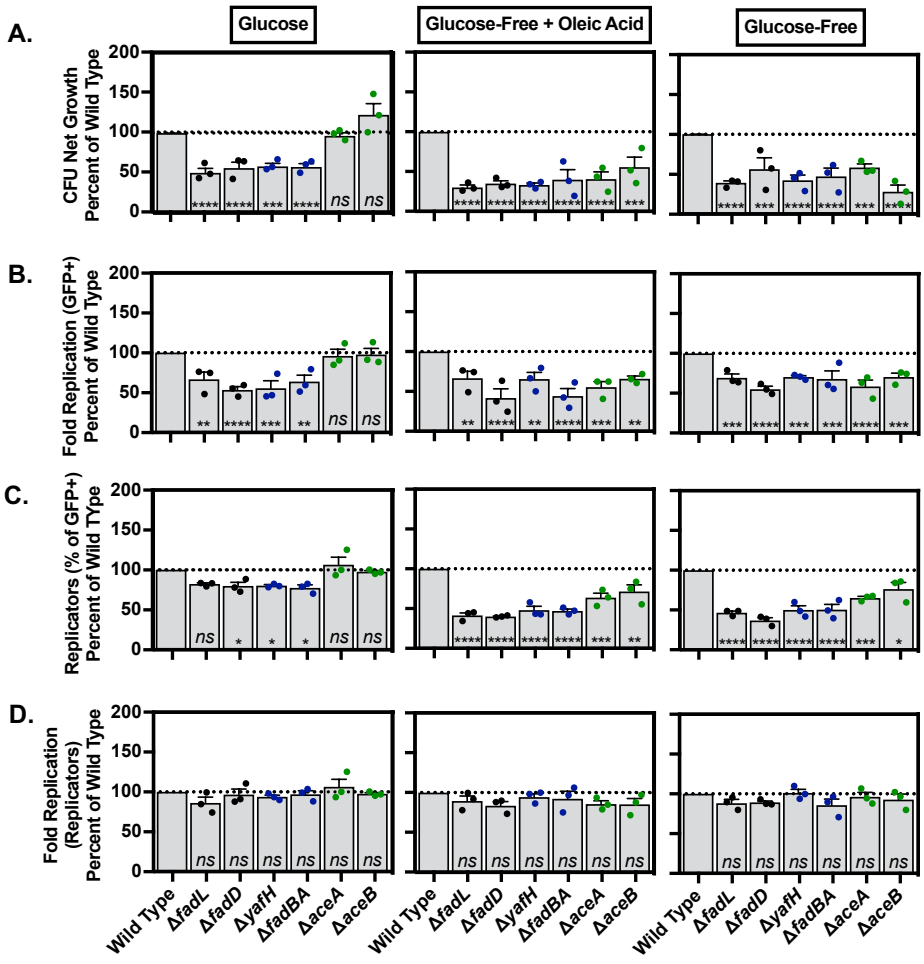

Figure 5-14. Fewer *Salmonella* replicate in IFN-γ-activated RAW 264.7 upon loss of lipid metabolism genes. Experiments and analyses were performed as in Figure 5-13, except macrophages were RAW 264.7. * $p < 0.05$; ** $p < 0.01$; *** $p < 0.001$; **** $p < 0.0001$ by one-way ANOVA.

indicating that *Salmonella* utilizes lipids during infection of macrophages with abundant amino acids. Strains lacking the glyoxylate shunt resembled wild type, indicating that when bacteria are using lipids for carbon and energy, other glycolytic carbon sources are available to replenish metabolic intermediates. Thus, although other carbon and energy sources contribute to growth, lipids are a key nutrient source during infection of certain types of macrophages.

E. FEWER BACTERIA REPLICATE WITHIN MACROPHAGES IN THE ABSENCE OF LIPID METABOLISM GENES

I next established whether the observed defects in replication were due to fewer replicating bacteria, which would suggest that only a subset of bacteria utilize lipids, or a reduced extent of replication for all replicating bacteria, which could indicate that all bacteria use lipids in addition

to other carbon sources. To distinguish between these possibilities, I employed fluorescence dilution and flow cytometry to directly measure bacterial replication. I focused on replicating bacteria, which comprised ~78% of the population during wild-type infection of glucose-rich macrophages (**Figure 5-11C**). I found that a smaller fraction of bacteria lacking import (black dots) or β-oxidation (blue dots) genes replicated relative to wild type (~62% of total) (**Figure 5-13C, left; Figure 5-14C, left**), but that the mutant bacteria that did replicate did so to a similar extent as wild type (**Figure 5-13D, left; Figure 5-14D, left**). Together, these data suggest that a subset of wild-type *Salmonella* primary utilize lipids, and the remaining bacteria primary utilize other carbon souces. In the absence of lipid metabolism genes, the "lipid-users" no longer replicate, but the "non-lipid-users" experience no change in replication.

To better visualize these data, I termed "non-lipid-users" the population that replicated in the absence of lipid metabolism genes (~62% of total), and "lipid-users" the difference between the proportion of replicating wild-type and mutant bacteria (~16% of total) **(Figure 5-15**). I also calculated the fraction of replicating bacteria that used lipids (~21% of replicators) and did not use lipids (~79%).

F. GLUCOSE LIMITATION INCREASES THE PROPORTION OF BACTERIA UTILIZING LIPIDS AND CONFERS A REQUIREMENT FOR THE GLYOXYLATE SHUNT IN MACROPHAGES

In vivo, *Salmonella* inhabits diverse macrophages, which may contain varying levels of glucose and lipids. I next tested the role of import and β-oxidation genes when NEAA-supplemented macrophages were cultured in the absence of glucose, with or without oleic acid. I hypothesized that lipids may play a more significant nutritional role for *Salmonella*, which would result in more severe defects in growth and replication for the mutants. Indeed, under these conditions, the proportion of replicating bacteria utilizing lipids increased from ~21% to ~48% based on the defects in the mutants (**Figure 5-13C, center; Figure 5-14C, center;**

Figure 5-15). Given that the overall replication of wild-type bacteria remained essentially unchanged in glucose-free medium with oleic acid, this indicates that more bacteria utilize lipids as a nutrient source under glucose limitation.

My previous results indicated that the glyoxylate shunt (green dots) was dispensable for growth in macrophages cultured with glucose and NEAA (**Figure 5-13 left; Figure 5-14 left**). The glyoxylate shunt is required during growth on lipids in the absence of glucose, and bridges the TCA cycle to replenish glycolytic intermediates that are withdrawn for biosynthesis. However, when NEAA-macrophages were cultured in glucose-free medium with or without oleic acid, mutants lacking the glyoxylate shunt had reduced growth and replication (**Figure 5-13,14 center, right**). Thus, for certain bacteria or in certain stages of infection, lipids may be the sole source for carbon, energy, and for replenishing metabolic intermediates, necessitating the activity of the glyoxylate shunt.

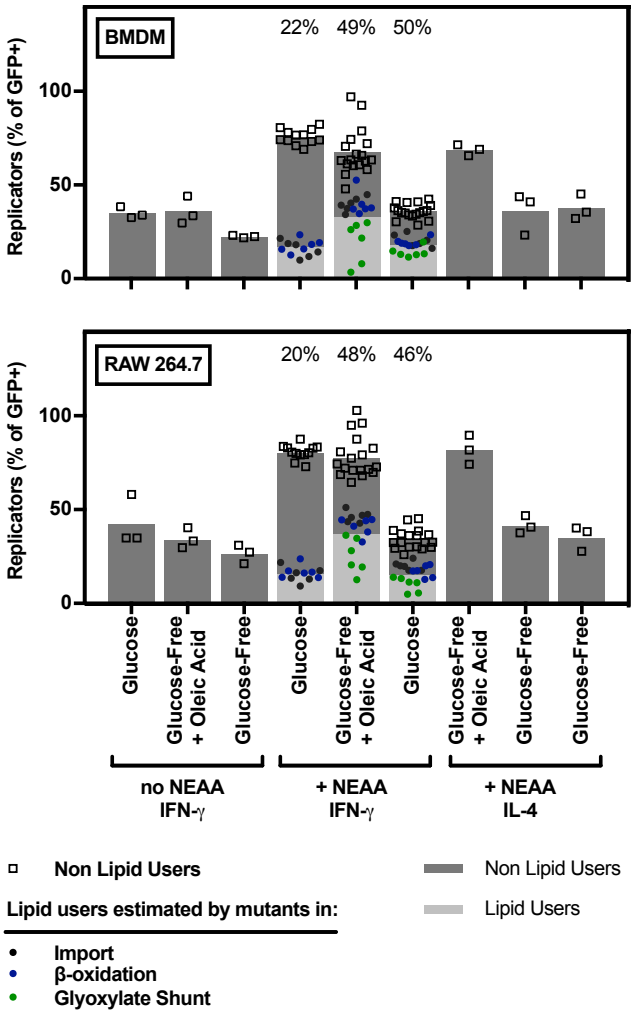

Figure 5-15. Calculated estimates of the proportion of wild-type bacteria using lipids based on mutant defects. Raw percentage of replicating bacteria from **Figures 5-9, 5-13, 5-14, 5-17, 5-18** were used to estimate the proportion of lipid-users and non-lipid-users. For mutants exhibiting defects in growth, replication, and percentage of replicating bacteria, the proportion of bacteria utilizing lipids was estimated as (% of wild-type replicators of total) – (% of mutant replicators of total). Each calculated estimate is represented as a dot (black = import; blue dots = **β**-oxidation; green dots = glyoxylate); mean estimate is the light gray bar. The proportion of non-lipid-users was determined as the percent of mutant replicators of total (open squares; dark gray bar). Lipid-users as a percentage of replicating bacteria are noted in text above the bars.

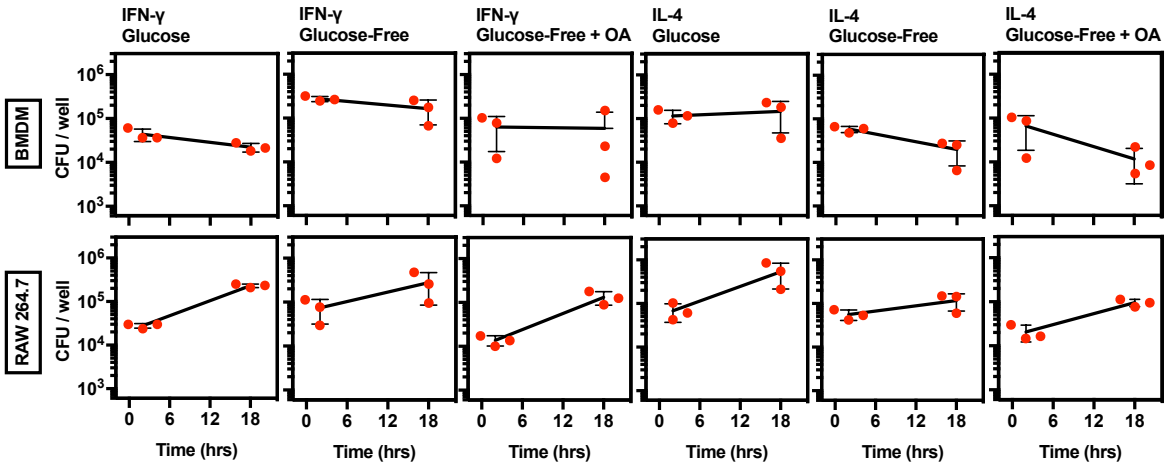

Figure 5-16. Unnormalized CFU data from Figures 5-13, 5-14, 5-17, 5-18. Average of triplicate samples from each of 3 independent biological replicates (red circles) is superimposed on mean and SEM. BMDMs are more permissive than RAW 264.7 macrophages. Interferon-γ-activated cells are better killers than interleukin-4-activated cells in the presence of glucose.

G. ANTI-INFLAMMATORY MACROPHAGES LIMIT *SALMONELLA* ACCESS TO LIPIDS

Salmonella may occupy differentially polarized macrophages, which differ in microbiocidal activities, overall function, and cellular metabolism (**Figure 5-16**) (Eisele et al., 2013; Saliba et al., 2016). My previous experiments were in M1 pro-inflammatory macrophages, which utilize glucose and may allow *Salmonella* increased access to lipids. In contrast, M2 macrophages use oxidative metabolism and *Salmonella* may not be able to acquire lipids. To investigate the role of lipids in alternatively activated macrophages, I treated BMDMs and RAW 264.7 cells with interleukin-4 (IL-4), which induces alternative M2 activation (Eisele et al., 2013). In IL-4-activated macrophages cultured with or without glucose or oleic acid, lipid metabolism mutants exhibited similar growth to wild-type bacteria (**Figure 5-17; Figure 5-18**), indicating lipids are not required for *Salmonella* growth in M2 anti-inflammatory macrophages. Further, I found that wild-type *Salmonella* had reduced growth and replication in M2 macrophages cultured in glucose-free medium with oleic acid, compared to M1 macrophages cultured in the same medium (**Figure 5-11**). Thus, alternative activation restricts *Salmonella* access to lipids.

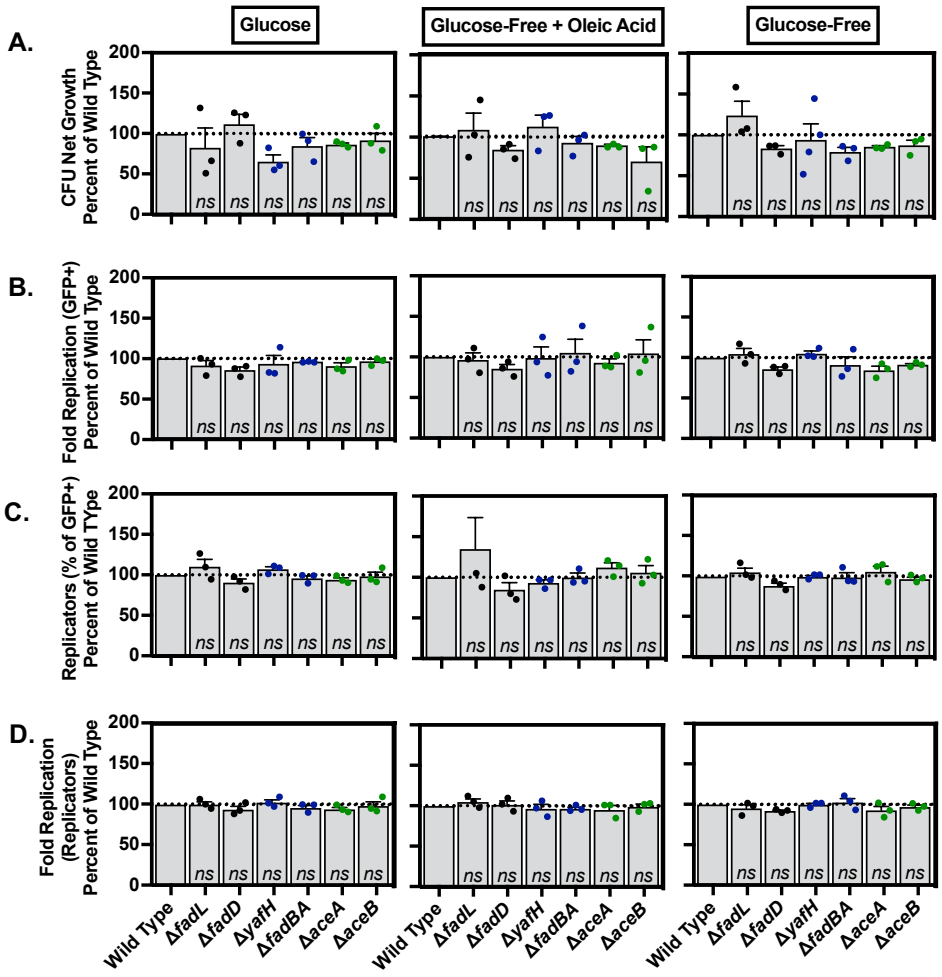

Figure 5-17. Loss of lipid metabolism genes does not affect replication in IL-4-activated BMDMs. Experiments and analyses were performed as in **Figure 5-13**, except macrophages were activated with interleukin-4 18-24 hours prior to infection. * $p < 0.05$; ** $p < 0.01$; *** $p < 0.001$; **** $p < 0.0001$ by one-way ANOVA.

H. DISCUSSION

The role of lipids as a nutrient source for *Salmonella* within host cells is not well understood. Several reports suggest lipid genes are dispensable in macrophages and epithelial cells (Bowden et al., 2010, 2014; Garcia-Gutierrez et al., 2016), but a recent study identified defects for several lipid mutants within macrophages (Diacovich et al., 2016). In this report, I found that a subset of *Salmonella* (~16% of total; ~21% of replicators) utilizes lipids as a carbon and energy source during infection of macrophages, based on defects in mutants lacking import and β-oxidation genes (**Figure 5-13, Figure 5-14**). These defects were specific for M1 macrophages where culture medium was supplemented with non-essential amino acids (NEAA), and I

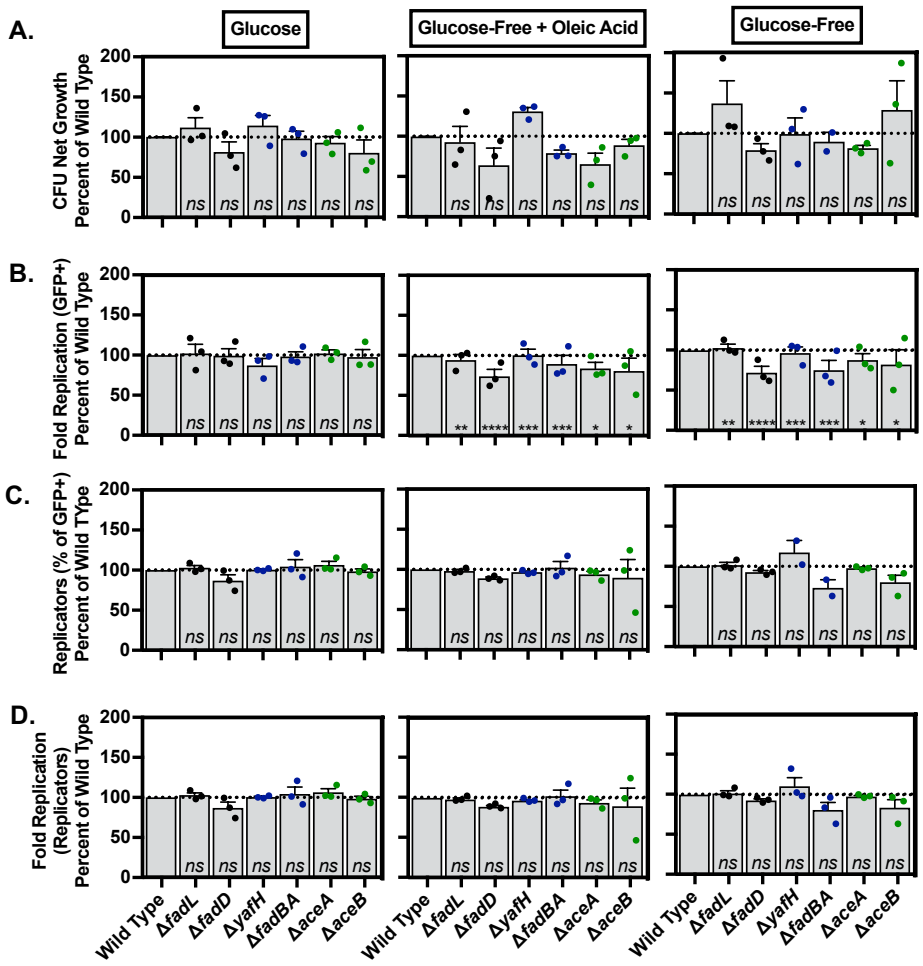

Figure 5-18. Loss of lipid metabolism genes does not affect replication in IL-4-activated RAW 264.7. Experiments and analyses were performed as in **Figure 5-17**, except macrophages were RAW 264.7. * $p < 0.05$; ** $p < 0.01$; *** $p < 0.001$; **** $p < 0.0001$ by one-way ANOVA.

observed similar defects between primary BMDMs and RAW 264.7 cells. I also found that eliminating glucose from the macrophage culture medium conferred an additional requirement for the glyoxylate shunt, which replenishes TCA cycle intermediates in the absence of glucose. Thus, lipids represent a relevant nutrient source for *Salmonella* during infection of specific kinds of macrophages, and provide the sole carbon source during growth in glucose-limited macrophages.

What determines whether *Salmonella* utilizes lipids within macrophages? One possibility is that bacteria switch to utilizing lipids as glucose is depleted over time. However, this is inconsistent with the finding that a large proportion of bacteria lacking lipid metabolism genes still replicate similarly to wild-type (**Figure 5-13C; Figure 5-14C**). This supports the existence of

separate groups of “lipid-users” that cannot replicate in the absence of lipid metabolism genes and “non-lipid-users” which do replicate in the absence of lipid metabolism genes, and thus likely never utilize lipids (**Figure 5-15**). It is possible that these two subpopulations are in distinct subcellular locations within the macrophage which influences replication (Knodler et al., 2014; Wrande et al., 2016), or within distinct macrophages in the same culture dish (Saliba et al., 2016). Future work to elucidate replication of individual bacteria from isolated cells or subcellular compartments could examine these possibilities.

Alternatively, interbacterial competition for nutrients and niches could drive a subset of bacteria to utilize lipids under certain circumstances. When glucose was removed from the macrophage culture medium, mutants lacking lipid metabolism genes exhibited a larger defect in the proportion of replicating bacteria (**Figure 5-13C center; Figure 5-14C center**) (Diacovich et al., 2016). This result suggests some “non-lipid-users” become “lipid-users” in order to replicate when glucose is limited in the macrophage culture medium (**Figure 5-15**), which supports the idea that competition drives bacteria to metabolize lipids. I also found that lipid metabolism genes were only required when macrophage culture medium was supplemented with NEAA (**Figure 5-13; Figure 5-14**), which increased wild-type *Salmonella* growth. Further, a larger proportion of bacteria replicated in macrophages with NEAA than without (**Figure 5-11**). As *Salmonella* acquires the majority of amino acids from the host (Steeb et al., 2013), surplus exogenous NEAA may increase replicative capacity, driving some bacteria to metabolize lipids. However, I found different results for *Salmonella* in RAW 264.7 cells, which also enable increased bacterial growth due to surplus iron (**Figure 5-11, Figure 5-16**) (Fritsche et al., 2012). Mutation of lipid metabolism genes did not confer a defect for *Salmonella* in the absence of NEAA, nor a larger defect in the presence of NEAA (**Figure 5-9, Figure 5-14**). Accordingly, I found that the same proportion of bacteria replicated in RAW 264.7 as in BMDMs, indicating there was no change in access to replicative niches (**Figure 5-11**). Thus, non-lipid carbon is not limited for replicating bacteria in RAW 264.7 and BMDMs, but availability of non-lipid replicative

niches is limited. Taken together, these data suggest that lipid utilization is driven by competition for replicative niches. In the presence of NEAA, *Salmonella* appears to gain access to additional replicative niches replete with lipids where otherwise nonreplicating *Salmonella* can replicate. Thus, amino acids may play a key role in determining the metabolic strategy of intracellular *Salmonella* (Eriksson et al., 2003; Liu et al., 2017; Shi et al., 2006).

Finally, I demonstrated that *Salmonella* does not utilize lipids in anti-inflammatory M2 macrophages (**Figure 5-17, 5-18**), which utilize oxidative phosphorylation of fatty acids (Galván-Peña and O'Neill, 2014; Jha et al., 2015). M2 macrophage metabolism may thus limit *Salmonella* access to lipids. Furthermore, *Salmonella* replication was primarily dependent on glucose levels, as culturing macrophages in glucose-free medium strongly reduced wild type growth and replication and this reduction was not rescued with oleic acid supplementation (**Figure 5-11**). This result supports the idea that macrophage metabolism restricts availability of nutrients for intracellular bacteria (Galván-Peña and O'Neill, 2014; Jha et al., 2015; Rodriguez-Prados et al., 2010), and that the host immune activation state can influence pathogen virulence (Eisele et al., 2013; Muraille et al., 2014; Saliba et al., 2016).

I also investigated the role of lipid metabolism genes *in vivo*. I demonstrated that loss of lipid degradation genes attenuates *Salmonella* infection in the 129Sv mouse chronic typhoid model (**Figure 5-5, 5-6, 5-7**). The *in vivo* results are in agreement with another report, which also used 129Sv mice and competitive infection (Fang et al., 2005); however, they only found a phenotype in the mesenteric lymph nodes. This could be due to more rapid clearance of bacteria in other organs, as the authors used an auxotrophic *Salmonella* background. An additional report found a subtle defect for lipid mutants during infection of BALB/c mice, which model acute infection (Steeb et al., 2013). In contrast to these results, several published studies have not shown systemic phenotypes for lipid mutants in BALB/c mice (Becker et al., 2006; Fang et al., 2005; Golubeva et al., 2016; Kim et al., 2006; Spector et al., 1999; Tchawa Yimga et al., 2006b). It is possible that this difference is due to different requirements for lipid

metabolism in acute and chronic infection, though one study found no defect in a transgenic immunocompetent BALB/c model of chronic infection (Kim et al., 2006).

I propose instead that underlying biases in the host cytokine response influence macrophage polarization and thus *Salmonella* lipid utilization, consistent with the macrophage data that *Salmonella* utilizes lipids in M1 macrophages. 129Sv mice initially respond to infection by *Salmonella* and other microbes with production of Th1 cytokines, which in turn polarize macrophages toward an M1 pro-inflammatory state (Eisele et al., 2013; Mills et al., 2000; Muraille et al., 2014; Rivera and Tessarollo, 2008; Sellers et al., 2011; Swihart et al., 1995). Thus, during early infection of 129Sv mice, *Salmonella* is likely within M1 macrophages. The data indicate that *Salmonella* utilizes lipids in M1 macrophages *in vitro*, so it is probable that lipid mutant defects *in vivo* are due to the inability to replicate in M1 macrophages early in infection. The data also shows that *Salmonella* does not use lipids in M2 macrophages; this supports the idea that *Salmonella* exclusively uses glucose at later timepoints in 129Sv mice, when M2 macrophages predominate as the infection transitions toward a chronic state (Brown et al., 2010; Eisele et al., 2013; Thompson et al., 2009).

In contrast to 129Sv and many other mouse strains, BALB/c mice are biased toward a Th2 anti-inflammatory phenotype in response to infection (Davis et al., 2013; Tumitan et al., 2007; Wells et al., 2003), though this has not been demonstrated specifically for *Salmonella* infection. As a result, I propose that in BALB/c mice *Salmonella* is predominantly within M2 macrophages and does not use lipids, which is consistent with the data that *Salmonella* lipid mutants have no defects in M2 macrophages. This rationale would explain why *Salmonella* lipid mutants are defective in Th1-biased 129Sv mice in this study, but not in Th2-biased BALB/c mice in many other studies.

My study employed mutants lacking genes in every step of lipid metabolism. In addition to the canonical acyl-coA-dehydrogenase (*fadD*) and β-oxidation enzymes (*yafH-fadB-fadA*), *Salmonella* encodes secondary enzymes (*ydiD, ydiO-yfcX-yfcY*), which are required for

anaerobic growth on fatty acids in *E. coli* (Campbell et al., 2003; Morgan-Kiss and Cronan, 2004). I found that *fadD* was required for both aerobic and anaerobic growth as well as *in vivo* infection; *ydiD* was dispensable. The two β-oxidation pathways were generally specific for aerobic and anaerobic growth *in vitro* (**Figure 5-2, Table 5-1**). In mice, the two pathways were surprisingly able to compensate for each other, though it is unclear whether this occurs within a single bacterium or across the population. In contrast, the secondary pathway was unable to compensate for loss of canonical genes during infection of macrophages. These results could suggest that *Salmonella* utilizes lipids in anaerobic environments to allow expression of the secondary pathway *in vivo*. Our understanding of lipid gene expression in *Salmonella* is limited to parallel work in *E. coli*, however, functional differences have been described (Iram and Cronan, 2006), so it is possible that additional host factors may activate expression of the secondary pathway. Defining the specific *in vivo* environment in which *Salmonella* utilizes lipids could facilitate our understanding of the interplay between these two beta-oxidation pathways.

In conclusion, lipids are a relevant nutrient source for *Salmonella* during infection. Although diverse pathogens are known to utilize fatty acids during infection (Daniel et al., 2011; Dunn et al., 2009; Kumar et al., 2006; Lindsey et al., 2008; Lorenz and Fink, 2001; McKinney et al., 2000; Wall et al., 2005), little is known about the specific microenvironments in which they do so. I found that *Salmonella* utilizes lipids in M1 macrophages, where glucose is limited but amino acids are abundant. This is consistent with the *in vivo* data using Th1-based 129Sv mice, which initially respond by polarizing macrophages toward an M1 state. Thus, the *Salmonella* nutritional strategy can be strongly affected by the host immune state and nutrient availability. Diverse pathogens likely alter their infectious strategy based on factors specific to the particular microenvironment, and these factors may influence metabolism, replication, and the outcome of infection.

I. MATERIALS AND METHODS

Bacterial strains and growth conditions. *Salmonella enterica* serovar typhimurium wild-type strain SL1344 (Merritt et al., 1984) (ALR#001; DET#0001) and derivatives were cultured in LB medium containing 30 µg/ml streptomycin, 50 µg/ml ampicillin, 30 µg/ml kanamycin, or 34 µg/ml chloramphenicol. Liquid cultures were incubated overnight at 37 °C with aeration. Deletion strains were marked at the indicated locus with kanamycin or chloramphenicol resistance cassettes (Datsenko and Wanner, 2000; Kim et al., 2014), which were P22 phage transduced into SL1344 (Davis et al., 1980) (ALR#009, #015, #077, #081, #085, #089, #097, #298, #439, #461, #526). The resistance cassette was removed by induction of FLP recombinase or I-SceI to yield a 84-bp scar or no scar, respectively (ALR#034, #038, #171, #175, #179, #183). Mutant strains were validated by PCR and growth on oleic acid.

Complementation plasmids were derived from medium-copy plasmid pRB3-273c (Berggren et al., 1995). The target gene and its promoter were amplified from *Salmonella* genomic DNA (350 bp upstream and 50 bp downstream of the gene) using PCR primers containing restriction digest sites for BamHI and HindIII (*fadL*, *aceA*, *aceB*) or BamHI and KpnI (*fadD*). For *aceA*, two amplicons were initially generated: the *aceBA* promoter region with a downstream KpnI recognition sequence, and the *aceA* gene with *aceB* Shine-Dalgarno sequence and KpnI recognition sequence engineered into the upstream PCR primer. The two amplicons were digested using KpnI, ligated, and amplified as a single fragment using PCR. For *aceB*, the entire *aceBA* operon was amplified, digested with HpaI to remove 1157 bp of the *aceA* gene, ligated, and amplified as a single fragment using PCR. The fragment thus contained the promoter, *aceB*, the 31 bp intergenic region, the initial 117 nucleotides and final 31 bp of *aceA*. This approach was employed because the promoter-*aceB* amplicon only partially complemented mutants lacking *aceB* for unknown reasons. Amplicons were digested with BamHI and HindIII or KpnI, gel-purified, ligated into linearized pRB3-273c, and verified by sequencing of the entire

insertion prior to transformation into mutant strains (ALR#493, #495, #497, #499, #510, #512, #591, #603).

For fluorescence dilution experiments, strains were transformed with pDiGi and chromosomally marked with GFP at the *rpsM* locus using P22 phage transduction (Vazquez-Torres et al., 1999) (ALR#258, #259, #260, #261, #262, #282, #286). To induce expression of dsRed prior to infection, strains were cultured overnight in medium containing 170 mM MES pH 5.0, 5 mM KCl, 7.5 mM $(NH_4)_2SO_4$, 0.5 mM K_2SO_4, 1 mM KH_2PO_4, 10 mM $MgCl_2$, 0.3% glycerol, 0.1% casamino acids, 10 mM arabinose with appropriate antibiotics (Helaine et al., 2010). We found that pDiGc, which encodes GFP under the *rpsM* promoter, significantly hindered Salmonella infection, presumably due to high GFP expression (**Appendix E**).

Bacterial growth assays. For broth growth experiments, overnight cultures were washed in PBS and diluted to an OD_{600} of 0.01 in 300 µl of LB or M9 minimal medium supplemented with 0.004% histidine, 1 mM $MgSO_4$, 100 µM $CaCl_2$ and either 0.4% dextrose, 0.4% glycerol, or 0.1% sodium oleate and 1% igepal CA-630, which was necessary to solubilize oleate. Bacteria were grown in 96-well plates shaking in an Eon or Synergy H1 Microplate Spectrophotometer (BioTek) at 37 °C, and the OD600 was recorded every 20 minutes.

For growth on solid medium, overnight cultures were washed in PBS, resuspended in PBS to OD_{600} of 1.0, and 3 µL was spread onto M9 minimal agar plates supplemented with 1 mM $MgSO_4$, 100 µM $CaCl_2$, 0.004% histidine, 1.5% agar, 1% igepal CA-630, and either 0.4% dextrose, 0.1% sodium oleate, 0.1% sodium decanoate, or 0.1% sodium octanoate. No growth was observed in the absence of carbon. For anaerobic growth, plates were supplemented with 25 mM nitrate as an alternative electron acceptor; no anaerobic growth was observed in the absence of nitrate. Anaerobic plates were grown at 37 °C within GasPak EZ anaerobe pouches (BD).

Cell culture and bone marrow derived macrophage (BMDM) generation. Macrophages were routinely cultured in DMEM high glucose (Sigma) supplemented with 10% fetal bovine

serum, 2 mM L-glutamine, 1 mM sodium pyruvate, 10 mM HEPES, and 50 μM β-mercaptoethanol. To generate bone-marrow derived macrophages, femurs and tibias from 4-10 week old wild-type 129S6/SvEvTac mice (Taconic Laboratories) were flushed with PBS to recover bone marrow, layered over Histopaque-1083 (Sigma), and centrifuged for 25 minutes at 500 x *g*. The mononuclear cell fraction was recovered and washed in complete media. Cells were seeded at 1-2 x 10^5 cells/ml in complete medium supplemented with 30-35% conditioned medium from 3T3 cells expressing MCSF, and fed 3 days later. After 1 week in culture, BMDMs typically replicated 5-10 fold under these conditions. Twenty-four hours prior to infection, macrophages were transferred into defined glucose-free DMEM supplemented with 10% fetal bovine serum, 2 mM L-glutamine, 10 mM HEPES, 50 μM β-mercaptoethanol, and 1X non-essential amino acids (Sigma). Importantly, we observed minimal replication of *Salmonella* within macrophages when defined DMEM medium did not contain non-essential amino acids (**Figure 5-11**). Glucose-free medium was supplemented with 4.5 g/L glucose or 600 μM oleic acid (conjugated 6:1 with BSA; concentrated oleic acid dissolved in 0.1 M Na_2CO_3 at 55 °C was added to BSA dissolved in PBS, stirred for 1 hour at 37 °C, filter-sterilized, and stored at -20 °C). Supplementation with BSA vehicle control yielded results identical to glucose-free medium. Macrophages were activated with 2 ng/ml recombinant murine IFN-γ (PeproTech) or 20 ng/ml recombinant murine IL-4 (PeproTech) for 18-24 hours prior to infection.

Infection of cell culture macrophages. For fluorescence dilution experiments, bacteria were added to BMDMs at a concentration of 3 x 10^7 CFU/ml in media. We found that this protocol reproducibly yielded infection of 70-80% of BMDMs with dsRed-expressing bacteria by flow cytometry (data not shown). After 45 minutes and 2 hours, medium was exchanged for medium containing 100 and 10 μg/ml gentamicin, respectively. At 2 and 18 hours post infection, parallel samples were washed three times with PBS and lysed with 0.1% Triton X-100. A portion of the lysate was diluted in PBS and plated to determine colony-forming units (CFU). Net growth was calculated as the recovered CFU at 18 hours divided by that at 2 hours. The remainder of

the lysate was centrifuged for 20 minutes at 2500 x *g* at 10 °C, fixed with 1.6% paraformaldehyde, and analyzed using a CyAn ADP cytometer (Beckman Coulter). A minimum of 30,000 GFP+ events were collected for analysis. Data were analyzed with FlowJo. Samples were gated for GFP-positive bacteria. Bacterial fold replication was calculated as the dsRed geometric mean of the inoculum divided by that of the GFP+ population at 18 hours post infection.

Mouse infections. Experimental protocols were approved by the University of Colorado Institutional Committee for Animal Care and Use. Seven-week-old male and female 129S6/SvEvTac mice (Taconic Laboratories) were used for competitive infection studies. Mice were inoculated with a 1:1 mixture of two differentially marked strains. For orogastric infections, animals were fasted 8-12 hours prior to oral gavage with 1×10^9 each strain (2×10^9 total in 100 µl). For intraperitoneal infections, animals were inoculated with 1×10^3 each strain (2×10^3 total in 100 µl). At two weeks post infection animals were euthanized by CO_2 asphyxiation followed by cervical dislocation. Cecum, Peyer's patches, mesenteric lymph nodes, spleen, and liver were harvested, homogenized in PBS, and serially diluted to enumerate CFU. The competitive index (CI) for each organ was calculated as ($CFU_{strain\ A}$ / $CFU_{strain\ B}$) output / ($CFU_{strain\ A}$ / $CFU_{strain\ B}$) input.

Statistics. *p*-values were calculated using one-way ANOVA or one-sample t test (GraphPad Prism) and considered significant if $p < 0.05$ as described in the figure legends

CHAPTER 6. *SALMONELLA* REPLICATES MORE IN MACROPHAGES CO-CULTURED WITH HEALTHY ERYTHROCYTES, T CELLS, OR SENESCENT ERYTHROCYTES

A. INTRODUCTION

In vivo, immune cells constantly interact with other host cells, and these interactions can drive changes in cellular polarization and function. Macrophages interact with healthy and damaged erythrocytes, lymphocytes, endothelial cells, and hepatocytes, among others. Although we know how certain macrophage interactions contribute to the systemic immune response, we know little about how they affect the outcome of individual infected macrophages. Since macrophages are a critical niche for certain intracellular pathogens (Thi et al., 2012), understanding the cellular interactions that affect the outcome of infection for the macrophage is relevant fo understanding the outcome of infection for the host.

Erythrocytes outnumber macrophages by at least two orders of magnitude, and these cells frequently interact in the bone marrow, spleen, and circulation. In the bone marrow, macrophages support erythropoiesis via direct signaling interactions and secretion of cytokines and other soluble factors (Gordon and Martinez-Pomares, 2017). In the spleen, macrophages phagocytose senescent erythrocytes, identified by surface changes including exposure of phosphatidylserine (Bratosin et al., 1998). Circulating macrophages also import hemoglobin released from damaged erythrocytes to protect other cells from oxidation by free heme (Alam et al., 2017; de Back et al., 2014). Within macrophages, hemoglobin-derived iron is recycled, stored, and released as needed by several iron-metabolism proteins including heme oxygenase, hepcidin, and ferroportin (Alam et al., 2017). Macrophages also clear immune complexes and pathogens bound to erythrocyte surface complement receptors (de Back et al., 2014), as well as hemophagocytose whole healthy erythrocytes during pathological macrophage activation (Akilesh et al., 2019; Behrens et al., 2011; Milner et al., 2010; Ohyagi et al., 2013; Zoller et al., 2011). Thus, macrophages extensively interact with erythrocytes directly and indirectly in many tissues.

T cell activation is dependent on interactions with macrophages and other antigen-presenting cells (Smith-Garvin et al., 2009). Macrophages digest foreign material and display it on surface molecules which match receptors on particular T cells. During infection, pathogen products drive expression of additional macrophage surface molecules and stimulate proliferation and direct the differentiation of matching T cells. Macrophages and T cells also interact indirectly via production of cytokines, including interferon-γ, interleukin-4, and interleukin-10 and other soluble factors which influence cellular function (Bingisser et al., 1998; Hsieh et al., 1993). During infection with *Mycobacterium tuberculosis* and other granulomatous pathogens, infected and uninfected macrophages concentrate to contain bacteria; T cells typically ring the macrophages and secrete cytokines to activate macrophages (Co et al., 2004; Egen et al., 2008). Finally, in certain instances, macrophages phagocytose healthy T cells (Nix et al., 2007; Ohyagi et al., 2013), similar to hemophagocytosis of healthy erythrocytes as describe above.

To study the effect of host-host interactions on infection of macrophages, I employed the bacterial pathogen *Salmonella enterica* serovar Typhimurium, which relies on infection of macrophages to cause systemic disease (Fields et al., 1986; Vazquez-Torres et al., 1999). *Salmonella* is ingested through contaminated food or water, traverses the intestinal epithelium, and is phagocytosed by macrophages. Within macrophages, *Salmonella* disseminates systemically to the spleen, liver, and circulation (Bauler et al., 2017; Vazquez-Torres et al., 1999) and can persist within macrophages to cause chronic infections (Monack, 2004). Thus, interactions of erythrocytes or T cells with *Salmonella*-infected macrophages could affect the outcome of colonization. Indeed, we have previously shown that co-culture of macrophages and erythrocytes or T cells increases *Salmonella* load (Nagy et al., 2014; Pilonieta et al.; Silva-Herzog and Detweiler, 2010). Direct or indirect interactions could affect macrophage polarization and function. We have also previously shown that *Salmonella*-infected macrophages hemophagocytose healthy erythrocytes and T cells (McDonald et al., 2016; Nix et

al., 2007), which may affect macrophage function (Gill et al., 1966; Hand and King-Thompson, 1983; Hook et al., 1967). In this study, I established the mechanisms through which erythrocyte and T cell co-culture lead to increased *Salmonella* replication.

B. ERYTHROCYTE CO-CULTURE INCREASES *SALMONELLA* REPLICATION WITHIN MACROPHAGES IN A CONTACT-DEPENDENT MANNER

Macrophages routinely encounter intact nonsenescent erythrocytes, but the impact of these interactions for infected macrophages is unknown. I probed the effect of freshly isolated erythrocytes on intracellular bacterial replication and survival using a cell culture model of *Salmonella* infection of primary bone-marrow derived macrophages (BMDMs). *Salmonella* is rapidly phagocytosed and activates a transcriptional program to defend against macrophage antimicrobials and establish a replication niche (Haraga et al., 2008). BMDMs were infected with *Salmonella* and erythrocytes added after 2 hours. At 18 hours post infection I quantified *Salmonella* bacterial load using plating for CFU and replication using the pDiGi system of bacterial fluorescence dilution (Helaine et al., 2010) (**Figure 5-10**)**.** Inclusion of erythrocytes during infection increased *Salmonella* replication and bacterial load in a dose-dependent manner, but co-culture of macrophages with inert microspheres did not (**Figure 6-1**).

Co-culture could indirectly affect macrophage infection, independent of any interactions between erythrocytes and macrophages. For example, erythrocytes could consume nutrients or signaling factors in the media, reducing those available for macrophages or *Salmonella*. Alternatively, release of soluble factors from erythrocytes such as apoptotic bodies or extracellular vesicles could interact with macrophages. To evaluate whether contact is required for the observed effects on *Salmonella* replication, I separated erythrocytes and macrophages during co-culture by about 1000 μm using a transwell insert (**Figure 6-2A**). The transwell membrane had 0.4 μm pores, which prevents passage of erythrocytes (**Figure 6-2B**) but allows diffusion of some extracellular vesicles, which range in size from 0.04-2 μm

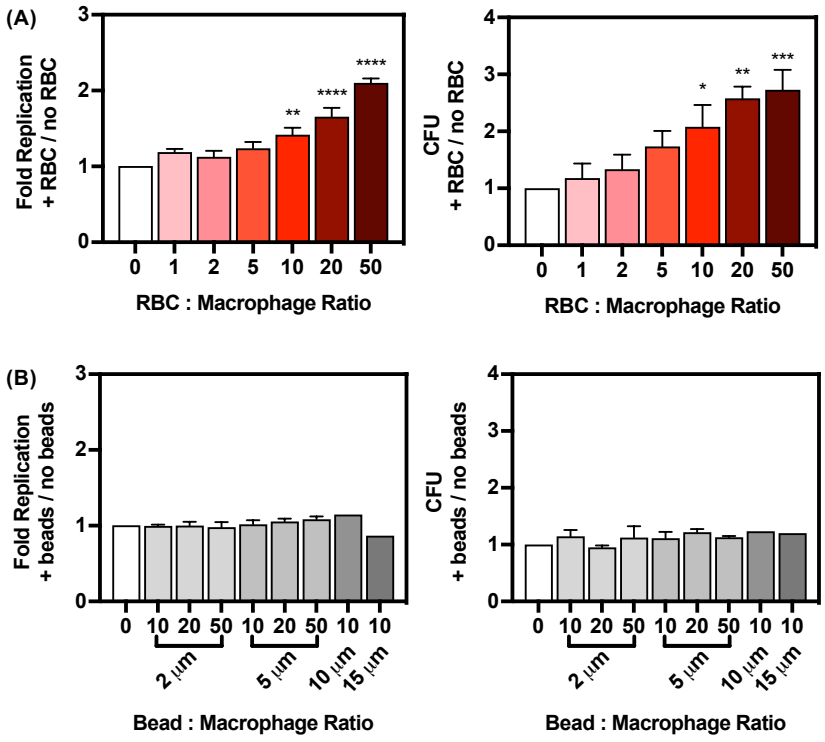

Figure 6-1. Co-culture of erythrocytes but not beads increases *Salmonella* replication and load. BMDMs were infected with *Salmonella* and co-cultured with erythrocytes **(A)** or inert beads **(B)** at the indicated ratios. Fold replication **(left)** and CFU **(right)** are normalized to no co-culture. Data are aggregated mean and SEM of at least 3 biological replicates, except for 10 and 15 μm beads, which are a single experiment. * $p < 0.05$; ** $p < 0.01$; *** $p < 0.001$; **** $p < 0.0001$ by one-way ANOVA compared to no co-culture.

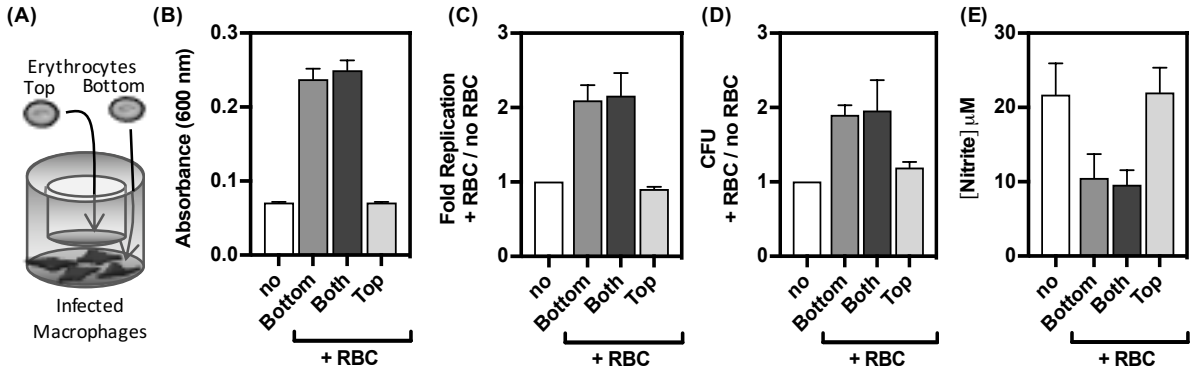

Figure 6-2. Separating erythrocytes and macrophages blocks the effect of erythrocyte co-culture. (A) BMDM were infected and co-cultured with erythrocytes in the indicated compartments of transwell inserts with 0.4 μm pores. **(B)** Absorbance of media from the bottom compartment demonstrates cells from the top compartment did not pass through the transwell. Mean and SD of triplicate samples of a single biological replicate; representative of 3 biological replicates. Samples were processed at 18 hours post infection to determine bacterial replication **(C)**, CFU **(D)** and supernatant nitrite **(E).** Data are mean and SEM of 3 biological replicates.

(Zaborowski et al., 2015). When erythrocytes were added to the bottom compartment of the culture dish, *Salmonella* replicated more as expected (**Figure 6-2C,D**). However, when erythrocytes were added to the top compartment, there was no change to *Salmonella* replication. In case larger extracellular vesicles were blocked by the transwell membrane, I also

added conditioned medium from erythrocyte-macrophage co-cultures, but found conditioned medium had no effect on replication (**Figure 6-3**). Together, these data argue that contact or proximity within 1000 μm is required for erythrocyte co-culture to increase *Salmonella* replication.

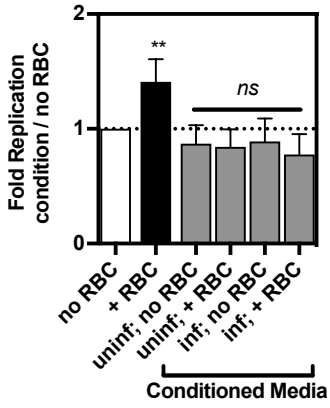

Figure 6-3. Conditioned media from infected macrophage-erythrocyte co-cultures does not increase *Salmonella* replication. BMDM were infected and incubated with conditioned media from uninfected or infected BMDM cultured with or without erythrocytes. Data shown are aggregated mean and SEM from 3 independent conditioned media, each used in 2 biological replicates. ** $p < 0.01$ by one-way ANOVA compared to no co-culture unless otherwise indicated.

C. INCREASED REPLICATION IS INDEPENDENT OF IRON OR LIPID UTILIZATION

Macrophages restrict microbial access to iron in response to infection (Nairz et al., 2007), but erythrocytes represent a source of iron in heme. Previous work suggested *Salmonella* acquired erythrocyte-derived iron because a mutant lacking the ferrous iron transporter FeoB was outcompeted by wild-type bacteria in macrophages co-cultured with erythrocytes (Nagy et al., 2014). However, using the more sensitive fluorescence dilution method to measure replication, I found no defects in an independently constructed *feoB*::cm mutant in macrophages co-cultured with erythrocytes (**Figure 6-4**). I also found that a mutant lacking FeoB and the ferric iron siderophores FepA and IroN, which has reduced ability to acquire iron and is defective in BMDMs, was not rescued by erythrocytes though it was rescued by iron supplementation (**Figure 6-5**). Supplementation of macrophage media with iron or chelation of iron did not modulate erythrocyte-enhanced replication (**Figure 6-6**). I also monitored expression of iron-related genes in *Salmonella* and in macrophages. *Salmonella* did not alter expression of ferrous or ferric iron transporters (*feoB*, *fepB*) during erythrocyte co-culture (**Figure 6-7A**). I also

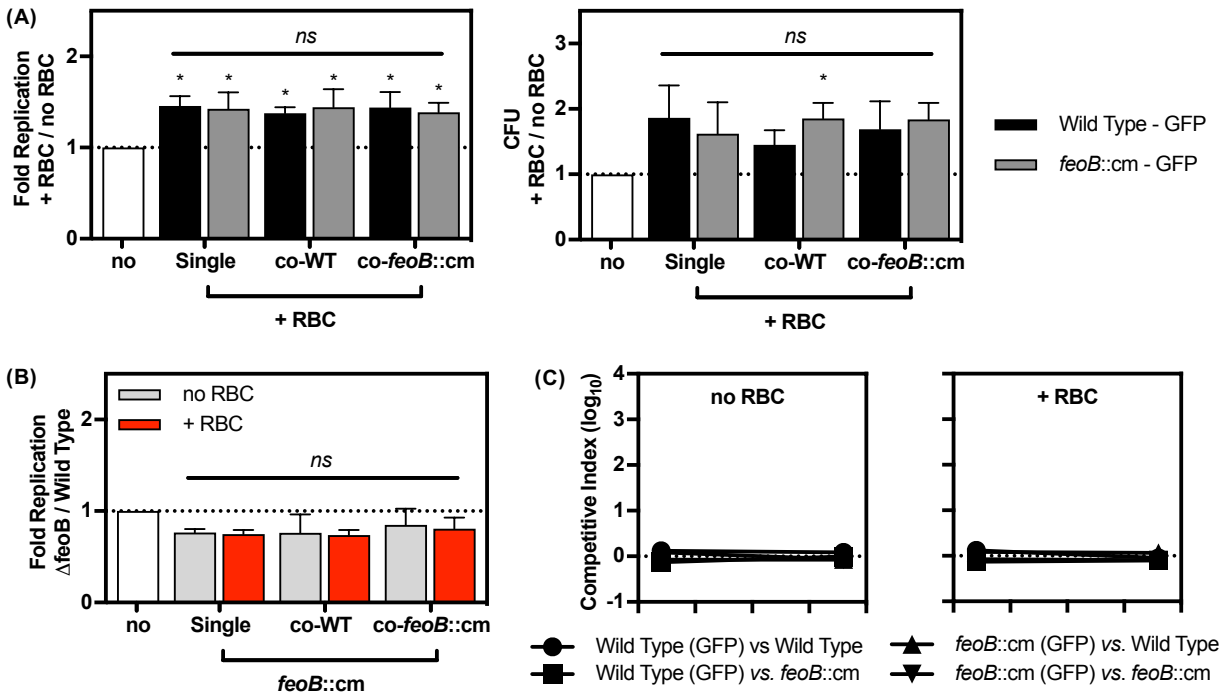

Figure 6-4. *Salmonella* does not require the FeoB ferrous iron transporter for colonization of macrophages or increased replication upon erythrocyte co-culture. BMDM were infected with pDiGi-harboring, GFP-expressing wild type or *feoB*::cm as single infections, or in combination with wild-type or *feoB*::cm bacteria containing pDiGi but not expressing GFP. Infected macrophages were co-cultured with 10:1 erythrocytes and processed at 18 hours post infection. **(A)** Fold replication (**left**) and CFU (**right**) of GFP-expressing bacteria during erythrocyte co-culture are normalized to that without erythrocyte co-culture for the indicated strain combination. **(B)** Fold replication of the *feoB*::cm strain with or without erythrocytes are normalized to that of wild type for the indicated strain combination. **(C)** CFUs were used to determine the competitive index for the indicated co-infections. Data shown are aggregated mean and SEM from at least 3 biological replicates. * $p < 0.05$ by one-way ANOVA compared to white bars unless otherwise noted.

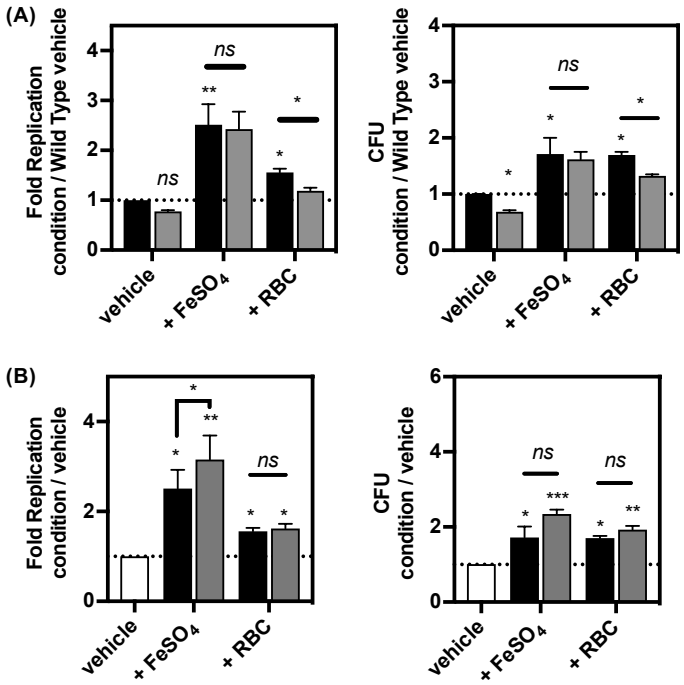

Figure 6-5. Iron supplementation but not erythrocyte co-culture rescues an iron uptake mutant in macrophages. BMDM were infected with the indicated strains and at 2 h.p.i. media was supplemented with 500 μM $FeSO_4$ or erythrocytes. Fold replication (**left**) and CFU (**right**) were normalized to vehicle for wild-type bacteria (**A**) or vehicle for each strain to determine the replication increase (**B**). Data shown are aggregated mean and SEM from at least 3 biological replicates. * $p < 0.05$; ** $p < 0.01$; *** $p < 0.001$; **** $p < 0.0001$ by one-way ANOVA compared to wild type vehicle unless otherwise noted.

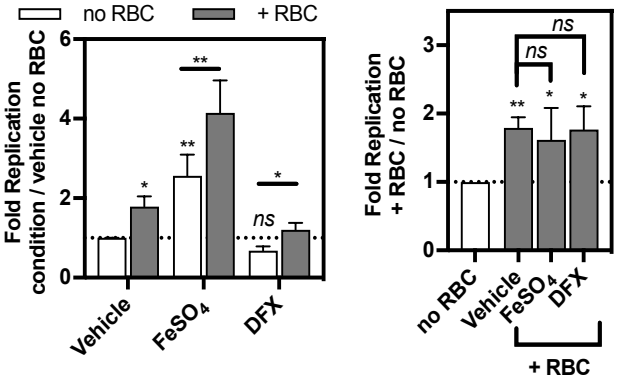

Figure 6-6. Iron chelation or supplementation does not affect erythrocyte-dependent replication increase. BMDM were infected and at 2 h.p.i. media was supplemented with 500 μM $FeSO_4$ or the iron chelator deferasirox (DFX) at 250 μM, with or without erythrocytes. Fold replication of the + RBC condition was normalized to the vehicle no RBC condition for (**left**) or the no RBC condition for each treatment to determine the replication increase (**right**). Data shown are aggregated mean and SEM from at least 3 biological replicates. * $p < 0.05$; ** $p < 0.01$ by one-way ANOVA compared to vehicle no erythrocytes unless otherwise noted.

observed no changes in macrophage expression of genes involved in iron storage, suggesting erythrocyte co-culture does not modulate iron flux in macrophages (**Figure 6-7B**). Finally, preliminary experiments by Toni Nagy indicated that *Salmonella* does not acquire erythrocyte-derived ^{57}Fe by ICP-MS. Together, these data argue that erythrocyte co-culture does not lead to increased iron availability for intracellular bacteria.

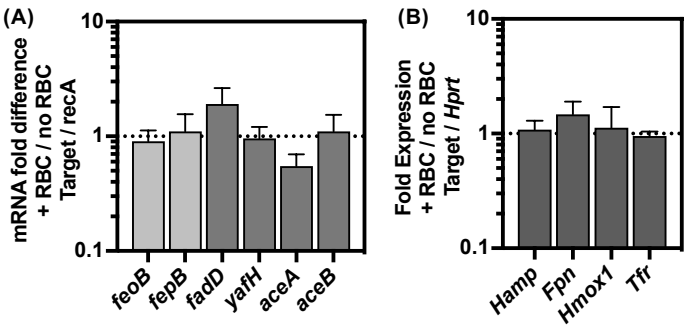

Figure 6-7. Erythrocyte co-culture does not alter expression of iron or lipid metabolism genes. BMDM were infected and co-cultured with erythrocytes. **(A)** At 18 h.p.i. macrophages were lysed to release bacteria and bacterial RNA was harvested. **(B)** Macrophage RNA was harvested at 18 h.p.i. Expression of the indicated genes was normalized to reference genes *recA* or *Hprt*, and to expression in the absence of erythrocytes. Data are aggregated mean and SEM of 3 biological replicates.

I showed in **Chapter 5** that *Salmonella* utilizes lipids as a nutrient source within macrophages. Macrophages phagocytose and degrade erythrocytes, leading to accumulation of lipid droplets (Brown et al., 2010). I next hypothesized that lipids from erythrocytes could serve as a supplementary carbon source for *Salmonella* within macrophages. However, I found that the erythrocyte-dependent replication boost did not require lipid metabolism genes, suggesting *Salmonella* does not use lipids from erythrocytes (**Figure 6-8**). I also observed no changes in mRNA expression of *Salmonella* lipid metabolism genes *fadD*, *yafH*, *aceA*, or *aceB* upon erythrocyte co-culture (**Figure 6-7A**), or acquisition of fluorescent lipids from erythrocytes (**Figure 6-9**). Together, these data suggest erythrocyte co-culture does not induce changes in lipid availability.

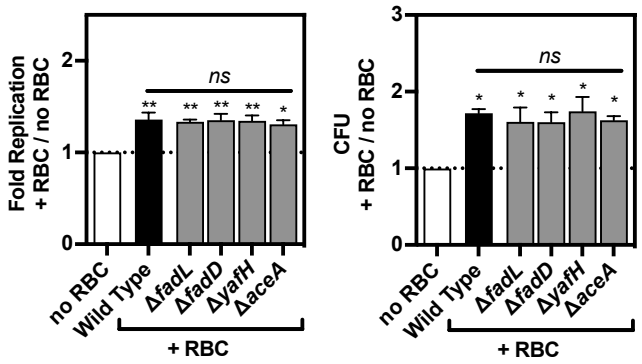

Figure 6-8. *Salmonella* does not require lipid metabolism for increased replication upon erythrocyte co-culture. BMDM were infected with wild type or the indicated mutants and co-cultured with erythrocytes. Fold replication (**left**) and CFU (**right**) are normalized to that of bacteria from the no erythrocyte condition for each strain (white bar) to determine the replication increase. Data shown are aggregated mean and SEM from at least 3 biological replicates. * $p < 0.05$; ** $p < 0.01$by one-way ANOVA compared to no co-culture unless otherwise noted.

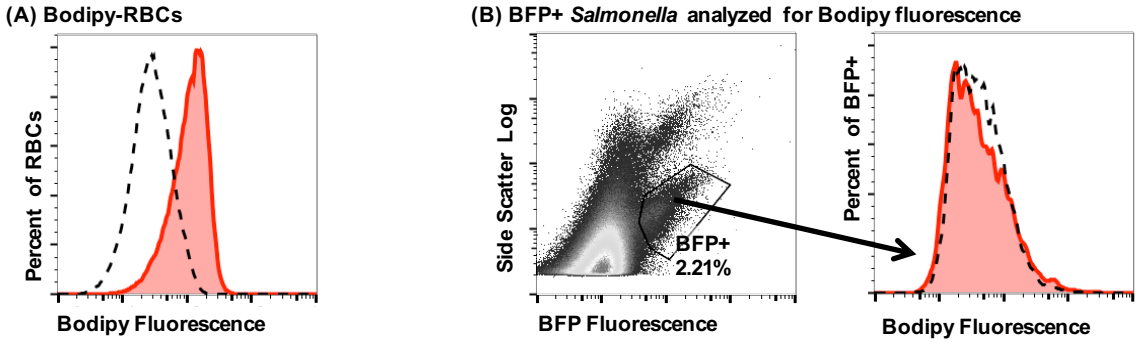

Figure 6-9. *Salmonella* does not acquire fluorescent lipids from erythrocytes. (A) Flow cytometry histogram of unstained (black dotted line) and Bodipy-stained erythrocytes (red shadow). **(B)** BMDM were infected with BFP-expressing *Salmonella* and co-cultured with Bodipy-stained erythrocytes. At 18 hours post infection, macrophages were lysed to release bacteria and Bodipy fluorescence of bacteria was measured using flow cytometry. Representative flow cytometry gating scheme and Bodipy histograms of triplicate samples from one experiment are shown. Histograms are Bodipy fluorescence of bacteria from macrophages co-cultured with erythrocytes (black dotted line) and Bodipy-stained erythrocytes (red shadow).

D. ERYTHROCYTE CO-CULTURE RELIEVES NITRIC-OXIDE MEDIATED REPRESSION OF *SALMONELLA* REPLICATION

Salmonella intracellular replication and survival is suppressed by antimicrobial effectors. I next hypothesized that erythrocyte co-culture could blunt key macrophage effects, thereby permitting increased bacterial replication. I tested whether *Salmonella* experienced reduced stress by quantifying expression of bacterial genes involved in defense against reactive oxygen species (ROS), reactive nitrogen species (RNS), antimicrobial peptides, and acid stress. Bacteria from macrophages co-cultured with erythrocytes had reduced expression of the genes *hmpA* and *ytfE* (**Figure 6-10**), which are involved in defense against RNS (Burton et al., 2014). RNS primary inhibit bacterial replication by disrupting metal and thiol cofactors in enzymes involved in respiration and DNA replication (Fang, 2004b; Henard and Vazquez-Torres, 2011; Vazquez-Torres et al., 2000b). Macrophages produce nitric oxide through the action of inducible nitric oxide synthase (iNos); nitric oxide reacts with ROS to form other RNS and may synergize with ROS to effect bacterial killing. Nitric oxide is freely permeable through host and bacterial membranes and spontaneously oxidizes to nitrite.

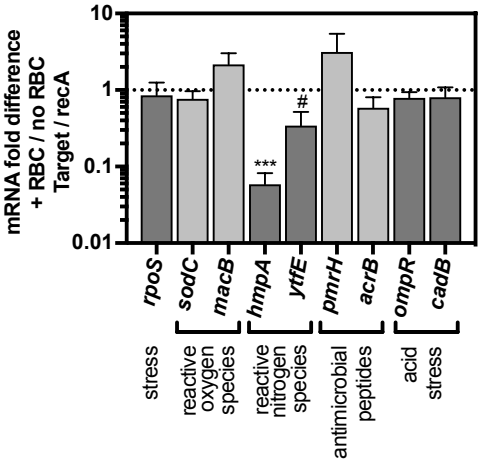

Figure 6-10. *Salmonella* expression of *hmpA* is decreased in macrophages co-cultured with erythrocytes. As in Figure 6-7A.

I verified that *Salmonella* experiences less RNS during erythrocyte co-culture using a Δ*hmpA* mutant, which is defective in macrophages due to a defect in detoxifying nitric oxide (**Figure 6-11**). I first confirmed that supplementing media with the iNos inhibitor increased bacterial replication and eliminated supernatant nitrite (a proxy for nitric oxide production), indicating nitric oxide limits replication. As expected, treatment with the iNos inhibitor L-NIL fully rescued Δ*hmpA* replication to the same level as wild type, resulting in an enhanced replication

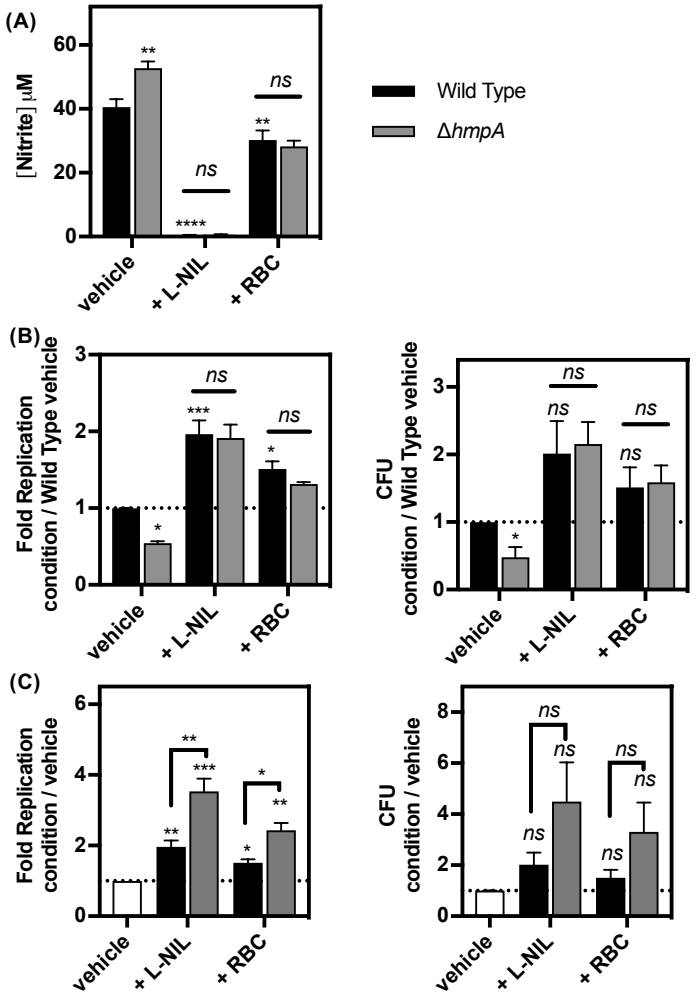

Figure 6-11. Erythrocyte co-culture or iNos inhibition reduces NO and rescues an NO-sensitive *Salmonella* mutant. BMDMs were infected with wild type or Δ*hmpA* *Salmonella* and treated with erythrocytes or 50 μM L-NIL. Supernatant nitrite **(A),** bacterial replication (**B,C left**), and CFU (**B,C right**) were measured at 18 hours post infection. Replication and CFU are normalized to vehicle for wild type (**B**) or vehicle for each strain to determine the replication increase (**C**). Data shown are aggregated mean and SEM from at least 3 biological replicates. * $p < 0.05$; ** $p < 0.01$; *** $p < 0.001$; **** $p < 0.0001$ by one-way ANOVA compared to no co-culture.

increase for Δ*hmpA* than for wild type when normalized to replication for each strain in the absence of L-NIL (**Figure 6-11**). Similar to L-NIL, erythrocyte co-culture reduced nitrite and rescued Δ*hmpA* replication to the same level as wild type, again affording an enhanced replication increase for mutant than for wild type. These data indicate that the replication increase induced by erythrocyte co-culture is due to reduced exposure to nitric oxide or other derivative RNS.

I next tested whether erythrocyte-induced replication required nitric oxide. Erythrocyte co-culture in the presence of L-NIL, which fully inhibited nitrite production, did not increase *Salmonella* replication (**Figure 6-12A-C**). To rule out the possibility that L-NIL treatment maximally increased bacterial replication leading to no further increase upon erythrocyte

treatment, I co-treated macrophages with L-NIL and iron and found that *Salmonella* replication in the presence of L-NIL was enhanced by iron. Thus, the lack of erythrocyte-induced increase in the presence of L-NIL is due to elimination of nitric oxide.

Similar results were observed with the cell-impermeable nitric oxide scavenger PTIO, indicating that eliminating extracellular nitric oxide is sufficient to block erythrocyte-dependent replication (**Figure 6-12A-C**). (PTIO reacts with nitric oxide to form nitrite, leading to an increase in measured supernatant nitrite when nitric oxide is eliminated.) Next, I tested whether macrophage-derived nitric oxide was required. Supplementing media with the nitric oxide donor diethylenetriamine NONOate (dNO; $t_{1/2}$ 20 hours at 37 °C) rescued the effect of L-NIL treatment but did not alter the effect of erythrocyte co-culture (**Figure 6-12A,B**). This result is consistent

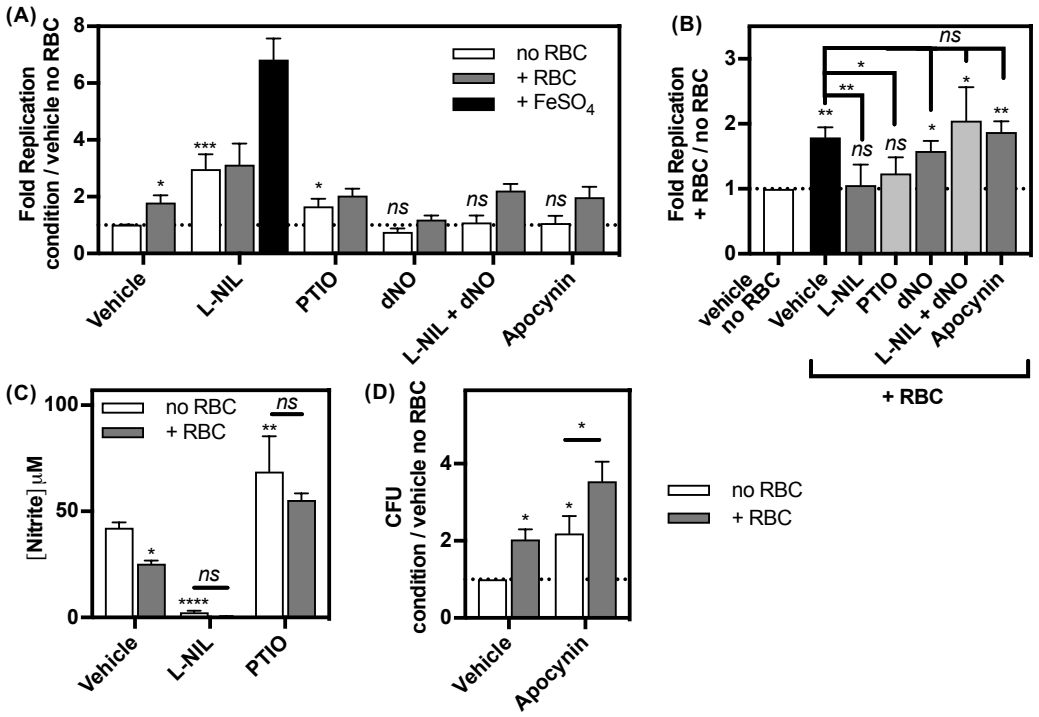

Figure 6-12. Erythrocyte-induced replication is mediated by reduced nitric oxide. BMDM were infected and co-cultured with erythrocytes and the indicated reagents: L-NIL (50 μM); PTIO (1 mM); diethylenetriamine-NONOate (dNO; 1 mM); apocynin (250 μM); $FeSO_4$ (500 μM). Replication is normalized to no erythrocyte vehicle (**A**) or no erythrocyte for each reagent to determine replication increase (**B**). Supernatant nitrite (**C**) and CFU (**D**) are shown for indicated samples. Data shown are aggregated mean and SEM from at least 3 biological replicates. *p*-values were determined using two-way ANOVA and are compared to vehicle no erythrocyte unless otherwise indicated.

with the idea that nitric oxide freely moves through membranes, and that nitric oxide is necessary and sufficient for the replication increase caused by erythrocyte co-culture.

Nitric oxide can react with ROS to form additional RNS which can suppress bacterial replication. To test whether derivative RNS were required for the effect of erythrocyte co-culture, I disrupted macrophage ROS production. Treatment with the NADPH oxidase inhibitor apocynin increased bacterial load monitored by CFU, as expected for reducing bactericidal ROS (**Figure 6-12D**). Apocynin did not affect replication or erythrocyte-induced replication (**Figure 6-12A,B**), indicating that the reaction of ROS with nitric oxide to form derivative RNS is not relevant. It is possible that macrophages primed with interferon-γ, which have increased NADPH oxidase activity upon infection (Lowenstein et al., 1993), would display a greater contribution of ROS.

Together, these results indicate that erythrocytes lead to changes in *Salmonella* exposure to nitric oxide, which permits increased replication. Given my previous data showing that macrophage-erythrocyte contact or proximity is required, I next tested several possible mechanisms for erythrocytes to reduce nitric oxide: erythrocyte scavenging, hemophagocytosis, or signaling-mediated activation changes.

E. ERYTHROCYTES SCAVENGE NITRIC OXIDE

Free hemoglobin is an efficient scavenger and detoxifier of NO (Luchsinger et al., 2003). Although erythrocyte membranes limit the ability of cellular hemoglobin to scavenge low concentrations of endothelial-derived NO during homeostasis (100-300 nM) (Han et al., 2005; Kelm, 1999; Liu et al., 1998), intact erythrocytes have been shown to reduce the effect of phagocyte-derived NO during infection (Kim et al., 1996). I first tested whether erythrocytes scavenge nitric oxide at concentrations equivalent to those in the above experiments (40-100 μM), using a real-time assay of nitric oxide production from the NO donor diethylamine-NONOate (deaNO; $t_{1/2}$ 15 minutes at room temperature) (Ridnour et al., 2000). I found that known scavengers quercetin, PTIO, and cell-free hemoglobin reduced NO in a dose-dependent

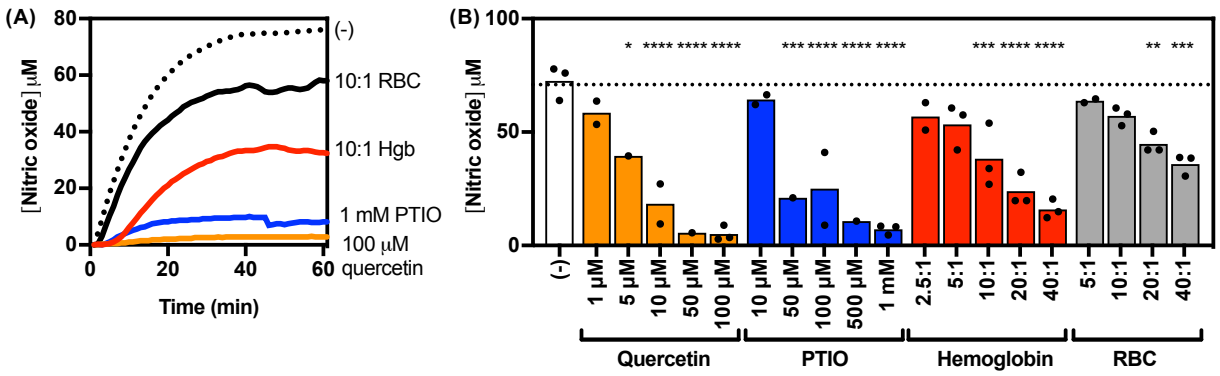

Figure 6-13. Erythrocytes scavenge nitric oxide. Production of nitric oxide from 100 μM deaNO in cell culture media was measured in real time using the Neutral Griess Reagent as described in the methods. Erythrocytes were added at concentrations corresponding to the indicated ratios used in macrophage co-culture experiments (5 x 10^6, 1 x 10^7, 2 x 10^7, 4 x 10^7). Hemoglobin was freshly obtained from erythrocytes and added to correspond to the amount in the indicated ratios of erythrocytes (41.7 μg/ml, 83.3 μg/ml, 166.7 μg/ml, 333.3 μg/ml, 666.7 μg/ml). **(A)** Representative kinetic plot of nitric oxide production. **(B)** Total nitric oxide produced as of 60 minutes was plotted for the indicated scavengers. Individual data points from 1-3 biological replicates (black dots) are superimposed on the mean. * $p < 0.05$; ** $p < 0.01$; *** $p < 0.001$; **** $p < 0.0001$ by one-way ANOVA compared to no co-culture.

manner (**Figure 6-13**). I also found that intact erythrocytes reduced NO at similar concentrations to what I used in my previous experiments (10:1 erythrocyte:macrophage ratio is typically 1 x 10^7 erythrocytes / ml). Notably, intact erythrocytes scavenged NO about half as well as cell-free hemoglobin, suggesting that at high concentrations of NO, diffusion through erythrocyte membranes plays a less significant role in the reaction. Thus, erythrocytes are likely scavenging nitric oxide during co-culture with infected macrophages.

To establish whether erythrocyte scavenging of nitric oxide mediates increased *Salmonella* replication with macrophage during co-culture, I next tested whether erythrocyte hemoglobin is required. I prepared erythrocyte ghosts, which have been permeabilized by sequential washes in hypotonic saline to release intracellular contents and resealed (Loegering et al., 1987). I found that addition of hemoglobin-free ghosts at equivalent or 10 times higher numbers did not increase *Salmonella* replication (**Figure 6-14**). Further, I previously showed that contact or proximity within 1000 μm is required for the effect on *Salmonella* replication and for reductions

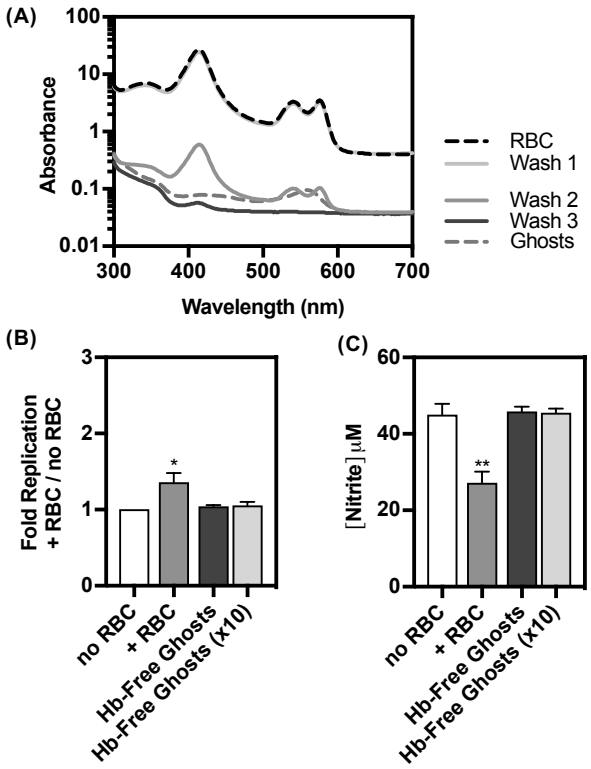

Figure 6-14. Hemoglobin-free erythrocyte ghosts do not increase *Salmonella* replication in macrophages. Hemoglobin-free erythrocyte ghosts were prepared using repeated washes in hypotonic saline and added to infected macrophages. **(A)** Representative absorbance spectra of lysed RBCs, cellular contents leaking into the supernatant over 3 washes, and lysed ghosts after 3 washes. Reduced hemoglobin peaks at approximately 404, 540, and 580 nm. **(B)** Fold replication of bacteria recovered from macrophages and **(C)** supernatant nitrite after co-culture with the indicated erythrocytes. Data are aggregated mean and SEM of at least 3 biological replicates. * $p < 0.05$ by one-way ANOVA compared to no co-culture.

in nitric oxide (**Figure 6-2**). This result is consistent with the diffusion and auto-oxidation rates of NO, which together suggest NO has an effective distance of less than 500 µm from the producing-cell (Kelm, 1999; Thomas et al., 2001; Vaughn et al., 1998). Together, these data suggest that scavenging of NO by erythrocyte hemoglobin likely contributes to the observed increases in *Salmonella* replication upon co-culture.

F. INCREASED REPLCATION IS NOT UNIQUE TO HEMOPHAGOCYTES AND IS NOT MEDIATED BY SECRETED FACTORS OR PHAGOCYTOSIS

Approximately 4-6% of macrophages phagocytose erythrocytes in response to infection with *Salmonella* (McDonald et al., 2016). Hemophagocytes may adopt an anti-inflammatory phenotype and produce less nitric oxide, which could affect *Salmonella* within hemophagocytes or in neighboring macrophages (Loegering et al., 1987; Ohyagi et al., 2013). Given that contact is required for the effect of erythrocyte co-culture, I hypothesized that hemophagocytes could contribute to reduced *Salmonella* exposure to nitric oxide, in addition to nitric oxide scavenging

by extracellular erythrocytes. I first tested whether *Salmonella* replication was altered within hemophagocytes relative to non-hemophagocytes from the same well. I sorted macrophages based on intracellular Ter119, an erythrocyte surface marker using FACS and harvested bacteria. I found no difference in bacterial replication between the Ter119+ and Ter119- populations (**Figure 6-15**). Work by Erin McDonald also demonstrated there was no difference in macrophage mRNA expression of several pro-inflammatory and anti-inflammatory genes, including *iNos*, between hemophagocytes and non-hemophagocytes. Likewise, flow cytometric profiling yielded no differences in expression of several infection-relevant macrophage surface proteins (Heidi Nick).

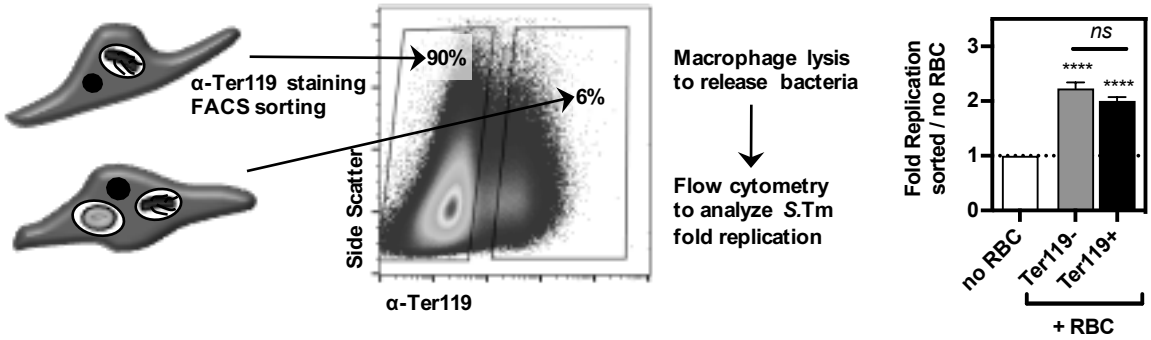

Figure 6-15. *Salmonella* replicates similarly in hemophagocytes and non-hemophagocytes from the same well. BMDM were infected, co-cultured with erythrocytes, and at 18 hours post infection macrophages were fixed and stained for intracellular Ter119 and sorted using FACS into Ter119- and Ter119+. Bacteria from lysates were analyzed for dsRed fluorescence and fold replication. Data are mean + SEM from 3 independent biological replicates. **** $p < 0.0001$ by one-way ANOVA compared to no co-culture unless otherwise indicated.

It is possible that hemophagocytes could influence neighboring cells through a secreted factor; however as previously shown, I found that conditioned media from macrophage-erythrocyte co-cultures had no effect on *Salmonella* replication with naïve macrophages (**Figure 6-3**). Finally, I inhibited hemophagocytosis using cytochalasin D, which blocks actin polymerization. Though I observed a dose-dependent effect of cytochalasin D on hemophagocytosis, there was no effect on *Salmonella* replication or supernatant nitrite (**Figure 6-16**). These data indicate that in this model, there is no different between hemophagocytes and

non-hemophagocytes and that hemophagocytosis has no effect on macrophage activation or *Salmonella* infection.

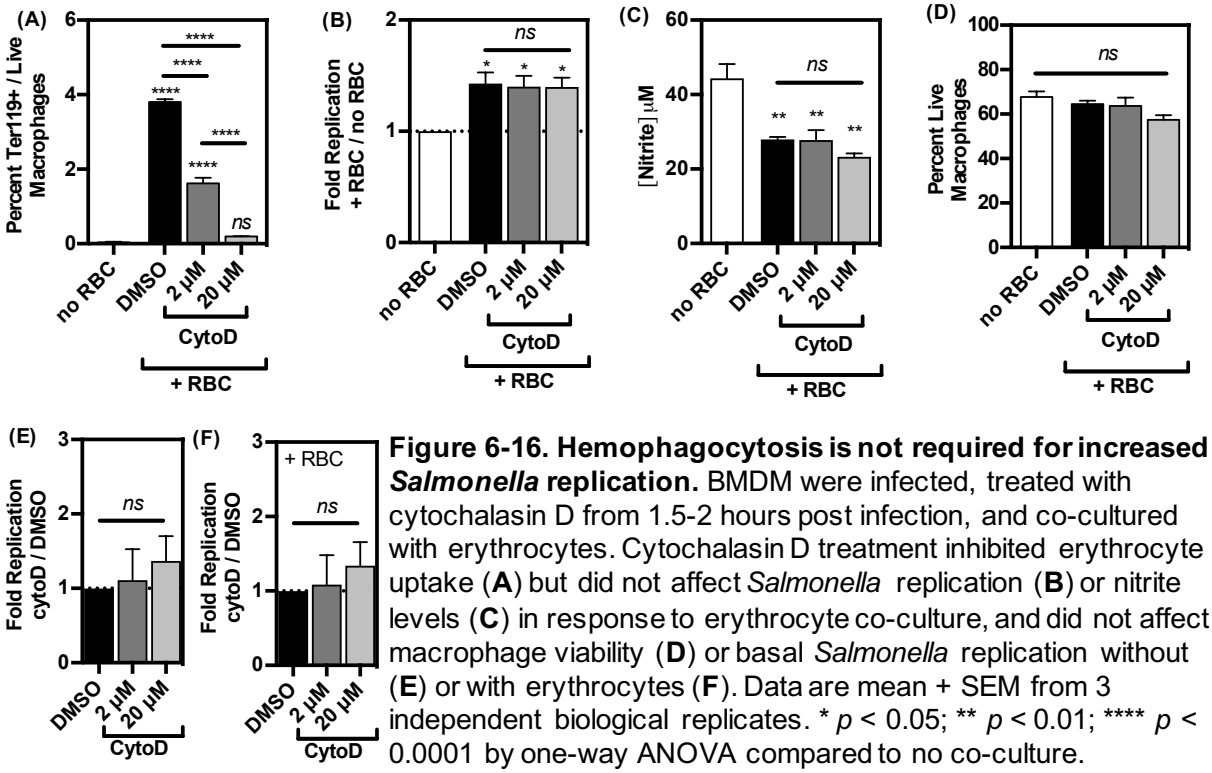

Figure 6-16. Hemophagocytosis is not required for increased *Salmonella* replication. BMDM were infected, treated with cytochalasin D from 1.5-2 hours post infection, and co-cultured with erythrocytes. Cytochalasin D treatment inhibited erythrocyte uptake (**A**) but did not affect *Salmonella* replication (**B**) or nitrite levels (**C**) in response to erythrocyte co-culture, and did not affect macrophage viability (**D**) or basal *Salmonella* replication without (**E**) or with erythrocytes (**F**). Data are mean + SEM from 3 independent biological replicates. * $p < 0.05$; ** $p < 0.01$; **** $p < 0.0001$ by one-way ANOVA compared to no co-culture.

G. ERYTHROCYTES DO NOT MODULATE MACROPHAGE PHENOTYPE

Erythrocyte surface molecules have been implicated in signaling interactions with other cell types (Sadallah et al., 2008). Given my earlier data that contact is required for the effect of erythrocyte co-culture but not phagocytosis, I hypothesized that extracellular erythrocytes could engage in signaling interactions with macrophages and modulate macrophage activation state in addition to scavenging nitric oxide as shown above. In particular, phosphatidylserine (PS) exposure on senescent erythrocytes induces IL-10 production and shifts macrophages to an anti-inflammatory phenotype (Birge et al., 2016; Chung et al., 2007; Huynh et al., 2002; Voll et al., 1997). Indeed, I found that PS-erythrocytes increased *Salmonella* replication (**Figure 6-17A**). Infected macrophages could damage co-cultured erythrocytes and lead to PS-exposure. However, I found that few erythrocytes exposed PS after co-culture with infected macrophages

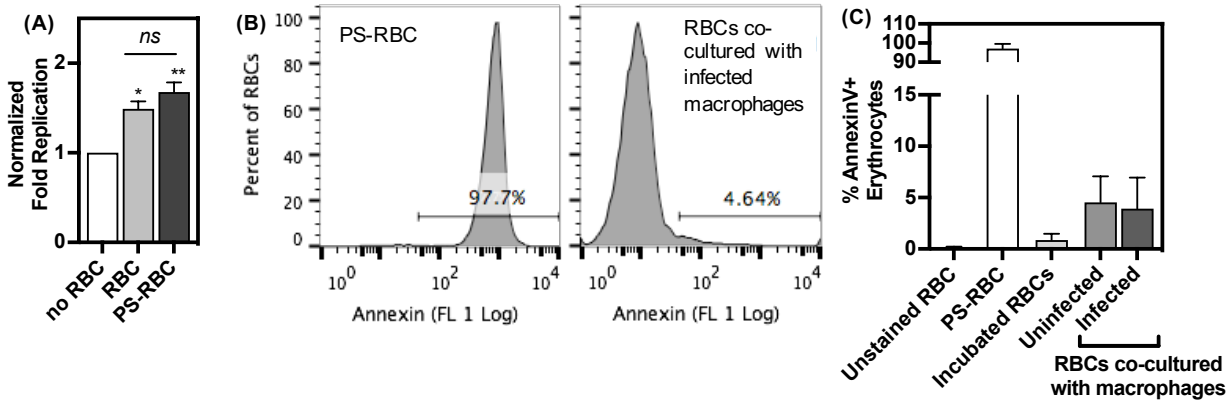

Figure 6-17. Few erythrocytes expose phosphatidylserine after co-culture. Macrophages were infected and incubated with healthy or oxidized erythrocytes. (**A)** At 18 h.p.i. bacteria were harvested to determine fold replication. **(B,C)** At 18 h.p.i. erythrocytes were harvested and analyzed for phosphatidlyserine exposure using annexin staining. Representative gating (**B**) and quantification after the indicated treatments or incubations (**C**). Data are mean + SEM of at least 3 independent biological replicates. * $p < 0.05$; ** $p < 0.01$ by one-way ANOVA compared to no co-culture.

or incubation in PBS, indicating any PS-signaling does not contribute to the effects of healthy erythrocyte co-culture (**Figure 6-17B,C**). To further test whether other erythrocyte surface molecules could contribute to increased *Salmonella* replication, I treated erythrocytes with proteinase K to digest surface proteins, neuraminidase to disrupt surface glycans, or glutaraldehyde to prevent ligand clustering. Removing surface molecules did not abolish erythrocyte-induced replication (**Figure 6-18**). I also found that disrupting macrophage signaling pathways using a panel of inhibitors did not affect the erythrocyte-induced replication increase, though inhibition of several signaling pathways independently affected nitric oxide production and *Salmonella* replication (**Figure 6-19**). Finally, I compared the phenotypes of macrophages cultured with and without erythrocytes during infection and found that erythrocyte co-culture did not modulate macrophage expression of genes or cytokines associated with activation state (**Figure 6-20**). Thus, I could not identify a surface interaction, signaling pathway, or activation marker that could mediate changes in production of nitric oxide during erythrocyte co-culture.

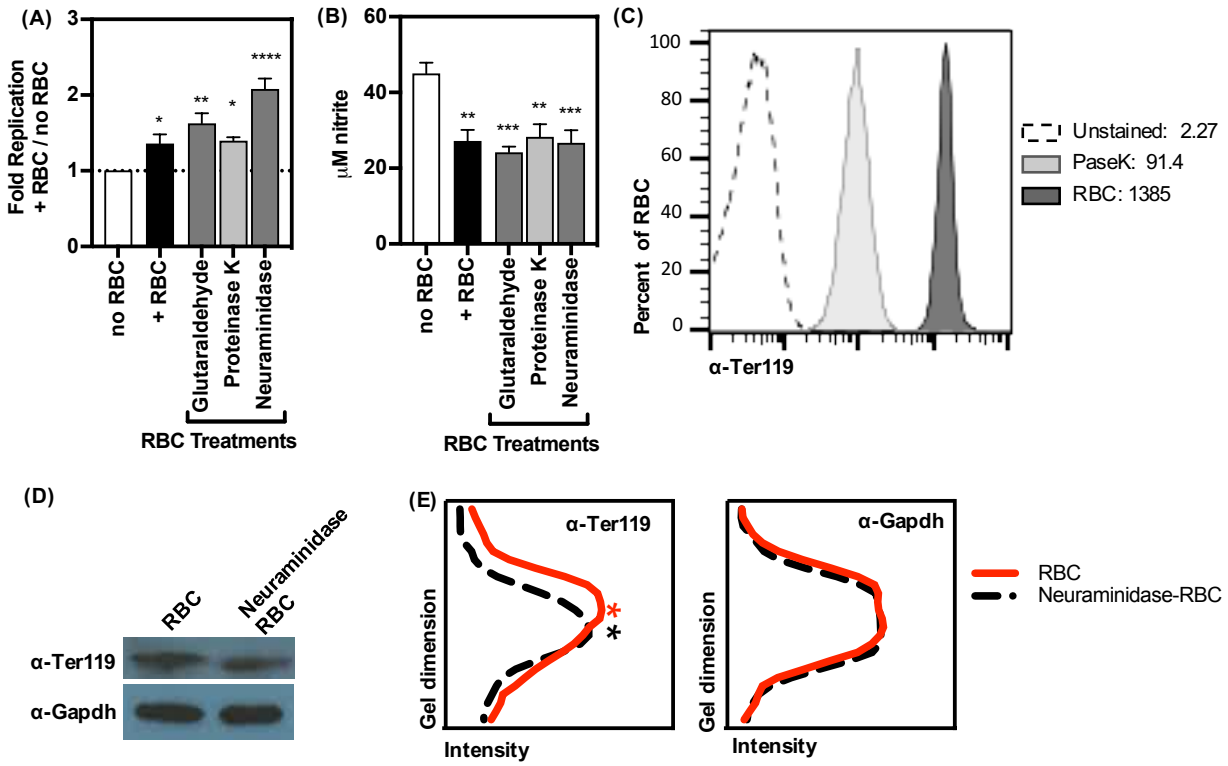

Figure 6-18. Disrupting erythrocyte surface ligands does not alter the effect of erythrocyte co-culture. Erythocytes were treated with the indicated reagents and added to infected macrophages. *Salmonella* replication **(A)** and supernatant nitrite **(B)** were measured at 18 h.p.i. Data are mean + SEM of at least 3 independent biological replicates. * $p < 0.05$; ** $p < 0.01$; *** $p < 0.001$ by one-way ANOVA compared to no co-culture. (**C**) Untreated and Proteinase K-treated erythrocytes were stained for surface Ter119; protease treatment reduced surface Ter119. Median fluorescence intensities are noted in the legend. (**D**) Protein from untreated and neuraminidase-treated erythrocytes was probed using Western blotting. Neuraminidase treatment decreases the molecular weight of Ter119, as evident by a downward shift in the average of 6-7 linescans through the band (**E**).

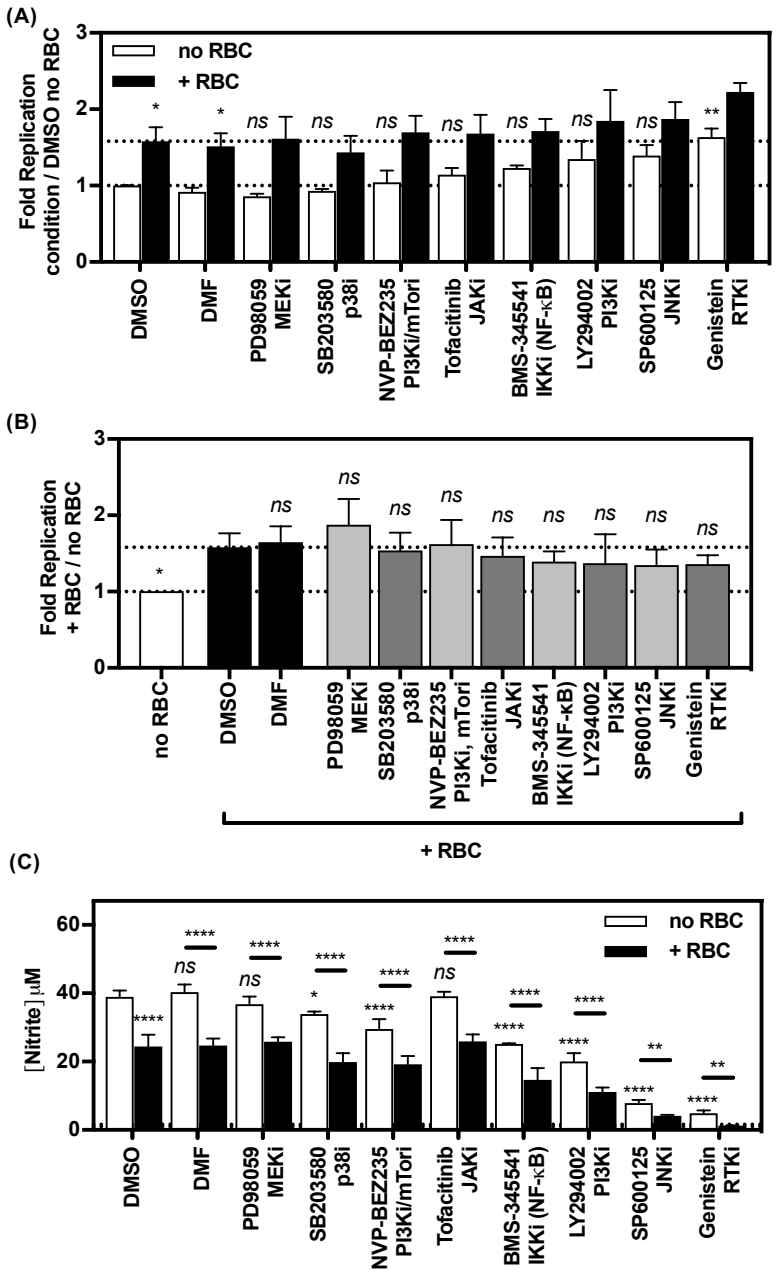

Figure 6-19. Disrupting macrophage signaling using inhibitors of key pathways does not alter the ability of erythrocytes to increase intracellular *Salmonella* replication. Infected macrophages were treated with the indicated inhibitors beginning at 1 h.p.i., and co-cultured with erythrocytes beginning at 2 h.p.i. At 18 h.p.i. bacteria were harvested and fold replication was calculated and normalized to DMSO no RBC **(A)** or the no RBC condition for each drug **(B)**. Supernatant nitrite was determined using the Griess assay **(C)**.

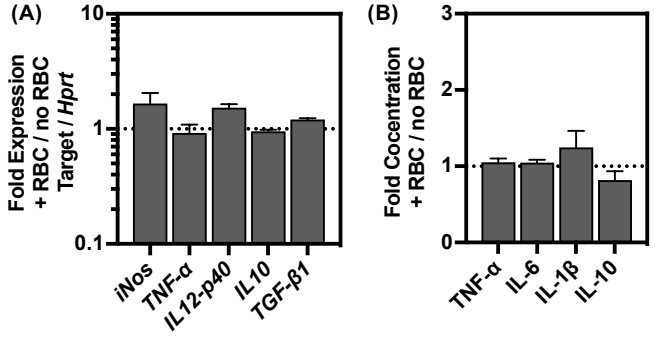

Figure 6-20. Erythrocyte co-culture does not affect mRNA or protein levels for differential markers of macrophage activation. (A) As in **Figure 6-7B**. **(B)** Levels of the indicated cytokines in the supernatant from macrophages co-cultured with and without erythrocytes were quantified as described in the methods. Data are aggregated mean and SEM of at least 3 biological replicates.

H. HEMOPHAGOCYTOSIS OF T CELLS ALTERS MACROPHAGE ACTIVATION AND IRON HOMEOSTASIS IN A CELL-INTRINSIC MANNER

Macrophages interact extensively with T cells during infection. I next explored how T cells affect *Salmonella* infection of macrophages. I found that T cells increased *Salmonella* replication and growth in a dose-dependent manner, but did not cause a significant reduction in supernatant NO (**Figure 6-21A**), in contrast to my previous experiments with erythrocytes. I also found that the T-cell-mediated replication increase was independent of NO production (**Figure 6-21B**) and that T cells did not rescue an NO-sensitive *Salmonella* mutant (**Figure 6-21C,D**). Further, T cells were unable to scavenge NO (**Figure 6-21E**). Together, these data indicate that although T cells have a similar impact as erythrocytes on *Salmonella* infection of macrophages, their effect is mediated by a different mechanism.

Iron is a key driver of *Salmonella* replication. I next tested whether T cells mediate increased iron activation for *Salmonella*. I found that supplementing medium with iron blocked the effect of T cell co-culture (**Figure 6-22A**) and that T cells rescued a *Salmonella* mutant with defects in iron uptake (**Figure 6-22B,C**).

I next profiled bacterial and macrophage gene expression and macrophage cytokine expression. I found that T cell co-culture increased macrophage anti-inflammatory markers, including IL-10, TGF-β, and arginase 1 (**Figure 6-23A**). I also found changes, though not significant, in macrophage iron metabolism genes, including hepcidin, ferroportin, and heme oxygenase. These data suggest that T cells alter macrophage activation and iron homeostasis, which together could explain why *Salmonella* replicates more during T cell co-culture.

To probe the T cell-macrophage interaction, I next evaluated whether contact is required for the effects on *Salmonella* replication. I found that adding T cells to the top compartment of a transwell insert had no effect on *Salmonella* replication (**Figure 6-24A**). I also found that inhibiting phagocytosis using cytochalasin D blocked the ability of T cells to increase *Salmonella* replication (**Figure 6-24C**). I next sorted macrophages based on uptake of T cells, and I found

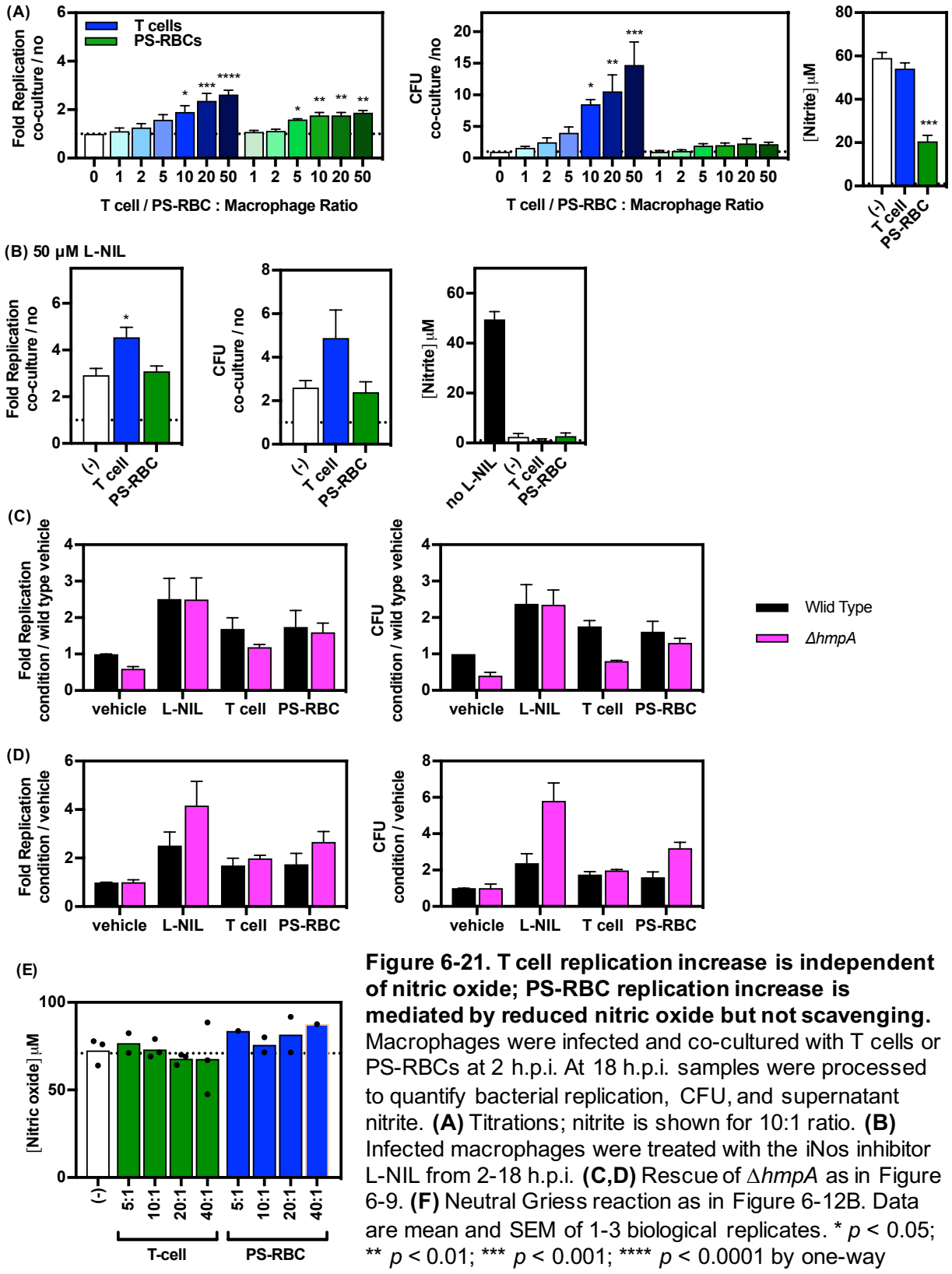

Figure 6-21. T cell replication increase is independent of nitric oxide; PS-RBC replication increase is mediated by reduced nitric oxide but not scavenging. Macrophages were infected and co-cultured with T cells or PS-RBCs at 2 h.p.i. At 18 h.p.i. samples were processed to quantify bacterial replication, CFU, and supernatant nitrite. **(A)** Titrations; nitrite is shown for 10:1 ratio. **(B)** Infected macrophages were treated with the iNos inhibitor L-NIL from 2-18 h.p.i. **(C,D)** Rescue of Δ*hmpA* as in Figure 6-9. **(F)** Neutral Griess reaction as in Figure 6-12B. Data are mean and SEM of 1-3 biological replicates. * $p < 0.05$; ** $p < 0.01$; *** $p < 0.001$; **** $p < 0.0001$ by one-way ANOVA compared to no co-culture.

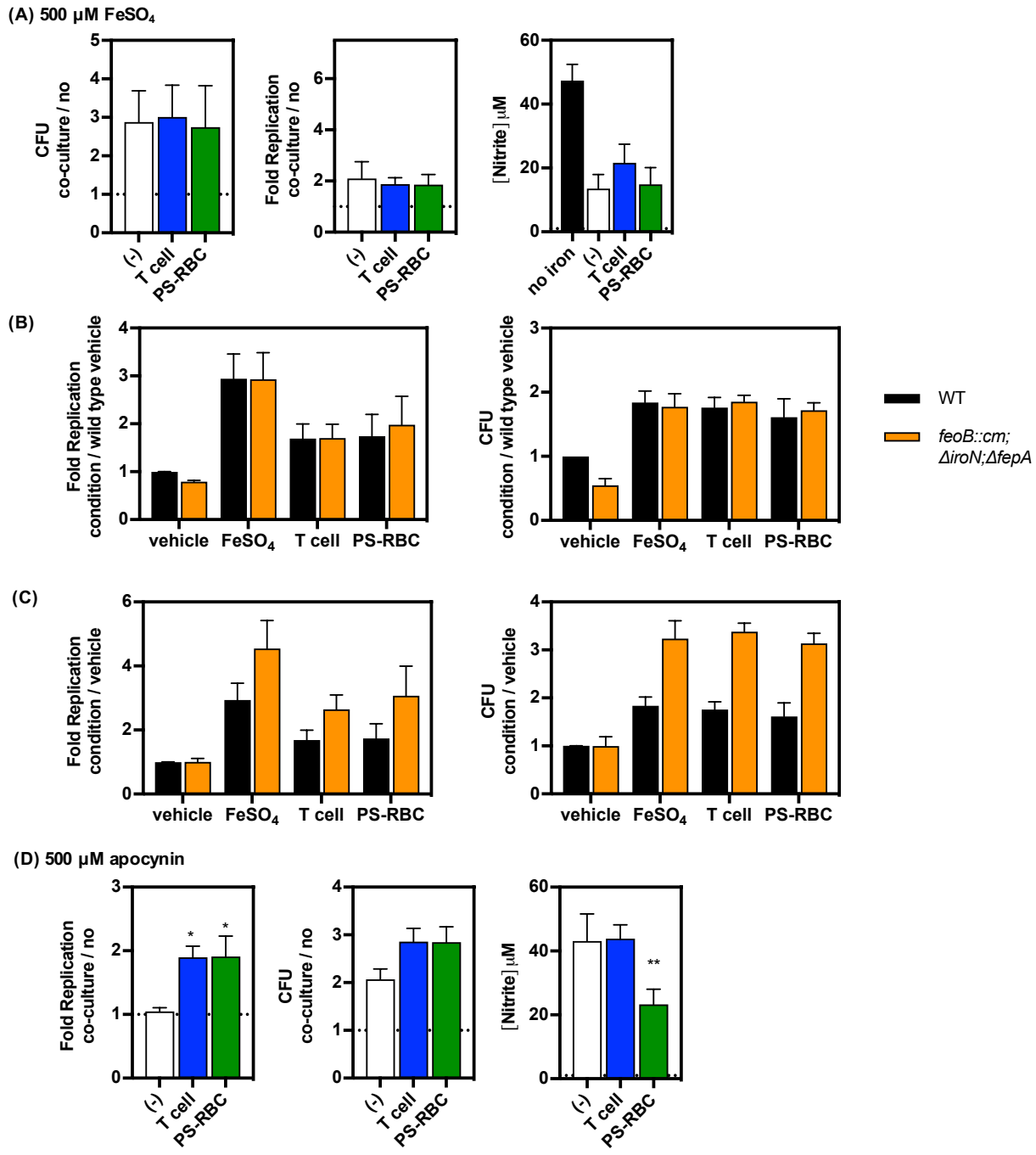

Figure 6-22. T cell and PS-RBC replication increases are mediated by increased iron availability. Macrophages were infected and co-cultured with T cells or PS-RBCs at 2 h.p.i. At 18 h.p.i. samples were processed to quantify bacterial replication, CFU, and supernatant nitrite. **(A)** Infected macrophages were incubated with $FeSO_4$ from 2-18 h.p.i. **(B,C)** Rescue of an iron uptake mutant as in Figure 6-3. **(D)** Infected macrophages were incubated with the NADPH oxidase inhibitor apocynin from 2-18 h.p.i. Data are mean and SEM of 1-3 biological replicates. * $p < 0.05$; ** $p < 0.01$ by one-way ANOVA compared to no co-culture.

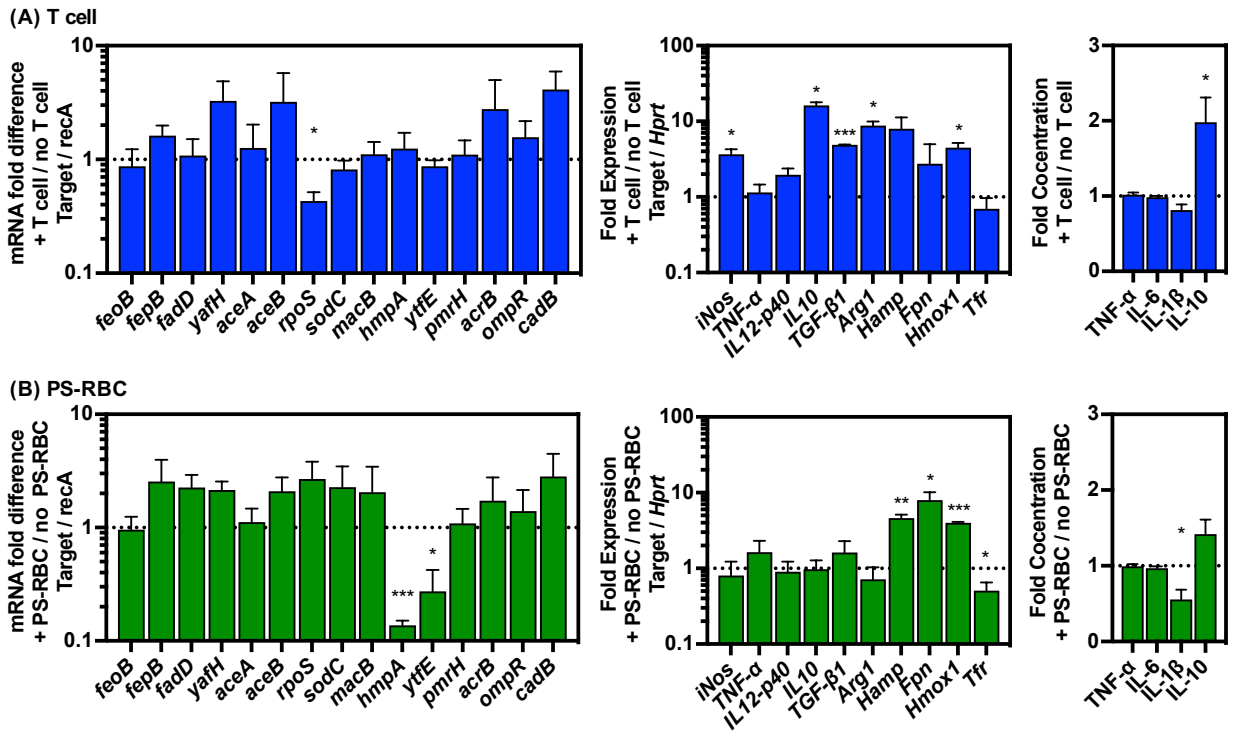

Figure 6-23. T cell or PS-RBC co-culture alters bacterial stress response genes, macrophage activation markers, and macrophage iron homeostasis gene expression. Bacterial gene expression, macrophage gene expression, and macrophage cytokine production were quantified as in Figures 6-7 and 6-20B after co-culture with T cells **(A)** or PS-RBCs **(B).**

that bacteria replicated more specifically within macrophages that had taken up T cells (**Figure 6-24D**). These data suggest that uptake of T cells could alter macrophage activation and iron homeostasis in a cell-intrinsic manner, resulting in increased *Salmonella* replication within these cells. Indeed, I found no evidence that a secreted factor affected bacterial replication, as treatment of infected macrophages with conditioned media from T cell co-culture samples did not affect replication (**Figure 6-25E**).

I. CO-CULTURE WITH SENESCENT ERYTHROCYTES ALTERS MACROPHAGE ACTIVATION, IRON HOMEOSTASIS, AND NITRIC OXIDE LEVELS

A key role of macrophages is to phagocytose senescent erythrocytes, which expose phosphatidylserine due to oxidation of cellular hemoglobin (Kiefer and Snyder, 2000). I generated senescent erythrocytes (PS-RBCs) via chemical oxidation (Sambrano and Steinberg,

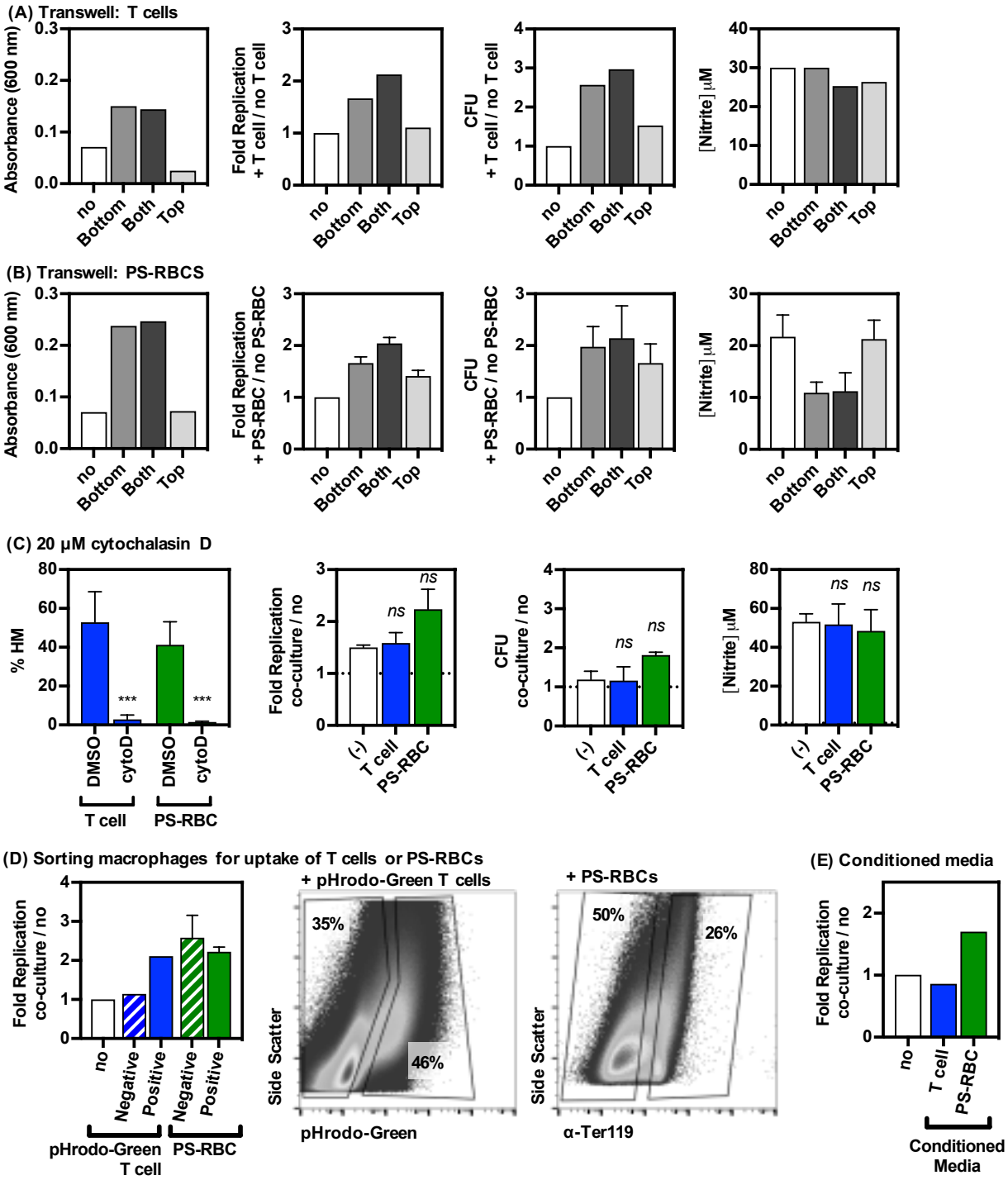

Figure 6-24. T cell and PS-RBC replication increases require contact. (A,B) As in **Figure 6-2. (C)** As in **Figure 6-16. (D)** Macrophages were sorted based on uptake of T cells or PS-RBCs (see methods) and bacteria from each population were analyzed for replication as in **Figure 6-15**, except that T cell co-cultured macrophages were infected with bacteria only harboring pDiGi, and sorted samples were lysed and stained with 10 µM DAPI to identify bacteria using flow cytometry. **(E)** Conditioned medium from infected macrophages co-cultured with the indicated cells was filtered and added to separately infected macrophages.

1995; Tanaka et al., 2001), which leads to phosphatidylserine exposure (**Figure 6-17**). I found that co-culture of PS-RBCs with infected macrophages led to increased *Salmonella* replication and decreased NO production (**Figure 6-21A**), as I previously observed with healthy erythrocytes. Treatment with L-NIL to inhibit NO production blocked the effect of PS-RBCs on *Salmonella* replication (**Figure 6-21B**), and PS-RBCs rescued the NO-sensitive *Salmonella* mutant (**Figure 6-21C,D**). These data indicate that PS-RBCs increase *Salmonella* replication by decreasing exposure to NO. However, unlike I observed with healthy erythrocytes, PS-RBCs do not scavenge NO (**Figure 6-21E**). This result is consistent with the fact that hemoglobin within PS-RBCs is oxidized, and oxidized hemoglobin is a poor scavenger of NO (Luchsinger et al., 2003). Thus, PS-RBCs must decrease NO exposure by another mechanism.

Regulation of iNos is tightly intertwined with iron levels during infection (Nairz et al., 2013). Indeed, iron supplementation significantly decreases NO production (**Figure 6-22A**). I next tested whether PS-RBC co-culture also increases iron access for *Salmonella*. I found that supplementing medium with excess iron blocked the ability of PS-RBCs to increase *Salmonella* replication (**Figure 6-22A**), and that PS-RBC co-culture rescued a *Salmonella* mutant with defects in iron uptake (**Figure 6-22B,C**). Thus, PS-RBC co-culture appears to both reduce NO and liberate iron for *Salmonella*, together resulting in increased replication. Indeed, PS-RBC co-culture reduced expression of *Salmonella* NO-responsive genes, and altered expression of iron regulatory genes (**Figure 6-23B**). These changes may be due to alterations in certain cytokines, as I also found decreased expression of the pro-inflammatory cytokine IL-1β (**Figure 6-23B**).

Uptake of PS-RBCs has been shown to have immunosuppressive effects on macrophages (Birge et al., 2016; Huynh et al., 2002; Voll et al., 1997). Although I found that contact was required for the effects of PS-RBCs using transwells (**Figure 6-24B**), inhibition of uptake using cytochalasin D did not prevent increases in *Salmonella* replication (**Figure 6-24C**). Further, *Salmonella* replicated equally in macrophages that had and had not taken up PS-RBCs (**Figure 6-24D**), and conditioned media from co-culture samples did not affect replication (**Figure 6-24E**)

These result suggests that efferocytosis of PS-RBCs does not mediate increased *Salmonella* replication, but rather than surface interactions may lead to changes in macrophage activation and immune responses.

J. DISCUSSION

Macrophages interact with other cell types during infection, but the implications of these interactions are largely unstudied. Several studies have explored the effect of co-culturing macrophages with epithelial cells during infection and have identified modulatory effects on macrophage activation and cytokine secretion in macrophages, as well as effects on epithelial cells (Bodet et al., 2005; Noel et al., 2017; Stříž et al., 2001; Verway et al., 2013). However, macrophages also interact with leukocytes during infection, and the impact of these interactions is unknown. In this study I found that co-culture of three kinds of leukocytes led to increased *Salmonella* replication within macrophages.

I found that healthy erythrocytes efficiently scavenge nitric oxide thereby increasing *Salmonella* replication. Along with other studies, this result illustrates the importance of nitric oxide in controlling *Salmonella* replication within macrophages (Burton et al., 2014; Chakravortty et al., 2002; De Groote et al., 1996; Henard and Vazquez-Torres, 2011; Vazquez-Torres et al., 2000b). Surprisingly, I found no evidence that other interactions between macrophage and erythrocyte affect the *Salmonella*-macrophage interface, in contrast to evidence that signaling with or uptake of erythrocytes affects the macrophage immune response (Hand and King-Thompson, 1983; Kim et al., 1996; Loegering et al., 1987; Sadallah et al., 2008). Erythrocytes and infected macrophages likely interact in the spleen, where macrophages survey leukocytes for senescent erythrocytes and a key tissue colonized by Salmonella (Borges da Silva et al., 2015; Salcedo et al., 2001). Thus, nitric oxide scavenging by passing erythrocytes may reduce the effective concentration of nitric oxide and enable increased bacterial replication in the spleen.

During infection by *Salmonella* and certain pathological inflammatory conditions, macrophages hemophagocytose healthy T cells (Brown et al., 2010; Nix et al., 2007; Ohyagi et al., 2013). We have previously demonstrated that *Salmonella* replicates more in hemophagocytes (Silva-Herzog and Detweiler, 2010), but the mechanism of this replication is unknown. My study suggests that hemophagocytosis of T cells leads to increased iron available for *Salmonella* within hemophagocytes. Iron homeostasis is connected to immune activation, and I indeed found that T cell co-culture induced the anti-inflammatory cytokine IL-10. IL-10 induces expression of heme oxygenase which increases intracellular iron within macrophages and could explain the excess iron available to *Salmonella* (Philippidis P. et al., 2004; Sierra-Filardi et al., 2010). However, I also found increased expression of ferroportin, which exports iron, and hepcidin, which blocks ferroportin, so the overall effect on iron levels is not readily apparent. Additional work is required to reveal the pathways that connect to produce increased iron available for *Salmonella*.

Finally, I found that senescent erythrocytes (PS-RBCs) also increase *Salmonella* replication in macrophages. Although senescent erythrocytes are readily phagocytosed by macrophages, uptake was not required for an effect on *Salmonella* replication. However, I found that PS-RBCs reduce nitric oxide, increase iron access, and decrease expression of the pro-inflammatory cytokine IL-1β. Connections between these pathways have been observed, but the causation in this case remains unclear. Expression of iNos can be affected by iron levels (Weiss et al., 1994), and nitric oxide affects regulation of the iron exporter ferroportin (Nairz et al., 2013). IL-1β may also be involved in regulation of iNos and hepcidin (Katayama et al., 1998; Lee et al., 2005; Skorokhod et al., 2007). Thus, although we understand how *Salmonella* benefits from PS-RBC co-culture, the changes in the macrophage that lead to increased iron and reduced nitric oxide remain unclear.

Taken together, my data demonstrates that interactions between macrophages and other cell types can alter the balance of infection between host and pathogen. These effects can be mediated by chemical interactions, signaling, polarization, and nutritional changes. These observations are in line with the idea that infection is extremely heterogeneous; macrophages likely interact with different host cells *in vivo* and thus respond uniquely to infection. As a result, intracellular pathogens experience a different host cell environment, and infection may have a different outcome. Thus, future studies connecting host cell phenotypes and interactions with infection outcome and pathogen strategies *in vitro* and *in vivo* may reveal key players that drive pathogen success.

K. MATERIALS AND METHODS

Bacterial strains and growth conditions. Bacterial strains were *Salmonella enterica* serovar Typhimurium strain SL1344 with *rpsM*::GFP (SM022, (Vazquez-Torres et al., 1999)) harboring pDiGi and were cultured at 37°C with aeration. For fluorescence dilution experiments (Helaine et al., 2010), we found that use of pDiGc, which encodes GFP under the *rpsM* promoter, significantly hindered *Salmonella* infection, presumably due to high GFP expression from the plasmid (**Appendix E**). Thus, strains were transformed with pDiGi and chromosomally marked with GFP at the *rpsM* locus using P22 phage transduction (Vazquez-Torres et al., 1999) (ALR#258, #259, #260, #261, #262, #391, #584, #601). Strains were induced overnight in medium containing 170 mM MES pH 5.0, 5 mM KCl, 7.5 mM $(NH_4)_2SO_4$, 0.5 mM K_2SO_4, 1 mM KH_2PO_4, 10 mM $MgCl_2$, 0.3% glycerol, 0.1% casamino acids, 10 mM arabinose with 30 μg/ml streptomycin, 50 μg/ml ampicillin, and 30 μg/ml kanamycin prior to infection (Helaine et al., 2010). BFP-expressing *Salmonella* were transformed with a plasmid encoding blue fluorescent protein (BFP) driven by the *rpsM* promoter (ALR#234; DET#1271) (McQuate et al., 2017).

Strains with deletions of iron or lipid metabolism genes were constructed and the locus marked with kanamycin or chloramphenicol resistance cassettes (Datsenko and Wanner, 2000;

Kim et al., 2014), which was P22 phage transduced into SL1344 (Nagy et al., 2013). An *hmpA*::kan strain was a kind gift from Andreas Vazquez-Torres (McCollister et al., 2008). The antibiotic resistance gene was removed by induction of FLP recombinase or I-SceI to yield a 84-bp scar or no scar, depending on the method. Mutant strains were validated by PCR.

Mammalian cell culture. Macrophages were routinely cultured at 37 °C with 5% CO_2 in DMEM high glucose (Sigma) supplemented with 10% fetal bovine serum, 2 mM L-glutamine, 1 mM sodium pyruvate, 10 mM HEPES, and 50 μM β-mercaptoethanol. To generate bone-marrow derived macrophages, femurs and tibias from 4-10 week old wild-type 129S6/SvEvTac (Taconic) mice were flushed with PBS to recover bone marrow, layered over Histopaque-1083, and centrifuged for 25 minutes at 500 x *g*. The mononuclear cell fraction was recovered and washed in complete media. Cells were seeded at 1-2 x 10^5 cells/ml in complete medium supplemented with 30-35% conditioned medium from 3T3 cells expressing MCSF, and fed 3-4 days later. After 1 week in culture, BMDMs typically replicated 5-10 fold under these conditions. When applicable, macrophages were activated with 2 ng/ml recombinant murine IFNγ (PeproTech) for 18-24 hours prior to infection. Jurkat human T cells were cultured in RPMI 1640 with 10% FBS.

Erythrocyte treatments. Erythrocytes were harvested from 129S6/SvEvTac mice and washed with PBS. To produce phosphatidyl-serine-expressing erythrocytes, cells were resuspended in 0.2 mM $CuSO_4$ and freshly prepared 5 mM L-ascorbic acid at 8 x 10^6 cells/ml in PBS and incubated for 90 minutes at 37°C, washed three times in PBS with 6.8 mM EDTA followed by a final wash in PBS (Sambrano and Steinberg, 1995; Tanaka et al., 2001). Exposure of phosphatidylserine was confirmed using annexin staining (**Figure 6-17B**). Two million erythrocytes were washed in PBS, stained with 100 μl 1:50 annexin V conjugated to Alexa-488 (Invitrogen) in annexin binding buffer (ABB; 10 mM HEPES pH 7.4, 140 mM NaCl, 2.5 mM $CaCl_2$) for 15 minutes at room temperature, washed twice in ABB, resuspended in 2 ml

ABB and immediately analyzed by flow cytometry.

To prepare hemoglobin-free ghosts, erythrocytes were pelleted at high speed and resuspended in 5 mM $NaPO_4$, pH 8.0 at 3 x 10^8 cells/ml three times after which no additional hemoglobin leakage was observed (Loegering et al., 1987). Hemoglobin leakage into the wash supernatant was monitored using absorbance and compared to untreated erythrocytes or ghosts lysed with 1% Triton X-100 in water (**Figure 6-13A**) (Himbert et al., 2017; Jiang et al., 2007).

Erythrocytes were fixed at 8 x 10^6 cells/ml using 2.5% glutaraldehyde in PBS for 90 minutes at 37°C and washed 3 times in PBS; treated erythrocytes showed no lysis during long-term storage at 4°C indicating fixation.

Protease-treated erythrocytes were incubated at 1 x 10^8 cells/ml in PBS with 30 μg/ml proteinase K for 1 hour at 37°C with rolling; loss of surface Ter119 was validated using flow cytometry as for intracellular Ter119 staining of macrophages without the permeabilization step. (**Figure 6-18C**).

Glycosidase-treated erythrocytes were incubated at 5 x 10^8 cells/ml in PBS with 100 mU/ml neuraminidase from *Vibrio cholerae* (Sigma) 1 hour at 37°C; reduction in Ter119 molecular weight was validated using Western blot (**Figure 6-18D,E**). Two hundred thousand erythroctyes were lysed using RIPA buffer with protease inhibitors and loaded into a 15% polyacrylamide gel, transferred to PVDF membrane (Bio-Rad) and probed overnight with anti-Ter119 antibody (eBioscience) at 1:15,000 and goat anti-rat-HRP (Invitrogen) for 1 hour at 1:5000 in TBS with 0.1% Tween-20. Membranes were stripped using Restore (Thermo) and reprobed overnight with anti-GAPDH (clone GA1R, Invitrogen) at 1:3000 and anti-mouse-HRP (Cell Signaling Technologies) at 1:3000 in PBS with 0.1% Tween-20. Membranes were imaged with SuperSignal West Pico PLUS Chemiluminescence (Thermo) and analyzed using ImageJ.

To prepare cell-free hemoglobin, erythrocytes were resuspended in 5 mM $NaPO_4$, pH 8.0 at

3 x 10^8 cells/ml and incubated for 30 minutes at room temperature with agitation, then filter-sterilized (Hand and King-Thompson, 1983). Concentration was calibrated using absorbance at 404 nm based on a standard curve of bovine hemoglobin (Sigma). Oxidized hemoglobin was obtained by incubating fresh hemoglobin at 37°C for 7 days. Redox state was validated using absorbance spectroscopy compared to fresh erythrocytes lysed with 1% Triton X-100 and bovine methemoglobin (Sigma).

Bodipy-stained erythrocytes were prepared by incubating erythrocytes at 1 x 10^8 / ml in PBS with 5 µg/ml Bodipy-500/510-C12 (Invitrogen) for 1 hours at 37°C, then washing twice in PBS prior to addition to infected macrophages.

Infection of cell culture macrophages. Bacteria from overnight cultures were diluted to 3e7 cfu/ml in complete cell culture medium and used to infect BMDMs. In some experiments, fluorescence dilution strains harboring pDiGi and *rpsM*::GFP (ALR#258, #391) were co-infected with strains harboring pDiGi (ALR#228, #383), both at 3e7 cfu/ml (**Appendix E**). After 45 minutes, medium was exchanged for medium containing 100 µg/ml gentamicin to kill extracellular bacteria. Where indicated, at 90 minutes post infection cytochalasin D was spiked into wells to yield a final concentration of 20 µM unless otherwise indicated. At 2 hours post infection, medium was exchanged for medium containing 10 µg/ml gentamicin and additional reagents as indicated in figure legends. Erythrocytes were added at a ratio of 10 erythrocytes per macrophage unless otherwise indicated. In some experiments, conditioned medium from infected wells was collected at 18 h.p.i., pelleted and the supernatant frozen at -20°C, and added to freshly infected macrophages at 2 h.p.i. For experiments with transwells, macrophages were derived and infected as described. At 2 h.p.i. polyester transwell inserts with 0.4 µm pores (Greiner) were added to wells and medium was added to both compartments, yielding twice the final volume as in experiments without transwells.

For experiments with signaling inhibitors, infected macrophages were treated with drugs

from 1-18 h.p.i. Concentrated drug was added at 1 h.p.i. and again when medium was exchanged for low gentamicin at 2 h.p.i. All drugs were dissolved in DMSO except where indicated. Final concentrations were as follows: PD98059: 50 μM. SB203580: 50 μM. NVP-BEZ235: 500 nM (DMF). Tofacitinib: 500 nM. BMS-345541: 2 μM. LY294002: 10 μM. SP600125: 50 μm. Genistein: 200 μM.

At 18 hours post infection, samples were washed three times with PBS and lysed with 0.1% Triton X-100. A portion of the lysate was diluted in PBS and plated to determine colony-forming units (CFU). The remainder of the lysate was centrifuged for 20 minutes at 2500 x *g* at 10 °C, fixed with 1.6% paraformaldehyde, and analyzed using a CyAn ADP flow cytometer (Beckman Coulter). A minimum of 30,000 GFP+ events were collected for analysis. Data were analyzed with FlowJo. Samples were gated for GFP-positive bacteria. Bacterial fold replication was calculated as the dsRed geometric mean of the inoculum divided by that of the GFP+ population at 18 hours post infection (Helaine et al., 2010).

For samples from fixed macrophages, populations were sorted (see below) into 0.1% Triton X-100, pelleted, resuspended in 0.1% Triton X-100, vortexed, and incubated for 30 minutes at room temperature to release bacteria prior to washing with PBS and analysis by flow cytometry as described above. For samples from macrophages sorted for uptake of pHrodo-Green-labeled T cells, macrophages were infected with bacteria harboring pDiGi only (without *rpsM*::GFP). After sorting and lysis, samples were stained with 10 μM DAPI for 20 minutes at room temperature and analyzed via flow cytometry; bacteria were identified using FL-6 fluorescence and dsRed fluorescence was quantified as above.

Where indicated, supernatants were collected by pipetting without disturbing settled cells and [nitrite] was quantified using the colorimetric Griess assay (Sigma) following the manufacturer's instructions. Raw absorbance was converted to μM nitrite using a standard curve of sodium nitrite dissolved in cell culture media.

Neutral Griess reaction. Nitric oxide production was measured in real-time (Ridnour et al., 2000) using the neutral Griess reagent (100 mM phosphate buffer, pH 7.4, 17 mM sulfanilamide, and 0.4 mM N-(1-Naphthyl)ethyleediamine). Briefly, the indicated concentrations of scavengers in complete medium were combined with 2X neutral Griess reagent and 100 μM diethylamine-NONOate (deaNONO) and the absorbance at 496 nm was measured every 1 minute for 1 hour. The reported extinction coefficient in 100 mM phosphate buffer (ε = 6600 M^{-1} cm^{-1}) was used to calculate nitric oxide concentration using Beer's law (c = A / ε * pathlength).

Flow cytometry and FACS of hemophagocytes. To detect erythrocytes within macrophages for analysis or FACS, samples were processed essentially as described (McDonald et al., 2016; Pilonieta et al., 2014). Macrophages were infected with nonfluroescent wild-type bacteria. Wells were washed with ACK lysis buffer (150 mM NH_4Cl, 10 mM $KHCO_3$, 100 μM EDTA, pH 7.4) for 1 minute to lyse extracellular erythrocytes, then treated with cold ion-free PBS, 2.5 mM EDTA at 4°C for 10-15 minutes prior to gentle scraping to suspend adherent cells. Samples were pelleted and stained with Live/Dead Near-IR stain (Life Technologies) at 1:3000 in PBS for 20 minutes and washed in PBS. Samples were then Fc-blocked with anti-CD16/32 (eBioscience) in staining buffer for 20 minutes prior to fixation, permeabilization, and staining with anti-Ter119-APC at 1:200 (eBioscience) as described.

For experiments with T cells, the pH-sensitive dye pHrodo-Green STP Ester (Invitrogen) was used to detect internalized cells. One hundred million Jurkats in 10 mL PBS were stained with 1 μL dye for 1 hour at 37 °C and washed twice in complete medium prior to addition to infected macrophages. Processing for flow cytometry or FACS was performed as for experiments with erythrocytes, except that the ACK lysis step was replaced with a PBS wash, and samples were fixed and analyzed after Live/Dead staining.

Cytokine profiling. Cell culture supernatants were harvested, pelleted, and supernatants were frozen at -80 °C until analysis using the ProcartaPlex Multiplex Immunoassay kit. Samples were analyzed using a Luminex Magpix system.

RNA extraction and quantitative PCR. Bacteria from infected macrophages were pelleted and lysed using lysozyme and RLT according to the Qiagen RNeasy kit. RNA was extracted following the PureLink kit except with 70% EtOH to precipitate nucleic acids, followed by DNase digestion (Qiagen RNase-free DNase) for 30 minutes at room temperature, followed by inactivation using heat/EDTA. Five micrograms RNA in 100 microliters was reverse transcribed using the iScript cDNA synthesis kit, diluted 3.5 fold, and 8 microliters was used as template in SYBR-Green quantitative PCR. Cts were normalized to the reference gene *recA*, and normalized as indicated in the figure legend following the 2^- ΔΔCt method.

Mammalian RNA was extracted following the RNeasy kit including on-column DNase treatment and quantitifed using reverse-transcriptase quantitative PCR. One microgram RNA in 20 microliters was reverse transcribed using the iScript cDNA synthesis kit, diluted 10-fold, and 8-10 microliters was used as template in SYBR-Green quantitative PCR. Cts were normalized to the reference genes *Hprt*, and normalized as described in the legends following the 2^- ΔΔCt method.

CHAPTER 7. FUTURE DIRECTIONS AND CLOSING REMARKS

A. INTRODUCTION: EXTREME *SALMONELLA*

Salmonella enterica serovar Typhimurium infection of mice has been studied for decades as a model for human typhoid fever. Some of the first mechanistic studies identified the *PhoPQ* operon as a key transcriptional regulator of virulence (Groisman et al., 1989; Miller et al., 1989b). Extensive characterization of two type III secretion systems (T3SS) and dozens of exported effectors illuminated how *Salmonella* modifies its host cells (Galán and Curtiss, 1989; Hensel et al., 1995, 1997, 1998; Ochman et al., 1996). Macrophages were identified as the central host cell for systemic infection and persistence (Monack, 2004; Vazquez-Torres et al., 1999), and many studies demonstrated how *Salmonella* survives macrophage insults (Alpuche Aranda et al., 1992; De Groote et al., 1996; Fang et al., 1992; Uchiya et al., 1999; Vazquez-Torres et al., 2000a). Transcriptional and proteomic profiling have yielded a larger picture of how *Salmonella* adapts to the host environment (Becker et al., 2006; Eriksson et al., 2003; Rollenhagen and Bumann, 2006; Shi et al., 2006; Steeb et al., 2013). Recently, new techniques have demonstrated that *Salmonella* infection is heterogeneous (Helaine et al., 2014; Saliba et al., 2016). Through these studies, we have built a highly detailed picture of the challenging host environment in which *Salmonella* survives, replicates, and causes infection.

I sought to add a few more details to our understanding of *Salmonella* host-pathogen interactions, and to leverage what we already know about *Salmonella* pathogenesis to identify novel therapeutic strategies. I employed an unbiased screen, hypothesis-driven approaches, and serendipitous observations on the path toward these results. My data suggests that there are myriad infection-specific pathways involved in *Salmonella* virulence, including bacterial efflux pumps and host autophagy. I also found that the macrophage niche is influenced by polarization, nutritional landscape, and other host cells, and that these factors alter the microenvironment experienced by *Salmonella* and the outcome of infection. Together, these

studies illustrate the complexity and uniqueness of the extreme *Salmonella*-macrophage host-pathogen interface.

B. *SALMONELLA* INFECTION OF MACROPHAGES YIELDS INFECTION-SPECIFIC ANTIMICROBIALS

Salmonella survives and replicates in a challenging environment using a variety of evasive strategies. We decided to search for small molecules that disrupt this host-pathogen interface. Similar studies have identified putative therapeutics and probes that illuminate novel aspects of host-pathogen interactions (Lieberman and Higgins, 2009; Maudet et al., 2014; Rybniker et al., 2014; Samantaray et al., 2016; Stanley et al., 2014).

I developed a medium-throughput screen to quantify *Salmonella* infection of cultured macrophages using fluorescence microscopy. I first assessed the importance of several elements of the standard infection protocol (Nagy et al., 2013). I found that several steps meant to enhance *Salmonella* uptake/invasion had minimal effects on bulk infection (**Appendix A**). However, I cannot rule out that these changes could affect infection on a single-cell level, which could alter the physiological relevance of the infection model. For example, I found that opsonization of bacteria did not affect uptake or infection kinetics *in vitro*, but *Salmonella* is likely coated with complement *in vivo* and this could affect bacterial virulence gene expression. I also found no difference removing remaining extracellular bacteria after the internalization step and leaving them in culture with infected macrophages for 18 hours, though the increased extracellular LPS could affect the macrophage immune response. I also found that intracellular bacterial growth proceeded similarly regardless of the starting number of bacteria within macrophages, though higher bacterial loads caused more macrophage death. Thus, it is unclear what *in vitro* factors most truly resemble *in vivo* infection, and whether those factors are relevant for the outcome of infection.

We used the final streamlined assay to screen for small molecules that reduced bacterial load within macrophages (**Chapter 2**). Of the best 60 hits, only 7 affected bacterial growth in broth, indicating that many of the hits likely target bacterial or host factors specific to infection. Some of the hits have also been identified in other infection-based screens. Further, we also identified a variety of known bioactive compounds which were not known to possess antimicrobial activity. Thus, searching for compounds that perturb the *Salmonella* host-pathogen interface is an attractive strategy to identify novel antimicrobials.

A key future direction is to identify the mechanism of action of our anti-*Salmonella* compounds. I discuss some approaches and my work to that end below, but much of hit characterization and development is dependent on luck. Thus, amassing a larger collection of anti-*Salmonella* compounds is another key future direction to facilitate additional studies. Diverse small molecule libraries are available, including FDA-approved drugs, targeted screening collections, synthetic diversity libraries, and natural products. Investigating many different types of compounds may increase the likelihood of identifying an exciting hit. I screened a small library of synthetically modified natural products and identified several interesting structural classes (**Appendix D**); others are already screening other libraries to add to our collection of anti-*Salmonella* small molecules.

C. IDENTIFICATION OF DRUG TARGETS REVEALS KEY INTERACTIONS BETWEEN HOST AND PATHOGEN

Though it is relatively straightforward to screen for compounds that perturb *Salmonella* infection of macrophages, further studies to prioritize, characterize, and develop resulting hits are more challenging and mostly rely on luck. An attractive approach is to perform secondary screens for inhibition of pathogen or host functions; this approach can quickly identify a potential target pathway (Maudet et al., 2014; Rybniker et al., 2014). However, this approach is limited by the availability of secondary screens, and the creativity to develop new assays. We performed a

secondary screen on our hits for anti-efflux activity (Coldham et al., 2010), and found three compounds that inhibit *Salmonella* efflux of fluorescent dyes *in vitro* (**Chapter 3**). Small molecules can disrupt efflux by disrupting bacterial membrane potential, but we found no evidence that our drugs did so. We also found that the drugs bound a key efflux pump in *Salmonella*, AcrAB, suggesting they may directly inhibit the pump. We next hypothesized that efflux inhibition could sensitize bacteria to host antimicrobials within the macrophage, leading to increased killing. In support of this idea, the drugs synergized with antimicrobial peptides in broth, and also are active against *Salmonella* within HeLa cells, which express antimicrobial peptides (Mineshiba et al., 2005; Park et al., 2011). However, we were unable to test this hypothesis in macrophages for several reasons. First, macrophages express multiple (some unknown) antimicrobial peptides, so we were unable to demonstrate that anti-*Salmonella* activity required host antimicrobial peptides (Nguyen et al., 2011). Secondly, deletion of *Salmonella* efflux pump genes leads to upregulation of other efflux pumps which compensate for the missing pump (Wang-Kan et al., 2017). As a result, drug treatment of intracellular bacteria missing AcrAB yielded similar inhibition as treatment of intracellular wild-type bacteria. This data is consistent with the idea that the mutant strain has upregulation of other efflux pumps, which are then targeted by the inhibitor, but it could also suggest that efflux inhibition does not mediate activity against intracellular *Salmonella*. We initiated efforts to construct a point mutant in AcrAB which does not display compensatory expression of other pumps to further investigate this possibility. However, it may be challenging to perform studies with drug treatment of intracellular bacterial mutants, as if the mutation independently causes a severe defect it is impossible the measure the activity of the drug. Thus, it remains unclear whether efflux pump inhibition actually mediates anti-*Salmonella* activity of these drugs. Indeed, additional work by Amy Crooks has shown that derivatives of these drugs with improved anti-*Salmonella* activity do not have improved anti-efflux activity.

Thus, secondary screens have a key limitation as a path to target identification: Even though a drug may inhibit a particular pathogen or host function in a secondary assay, additional studies are required to verify whether that identified activity mediates the antibacterial activity. We have employed other secondary screens to assay other potential mechanisms of action, including induction of autophagy, disruption of bacterial membranes, and inhibition of *Salmonella* virulence gene expression. Future work will involve developing additional secondary screens based on possible mechanisms of action for anti-*Salmonella* compounds.

An alternative approach to target identification is to focus on known compounds with information about toxicity and chemistry. With luck, this approach can be a quick route to a mechanism (Kouznetsova et al., 2014; Stanley et al., 2014), but we and others have encountered roadblocks (Andersson et al., 2016; Lieberman and Higgins, 2009, 2010). I studied the small molecule clomipramine, a known tricyclic antidepressant, but the antibacterial mechanism remains unclear (**Chapter 4**). Clomipramine inhibits the serotonin reuptake transporter (SERT) which can alter macrophage activation state (de las Casas-Engel et al., 2013), but extracellular serotonin levels or SERT expression did not alter clomipramine anti-*Salmonella* activity. Clomipramine also targets other neurotransmitter transporters, but we found no evidence using related compounds with differing specificities that this activity mediated anti-*Salmonella* activity. TCAs have been shown to disrupt bacterial efflux and host calmodulin / calcium signaling (Asano, 1989; Prozialeck and Weiss, 1982a; Rodrigues et al., 2008), but I found no evidence that these activities mediated activity against intracellular *Salmonella*. Other reports indicate that TCAs modulates autophagy (Guan et al., 2018; Rossi et al., 2009), and we indeed found that clomipramine induces accumulation of autophagosomes in uninfected macrophages. Additional work is required to establish whether and how autophagy induced by clomipramine leads to bacterial killing. Thus, although clomipramine is a known drug, its antibacterial target remains unknown.

An additional possible future approach to target identification is to incorporate *in silico* techniques to screening and characterization. Recently, other groups have employed multiparameter assays and systems biology integration to identify putative targets (Christophe et al., 2009; Korbee et al., 2018; Sundaramurthy et al., 2013); these approaches may revolutionize downstream assays of hits from empirical small molecule screens. However, even this approach has the limitation of whether an identified target pathway is the target that mediates antimicrobial activity. Thus, validation experiments in the primary assay will always be required to truly understand how a novel compound eliminates intracellular bacteria.

Successful identification of the target of a novel antimicrobial represents a large step forward for understanding how pathogens cause disease as well as future efforts toward developing therapeutics. Repurposed drugs that target host pathways could reveal a new player in the interactions between host and pathogen (Stanley et al., 2014). Novel drugs that inhibit known therapeutic targets could be developed into a clinical drug, such as our putative efflux pump inhibitors. Previously unknown therapeutic targets could be identified and exploited for future drug development (Rybniker et al., 2014). Thus, screening for antimicrobials must be united with creative approaches to target identification to not only characterize the initial hits, but also to lay the foundation for future progress.

D. DIVERSE HOST MICROENVIRONMENTS PRODUCE UNIQUE INTERACTIONS BETWEEN HOST AND PATHOGEN

Early studies with *Salmonella* emphasized the centrality of macrophages for infection (Monack, 2004; Vazquez-Torres et al., 1999), but we are beginning to better understand the full diversity of macrophages (Mosser and Edwards, 2008). Indeed, other studies have recently shown that *Salmonella* infection varies in certain macrophage subclasses (Burton et al., 2014; Diacovich et al., 2016; Eisele et al., 2013), suggesting unique niches impact bacterial strategies and the outcome of infection. I studied *in vitro* infection of several kinds of macrophages and

found that *Salmonella* nutrient use and replication was strongly affected by macrophage activation and by co-culture of other host cells.

Macrophage polarization and metabolism are tightly linked (Galván-Peña and O'Neill, 2014; Jha et al., 2015), and host cell metabolism likely affects the nutrients available for intracellular bacteria (Eisenreich et al., 2015). Using a series of *Salmonella* mutants lacking lipid metabolism genes, I found that *Salmonella* utilizes lipids in pro-inflammatory but not anti-inflammatory macrophages (**Chapter 5**). Also, this defect was only present when macrophages were supplemented with non-essential amino acids, which appeared to increase *Salmonella* replication. As *Salmonella* acquires the majority of its amino acids from the host (Eriksson et al., 2003), surplus amino acids may license enhanced replication and confer a requirement for lipids for some replicating bacteria. Indeed, other evidence suggests that only a subset of bacteria with pro-inflammatory amino-acid-rich macrophages use lipids. This raises the question of whether bacteria within the same macrophage experience different nutritional microenvironments and thus employ different nutritional strategies. Future work could use microscopic correlation of growth and localization or single-cell RNA-sequencing to characterize the conditions that drive certain bacteria to utilize lipids (Helaine et al., 2010; Saliba et al., 2016).

I also explored the role of lipid metabolism genes during infection of mice. I found that mutants lacking lipid metabolism genes were defective, and that two β-oxidation pathways that metabolize lipids can compensate *in vivo*. This result is surprisingly, given that the pathways are primarily utilized for aerobic and anaerobic growth respectively *in vitro*. However, other factors may regulate their expression *in vivo*. Thus, future work to define in what kinds of *in vivo* cells *Salmonella* uses lipids could help define the regulatory cues of these two compensatory pathways.

Macrophages interact with multiple host cell types during infection, and host cell interactions can influence macrophage activation and immune response (de Back et al., 2014;

Co et al., 2004; Egen et al., 2008; Ohyagi et al., 2013; Voll et al., 1997). However, little is known about the impact of cellular interactions on replication of intracellular pathogens. I found that co-culture of infected macrophages with healthy erythrocytes, senescent erythrocytes, or T cells increased intracellular *Salmonella* replication (**Chapter 6**). Surprisingly, the replication increase for each cell type was mediated by a unique mechanism. Healthy erythrocytes did not affect macrophage activation or contribute nutrients to *Salmonella*, but instead scavenged nitric oxide and reduced nitrosative stress, enabling increased replication. In contrast, co-culture with senescent erythrocytes disrupted macrophage iron homeostasis and nitric oxide, likely through altering the inflammatory response. Finally, co-culture with T cells shifted macrophages toward an anti-inflammatory phenotype and increased iron access for *Salmonella*. Excitingly, this effect was dependent on uptake and occurred only within macrophages that had phagoytosed T cells, suggesting internal sensing of T cells may alter cell-intrinsic signaling or intercellular communication.

Taken together, these data argue that external factors strongly alter the macrophage microenvironment experienced by *Salmonella* and can change the progression of infection within macrophages. As additional studies detail the unique host-pathogen interface in many diverse microenvironments, we can broaden our understanding of infection across time, space, and hosts.

E. CONCLUSION: EXTREME ENVIRONMENTS AS A FRAMEWORK FOR STUDYING HOST-PATHOGEN INTERACTIONS

Though much is known about the challenging macrophage environment which *Salmonella* colonizes, new techniques and approaches will allow us to further probe this host-pathogen interface. Unbiased approaches such as small molecule screens and subsequent identification of infection-relevant targets have the potential to crack open new host and pathogen pathways involved in infection. Are there host pathways that can be activated to clear *Salmonella*? What

host pathways are required for *Salmonella* infection? Are bacteria in different subsets of macrophages targeted differently by drugs? The idea of pathogen and host heterogeneity represents a paradigm shift in defining host-pathogen interactions, and expands the possible lines of investigation. How does *Salmonella* nutrient use change between acute and chronic infection? What flavors of macrophages host replicating and non-replicating bacteria? How do infected macrophages interact with uninfected macrophages? Answering questions like these will continue to add color to the fascinating picture of how *Salmonella* causes infection.

For other pathogens, many of these themes and questions will also expand our understanding of disease. Macrophages are a host cell for many other pathogens, including *Brucella abortus*, *Mycobacterium tuberculosis, Coxiella burnetii*, *Legionella pneumophila*, and *Listeria monocytogenes*. Similar to my studies in *Salmonella*, questions remain about bacterial and host pathways that could be targeted by small molecules and how bacterial nutrition and replication is influenced by the unique macrophage state, including activation and cellular interactions. These themes also apply to bacteria that colonize other host cell types, such as epithelial cells, as well as to extracellular pathogens. What players enable these microbes to survive in these challenging environments? What factors coalesce to shape the particular niche? How do unique microenvironments contribute to the progression and outcome of infection? Ultimately, exploring how pathogens survive and replicate in an extreme host environment is a compelling framework for studying host-pathogen interactions.

REFERENCES

Abouzeed, Y.M., Baucheron, S., and Cloeckaert, A. (2008). ramR Mutations Involved in Efflux-Mediated Multidrug Resistance in Salmonella enterica Serovar Typhimurium▽. Antimicrobial Agents and Chemotherapy *52*, 2428–2434.

Aderem, A., and Ulevitch, R.J. (2000). Toll-like receptors in the induction of the innate immune response. Nature *406*, 782–787.

Akilesh, H.M., Buechler, M.B., Duggan, J.M., Hahn, W.O., Matta, B., Sun, X., Gessay, G., Whalen, E., Mason, M., Presnell, S.R., et al. (2019). Chronic TLR7 and TLR9 signaling drives anemia via differentiation of specialized hemophagocytes. Science *363*, eaao5213.

Alam, M.Z., Devalaraja, S., and Haldar, M. (2017). The Heme Connection: Linking Erythrocytes and Macrophage Biology. Frontiers in Immunology *8*, 33.

Allen, R.C., Popat, R., Diggle, S.P., and Brown, S.P. (2014). Targeting virulence: can we make evolution-proof drugs? Nature Reviews Microbiology *12*, 300–308.

Alonso, A., and Martinez, J.L. (2001). Expression of Multidrug Efflux Pump SmeDEF by Clinical Isolates of Stenotrophomonas maltophilia. Antimicrobial Agents and Chemotherapy *45*, 1879–1881.

Alpuche Aranda, C.M., Swanson, J.A., Loomis, W.P., and Miller, S.I. (1992). Salmonella typhimurium activates virulence gene transcription within acidified macrophage phagosomes. Proc Natl Acad Sci USA *89*, 10079.

Amaral, L., and Viveiros, M. (2012). Why thioridazine in combination with antibiotics cures extensively drug-resistant Mycobacterium tuberculosis infections. International Journal of Antimicrobial Agents *39*, 376–380.

AMARAL, L., KRISTIANSEN, J., and LORIAN, V. (1992). Synergic effect of chiorpromazine on the activity of some antibiotics. Journal of Antimicrobial Chemotherapy *30*, 556–558.

Aminov, R.I. (2010). A Brief History of the Antibiotic Era: Lessons Learned and Challenges for the Future. Frontiers in Microbiology *1*, 134.

Andersen, J.L., He, G.-X., Kakarla, P., K C, R., Kumar, S., Lakra, W.S., Mukherjee, M.M., Ranaweera, I., Shrestha, U., Tran, T., et al. (2015). Multidrug efflux pumps from Enterobacteriaceae, Vibrio cholerae and Staphylococcus aureus bacterial food pathogens. International Journal of Environmental Research and Public Health *12*, 1487–1547.

Andersson, J.A., Fitts, E.C., Kirtley, M.L., Ponnusamy, D., Peniche, A.G., Dann, S.M., Motin, V.L., Chauhan, S., Rosenzweig, J.A., Sha, J., et al. (2016). New Role for FDA-Approved Drugs in Combating Antibiotic-Resistant Bacteria. Antimicrobial Agents and Chemotherapy *60*, 3717–3729.

Anuforom, O., Wallace, G.R., Buckner, M.M.C., and Piddock, L.J.V. (2016). Ciprofloxacin and ceftriaxone alter cytokine responses, but not Toll-like receptors, to *Salmonella* infection *in vitro*. Journal of Antimicrobial Chemotherapy dkw092.

Arnold, C.E., Gordon, P., Barker, R.N., and Wilson, H.M. (2015). The activation status of human macrophages presenting antigen determines the efficiency of Th17 responses. Immunobiology *220*, 10–19.

Asano, M. (1989). Divergent pharmacological effects of three calmodulin antagonists, N-(7-aminohexyl)-5-chloro-1-naphtalenesulfonamide (W-7), chlorpromazine and calmidazolium, on isometric tension development and myosin light chain phosphorylation in intact bovine tracheal smooth muscle. Journal of Experimental Medicine *251*, 764–773.

Ashburn, T.T., and Thor, K.B. (2004). Drug repositioning: identifying and developing new uses for existing drugs. Nature Reviews Drug Discovery *3*, 673–683.

de Back, D., Kostova, E., van Kraaij, M., van den Berg, T., and Van Bruggen, R. (2014). Of macrophages and red blood cells; a complex love story. Frontiers in Physiology *5*, 9.

Bals, R., Wang, X., Zasloff, M., and Wilson, J.M. (1998). The peptide antibiotic LL-37/hCAP-18 is expressed in epithelia of the human lung where it has broad antimicrobial activity at the airway surface. Proceedings of the National Academy of Sciences *95*, 9541–9546.

Barat, S., Steeb, B., Mazé, A., and Bumann, D. (2012). Extensive in vivo resilience of persistent Salmonella. PloS One *7*, e42007.

Baucheron, S., Imberechts, H., Chaslus-Dancla, E., and Cloeckaert, A. (2004). The AcrB Multidrug Transporter Plays a Major Role in High-Level Fluoroquinolone Resistance in Salmonella enterica Serovar Typhimurium Phage Type DT204. Microbial Drug Resistance *8*, 281–289.

Bauler, T.J., Starr, T., Nagy, T.A., Sridhar, S., Scott, D., Winkler, C.W., Steele-Mortimer, O., Detweiler, C.S., and Peterson, K.E. (2017). Salmonella Meningitis Associated with Monocyte Infiltration in Mice. The American Journal of Pathology *187*, 187–199.

Becker, D., Selbach, M., Rollenhagen, C., Ballmaier, M., Meyer, T.F., Mann, M., and Bumann, D. (2006). Robust Salmonella metabolism limits possibilities for new antimicrobials. Nature *440*, 303–307.

Behrens, E.M., Canna, S.W., Slade, K., Rao, S., Kreiger, P.A., Paessler, M., Kambayashi, T., and Koretzky, G.A. (2011). Repeated TLR9 stimulation results in macrophage activation syndrome–like disease in mice. Journal of Clinical Investigation *121*, 2264–2277.

Bellora, F., Castriconi, R., Dondero, A., Reggiardo, G., Moretta, L., Mantovani, A., Moretta, A., and Bottino, C. (2010). The interaction of human natural killer cells with either unpolarized or polarized macrophages results in different functional outcomes. Proceedings of the National Academy of Sciences *107*, 21659–21664.

Benoit, M., Desnues, B., and Mege, J.-L. (2008). Macrophage Polarization in Bacterial Infections. J. Immunol. *181*, 3733.

Benson, T.J., McKie, J.H., Garforth, J., Borges, A., Fairlamb, A.H., and Douglas, K.T. (1992). Rationally designed selective inhibitors of trypanothione reductase. Phenothiazines and related tricyclics as lead structures. Biochem. J *286*, 9–11.

Berggren, R.E., Wunderlich, A., Ziegler, E., Schleicher, M., Duke, R.C., Looney, D., and Fang, F.C. (1995). HIV gp120-specific cell-mediated immune responses in mice after oral immunization with recombinant Salmonella. J Acquir Immune Defic Syndr Hum Retrovirol *10*, 489–495.

Berghaus, L.J., Moore, J.N., Hurley, D.J., Vandenplas, M.L., Fortes, B.P., Wolfert, M.A., and Boons, G.-J. (2010). Innate immune responses of primary murine macrophage-lineage cells and RAW 264.7 cells to ligands of Toll-like receptors 2, 3, and 4. Comparative Immunology, Microbiology and Infectious Diseases *33*, 443–454.

Bijlsma, J.J.E., and Groisman, E.A. (2005). The PhoP/PhoQ system controls the intramacrophage type three secretion system of Salmonella enterica. Mol Microbiol *57*, 85–96.

Bingisser, R.M., Tilbrook, P.A., Holt, P.G., and Kees, U.R. (1998). Macrophage-Derived Nitric Oxide Regulates T Cell Activation via Reversible Disruption of the Jak3/STAT5 Signaling Pathway. J. Immunol. *160*, 5729.

Birge, R.B., Boeltz, S., Kumar, S., Carlson, J., Wanderley, J., Calianese, D., Barcinski, M., Brekken, R.A., Huang, X., Hutchins, J.T., et al. (2016). Phosphatidylserine is a global immunosuppressive signal in efferocytosis, infectious disease, and cancer. Cell Death And Differentiation *23*, 962.

Birkenstock, T., Liebeke, M., Winstel, V., Krismer, B., Gekeler, C., Niemiec, M.J., Bisswanger, H., Lalk, M., and Peschel, A. (2012). Exometabolome Analysis Identifies Pyruvate Dehydrogenase as a Target for the Antibiotic Triphenylbismuthdichloride in Multiresistant Bacterial Pathogens. Journal of Biological Chemistry *287*, 2887–2895.

Birmingham, C.L., Smith, A.C., Bakowski, M.A., Yoshimori, T., and Brumell, J.H. (2006). Autophagy controls Salmonella infection in response to damage to the Salmonella-containing vacuole. J Biol Chem *281*, 11374–11383.

Biswas, S.K., and Mantovani, A. (2010). Macrophage plasticity and interaction with lymphocyte subsets: cancer as a paradigm. Nat Immunol *11*, 889–896.

Biswas, S.K., and Mantovani, A. (2012). Orchestration of Metabolism by Macrophages. Cell Metabolism *15*, 432–437.

Bode, C., Diedrich, B., Muenster, S., Hentschel, V., Weisheit, C., Rommelsheim, K., Hoeft, A., Meyer, R., Boehm, O., Knuefermann, P., et al. (2014). Antibiotics regulate the immune response in both presence and absence of lipopolysaccharide through modulation of Toll-like receptors, cytokine production and phagocytosis in vitro. International Immunopharmacology *18*, 27–34.

Bodet, C., Chandad, F., and Grenier, D. (2005). Modulation of cytokine production by Porphyromonas gingivalis in a macrophage and epithelial cell co-culture model. Microbes and Infection *7*, 448–456.

Bogdan, C., and Nathan, C. (1993). Modulation of macrophage function by transforming growth factor beta, interleukin-4, and interleukin-10. Ann N Y Acad Sci *685*, 713–739.

Bogomolnaya, L.M., Andrews, K.D., Talamantes, M., Maple, A., Ragoza, Y., Vazquez-Torres, A., and Andrews-Polymenis, H. (2013). The ABC-Type Efflux Pump MacAB Protects Salmonella enterica serovar Typhimurium from Oxidative Stress. MBio *4*, e00630-13-e00630-13.

Bohnert, J.A., Karamian, B., and Nikaido, H. (2010). Optimized Nile Red Efflux Assay of AcrAB-TolC Multidrug Efflux System Shows Competition between Substrates. Antimicrobial Agents and Chemotherapy *54*, 3770–3775.

Borges da Silva, H., Fonseca, R., Pereira, R.M., Cassado, A. dos A., Álvarez, J.M., and D'Império Lima, M.R. (2015). Splenic Macrophage Subsets and Their Function during Blood-Borne Infections. Frontiers in Immunology *6*, 480.

Boucrot, E. (2005). The Intracellular Fate of Salmonella Depends on the Recruitment of Kinesin. Science *308*, 1174–1178.

Bowden, S.D., Rowley, G., Hinton, J.C.D., and Thompson, A. (2009). Glucose and Glycolysis Are Required for the Successful Infection of Macrophages and Mice by Salmonella enterica Serovar Typhimurium. Infection and Immunity *77*, 3117–3126.

Bowden, S.D., Ramachandran, V.K., Knudsen, G.M., Hinton, J.C.D., and Thompson, A. (2010). An Incomplete TCA Cycle Increases Survival of Salmonella Typhimurium during Infection of Resting and Activated Murine Macrophages. PLoS ONE *5*, e13871.

Bowden, S.D., Hopper-Chidlaw, A.C., Rice, C.J., Ramachandran, V.K., Kelly, D.J., and Thompson, A. (2014). Nutritional and Metabolic Requirements for the Infection of HeLa Cells by Salmonella enterica Serovar Typhimurium. PLOS ONE *9*, e96266.

Bratosin, D., Mazurier, J., Tissier, J.P., Estaquier, J., Huart, J.J., Ameisen, J.C., Aminoff, D., and Montreuil, J. (1998). Cellular and molecular mechanisms of senescent erythrocyte phagocytosis by macrophages. A review. Biochimie *80*, 173–195.

Brideau, C., Gunter, B., Pikounis, B., and Liaw, A. (2003). Improved Statistical Methods for Hit Selection in High-Throughput Screening. Journal of Biomolecular Screening *8*, 634–647.

British Medical Association, Royal Pharmaceutical Society of Great Britain, and Joint Formulary Committee (Great Britain) (2006). BNF (London: BMJ).

Brodin, P., Poquet, Y., Levillain, F., Peguillet, I., Larrouy-Maumus, G., Gilleron, M., Ewann, F., Christophe, T., Fenistein, D., Jang, J., et al. (2010). High Content Phenotypic Cell-Based Visual Screen Identifies Mycobacterium tuberculosis Acyltrehalose-Containing Glycolipids Involved in Phagosome Remodeling. PLoS Pathogens *6*, e1001100.

Brown, D.E., McCoy, M.W., Pilonieta, M.C., Nix, R.N., and Detweiler, C.S. (2010). Chronic Murine Typhoid Fever Is a Natural Model of Secondary Hemophagocytic Lymphohistiocytosis. PLoS ONE *5*, e9441.

Brumell, J.H., and Grinstein, S. (2004). Salmonella redirects phagosomal maturation. Current Opinion in Microbiology *7*, 78–84.

Brumell, J.H., Goosney, D.L., and Finlay, B.B. (2002). SifA, a type III secreted effector of Salmonella typhimurium, directs Salmonella-induced filament (Sif) formation along microtubules. Traffic *3*, 407–415.

Buchmeier, N.A., and Heffron, F. (1991). Inhibition of macrophage phagosome-lysosome fusion by Salmonella typhimurium. Infect Immun *59*, 2232–2238.

Buckley, A.M., Webber, M.A., Cooles, S., Randall, L.P., La Ragione, R.M., Woodward, M.J., and Piddock, L.J.V. (2006). The AcrAB-TolC efflux system of Salmonella enterica serovar Typhimurium plays a role in pathogenesis. Cellular Microbiology *8*, 847–856.

Bumann, D. (2015). Heterogeneous Host-Pathogen Encounters: Act Locally, Think Globally. Cell Host & Microbe *17*, 13–19.

Bumann, D., and Schothorst, J. (2017). Intracellular Salmonella metabolism. Cell Microbiol *19*.

Burger, P., Hilarius-Stokman, P., de Korte, D., van den Berg, T.K., and van Bruggen, R. (2012). CD47 functions as a molecular switch for erythrocyte phagocytosis. Blood *119*, 5512–5521.

Burton, N.A., Schürmann, N., Casse, O., Steeb, A.K., Claudi, B., Zankl, J., Schmidt, A., and Bumann, D. (2014). Disparate Impact of Oxidative Host Defenses Determines the Fate of Salmonella during Systemic Infection in Mice. Cell Host & Microbe *15*, 72–83.

Cairo, G., Recalcati, S., Mantovani, A., and Locati, M. (2011). Iron trafficking and metabolism in macrophages: contribution to the polarized phenotype. Trends in Immunology *32*, 241–247.

Campbell, J.W., and Cronan, J.E. (2002). The Enigmatic Escherichia coli fadE Gene Is yafH. Journal of Bacteriology *184*, 3759–3764.

Campbell, J.W., Morgan-Kiss, R.M., and E Cronan, J. (2003). A new Escherichia coli metabolic competency: growth on fatty acids by a novel anaerobic β-oxidation pathway. Molecular Microbiology *47*, 793–805.

Canton, J., Neculai, D., and Grinstein, S. (2013). Scavenger receptors in homeostasis and immunity. Nat Rev Immunol *13*, 621–634.

Carey, K.L., Westwood, N.J., Mitchison, T.J., and Ward, G.E. (2004). A small-molecule approach to studying invasive mechanisms of Toxoplasma gondii. Proceedings of the National Academy of Sciences of the United States of America *101*, 7433–7438.

Carlier, M.-B., Scorneaux, B., Zenebergh, A., Desnottes, J.-F., and Tulkens, P.M. (1990). Cellular uptake, localization and activity of fluoroquinolones in uninfected and infected macrophages. Journal of Antimicrobial Chemotherapy *26*, 27–39.

Carryn, S., Chanteux, H., Seral, C., Mingeot-Leclercq, M.-P., Van Bambeke, F., and Tulkens, P.M. (2003). Intracellular pharmacodynamics of antibiotics. Infectious Disease Clinics of North America *17*, 615–634.

de las Casas-Engel, M., Dominguez-Soto, A., Sierra-Filardi, E., Bragado, R., Nieto, C., Puig-Kroger, A., Samaniego, R., Loza, M., Corcuera, M.T., Gomez-Aguado, F., et al. (2013).

Serotonin Skews Human Macrophage Polarization through HTR2B and HTR7. The Journal of Immunology *190*, 2301–2310.

Cederlund, H., and Mardh, P.A. (1993). Antibacterial activities of non-antibiotic drugs. J Antimicrob Chemother *32*, 355–365.

Cegelski, L., Marshall, G.R., Eldridge, G.R., and Hultgren, S.J. (2008). The biology and future prospects of antivirulence therapies. Nature Reviews Microbiology *6*, 17–27.

Chakravortty, D., Hansen-Wester, I., and Hensel, M. (2002). Salmonella pathogenicity island 2 mediates protection of intracellular Salmonella from reactive nitrogen intermediates. J Exp Med *195*, 1155–1166.

Chan, Y.Y., and Chua, K.L. (2005). The Burkholderia pseudomallei BpeAB-OprB Efflux Pump: Expression and Impact on Quorum Sensing and Virulence. Journal of Bacteriology *187*, 4707–4719.

Chan, C., Yin, H., Garforth, J., McKie, J.H., Jaouhari, R., Speers, P., Douglas, K.T., Rock, P.J., Yardley, V., Croft, S.L., et al. (1998). Phenothiazine inhibitors of trypanothione reductase as potential antitrypanosomal and antileishmanial drugs. Journal of Medicinal Chemistry *41*, 148–156.

Chan, J.H., Hong, J.S., Kuyper, L.F., Baccanari, D.P., Joyner, S.S., Tansik, R.L., Boytos, C.M., and Rudolph, S.K. (1995). Selective Inhibitors of Candida albicans Dihydrofolate Reductase: Activity and Selectivity of 5-(Arylthio)-2,4-diaminoquinazolin. J. Med. Chem *38*, 3608–3616.

Chevalier, J., Mahamoud, A., Baitiche, M., Adam, E., Viveiros, M., Smarandache, A., Militaru, A., Pascu, M.L., Amaral, L., and Pagès, J.-M. (2010). Quinazoline derivatives are efficient chemosensitizers of antibiotic activity in Enterobacter aerogenes, Klebsiella pneumoniae and Pseudomonas aeruginosa resistant strains. International Journal of Antimicrobial Agents *36*, 164–168.

Christophe, T., Jackson, M., Jeon, H.K., Fenistein, D., Contreras-Dominguez, M., Kim, J., Genovesio, A., Carralot, J.-P., Ewann, F., Kim, E.H., et al. (2009). High Content Screening Identifies Decaprenyl-Phosphoribose 2′ Epimerase as a Target for Intracellular Antimycobacterial Inhibitors. PLOS Pathogens *5*, e1000645.

Chung, E.Y., Liu, J., Homma, Y., Zhang, Y., Brendolan, A., Saggese, M., Han, J., Silverstein, R., Selleri, L., and Ma, X. (2007). Interleukin-10 expression in macrophages during phagocytosis of apoptotic cells is mediated by homeodomain proteins Pbx1 and Prep-1. Immunity *27*, 952–964.

Cirillo, D.M., Valdivia, R.H., Monack, D.M., and Falkow, S. (1998). Macrophage-dependent induction of the Salmonella pathogenicity island 2 type III secretion system and its role in intracellular survival. Molecular Microbiology *30*, 175–188.

Clardy, J., Fischbach, M.A., and Walsh, C.T. (2006). New antibiotics from bacterial natural products. Nat Biotech *24*, 1541–1550.

Clark, D., and Cronan, J. (2005). Two-Carbon Compounds and Fatty Acids as Carbon Sources. EcoSal Plus.

Clatworthy, A.E., Pierson, E., and Hung, D.T. (2007). Targeting virulence: a new paradigm for antimicrobial therapy. Nature Chemical Biology *3*, 541–548.

Co, D.O., Hogan, L.H., Kim, S.-I., and Sandor, M. (2004). Mycobacterial granulomas: keys to a long-lasting host–pathogen relationship. Clinical Immunology *113*, 130–136.

Coldham, N.G., Webber, M., Woodward, M.J., and Piddock, L.J.V. (2010). A 96-well plate fluorescence assay for assessment of cellular permeability and active efflux in Salmonella enterica serovar Typhimurium and Escherichia coli. Journal of Antimicrobial Chemotherapy *65*, 1655–1663.

Corna, G., Campana, L., Pignatti, E., Castiglioni, A., Tagliafico, E., Bosurgi, L., Campanella, A., Brunelli, S., Manfredi, A.A., Apostoli, P., et al. (2010). Polarization dictates iron handling by inflammatory and alternatively activated macrophages. Haematologica *95*, 1814.

Costa, S.S., Lopes, E., Azzali, E., Machado, D., Coelho, T., da Silva, P.E.A., Viveiros, M., Pieroni, M., and Couto, I. (2016). An Experimental Model for the Rapid Screening of Compounds with Potential Use Against Mycobacteria. ASSAY and Drug Development Technologies *14*, 524–534.

Cremades, N., Velázquez-Campoy, A., Martínez-Júlvez, M., Neira, J.L., Pérez-Dorado, I., Hermoso, J., Jiménez, P., Lanas, A., Hoffman, P.S., and Sancho, J. (2009). Discovery of Specific Flavodoxin Inhibitors as Potential Therapeutic Agents against *Helicobacter pylori* Infection. ACS Chemical Biology *4*, 928–938.

Crouch, M.-L.V., Castor, M., Karlinsey, J.E., Kalhorn, T., and Fang, F.C. (2008). Biosynthesis and IroC-dependent export of the siderophore salmochelin are essential for virulence of Salmonella enterica serovar Typhimurium. Molecular Microbiology *67*, 971–983.

Crump, J.A., Luby, S.P., and Mintz, E.D. (2004). The global burden of typhoid fever. Bulletin of the World Health Organization *82*, 346–353.

Czyz, D.M., Potluri, L.-P., Jain-Gupta, N., Riley, S.P., Martinez, J.J., Steck, T.L., Crosson, S., Shuman, H.A., and Gabay, J.E. (2014). Host-Directed Antimicrobial Drugs with Broad-Spectrum Efficacy against Intracellular Bacterial Pathogens. MBio *5*, e01534-14-e01534-14.

Dandekar, T., Fieselmann, A., Fischer, E., Popp, J., Hensel, M., and Noster, J. (2014). Salmonella-how a metabolic generalist adopts an intracellular lifestyle during infection. Front Cell Infect Microbiol *4*, 191.

Daniel, J., Maamar, H., Deb, C., Sirakova, T.D., and Kolattukudy, P.E. (2011). Mycobacterium tuberculosis Uses Host Triacylglycerol to Accumulate Lipid Droplets and Acquires a Dormancy-Like Phenotype in Lipid-Loaded Macrophages. PLoS Pathogens *7*, e1002093.

Daniels, J.B., Call, D.R., Hancock, D., Sischo, W.M., Baker, K., and Besser, T.E. (2009). Role of Ceftiofur in Selection and Dissemination of blaCMY-2-Mediated Cephalosporin Resistance in Salmonella enterica and Commensal Escherichia coli Isolates from Cattle. Applied and Environmental Microbiology *75*, 3648–3655.

Datsenko, K.A., and Wanner, B.L. (2000). One-step inactivation of chromosomal genes in Escherichia coli K-12 using PCR products. Proceedings of the National Academy of Sciences *97*, 6640–6645.

Davis, M.J., Tsang, T.M., Qiu, Y., Dayrit, J.K., Freij, J.B., Huffnagle, G.B., and Olszewski, M.A. (2013). Macrophage M1/M2 Polarization Dynamically Adapts to Changes in Cytokine Microenvironments in Cryptococcus neoformans Infection. MBio *4*, e00264-13.

Davis, R.W., Botstein, D., and Roth, J.R. (1980). Advanced bacterial genetics: a manual for genetic engineering. Cold Spring Harbor Laboratory.

De Groote, M.A., Testerman, T., Xu, Y., Stauffer, G., and Fang, F.C. (1996). Homocysteine antagonism of nitric oxide-related cytostasis in Salmonella typhimurium. Science *272*, 414–417.

Deiwick, J., Nikolaus, T., Erdogan, S., and Hensel, M. (1999). Environmental regulation of Salmonella pathogenicity island 2 gene expression. Mol Microbiol *31*, 1759–1773.

Dellomonaco, C., Clomburg, J.M., Miller, E.N., and Gonzalez, R. (2011). Engineered reversal of the [bgr]-oxidation cycle for the synthesis of fuels and chemicals. Nature *476*, 355–359.

Dell'Osso, B., Nestadt, G., Allen, A., and Hollander, E. (2006). Serotonin-Norepinephrine Reuptake Inhibitors in the Treatment of Obsessive-Compulsive Disorder: A Critical Review. J Clin Psychiatry *67*, 600–610.

Denyer, S.P., and Maillard, J.-Y. (2002). Cellular impermeability and uptake of biocides and antibiotics in Gram-negative bacteria. Journal of Applied Microbiology *92*.

Diacovich, L., Lorenzi, L., Tomassetti, M., Méresse, S., and Gramajo, H. (2016). The infectious intracellular lifestyle of *Salmonella enterica* relies on the adaptation to nutritional conditions within the *Salmonella* -containing vacuole. Virulence 1–18.

Donia, M., and Hamann, M.T. (2003). Marine natural products and their potential applications as anti-infective agents. The Lancet Infectious Diseases *3*, 338–348.

Dragiev, P., Nadon, R., and Makarenkov, V. (2011). Systematic error detection in experimental high-throughput screening. BMC Bioinformatics *12*, 25.

Dunn, M.F., Ramirez-Trujillo, J.A., and Hernandez-Lucas, I. (2009). Major roles of isocitrate lyase and malate synthase in bacterial and fungal pathogenesis. Microbiology *155*, 3166–3175.

Durk, R.C., Singh, K., Cornelison, C.A., Rai, D.K., Matzek, K.B., Leslie, M.D., Schafer, E., Marchand, B., Adedeji, A., Michailidis, E., et al. (2010). Inhibitors of Foot and Mouth Disease Virus Targeting a Novel Pocket of the RNA-Dependent RNA Polymerase. PLoS ONE *5*, e15049.

Edwards, J.P., Zhang, X., Frauwirth, K.A., and Mosser, D.M. (2006). Biochemical and functional characterization of three activated macrophage populations. Journal of Leukocyte Biology *80*, 1298–1307.

Egen, J.G., Rothfuchs, A.G., Feng, C.G., Winter, N., Sher, A., and Germain, R.N. (2008). Macrophage and T Cell Dynamics during the Development and Disintegration of Mycobacterial Granulomas. Immunity *28*, 271–284.

Ehrlich, P., 1854-1915 (1910). Die experimentelle Chemotherapie der Spirillosen (Syphilis, R ückfallfieber, Hühnerspirillose, Frambösie) (Berlin : J. Springer, 1910.).

Eisele, N.A., Ruby, T., Jacobson, A., Manzanillo, P.S., Cox, J.S., Lam, L., Mukundan, L., Chawla, A., and Monack, D.M. (2013). Salmonella Require the Fatty Acid Regulator PPARδ for the Establishment of a Metabolic Environment Essential for Long-Term Persistence. Cell Host & Microbe *14*, 171–182.

Eisenreich, W., Heesemann, J., Rudel, T., and Goebel, W. (2015). Metabolic Adaptations of Intracellullar Bacterial Pathogens and their Mammalian Host Cells during Infection ("Pathometabolism"). Microbiol Spectr *3*.

Ellermeier, J.R., and Slauch, J.M. (2007). Adaptation to the host environment: regulation of the SPI1 type III secretion system in Salmonella enterica serovar Typhimurium. Current Opinion in Microbiology *10*, 24–29.

Eriksson, S., Lucchini, S., Thompson, A., Rhen, M., and Hinton, J.C. (2003). Unravelling the biology of macrophage infection by gene expression profiling of intracellular Salmonella enterica. Molecular Microbiology *47*, 103–118.

Ernst, R.K., Guina, T., and Miller, S.I. (2001). Salmonella typhimurium outer membrane remodeling: role in resistance to host innate immunity. Microbes and Infection *3*, 1327–1334.

Evans, M.J., Saghatelian, A., Sorensen, E.J., and Cravatt, B.F. (2005). Target discovery in small-molecule cell-based screens by in situ proteome reactivity profiling. Nature Biotechnology *23*, 1303–1307.

Faber, F., Thiennimitr, P., Spiga, L., Byndloss, M.X., Litvak, Y., Lawhon, S., Andrews-Polymenis, H.L., Winter, S.E., and Bäumler, A.J. (2017). Respiration of Microbiota-Derived 1,2-propanediol Drives Salmonella Expansion during Colitis. PLOS Pathogens *13*, e1006129.

Fairweather, D., and Cihakova, D. (2009). Alternatively activated macrophages in infection and autoimmunity. Journal of Autoimmunity *33*, 222–230.

Fang, F.C. (2004). Antimicrobial reactive oxygen and nitrogen species: concepts and controversies. Nat Rev Micro *2*, 820–832.

Fang, F.C. (2011). Antimicrobial actions of reactive oxygen species. MBio *2*.

Fang, F.C., Libby, S.J., Buchmeier, N.A., Loewen, P.C., Switala, J., Harwood, J., and Guiney, D.G. (1992). The alternative sigma factor katF (rpoS) regulates Salmonella virulence. Proc Natl Acad Sci U S A *89*, 11978–11982.

Fang, F.C., Libby, S.J., Castor, M.E., and Fung, A.M. (2005). Isocitrate Lyase (AceA) Is Required for Salmonella Persistence but Not for Acute Lethal Infection in Mice. Infection and Immunity *73*, 2547–2549.

Faucher, S.P., Porwollik, S., Dozois, C.M., McClelland, M., and Daigle, F. (2006). Transcriptome of Salmonella enterica serovar Typhi within macrophages revealed through the selective capture of transcribed sequences. Proceedings of the National Academy of Sciences of the United States of America *103*, 1906–1911.

Fauro, R., Presti, S.L., Bazan, C., Baez, A., Strauss, M., Triquell, F., Cremonezzi, D., Negrete, O.S., Willhuber, G.C., Paglini-Oliva, P., et al. (2013). Use of clomipramine as chemotherapy of the chronic phase of Chagas disease. Parasitology *140*, 917–927.

Feng, J., Wang, T., Zhang, S., Shi, W., and Zhang, Y. (2014). An Optimized SYBR Green I/PI Assay for Rapid Viability Assessment and Antibiotic Susceptibility Testing for Borrelia burgdorferi. PLoS ONE *9*, e111809.

Fields, P.I., Swanson, R.V., Haidaris, C.G., and Heffron, F. (1986). Mutants of Salmonella typhimurium that cannot survive within the macrophage are avirulent. Proceedings of the National Academy of Sciences *83*, 5189–5193.

Fischbach, M.A., and Walsh, C.T. (2009). Antibiotics for emerging pathogens. Science *325*, 1089–1093.

Fisman, D.N. (2000). Hemophagocytic syndromes and infection. Emerging Infectious Diseases *6*, 601.

Flannagan, R.S., Cosio, G., and Grinstein, S. (2009). Antimicrobial mechanisms of phagocytes and bacterial evasion strategies. Nat Rev Micro *7*, 355–366.

Fleming, A. (1929). On the Antibacterial Action of Cultures of a Penicillium, with Special Reference to their Use in the Isolation of B. influenzæ. British Journal of Experimental Pathology *10*, 226–236.

Freiberg, C., Fischer, H.P., and Brunner, N.A. (2005). Discovering the Mechanism of Action of Novel Antibacterial Agents through Transcriptional Profiling of Conditional Mutants. Antimicrobial Agents and Chemotherapy *49*, 749–759.

Fritsche, G., Nairz, M., Libby, S.J., Fang, F.C., and Weiss, G. (2012). Slc11a1 (Nramp1) impairs growth of Salmonella enterica serovar typhimurium in macrophages via stimulation of lipocalin-2 expression. Journal of Leukocyte Biology *92*, 353–359.

Galán, J.E., and Curtiss, R. (1989). Cloning and molecular characterization of genes whose products allow Salmonella typhimurium to penetrate tissue culture cells. Proc Natl Acad Sci USA *86*, 6383.

Galván-Peña, S., and O'Neill, L.A.J. (2014). Metabolic Reprograming in Macrophage Polarization. Frontiers in Immunology *5*, 420.

Garcia-del Portillo, F., Zwick, M.B., Leung, K.Y., and Finlay, B.B. (1993). Salmonella induces the formation of filamentous structures containing lysosomal membrane glycoproteins in epithelial cells. Proceedings of the National Academy of Sciences *90*, 10544–10548.

Garcia-Gutierrez, E., Chidlaw, A.C., Le Gall, G., Bowden, S.D., Tedin, K., Kelly, D.J., and Thompson, A. (2016). A Comparison of the ATP Generating Pathways Used by S. Typhimurium

to Fuel Replication within Human and Murine Macrophage and Epithelial Cell Lines. PLOS ONE *11*, e0150687.

Garvis, S.G., Beuzon, C.R., and Holden, D.W. (2001). A role for the PhoP/Q regulon in inhibition of fusion between lysosomes and Salmonella-containing vacuoles in macrophages. Cell Microbiol *3*, 731–744.

Ghia, J., Li, N., Wang, H., Collins, M., Deng, Y., El–Sharkawy, R.T., Côté, F., Mallet, J., and Khan, W.I. (2009). Serotonin Has a Key Role in Pathogenesis of Experimental Colitis. Gastroenterology *137*, 1649–1660.

Gill, F.A., Kaye, D., and Hook, E.W. (1966). THE INFLUENCE OF ERYTHROPHAGOCYTOSIS ON THE INTERACTION OF MACROPHAGES AND SALMONELLA IN VITRO. J Exp Med *124*, 173.

Golubeva, Y.A., Ellermeier, J.R., Cott Chubiz, J.E., and Slauch, J.M. (2016). Intestinal Long-Chain Fatty Acids Act as a Direct Signal To Modulate Expression of the Salmonella Pathogenicity Island 1 Type III Secretion System. MBio *7*.

Gordon, S. (2003). Alternative activation of macrophages. Nat Rev Immunol *3*, 23–35.

Gordon, S., and Martinez-Pomares, L. (2017). Physiological roles of macrophages. Pflügers Archiv - European Journal of Physiology *469*, 365–374.

Gottlieb, Y., Topaz, O., Cohen, L.A., Yakov, L.D., Haber, T., Morgenstern, A., Weiss, A., Chait Berman, K., Fibach, E., and Meyron-Holtz, E.G. (2012). Physiologically aged red blood cells undergo erythrophagocytosis in vivo but not in vitro. Haematologica *97*, 994–1002.

Gotz, A., Eylert, E., Eisenreich, W., and Goebel, W. (2010). Carbon metabolism of enterobacterial human pathogens growing in epithelial colorectal adenocarcinoma (Caco-2) cells. PLoS One *5*, e10586.

Gould, K. (2016). Antibiotics: from prehistory to the present day. Journal of Antimicrobial Chemotherapy *71*, 572–575.

Grant, S.S., and Hung, D.T. (2013). Persistent bacterial infections, antibiotic tolerance, and the oxidative stress response. Virulence *4*, 273–283.

Groisman, E.A., Chiao, E., Lipps, C.J., and Heffron, F. (1989). Salmonella typhimurium phoP virulence gene is a transcriptional regulator. Proceedings of the National Academy of Sciences *86*, 7077–7081.

Groisman, E.A., Parra-Lopez, C., Salcedo, M., Lipps, C.J., and Heffron, F. (1992). Resistance to host antimicrobial peptides is necessary for Salmonella virulence. Proceedings of the National Academy of Sciences *89*, 11939–11943.

Grom, A.A., and Mellins, E.D. (2010). Macrophage activation syndrome: advances towards understanding pathogenesis. Current Opinion in Rheumatology *22*, 561–566.

Guan, Y., Li, X., Umetani, M., Boini, K.M., Li, P.-L., and Zhang, Y. (2018). Tricyclic antidepressant amitriptyline inhibits autophagic flux and prevents tube formation in vascular endothelial cells. Basic & Clinical Pharmacology & Toxicology *0*.

Gunics, G., Motohashi, N., Amaral, L., Farkas, S., and Molnár, J. (2000). Interaction between antibiotics and non-conventional antibiotics on bacteria. International Journal of Antimicrobial Agents *14*, 239–242.

Gunn, J.S., Marshall, J.M., Baker, S., Dongol, S., Charles, R.C., and Ryan, E.T. (2014). Salmonella chronic carriage: epidemiology, diagnosis, and gallbladder persistence. Trends in Microbiology *22*, 648–655.

Hammer, N.D., Cassat, J.E., Noto, M.J., Lojek, L.J., Chadha, A.D., Schmitz, J.E., Creech, C.B., and Skaar, E.P. (2014). Inter- and Intraspecies Metabolite Exchange Promotes Virulence of Antibiotic-Resistant Staphylococcus aureus. Cell Host & Microbe *16*, 531–537.

Han, T.H., Pelling, A., Jeon, T.-J., Gimzewski, J.K., and Liao, J.C. (2005). Erythrocyte nitric oxide transport reduced by a submembrane cytoskeletal barrier. Biochim Biophys Acta *1723*, 135–142.

Hand, W.L., and King-Thompson, N.L. (1983). Effect of erythrocyte ingestion on macrophage antibacterial function. Infect. Immun. *40*, 917.

Haraga, A., Ohlson, M.B., and Miller, S.I. (2008). Salmonellae interplay with host cells. Nature Reviews Microbiology *6*, 53–66.

Harvey, A.L., Edrada-Ebel, R., and Quinn, R.J. (2015). The re-emergence of natural products for drug discovery in the genomics era. Nature Reviews Drug Discovery *14*, 111.

Heaslip, A.T., Leung, J.M., Carey, K.L., Catti, F., Warshaw, D.M., Westwood, N.J., Ballif, B.A., and Ward, G.E. (2010). A Small-Molecule Inhibitor of T. gondii Motility Induces the Posttranslational Modification of Myosin Light Chain-1 and Inhibits Myosin Motor Activity. PLoS Pathogens *6*, e1000720.

Heath, R.J., Jackowski, S., and Rock, C.O. (2002). Fatty acid and phospholipid metabolism in prokaryotes. New Comprehensive Biochemistry *36*, 55–92.

Helaine, S., Thompson, J.A., Watson, K.G., Liu, M., Boyle, C., and Holden, D.W. (2010). Dynamics of intracellular bacterial replication at the single cell level. Proceedings of the National Academy of Sciences *107*, 3746–3751.

Helaine, S., Cheverton, A.M., Watson, K.G., Faure, L.M., Matthews, S.A., and Holden, D.W. (2014). Internalization of Salmonella by Macrophages Induces Formation of Nonreplicating Persisters. Science *343*, 204–208.

Henard, C., and Vazquez-Torres, A. (2011). Nitric Oxide and Salmonella Pathogenesis. Frontiers in Microbiology *2*, 84.

Hensel, M. (2000). Salmonella pathogenicity island 2. Mol Microbiol *36*, 1015–1023.

Hensel, M., Shea, J., Gleeson, C., Jones, M., Dalton, E., and Holden, D. (1995). Simultaneous identification of bacterial virulence genes by negative selection. Science *269*, 400.

Hensel, M., Shea, J.E., Bäumler, A.J., Gleeson, C., Blattner, F., and Holden, D.W. (1997). Analysis of the boundaries of Salmonella pathogenicity island 2 and the corresponding chromosomal region of Escherichia coli K-12. J. Bacteriol. *179*, 1105.

Hensel, M., Shea, J.E., Waterman, S.R., Mundy, R., Nikolaus, T., Banks, G., Vazquez-Torres, A., Gleeson, C., Fang, F.C., and Holden, D.W. (1998). Genes encoding putative effector proteins of the type III secretion system of Salmonella pathogenicity island 2 are required for bacterial virulence and proliferation in macrophages. Molecular Microbiology *30*, 163–174.

Herbert, D.R., Hölscher, C., Mohrs, M., Arendse, B., Schwegmann, A., Radwanska, M., Leeto, M., Kirsch, R., Hall, P., Mossmann, H., et al. (2004). Alternative Macrophage Activation Is Essential for Survival during Schistosomiasis and Downmodulates T Helper 1 Responses and Immunopathology. Immunity *20*, 623–635.

Hernandez, L.D., Pypaert, M., Flavell, R.A., and Galán, J.E. (2003). A Salmonella protein causes macrophage cell death by inducing autophagy. J Cell Biol *163*, 1123.

Himbert, S., Alsop, R.J., Rose, M., Hertz, L., Dhaliwal, A., Moran-Mirabal, J.M., Verschoor, C.P., Bowdish, D.M.E., Kaestner, L., Wagner, C., et al. (2017). The Molecular Structure of Human Red Blood Cell Membranes from Highly Oriented, Solid Supported Multi-Lamellar Membranes. Scientific Reports *7*, 39661.

Hook, E.W., Kaye, D., and Gill, F.A. (1967). Factors influencing host resistance to salmonella infection. The effects of hemolysis and erythrophagocytosis. Transactions of the American Clinical and Climatological Association *78*, 230–241.

Hooper, L.V., Stappenbeck, T.S., Hong, C.V., and Gordon, J.I. (2003). Angiogenins: a new class of microbicidal proteins involved in innate immunity. Nature Immunology *4*, 269–273.

Hsieh, C., Macatonia, S., Tripp, C., Wolf, S., O'Garra, A., and Murphy, K. (1993). Development of TH1 CD4+ T cells through IL-12 produced by Listeria-induced macrophages. Science *260*, 547.

Huang, J.T., Welch, J.S., Ricote, M., Binder, C.J., Willson, T.M., Kelly, C., Witztum, J.L., Funk, C.D., Conrad, D., and Glass, C.K. (1999). Interleukin-4-dependent production of PPAR-[gamma] ligands in macrophages by 12/15-lipoxygenase. Nature *400*, 378–382.

Huigens III, R.W., Morrison, K.C., Hicklin, R.W., Flood Jr, T.A., Richter, M.F., and Hergenrother, P.J. (2013). A ring-distortion strategy to construct stereochemically complex and structurally diverse compounds from natural products. Nature Chemistry *5*, 195.

Hung, D.T., Shakhnovich, E.A., Pierson, E., and Mekalanos, J.J. (2005). Small-Molecule Inhibitor of Vibrio cholerae Virulence and Intestinal Colonization. Science *310*, 670–674.

Hurt, J.K., McQuade, T.J., Emanuele, A., Larsen, M.J., and Garcia, G.A. (2010). High-Throughput Screening of the Virulence Regulator VirF: A Novel Antibacterial Target for Shigellosis. Journal of Biomolecular Screening *15*, 379–387.

Huynh, M.-L.N., Fadok, V.A., and Henson, P.M. (2002). Phosphatidylserine-dependent ingestion of apoptotic cells promotes TGF-β1 secretion and the resolution of inflammation. J Clin Invest *109*, 41–50.

Imhoff, J.F., Labes, A., and Wiese, J. (2011). Bio-mining the microbial treasures of the ocean: New natural products. Biotechnology Advances *29*, 468–482.

Iram, S.H., and Cronan, J.E. (2006). The -Oxidation Systems of Escherichia coli and Salmonella enterica Are Not Functionally Equivalent. Journal of Bacteriology *188*, 599–608.

Ivnitski-Steele, I., Holmes, A.R., Lamping, E., Monk, B.C., Cannon, R.D., and Sklar, L.A. (2009). Identification of Nile red as a fluorescent substrate of the Candida albicans ATP-binding cassette transporters Cdr1p and Cdr2p and the major facilitator superfamily transporter Mdr1p. Analytical Biochemistry *394*, 87–91.

Jha, A.K., Huang, S.C.-C., Sergushichev, A., Lampropoulou, V., Ivanova, Y., Loginicheva, E., Chmielewski, K., Stewart, K.M., Ashall, J., Everts, B., et al. (2015). Network Integration of Parallel Metabolic and Transcriptional Data Reveals Metabolic Modules that Regulate Macrophage Polarization. Immunity *42*, 419–430.

Jiang, N., Tan, N.S., Ho, B., and Ding, J.L. (2007). Measurement of the red blood cell lysis by bacterial hemolysin.

Jiang, X., Zhang, W., Zhang, Y., Gao, F., Lu, C., Zhang, X., and Wang, H. (2008). Assessment of Efflux Pump Gene Expression in a Clinical Isolate Mycobacterium tuberculosis by Real-Time Reverse Transcription PCR. Microbial Drug Resistance *14*, 7–11.

Johnson, J.L., Ramadass, M., He, J., Brown, S.J., Zhang, J., Abgaryan, L., Biris, N., Gavathiotis, E., Rosen, H., and Catz, S.D. (2016). Identification of Neutrophil Exocytosis Inhibitors (Nexinhibs), Small Molecule Inhibitors of Neutrophil Exocytosis and Inflammation: DRUGGABILITY OF THE SMALL GTPase Rab27a. Journal of Biological Chemistry *291*, 25965–25982.

Jones, B.D., Ghori, N., and Falkow, S. (1994). Salmonella typhimurium initiates murine infection by penetrating and destroying the specialized epithelial M cells of the Peyer's patches. J Exp Med *180*, 15.

Kahnert, A., Seiler, P., Stein, M., Bandermann, S., Hahnke, K., Mollenkopf, H., and Kaufmann, S.H.E. (2006). Alternative activation deprives macrophages of a coordinated defense program to Mycobacterium tuberculosis. Eur J Immunol *36*, 631–647.

Katayama, I., Nishioka, K., Yamamoto, T., and Sawada, Y. (1998). Increased production of nitric oxide stimulated by interleukin-1beta in peripheral blood mononuclear cells in patients with systemic sclerosis. Rheumatology *37*, 1123–1125.

Kazemi, M.R., McDonald, C.M., Shigenaga, J.K., Grunfeld, C., and Feingold, K.R. (2005). Adipocyte Fatty Acid–Binding Protein Expression and Lipid Accumulation Are Increased During Activation of Murine Macrophages by Toll-Like Receptor Agonists. Arterioscler Thromb Vasc Bio *25*, 1220.

Kelm, M. (1999). Nitric oxide metabolism and breakdown. Biochim Biophys Acta *1411*, 273–289.

Kiefer, C.R., and Snyder, L.M. (2000). Oxidation and erythrocyte senescence. Curr Opin Hematol *7*, 113–116.

Kim, J., Webb, A.M., Kershner, J.P., Blaskowski, S., and Copley, S.D. (2014). A versatile and highly efficient method for scarless genome editing in Escherichia coli and Salmonella enterica. BMC Biotechnology *14*, 1.

Kim, S., Thiessen, P.A., Bolton, E.E., Chen, J., Fu, G., Gindulyte, A., Han, L., He, J., He, S., Shoemaker, B.A., et al. (2016). PubChem Substance and Compound databases. Nucleic Acids Research *44*, D1202–D1213.

Kim, Y.M., Hong, S.J., Billiar, T.R., and Simmons, R.L. (1996). Counterprotective effect of erythrocytes in experimental bacterial peritonitis is due to scavenging of nitric oxide and reactive oxygen intermediates. Infect Immun *64*, 3074–3080.

Kim, Y.R., Brinsmade, S.R., Yang, Z., Escalante-Semerena, J., and Fierer, J. (2006). Mutation of Phosphotransacetylase but Not Isocitrate Lyase Reduces the Virulence of Salmonella enterica Serovar Typhimurium in Mice. Infection and Immunity *74*, 2498–2502.

Knodler, L.A., Nair, V., and Steele-Mortimer, O. (2014). Quantitative Assessment of Cytosolic Salmonella in Epithelial Cells. PLOS ONE *9*, e84681.

Korbee, C.J., Heemskerk, M.T., Kocev, D., van Strijen, E., Rabiee, O., Franken, K.L.M.C., Wilson, L., Savage, N.D.L., Džeroski, S., Haks, M.C., et al. (2018). Combined chemical genetics and data-driven bioinformatics approach identifies receptor tyrosine kinase inhibitors as host-directed antimicrobials. Nature Communications *9*, 358.

Kouznetsova, J., Sun, W., Martínez-Romero, C., Tawa, G., Shinn, P., Chen, C.Z., Schimmer, A., Sanderson, P., McKew, J.C., Zheng, W., et al. (2014). Identification of 53 compounds that block Ebola virus-like particle entry via a repurposing screen of approved drugs. Emerging Microbes & Infections *3*, e84.

Kreider, T., Anthony, R.M., Urban, J.F., and Gause, W.C. (2007). Alternatively activated macrophages in helminth infections. Current Opinion in Immunology *19*, 448–453.

Krutzik, S.R., Tan, B., Li, H., Ochoa, M.T., Liu, P.T., Sharfstein, S.E., Graeber, T.G., Sieling, P.A., Liu, Y.-J., Rea, T.H., et al. (2005). TLR activation triggers the rapid differentiation of monocytes into macrophages and dendritic cells. Nature Medicine *11*, 653–660.

Kuhle, V., Jäckel, D., and Hensel, M. (2004). Effector proteins encoded by Salmonella pathogenicity island 2 interfere with the microtubule cytoskeleton after translocation into host cells. Traffic *5*, 356–370.

Kumar, Y., Cocchiaro, J., and Valdivia, R.H. (2006). The Obligate Intracellular Pathogen Chlamydia trachomatis Targets Host Lipid Droplets. Current Biology *16*, 1646–1651.

Kwon, Y.K., Lu, W., Melamud, E., Khanam, N., Bognar, A., and Rabinowitz, J.D. (2008). A domino effect in antifolate drug action in Escherichia coli. Nature Chemical Biology *4*, 602–608.

Labro, M.T. (1996). Intracellular bioactivity of macrolides. Clinical Microbiology and Infection *1*, S24–S30.

Lacroix, F.J., Cloeckaert, A., Grépinet, O., Pinault, C., Popoff, M.Y., Waxin, H., and Pardon, P. (1996). Salmonella typhimurium acrB-like gene: identification and role in resistance to biliary salts and detergents and in murine infection. FEMS Microbiology Letters *135*, 161–167.

Lamb, A.L. (2011). Pericyclic Reactions Catalyzed by Chorismate-Utilizing Enzymes. Biochemistry *50*, 7476–7483.

Lamers, R.P., Cavallari, J.F., and Burrows, L.L. (2013). The Efflux Inhibitor Phenylalanine-Arginine Beta-Naphthylamide (PAβN) Permeabilizes the Outer Membrane of Gram-Negative Bacteria. PLoS ONE *8*, e60666.

Law, G.L., Tisoncik-Go, J., Korth, M.J., and Katze, M.G. (2013). Drug repurposing: a better approach for infectious disease drug discovery? Current Opinion in Immunology *25*, 588–592.

Lawhon, S.D., Maurer, R., Suyemoto, M., and Altier, C. (2002). Intestinal short-chain fatty acids alter Salmonella typhimurium invasion gene expression and virulence through BarA/SirA. Molecular Microbiology *46*, 1451–1464.

Lee, P., Peng, H., Gelbart, T., Wang, L., and Beutler, E. (2005). Regulation of hepcidin transcription by interleukin-1 and interleukin-6. Proc Natl Acad Sci U S A *102*, 1906.

Lee, S.-J., Park, S.-Y., Jung, M.-Y., Bae, S.M., and Kim, I.-S. (2011). Mechanism for phosphatidylserine-dependent erythrophagocytosis in mouse liver. Blood *117*, 5215.

Lemoine, R.C., Glinka, T.W., Watkins, W.J., Cho, A., Yang, J., Iqbal, N., Singh, R., Madsen, D., Lolans, K., Lomovskaya, O., et al. (2004). Quinazolinone-based fungal efflux pump inhibitors. Part 1: Discovery of an (N-methylpiperazine)-containing derivative with activity in clinically relevant Candida spp. Bioorganic & Medicinal Chemistry Letters *14*, 5127–5131.

Leung, J.M., Tran, F., Pathak, R.B., Poupart, S., Heaslip, A.T., Ballif, B.A., Westwood, N.J., and Ward, G.E. (2014). Identification of T. gondii Myosin Light Chain-1 as a Direct Target of TachypleginA-2, a Small-Molecule Inhibitor of Parasite Motility and Invasion. PLoS ONE *9*, e98056.

Levine, M.M., Black, R.E., and Lanata, C. Precise estimation of the numbers of chronic carriers of Salmonella typhi in Santiago, Chile, an endemic area. Journal of Infectious Disease *146*, 724–726.

Lewis, K. (2013). Platforms for antibiotic discovery. Nature Reviews Drug Discovery *12*, 371–387.

Lewis, K. (2017). New approaches to antimicrobial discovery. Biochemical Pharmacology *134*, 87–98.

Li, N., Ghia, J.-E., Wang, H., McClemens, J., Cote, F., Suehiro, Y., Mallet, J., and Khan, W.I. (2011). Serotonin Activates Dendritic Cell Function in the Context of Gut Inflammation. The American Journal of Pathology *178*, 662–671.

Lieberman, L.A., and Higgins, D.E. (2009). A Small-Molecule Screen Identifies the Antipsychotic Drug Pimozide as an Inhibitor of Listeria monocytogenes Infection. Antimicrobial Agents and Chemotherapy *53*, 756–764.

Lieberman, L.A., and Higgins, D.E. (2010). Inhibition of Listeria monocytogenes infection by neurological drugs. International Journal of Antimicrobial Agents *35*, 292–296.

Lin, J., Sahin, O., Michel, L.O., and Zhang, Q. (2003). Critical Role of Multidrug Efflux Pump CmeABC in Bile Resistance and In Vivo Colonization of Campylobacter jejuni. Infection and Immunity *71*, 4250–4259.

Lin, L., Nonejuie, P., Munguia, J., Hollands, A., Olson, J., Dam, Q., Kumaraswamy, M., Rivera, H.J., Corriden, R., Rohde, M., et al. (2015). Azithromycin Synergizes with Cationic Antimicrobial Peptides to Exert Bactericidal and Therapeutic Activity Against Highly Multidrug-Resistant Gram-Negative Bacterial Pathogens. EBioMedicine *2*, 690–698.

Lindsey, T.L., Hagins, J.M., Sokol, P.A., and Silo-Suh, L.A. (2008). Virulence determinants from a cystic fibrosis isolate of Pseudomonas aeruginosa include isocitrate lyase. Microbiology *154*, 1616–1627.

Ling, L.L., Schneider, T., Peoples, A.J., Spoering, A.L., Engels, I., Conlon, B.P., Mueller, A., Schäberle, T.F., Hughes, D.E., Epstein, S., et al. (2015). A new antibiotic kills pathogens without detectable resistance. Nature *517*, 455–459.

Lipinski, C.A. (2000). Drug-like properties and the causes of poor solubility and poor permeability. Journal of Pharmacological and Toxicological Methods *44*, 235–249.

Liss, V., Swart, A.L., Kehl, A., Hermanns, N., Zhang, Y., Chikkaballi, D., Böhles, N., Deiwick, J., and Hensel, M. (2017). Salmonella enterica Remodels the Host Cell Endosomal System for Efficient Intravacuolar Nutrition. Cell Host & Microbe *21*, 390–402.

Liu, X., Miller, M.J., Joshi, M.S., Sadowska-Krowicka, H., Clark, D.A., and Lancaster, J.R.J. (1998). Diffusion-limited reaction of free nitric oxide with erythrocytes. J Biol Chem *273*, 18709–18713.

Liu, Y., Yu, K., Zhou, F., Ding, T., Yang, Y., Hu, M., and Liu, X. (2017). Quantitative Proteomics Charts the Landscape of Salmonella Carbon Metabolism within Host Epithelial Cells. J. Proteome Res. *16*, 788–797.

Livermore, D.M., on behalf of the British Society for Antimicrobial Chemotherapy Working Party on The Urgent Need: Regenerating Antibacterial Drug Discovery and Development, Blaser, M., Carrs, O., Cassell, G., Fishman, N., Guidos, R., Levy, S., Powers, J., Norrby, R., et al. (2011). Discovery research: the scientific challenge of finding new antibiotics. Journal of Antimicrobial Chemotherapy *66*, 1941–1944.

Loegering, D.J., Commins, L.M., Minnear, F.L., Gary, L.A., and Hill, L.A. (1987). Effect of Kupffer cell phagocytosis of erythrocytes and erythrocyte ghosts on susceptibility to endotoxemia and bacteremia. Infection and Immunity *55*, 2074–2080.

Lomovskaya, O., and Bostian, K.A. (2006). Practical applications and feasibility of efflux pump inhibitors in the clinic—A vision for applied use. Biochemical Pharmacology *71*, 910–918.

Lomovskaya, O., Warren, M.S., Lee, A., Galazzo, J., Fronko, R., Lee, M., Blais, J., Cho, D., Chamberland, S., Renau, T., et al. (2001). Identification and Characterization of Inhibitors of Multidrug Resistance Efflux Pumps in Pseudomonas aeruginosa: Novel Agents for Combination Therapy. Antimicrobial Agents and Chemotherapy *45*, 105–116.

Lorenz, M.C., and Fink, G.R. (2001). The glyoxylate shunt is required for fungal virulence. Nature *412*, 83–86.

Lowenstein, C.J., Alley, E.W., Raval, P., Snowman, A.M., Snyder, S.H., Russell, S.W., and Murphy, W.J. (1993). Macrophage nitric oxide synthase gene: two upstream regions mediate induction by interferon gamma and lipopolysaccharide. Proc Natl Acad Sci USA *90*, 9730.

Lucas, R.L., Lostroh, C.P., DiRusso, C.C., Spector, M.P., Wanner, B.L., and Lee, C.A. (2000). Multiple Factors Independently RegulatehilA and Invasion Gene Expression in Salmonella enterica Serovar Typhimurium. J. Bacteriol. *182*, 1872.

Luchsinger, B.P., Rich, E.N., Gow, A.J., Williams, E.M., Stamler, J.S., and Singel, D.J. (2003). Routes to S-nitroso-hemoglobin formation with heme redox and preferential reactivity in the beta subunits. Proc Natl Acad Sci U S A *100*, 461–466.

Luo, H., Zhu, H., Chen, J., Wang, K., Shi, L., He, L., Yang, L., and Mikailov, M. (2011). DRAR-CPI: a server for identifying drug repositioning potential and adverse drug reactions via the chemical–protein interactome. Nucleic Acids Research *39*, W492–W498.

M Nissink, J.W., and Blackburn, S. (2014). Quantification of frequent-hitter behavior based on historical high-throughput screening data. Future Medicinal Chemistry *6*, 1113–1126.

Macedo, D., Filho, A.J.M.C., Soares de Sousa, C.N., Quevedo, J., Barichello, T., Júnior, H.V.N., and Freitas de Lucena, D. (2017). Antidepressants, antimicrobials or both? Gut microbiota dysbiosis in depression and possible implications of the antimicrobial effects of antidepressant drugs for antidepressant effectiveness. Journal of Affective Disorders *208*, 22–32.

Majowicz, S.E., Musto, J., Scallan, E., Angulo, F.J., Kirk, M., O'Brien, S.J., Jones, T.F., Fazil, A., and Hoekstra, R.M. (2010). The Global Burden of Nontyphoidal Salmonella Gastroenteritis. Clinical Infectious Diseases *50*, 882–889.

Malik-Kale, P., Winfree, S., and Steele-Mortimer, O. (2012). The Bimodal Lifestyle of Intracellular Salmonella in Epithelial Cells: Replication in the Cytosol Obscures Defects in Vacuolar Replication. PLoS ONE *7*, e38732.

Malo, N., Hanley, J.A., Cerquozzi, S., Pelletier, J., and Nadon, R. (2006). Statistical practice in high-throughput screening data analysis. Nature Biotechnology *24*, 167–175.

Malubay, S.M.A. (2008). Modulation of the Serotonin Reuptake Transporter in RAW264. 7 Macrophages.

Mandal, A., Sinha, C., Kumar Jena, A., Ghosh, S., and Samanta, A. (2010). An Investigation on in vitro and in vivo Antimicrobial Properties of the Antidepressant: Amitriptyline Hydrochloride. Braz J Microbiol *41*, 635–645.

Mandal, D., Moitra, P.K., Saha, S., and Basu, J. (2002). Caspase 3 regulates phosphatidylserine externalization and phagocytosis of oxidatively stressed erythrocytes. FEBS Lett *513*, 184–188.

Maneglier, B., Guillemin, G.J., Clayette, P., Rogez-Kreuz, C., Brew, B.J., Dormont, D., Advenier, C., Therond, P., and Spreux-Varoquaux, O. (2008). Serotonin decreases HIV-1 replication in primary cultures of human macrophages through 5-HT1A receptors. British Journal of Pharmacology *154*, 174–182.

Manina, G., Dhar, N., and McKinney, J.D. (2015). Stress and Host Immunity Amplify Mycobacterium tuberculosis Phenotypic Heterogeneity and Induce Nongrowing Metabolically Active Forms. Cell Host & Microbe *17*, 32–46.

Martinez, F.O., Sica, A., Mantovani, A., and Locati, M. (2008). Macrophage activation and polarization. Front Biosci *13*, 453–461.

Martinez, J.L., Sánchez, M.B., Martínez-Solano, L., Hernandez, A., Garmendia, L., Fajardo, A., and Alvarez-Ortega, C. (2009). Functional role of bacterial multidrug efflux pumps in microbial natural ecosystems. FEMS Microbiology Reviews *33*, 430–449.

Martyn, D.C., Jones, D.C., Fairlamb, A.H., and Clardy, J. (2007). High-throughput screening affords novel and selective trypanothione reductase inhibitors with anti-trypanosomal activity. Bioorganic & Medicinal Chemistry Letters *17*, 1280–1283.

Mathew, M.D., Mathew, N.D., Miller, A., Simpson, M., Au, V., Garland, S., Gestin, M., Edgley, M.L., Flibotte, S., Balgi, A., et al. (2016). Using C. elegans Forward and Reverse Genetics to Identify New Compounds with Anthelmintic Activity. PLOS Neglected Tropical Diseases *10*, e0005058.

Matsumoto, Y., Hayama, K., Sakakihara, S., Nishino, K., Noji, H., Iino, R., and Yamaguchi, A. (2011). Evaluation of Multidrug Efflux Pump Inhibitors by a New Method Using Microfluidic Channels. PLoS ONE *6*, e18547.

Maudet, C., Mano, M., Sunkavalli, U., Sharan, M., Giacca, M., Förstner, K.U., and Eulalio, A. (2014). Functional high-throughput screening identifies the miR-15 microRNA family as cellular restriction factors for Salmonella infection. Nature Communications *5*, 4718.

Mazzilli, M., and Zecconi, A. (2010). Assessment of epithelial cells' immune and inflammatory response to Staphylococcus aureus when exposed to a macrolide. Journal of Dairy Research *77*, 404–410.

McCollister, B.D., Myers, J.T., Jones-Carson, J., Husain, M., Bourret, T.J., and Vázquez-Torres, A. (2008). N2O3 enhances the nitrosative potential of IFNγ-primed macrophages in response to Salmonella. Immunobiology *212*, 759–769.

McCoy, M.W., Moreland, S.M., and Detweiler, C.S. (2012). Hemophagocytic Macrophages in Murine Typhoid Fever Have an Anti-Inflammatory Phenotype. Infection and Immunity *80*, 3642–3649.

McDonald, E.M., Pilonieta, M.C., Nick, H.J., and Detweiler, C.S. (2016). Bacterial Stimulation of Toll-Like Receptor 4 Drives Macrophages To Hemophagocytose. Infection and Immunity *84*, 47–55.

McGourty, K., Thurston, T.L., Matthews, S.A., Pinaud, L., Mota, L.J., and Holden, D.W. (2012). Salmonella Inhibits Retrograde Trafficking of Mannose-6-Phosphate Receptors and Lysosome Function. Science *338*, 963.

McKinney, J.D., Honer zu Bentrup, K., Munoz-Elias, E.J., Miczak, A., Chen, B., Chan, W.T., Swenson, D., Sacchetini, J.C., Jacobs, W.R., and Russell, D.G. (2000). Persistence of Mycobacterium tuberculosis in macrophages and mice requires the glyoxylate shunt enzyme isocitrate lyase. Nature *406*, 735–738.

McQuate, S.E., Young, A.M., Silva-Herzog, E., Bunker, E., Hernandez, M., de Chaumont, F., Liu, X., Detweiler, C.S., and Palmer, A.E. (2017). Long-term live-cell imaging reveals new roles for *Salmonella* effector proteins SseG and SteA: New roles for *Salmonella* effector proteins. Cellular Microbiology *19*, e12641.

Medzhitov, R. (2007). Recognition of microorganisms and activation of the immune response. Nature *449*, 819–826.

Mercado-Lubo, R., Leatham, M.P., Conway, T., and Cohen, P.S. (2009). Salmonella enterica Serovar Typhimurium Mutants Unable To Convert Malate to Pyruvate and Oxaloacetate Are Avirulent and Immunogenic in BALB/c Mice. Infection and Immunity *77*, 1397–1405.

Merritt, F.F., Smith, B.P., Reina-Guerra, M., Habasha, F., and Johnson, E. (1984). Relationship of cutaneous delayed hypersensitivity to protection from challenge exposure with Salmonella typhimurium in calves. Am J Vet Res *45*, 1081–1085.

Mesquita, F.S., Thomas, M., Sachse, M., Santos, A.J.M., Figueira, R., and Holden, D.W. (2012). The Salmonella Deubiquitinase SseL Inhibits Selective Autophagy of Cytosolic Aggregates. PLOS Pathogens *8*, e1002743.

Miao, E.A., Brittnacher, M., Haraga, A., Jeng, R.L., Welch, M.D., and Miller, S.I. (2003). Salmonella effectors translocated across the vacuolar membrane interact with the actin cytoskeleton. Molecular Microbiology *48*, 401–415.

Miller, S.I., Kukral, A.M., and Mekalanos, J.J. (1989). A two-component regulatory system (phoP phoQ) controls Salmonella typhimurium virulence. Proceedings of the National Academy of Sciences *86*, 5054–5058.

Miller, Y.I., Choi, S.-H., Fang, L., and Harkewicz, R. (2009). Toll-Like Receptor-4 and Lipoprotein Accumulation in Macrophages. Trends in Cardiovascular Medicine *19*, 227–232.

Mills, C.D., Kincaid, K., Alt, J.M., Heilman, M.J., and Hill, A.M. (2000). M-1/M-2 macrophages and the Th1/Th2 paradigm. J Immunol *164*, 6166–6173.

Milner, J.D., Orekov, T., Ward, J.M., Cheng, L., Torres-Velez, F., Junttila, I., Sun, G., Buller, M., Morris, S.C., Finkelman, F.D., et al. (2010). Sustained IL-4 exposure leads to a novel pathway for hemophagocytosis, inflammation, and tissue macrophage accumulation. Blood *116*, 2476–2483.

Mineshiba, J., Myokai, F., Mineshiba, F., Matsuura, K., Nishimura, F., and Takashiba, S. (2005). Transcriptional regulation of Î²- *defensin - 2* by lipopolysaccharide in cultured human cervical carcinoma (HeLa) cells. FEMS Immunology & Medical Microbiology *45*, 37–44.

Misra, R., and Benson, S.A. (1988). Isolation and characterization of OmpC porin mutants with altered pore properties. J Bacteriol *170*, 528–533.

Misra, R., Morrison, K.D., Cho, H.J., and Khuu, T. (2015). Importance of Real-Time Assays To Distinguish Multidrug Efflux Pump-Inhibiting and Outer Membrane-Destabilizing Activities in Escherichia coli. Journal of Bacteriology *197*, 2479–2488.

Monack, D.M. (2004). Salmonella typhimurium Persists within Macrophages in the Mesenteric Lymph Nodes of Chronically Infected Nramp1+/+ Mice and Can Be Reactivated by IFN Neutralization. Journal of Experimental Medicine *199*, 231–241.

Monack, D.M., Mueller, A., and Falkow, S. (2004). Persistent bacterial infections: the interface of the pathogen and the host immune system. Nature Reviews Microbiology *2*, 747.

Moore, K., and Rees, S. (2001). Cell-Based Versus Isolated Target Screening: How Lucky Do You Feel? Journal of Biomolecular Screening *6*, 69–74.

Morgan-Kiss, R.M., and Cronan, J.E. (2004). The Escherichia coli fadK (ydiD) Gene Encodes an Anerobically Regulated Short Chain Acyl-CoA Synthetase. Journal of Biological Chemistry *279*, 37324–37333.

Mosser, D.M., and Edwards, J.P. (2008). Exploring the full spectrum of macrophage activation. Nature Reviews Immunology *8*, 958–969.

Munoz-Bellido, J.L., Munoz-Criado, S., and Garcìa-Rodrìguez, J.A. (2000). Antimicrobial activity of psychotropic drugs: Selective serotonin reuptake inhibitors. International Journal of Antimicrobial Agents *14*, 177–180.

Mura, C., Valenti, D., Floris, C., Sanna, R., De Luca, M.A., Fadda, A.M., and Loy, G. (2011). Metronidazole prodrugs: Synthesis, physicochemical properties, stability, and ex vivo release studies. European Journal of Medicinal Chemistry *46*, 4142–4150.

Muraille, E., Leo, O., and Moser, M. (2014). Th1/Th2 Paradigm Extended: Macrophage Polarization as an Unappreciated Pathogen-Driven Escape Mechanism? Frontiers in Immunology *5*, 603.

Murakami, S., Nakashima, R., Yamashita, E., and Yamaguchi, A. (2002). Crystal structure of bacterial multidrug efflux transporter AcrB. Nature *419*, 587–593.

Murakami, S., Nakashima, R., Yamashita, E., Matsumoto, T., and Yamaguchi, A. (2006). Crystal structures of a multidrug transporter reveal a functionally rotating mechanism. Nature *443*, 173–179.

Nagy, T.A., Moreland, S.M., Andrews-Polymenis, H., and Detweiler, C.S. (2013). The Ferric Enterobactin Transporter Fep Is Required for Persistent Salmonella enterica Serovar Typhimurium Infection. Infection and Immunity *81*, 4063–4070.

Nagy, T.A., Moreland, S.M., and Detweiler, C.S. (2014). Salmonella acquires ferrous iron from haemophagocytic macrophages. Molecular Microbiology *93*, 1314–1326.

Nairz, M., Theurl, I., Ludwiczek, S., Theurl, M., Mair, S.M., Fritsche, G., and Weiss, G. (2007). The co-ordinated regulation of iron homeostasis in murine macrophages limits the availability of iron for intracellular Salmonella typhimurium. Cellular Microbiology *9*, 2126–2140.

Nairz, M., Fritsche, G., Crouch, M.-L.V., Barton, H.C., Fang, F.C., and Weiss, G. (2009). Slc11a1 limits intracellular growth of *Salmonella enterica* sv. Typhimurium by promoting macrophage immune effector functions and impairing bacterial iron acquisition. Cellular Microbiology *11*, 1365–1381.

Nairz, M., Schleicher, U., Schroll, A., Sonnweber, T., Theurl, I., Ludwiczek, S., Talasz, H., Brandacher, G., Moser, P.L., Muckenthaler, M.U., et al. (2013). Nitric oxide–mediated regulation of ferroportin-1 controls macrophage iron homeostasis and immune function in Salmonella infection. J Exp Med *210*, 855.

Nakashima, R., Sakurai, K., Yamasaki, S., Hayashi, K., Nagata, C., Hoshino, K., Onodera, Y., Nishino, K., and Yamaguchi, A. (2013). Structural basis for the inhibition of bacterial multidrug exporters. Nature *500*, 102–106.

Nakayama, K., Ishida, Y., Ohtsuka, M., Kawato, H., Yoshida, K., Yokomizo, Y., Hosono, S., Ohta, T., Hoshino, K., Ishida, H., et al. (2003). MexAB-OprM-Specific efflux pump inhibitors in Pseudomonas aeruginosa. Part 1: Discovery and early strategies for lead optimization. Bioorganic & Medicinal Chemistry Letters *13*, 4201–4204.

Nathan, C.F., Murray, H.W., Wiebe, M.E., and Rubin, B.Y. (1983). Identification of interferon-gamma as the lymphokine that activates human macrophage oxidative metabolism and antimicrobial activity. J Exp Med *158*, 670.

Nguyen, L.T., Haney, E.F., and Vogel, H.J. (2011). The expanding scope of antimicrobial peptide structures and their modes of action. Trends in Biotechnology *29*, 464–472.

Nguyen, S.T., Kwasny, S.M., Ding, X., Cardinale, S.C., McCarthy, C.T., Kim, H.-S., Nikaido, H., Peet, N.P., Williams, J.D., Bowlin, T.L., et al. (2015). Structure–activity relationships of a novel pyranopyridine series of Gram-negative bacterial efflux pump inhibitors. Bioorganic & Medicinal Chemistry *23*, 2024–2034.

Nicklaus, M.C., and Sitzmann, M. (2016). CADD Group Chemoinformatics Tools and User Services. (National Cancer Institute).

Nikaido, H. (2009). Multidrug Resistance in Bacteria. Annual Review of Biochemistry *78*, 119–146.

Nishino, K., Latifi, T., and Groisman, E.A. (2006). Virulence and drug resistance roles of multidrug efflux systems of Salmonella enterica serovar Typhimurium. Molecular Microbiology *59*, 126–141.

Nishino, K., Nikaido, E., and Yamaguchi, A. (2009). Regulation and physiological function of multidrug efflux pumps in Escherichia coli and Salmonella. Biochimica et Biophysica Acta (BBA) - Proteins and Proteomics *1794*, 834–843.

Nix, R.N., Altschuler, S.E., Henson, P.M., and Detweiler, C.S. (2007). Hemophagocytic Macrophages Harbor Salmonella enterica during Persistent Infection. PLoS Pathogens *3*, e193.

Nodwell, M.B., Menz, H., Kirsch, S.F., and Sieber, S.A. (2012). Rugulactone and its Analogues Exert Antibacterial Effects through Multiple Mechanisms Including Inhibition of Thiamine Biosynthesis. ChemBioChem *13*, 1439–1446.

Noel, G., Baetz, N.W., Staab, J.F., Donowitz, M., Kovbasnjuk, O., Pasetti, M.F., and Zachos, N.C. (2017). A primary human macrophage-enteroid co-culture model to investigate mucosal gut physiology and host-pathogen interactions. Scientific Reports *7*, 45270.

Nonejuie, P., Burkart, M., Pogliano, K., and Pogliano, J. (2013). Bacterial cytological profiling rapidly identifies the cellular pathways targeted by antibacterial molecules. Proceedings of the National Academy of Sciences *110*, 16169–16174.

Ochman, H., Soncini, F.C., Solomon, F., and Groisman, E.A. (1996). Identification of a pathogenicity island required for Salmonella survival in host cells. Proc Natl Acad Sci USA *93*, 7800.

Ogushi, K. -i., Wada, A., Niidome, T., Mori, N., Oishi, K., Nagatake, T., Takahashi, A., Asakura, H., Makino, S. -i., Hojo, H., et al. (2001). Salmonella enteritidis FliC (Flagella Filament Protein) Induces Human -Defensin-2 mRNA Production by Caco-2 Cells. Journal of Biological Chemistry *276*, 30521–30526.

Ohl, M.E., and Miller, S.I. (2001). Salmonella: a model for bacterial pathogenesis. Annual Review of Medicine *52*, 259–274.

Ohyagi, H., Onai, N., Sato, T., Yotsumoto, S., Liu, J., Akiba, H., Yagita, H., Atarashi, K., Honda, K., Roers, A., et al. (2013). Monocyte-Derived Dendritic Cells Perform Hemophagocytosis to Fine-Tune Excessive Immune Responses. Immunity *39*, 584–598.

Oldenborg, P.A., Zheleznyak, A., Fang, Y.F., Lagenaur, C.F., Gresham, H.D., and Lindberg, F.P. (2000). Role of CD47 as a marker of self on red blood cells. Science *288*, 2051–2054.

O'Neil, D.A., Porter, E.M., Elewaut, D., Anderson, G.M., Eckmann, L., Ganz, T., and Kagnoff, M.F. (1999). Expression and regulation of the human β-defensins hBD-1 and hBD-2 in intestinal epithelium. The Journal of Immunology *163*, 6718–6724.

Opperman, T.J., Kwasny, S.M., Kim, H.-S., Nguyen, S.T., Houseweart, C., D'Souza, S., Walker, G.C., Peet, N.P., Nikaido, H., and Bowlin, T.L. (2014). Characterization of a Novel Pyranopyridine Inhibitor of the AcrAB Efflux Pump of Escherichia coli. Antimicrobial Agents and Chemotherapy *58*, 722–733.

Ordway, D., Viveiros, M., Leandro, C., Bettencourt, R., Almeida, J., Martins, M., Kristiansen, J.E., Molnar, J., and Amaral, L. (2003). Clinical Concentrations of Thioridazine Kill Intracellular Multidrug-Resistant Mycobacterium tuberculosis. Antimicrobial Agents and Chemotherapy *47*, 917–922.

Padilla, E., Llobet, E., Domenech-Sanchez, A., Martinez-Martinez, L., Bengoechea, J.A., and Alberti, S. (2010). Klebsiella pneumoniae AcrAB Efflux Pump Contributes to Antimicrobial Resistance and Virulence. Antimicrobial Agents and Chemotherapy *54*, 177–183.

Pages, J.-M., James, C.E., and Winterhalter, M. (2008). The porin and the permeating antibiotic: a selective diffusion barrier in Gram-negative bacteria. Nat Rev Micro *6*, 893–903.

Panday, A., Sahoo, M.K., Osorio, D., and Batra, S. (2015). NADPH oxidases: an overview from structure to innate immunity-associated pathologies. Cell Mol Immunol *12*, 5–23.

Park, K., Elias, P.M., Oda, Y., Mackenzie, D., Mauro, T., Holleran, W.M., and Uchida, Y. (2011). Regulation of Cathelicidin Antimicrobial Peptide Expression by an Endoplasmic Reticulum (ER) Stress Signaling, Vitamin D Receptor-independent Pathway. Journal of Biological Chemistry *286*, 34121–34130.

Parra-Lopez, C., Baer, M.T., and Groisman, E.A. (1993). Molecular genetic analysis of a locus required for resistance to antimicrobial peptides in Salmonella typhimurium. The EMBO Journal *12*, 4053.

Parra-Lopez, C., Lin, R., Aspedon, A., and Groisman, E.A. (1994). A Salmonella protein that is required for resistance to antimicrobial peptides and transport of potassium. The EMBO Journal *13*, 3964.

Pasquale, T.R., and Tan, J.S. (2005). Nonantimicrobial Effects of Antibacterial Agents. Clinical Infectious Diseases *40*, 127–135.

Payne, D.J., Gwynn, M.N., Holmes, D.J., and Pompliano, D.L. (2007). Drugs for bad bugs: confronting the challenges of antibacterial discovery. Nature Reviews Drug Discovery *6*, 29–40.

Peng, H., Guo, H., Pogoutse, O., Wan, C., Hu, L.Z., Ni, Z., and Emili, A. (2016). An Unbiased Chemical Proteomics Method Identifies FabI as the Primary Target of 6-OH-BDE-47. Environmental Science & Technology *50*, 11329–11336.

Perron, Y.G., Minor, W.F., Holdrege, C.T., Gottstein, W.J., Godfrey, J.C., Crast, L.B., Babel, R.B., and Cheney, L.C. (1960). Derivatives of 6-Aminopenicillanic Acid. I. Partially Synthetic Penicillins Prepared from α-Aryloxyalkanoic Acids. J. Am. Chem. Soc. *82*, 3934–3938.

Peyron, P., Vaubourgeix, J., Poquet, Y., Levillain, F., Botanch, C., Bardou, F., Daffé, M., Emile, J.-F., Marchou, B., Cardona, P.-J., et al. (2008). Foamy Macrophages from Tuberculous Patients' Granulomas Constitute a Nutrient-Rich Reservoir for M. tuberculosis Persistence. PLoS Pathogens *4*, e1000204.

Philippidis P., Mason J.C., Evans B.J., Nadra I., Taylor K.M., Haskard D.O., and Landis R.C. (2004). Hemoglobin Scavenger Receptor CD163 Mediates Interleukin-10 Release and Heme Oxygenase-1 Synthesis. Circulation Research *94*, 119–126.

Piddock, L.J. (2006). Multidrug-resistance efflux pumps? not just for resistance. Nature Reviews Microbiology *4*, 629–636.

Pilonieta, M.C., Moreland, S.M., English, C.N., and Detweiler, C.S. (2014). *Salmonella enterica* Infection Stimulates Macrophages to Hemophagocytose. MBio *5*, e02211-14.

Plenge-Tellechea, F., Soler, F., and Fernandez-Belda, F. (1999). Tricyclic antidepressants inhibit the Ca 2+-dependent ATPase activity from plasma membrane. Archives of Biochemistry and Biophysics *370*, 119–125.

Prozialeck, W.C., and Weiss, B. (1982). Inhibition of calmodulin by phenothiazines and related drugs: structure-activity relationships. Journal of Pharmacology and Experimental Therapeutics *222*, 509–516.

Racioppi, L., Noeldner, P.K., Lin, F., Arvai, S., and Means, A.R. (2012). Calcium/Calmodulin-dependent Protein Kinase Kinase 2 Regulates Macrophage-mediated Inflammatory Responses. Journal of Biological Chemistry *287*, 11579–11591.

Rajashekar, R., Liebl, D., Seitz, A., and Hensel, M. (2008). Dynamic remodeling of the endosomal system during formation of Salmonella-induced filaments by intracellular Salmonella enterica. Traffic *9*, 2100–2116.

Rasko, D.A., and Sperandio, V. (2010). Anti-virulence strategies to combat bacteria-mediated disease. Nature Reviews Drug Discovery *9*, 117–128.

Rasko, D.A., Moreira, C.G., Li, D.R., Reading, N.C., Ritchie, J.M., Waldor, M.K., Williams, N., Taussig, R., Wei, S., Roth, M., et al. (2008). Targeting QseC Signaling and Virulence for Antibiotic Development. Science *321*, 1078–1080.

Recalcati, S., Locati, M., Marini, A., Santambrogio, P., Zaninotto, F., De Pizzol, M., Zammataro, L., Girelli, D., and Cairo, G. (2010). Differential regulation of iron homeostasis during human macrophage polarized activation. Eur J Immunol *40*, 824–835.

Reens, A.L., Crooks, A.L., Su, C.-C., Nagy, T.A., Reens, D.L., Podoll, J.D., Edwards, M.E., Yu, E.W., and Detweiler, C.S. (2018). A cell-based infection assay identifies efflux pump modulators that reduce bacterial intracellular load. PLOS Pathogens *14*, e1007115.

Renau, T.E., Léger, R., Flamme, E.M., Sangalang, J., She, M.W., Yen, R., Gannon, C.L., Griffith, D., Chamberland, S., Lomovskaya, O., et al. (1999). Inhibitors of Efflux Pumps in *Pseudomonas a eruginosa* Potentiate the Activity of the Fluoroquinolone Antibacterial Levofloxacin. Journal of Medicinal Chemistry *42*, 4928–4931.

Richardson, J.L., Nett, I.R.E., Jones, D.C., Abdille, M.H., Gilbert, I.H., and Fairlamb, A.H. (2009). Improved Tricyclic Inhibitors of Trypanothione Reductase by Screening and Chemical Synthesis. ChemMedChem *4*, 1333–1340.

Ridnour, L.A., Sim, J.E., Hayward, M.A., Wink, D.A., Martin, S.M., Buettner, G.R., and Spitz, D.R. (2000). A spectrophotometric method for the direct detection and quantitation of nitric oxide, nitrite, and nitrate in cell culture media. Anal Biochem *281*, 223–229.

Rivarola, H.W., Fernández, A.R., Enders, J.E., Fretes, R., Gea, S., and Paglini-Oliva, P. (2001). Effects of clomipramine on< i> Trypanosoma cruzi</i> infection in mice. Transactions of the Royal Society of Tropical Medicine and Hygiene *95*, 529–533.

Rivarola, H.W., Bustamante, J.M., Lo Presti, S., Fernández, A.R., Enders, J.E., Gea, S., Fretes, R., and Paglini-Oliva, P. (2005). Trypanosoma cruzi: Chemotherapeutic effects of clomipramine in mice infected with an isolate obtained from an endemic area. Experimental Parasitology *111*, 80–86.

Rivera, J., and Tessarollo, L. (2008). Genetic Background and the Dilemma of Translating Mouse Studies to Humans. Immunity *28*, 1–4.

Rivera-Chávez, F., Zhang, L.F., Faber, F., Lopez, C.A., Byndloss, M.X., Olsan, E.E., Xu, G., Velazquez, E.M., Lebrilla, C.B., Winter, S.E., et al. (2016). Depletion of Butyrate-Producing Clostridia from the Gut Microbiota Drives an Aerobic Luminal Expansion of Salmonella. Cell Host & Microbe *19*, 443–454.

Rix, U., and Superti-Furga, G. (2009). Target profiling of small molecules by chemical proteomics. Nature Chemical Biology *5*, 616–624.

Rodrigues, L., Wagner, D., Viveiros, M., Sampaio, D., Couto, I., Vavra, M., Kern, W.V., and Amaral, L. (2008). Thioridazine and chlorpromazine inhibition of ethidium bromide efflux in Mycobacterium avium and Mycobacterium smegmatis. Journal of Antimicrobial Chemotherapy *61*, 1076–1082.

Rodriguez-Prados, J.-C., Traves, P.G., Cuenca, J., Rico, D., Aragones, J., Martin-Sanz, P., Cascante, M., and Bosca, L. (2010). Substrate fate in activated macrophages: a comparison between innate, classic, and alternative activation. J Immunol *185*, 605–614.

Rollenhagen, C., and Bumann, D. (2006). Salmonella enterica Highly Expressed Genes Are Disease Specific. Infection and Immunity *74*, 1649–1660.

Rollenhagen, C., Sörensen, M., Rizos, K., Hurvitz, R., and Bumann, D. (2004). Antigen selection based on expression levels during infection facilitates vaccine development for an intracellular pathogen. Proceedings of the National Academy of Sciences of the United States of America *101*, 8739–8744.

Rossi, M., Munarriz, E.R., Bartesaghi, S., Milanese, M., Dinsdale, D., Guerra-Martin, M.A., Bampton, E.T.W., Glynn, P., Bonanno, G., Knight, R.A., et al. (2009). Desmethylclomipramine induces the accumulation of autophagy markers by blocking autophagic flux. J. Cell Sci. *122*, 3330.

Rossi, M., Rotblat, B., Ansell, K., Amelio, I., Caraglia, M., Misso, G., Bernassola, F., Cavasotto, C.N., Knight, R.A., Ciechanover, A., et al. (2014). High throughput screening for inhibitors of the HECT ubiquitin E3 ligase ITCH identifies antidepressant drugs as regulators of autophagy. Cell Death and Disease *5*, e1203.

Rudd, M.L., Nicolas, A.N., Brown, B.L., Fischer-Stenger, K., and Stewart, J.K. (2005). Peritoneal macrophages express the serotonin transporter. Journal of Neuroimmunology *159*, 113–118.

Rybniker, J., Chen, J.M., Sala, C., Hartkoorn, R.C., Vocat, A., Benjak, A., Boy-Röttger, S., Zhang, M., Székely, R., Greff, Z., et al. (2014). Anticytolytic Screen Identifies Inhibitors of Mycobacterial Virulence Protein Secretion. Cell Host & Microbe *16*, 538–548.

Sadallah, S., Eken, C., and Schifferli, J.A. (2008). Erythrocyte-derived ectosomes have immunosuppressive properties. Journal of Leukocyte Biology *84*, 1316–1325.

Sakoulas, G., Kumaraswamy, M., Kousha, A., and Nizet, V. (2017). Interaction of Antibiotics with Innate Host Defense Factors against Salmonella enterica Serotype Newport. MSphere *2*.

Salcedo, S.P., Noursadeghi, M., Cohen, J., and Holden, D.W. (2001). Intracellular replication of Salmonella typhimurium strains in specific subsets of splenic macrophages in vivo. Cellular Microbiology *3*, 587–597.

Saliba, A.-E., Li, L., Westermann, A.J., Appenzeller, S., Stapels, D.A.C., Schulte, L.N., Helaine, S., and Vogel, J. (2016). Single-cell RNA-seq ties macrophage polarization to growth rate of intracellular Salmonella. Nature Microbiology *2*, 16206.

Salie, S., Hsu, N.-J., Semenya, D., Jardine, A., and Jacobs, M. (2014). Novel non-neuroleptic phenothiazines inhibit Mycobacterium tuberculosis replication. Journal of Antimicrobial Chemotherapy *69*, 1551–1558.

Samantaray, S., Correia, J.N., Garelnabi, M., Voelz, K., May, R.C., and Hall, R.A. (2016). Novel cell-based in vitro screen to identify small-molecule inhibitors against intracellular replication of Cryptococcus neoformans in macrophages. International Journal of Antimicrobial Agents *48*, 69–77.

Sambrano, G.R., and Steinberg, D. (1995). Recognition of oxidatively damaged and apoptotic cells by an oxidized low density lipoprotein receptor on mouse peritoneal macrophages: role of membrane phosphatidylserine. Proc Natl Acad Sci U S A *92*, 1396–1400.

Scharf, N.T., Molodtsov, V., Kontos, A., Murakami, K.S., and Garcia, G.A. (2016). Novel Chemical Scaffolds for Inhibition of Rifamycin-Resistant RNA Polymerase Discovered from High-Throughput Screening. Journal of Biomolecular Screening 1087057116679994.

Schenone, M., Dančík, V., Wagner, B.K., and Clemons, P.A. (2013). Target identification and mechanism of action in chemical biology and drug discovery. Nature Chemical Biology *9*, 232–240.

Seimon, T.A., Obstfeld, A., Moore, K.J., Golenbock, D.T., and Tabas, I. (2006). Combinatorial pattern recognition receptor signaling alters the balance of life and death in macrophages. Proceedings of the National Academy of Sciences *103*, 19794–19799.

Sellers, R.S., Clifford, C.B., Treuting, P.M., and Brayton, C. (2011). Immunological Variation Between Inbred Laboratory Mouse Strains: Points to Consider in Phenotyping Genetically Immunomodified Mice. Vet Pathol *49*, 32–43.

Seral, C., Van Bambeke, F., and Tulkens, P.M. (2003). Quantitative Analysis of Gentamicin, Azithromycin, Telithromycin, Ciprofloxacin, Moxifloxacin, and Oritavancin (LY333328) Activities against Intracellular Staphylococcus aureus in Mouse J774 Macrophages. Antimicrobial Agents and Chemotherapy *47*, 2283–2292.

Shafer, W.M., Qu, X.-D., Waring, A.J., and Lehrer, R.I. (1998). Modulation of Neisseria gonorrhoeae susceptibility to vertebrate antibacterial peptides due to a member of the resistance/nodulation/division efflux pump family. Proceedings of the National Academy of Sciences *95*, 1829–1833.

Shi, L., Adkins, J.N., Coleman, J.R., Schepmoes, A.A., Dohnkova, A., Mottaz, H.M., Norbeck, A.D., Purvine, S.O., Manes, N.P., Smallwood, H.S., et al. (2006). Proteomic Analysis of Salmonella enterica Serovar Typhimurium Isolated from RAW 264.7 Macrophages: IDENTIFICATION OF A NOVEL PROTEIN THAT CONTRIBUTES TO THE REPLICATION OF SEROVAR TYPHIMURIUM INSIDE MACROPHAGES. Journal of Biological Chemistry *281*, 29131–29140.

Shi, L., Chowdhury, S.M., Smallwood, H.S., Yoon, H., Mottaz-Brewer, H.M., Norbeck, A.D., McDermott, J.E., Clauss, T.R.W., Heffron, F., Smith, R.D., et al. (2009). Proteomic Investigation of the Time Course Responses of RAW 264.7 Macrophages to Infection with Salmonella enterica. Infection and Immunity *77*, 3227–3233.

Shin, B.-M., Paik, I.K., and Cho, H.I. (1994). Bone marrow pathology of culture proven typhoid fever. Journal of Korean Medical Science *9*, 57–63.

Sierra-Filardi, E., Vega, M.A., Sánchez-Mateos, P., Corbí, A.L., and Puig-Kröger, A. (2010). Heme Oxygenase-1 expression in M-CSF-polarized M2 macrophages contributes to LPS-induced IL-10 release. Immunobiology *215*, 788–795.

Silva-Herzog, E., and Detweiler, C.S. (2010). Salmonella enterica Replication in Hemophagocytic Macrophages Requires Two Type Three Secretion Systems. Infection and Immunity *78*, 3369–3377.

Silver, L.L. (2011). Challenges of Antibacterial Discovery. Clinical Microbiology Reviews *24*, 71–109.

Singh, V., Finke-Isami, J., Hopper-Chidlaw, A.C., Schwerk, P., Thompson, A., and Tedin, K. (2017). Salmonella Co-opts Host Cell Chaperone-mediated Autophagy for Intracellular Growth. J Biol Chem *292*, 1847–1864.

Sisson, G., Goodwin, A., Raudonikiene, A., Hughes, N.J., Mukhopadhyay, A.K., Berg, D.E., and Hoffman, P.S. (2002). Enzymes Associated with Reductive Activation and Action of Nitazoxanide, Nitrofurans, and Metronidazole in Helicobacter pylori. Antimicrobial Agents and Chemotherapy *46*, 2116–2123.

Sjuts, H., Vargiu, A.V., Kwasny, S.M., Nguyen, S.T., Kim, H.-S., Ding, X., Ornik, A.R., Ruggerone, P., Bowlin, T.L., Nikaido, H., et al. (2016). Molecular basis for inhibition of AcrB multidrug efflux pump by novel and powerful pyranopyridine derivatives. Proceedings of the National Academy of Sciences *113*, 3509–3514.

Skorokhod, O.A., Schwarzer, E., Ceretto, M., and Arese, P. (2007). Malarial pigment haemozoin, IFN-gamma, TNF-alpha, IL-1beta and LPS do not stimulate expression of inducible nitric oxide synthase and production of nitric oxide in immuno-purified human monocytes. Malaria Journal *6*, 73.

Slauch, J.M. (2011). How does the oxidative burst of macrophages kill bacteria? Still an open question. Molecular Microbiology *80*, 580–583.

Smith-Garvin, J.E., Koretzky, G.A., and Jordan, M.S. (2009). T Cell Activation. Annu. Rev. Immunol. *27*, 591–619.

Spector, M.P., DiRusso, C.C., Pallen, M.J., Del Portillo, F.G., Dougan, G., and Finlay, B.B. (1999). The medium-/long-chain fatty acyl-CoA dehydrogenase (fadF) gene of Salmonella typhimurium is a phase 1 starvation-stress response (SSR) locus. Microbiology *145*, 15–31.

Spinnenhirn, V., Farhan, H., Basler, M., Aichem, A., Canaan, A., and Groettrup, M. (2014). The ubiquitin-like modifier FAT10 decorates autophagy-targeted Salmonella and contributes to Salmonella resistance in mice. Journal of Cell Science *127*, 4883–4893.

Stanley, S.A., Barczak, A.K., Silvis, M.R., Luo, S.S., Sogi, K., Vokes, M., Bray, M.-A., Carpenter, A.E., Moore, C.B., Siddiqi, N., et al. (2014). Identification of Host-Targeted Small Molecules That Restrict Intracellular Mycobacterium tuberculosis Growth. PLoS Pathogens *10*, e1003946.

Steeb, B., Claudi, B., Burton, N.A., Tienz, P., Schmidt, A., Farhan, H., Mazé, A., and Bumann, D. (2013). Parallel Exploitation of Diverse Host Nutrients Enhances Salmonella Virulence. PLoS Pathogens *9*, e1003301.

Steele-Mortimer, O., Brumell, J.H., Knodler, L.A., Méresse, S., Lopez, A., and Finlay, B.B. (2002). The invasion-associated type III secretion system of Salmonella enterica serovar Typhimurium is necessary for intracellular proliferation and vacuole biogenesis in epithelial cells. Cellular Microbiology *4*, 43–54.

Stein, M., Keshav, S., Harris, N., and Gordon, S. (1992). Interleukin 4 potently enhances murine macrophage mannose receptor activity: a marker of alternative immunologic macrophage activation. J Exp Med *176*, 287.

Stříž, I., Slavčev, A., Kalanin, J., Jarešová, M., and Rennard, S.I. (2001). Cell–Cell Contacts with Epithelial Cells Modulate the Phenotype of Human Macrophages. Inflammation *25*, 241–246.

Su, C.-C., and Yu, E.W. (2007). Ligand-transporter interaction in the AcrB multidrug efflux pump determined by fluorescence polarization assay. FEBS Lett *581*, 4972–4976.

Sundaramurthy, V., Barsacchi, R., Samusik, N., Marsico, G., Gilleron, J., Kalaidzidis, I., Meyenhofer, F., Bickle, M., Kalaidzidis, Y., and Zerial, M. (2013). Integration of Chemical and RNAi Multiparametric Profiles Identifies Triggers of Intracellular Mycobacterial Killing. Cell Host & Microbe *13*, 129–142.

Sureka, K., Ghosh, B., Dasgupta, A., Basu, J., Kundu, M., and Bose, I. (2008). Positive Feedback and Noise Activate the Stringent Response Regulator Rel in Mycobacteria. PLOS ONE *3*, e1771.

Swihart, K., Fruth, U., Messmer, N., Hug, K., Behin, R., Huang, S., Del Giudice, G., Aguet, M., and Louis, J.A. (1995). Mice from a genetically resistant background lacking the interferon gamma receptor are susceptible to infection with Leishmania major but mount a polarized T helper cell 1-type CD4+ T cell response. J Exp Med *181*, 961–971.

Takano, A., Nag, S., Gulyás, B., Halldin, C., and Farde, L. (2011). NET occupancy by clomipramine and its active metabolite, desmethylclomipramine, in non-human primates in vivo. Psychopharmacology *216*, 279–286.

Tanaka, K., Usui, Y., and Kojo, S. (2001). Role of serum components in the binding and phagocytosis of oxidatively damaged erythrocytes by autologous mouse macrophages. Cell Mol Life Sci *58*, 1727–1733.

Tchawa Yimga, M., Leatham, M.P., Allen, J.H., Laux, D.C., Conway, T., and Cohen, P.S. (2006). Role of Gluconeogenesis and the Tricarboxylic Acid Cycle in the Virulence of Salmonella enterica Serovar Typhimurium in BALB/c Mice. Infection and Immunity *74*, 1130–1140.

Thi, E.P., Lambertz, U., and Reiner, N.E. (2012). Sleeping with the Enemy: How Intracellular Pathogens Cope with a Macrophage Lifestyle. PLOS Pathogens *8*, e1002551.

Thomas, D.D., Liu, X., Kantrow, S.P., and Lancaster, J.R. (2001). The biological lifetime of nitric oxide: Implications for the perivascular dynamics of NO and O_2. Proc Natl Acad Sci USA *98*, 355.

Thompson, L.J., Dunstan, S.J., Dolecek, C., Perkins, T., House, D., Dougan, G., Nguyen, T.H., Tran, T.P.L., Doan, C.D., Le, T.P., et al. (2009). Transcriptional response in the peripheral blood of patients infected with Salmonella enterica serovar Typhi. Proc Natl Acad Sci U S A *106*, 22433–22438.

Thornley, T.B., Fang, Z., Balasubramanian, S., Larocca, R.A., Gong, W., Gupta, S., Csizmadia, E., Degauque, N., Kim, B.S., Koulmanda, M., et al. (2014). Fragile TIM-4-expressing tissue resident macrophages are migratory and immunoregulatory. J Clin Invest *124*, 3443–3454.

Tulkens, P.M. (1991). Intracellular distribution and activity of antibiotics. European Journal of Clinical Microbiology and Infectious Diseases *10*, 100–106.

Tumitan, A.R.P., Monnazzi, L.G.S., Ghiraldi, F.R., Cilli, E.M., and Machado de Medeiros, B.M. (2007). Pattern of macrophage activation in yersinia-resistant and yersinia-susceptible strains of mice. Microbiol Immunol *51*, 1021–1028.

Uchiya, K., Barbieri, M.A., Funato, K., Shah, A.H., Stahl, P.D., and Groisman, E.A. (1999). A Salmonella virulence protein that inhibits cellular trafficking. The EMBO Journal *18*, 3924–3933.

Vargiu, A.V., Ruggerone, P., Opperman, T.J., Nguyen, S.T., and Nikaido, H. (2014). Molecular Mechanism of MBX2319 Inhibition of Escherichia coli AcrB Multidrug Efflux Pump and Comparison with Other Inhibitors. Antimicrobial Agents and Chemotherapy *58*, 6224–6234.

Vasan, M., Neres, J., Williams, J., Wilson, D.J., Teitelbaum, A.M., Remmel, R.P., and Aldrich, C.C. (2010). Inhibitors of the Salicylate Synthase (MbtI) from Mycobacterium tuberculosis Discovered by High-Throughput Screening. ChemMedChem *5*, 2079–2087.

Vats, D., Mukundan, L., Odegaard, J.I., Zhang, L., Smith, K.L., Morel, C.R., Wagner, R.A., Greaves, D.R., Murray, P.J., and Chawla, A. (2006). Oxidative metabolism and PGC-1beta attenuate macrophage-mediated inflammation. Cell Metab *4*, 13–24.

Vaughn, M.W., Kuo, L., and Liao, J.C. (1998). Effective diffusion distance of nitric oxide in the microcirculation. American Journal of Physiology-Heart and Circulatory Physiology *274*, H1705–H1714.

Vazquez-Torres, A., Jones-Carson, J., Baumler, A.J., Falkow, S., Valdivia, R., Brown, W., Le, M., Berggren, R., Parks, W.T., and Fang, F.C. (1999). Extraintestinal dissemination of Salmonella by CD18-expressing phagocytes. Nature *401*, 804–808.

Vazquez-Torres, A., Xu, Y., Jones-Carson, J., Holden, D.W., Lucia, S.M., Dinauer, M.C., Mastroeni, P., and Fang, F.C. (2000a). Salmonella pathogenicity island 2-dependent evasion of the phagocyte NADPH oxidase. Science *287*, 1655–1658.

Vazquez-Torres, A., Jones-Carson, J., Mastroeni, P., Ischiropoulos, H., and Fang, F.C. (2000b). Antimicrobial Actions of the Nadph Phagocyte Oxidase and Inducible Nitric Oxide Synthase in Experimental Salmonellosis. I. Effects on Microbial Killing by Activated Peritoneal Macrophages in Vitro. J Exp Med *192*, 227.

Velmurugan, D. (2015). Structure Based Discovery of inhibitors for Multidrug Efflux Pump-AcrB. Ommega Internations *1*, 1–8.

Venter, H., Mowla, R., Ohene-Agyei, T., and Ma, S. (2015). RND-type drug efflux pumps from Gram-negative bacteria: molecular mechanism and inhibition. Frontiers in Microbiology *06*.

Verway, M., Bouttier, M., Wang, T.-T., Carrier, M., Calderon, M., An, B.-S., Devemy, E., McIntosh, F., Divangahi, M., Behr, M.A., et al. (2013). Vitamin D Induces Interleukin-1β Expression: Paracrine Macrophage Epithelial Signaling Controls M. tuberculosis Infection. PLOS Pathogens *9*, e1003407.

Viarengo, G., Sciara, M.I., Salazar, M.O., Kieffer, P.M., Furlan, R.L.E., and Garcia Vescovi, E. (2013). Unsaturated long-chain free fatty acids are input signals of the Salmonella enterica PhoP/PhoQ regulatory system. Journal of Biological Chemistry.

Voll, R.E., Herrmann, M., Roth, E.A., Stach, C., Kalden, J.R., and Girkontaite, I. (1997). Immunosuppressive effects of apoptotic cells. Nature *390*, 350.

Wall, D.M., Duffy, P.S., DuPont, C., Prescott, J.F., and Meijer, W.G. (2005). Isocitrate Lyase Activity Is Required for Virulence of the Intracellular Pathogen Rhodococcus equi. Infect. Immun. *73*, 6736.

Wang, Y., Suzek, T., Zhang, J., Wang, J., He, S., Cheng, T., Shoemaker, B.A., Gindulyte, A., and Bryant, S.H. (2014). PubChem BioAssay: 2014 update. Nucleic Acids Research *42*, D1075–D1082.

Wang-Kan, X., Blair, J.M.A., Chirullo, B., Betts, J., La Ragione, R.M., Ivens, A., Ricci, V., Opperman, T.J., and Piddock, L.J.V. (2017). Lack of AcrB Efflux Function Confers Loss of Virulence on Salmonella enterica Serovar Typhimurium. MBio *8*.

Waterman, S.R., and Holden, D.W. (2003). Functions and effectors of the Salmonella pathogenicity island 2 type III secretion system. Cellular Microbiology *5*, 501–511.

Webber, M.A. (2003). The importance of efflux pumps in bacterial antibiotic resistance. Journal of Antimicrobial Chemotherapy *51*, 9–11.

Weiss, G., Werner-Felmayer, G., Werner, E.R., Grunewald, K., Wachter, H., and Hentze, M.W. (1994). Iron regulates nitric oxide synthase activity by controlling nuclear transcription. J Exp Med *180*, 969–976.

Wells, C.A., Ravasi, T., Faulkner, G.J., Carninci, P., Okazaki, Y., Hayashizaki, Y., Sweet, M., Wainwright, B.J., and Hume, D.A. (2003). Genetic control of the innate immune response. BMC Immunology *4*, 5.

Whitlow, M., Howard, A.J., Stewart, D., Hardman, K.D., Chan, J.H., Baccanari, D.P., Tansik, R.L., Hong, J.S., and Kuyper, L.F. (2001). X-ray Crystal Structures of *Candida a lbicans*

Dihydrofolate Reductase: High Resolution Ternary Complexes in Which the Dihydronicotinamide Moiety of NADPH Is Displaced by an Inhibitor. Journal of Medicinal Chemistry *44*, 2928–2932.

Wild, P., Farhan, H., McEwan, D.G., Wagner, S., Rogov, V.V., Brady, N.R., Richter, B., Korac, J., Waidmann, O., Choudhary, C., et al. (2011). Phosphorylation of the Autophagy Receptor Optineurin Restricts Salmonella Growth. Science *333*, 228.

Wilson, R.B., and Maloy, S.R. (1987). Isolation and characterization of Salmonella typhimurium glyoxylate shunt mutants. Journal of Bacteriology *169*, 3029–3034.

Wrande, M., Andrews-Polymenis, H., Twedt, D.J., Steele-Mortimer, O., Porwollik, S., McClelland, M., and Knodler, L.A. (2016). Genetic Determinants of Salmonella enterica Serovar Typhimurium Proliferation in the Cytosol of Epithelial Cells. Infection and Immunity *84*, 3517–3526.

Wright, G.W., and Simon, R.M. (2003). A random variance model for detection of differential gene expression in small microarray experiments. Bioinformatics *19*, 2448–2455.

Wright, M.H., and Sieber, S.A. (2016). Chemical proteomics approaches for identifying the cellular targets of natural products. Nat. Prod. Rep. *33*, 681–708.

Yep, A., McQuade, T., Kirchhoff, P., Larsen, M., and Mobley, H.L.T. (2014). Inhibitors of TonB Function Identified by a High-Throughput Screen for Inhibitors of Iron Acquisition in Uropathogenic Escherichia coli CFT073. MBio *5*, e01089-13-e01089-13.

Yoshida, K., Nakayama, K., Ohtsuka, M., Kuru, N., Yokomizo, Y., Sakamoto, A., Takemura, M., Hoshino, K., Kanda, H., Nitanai, H., et al. (2007). MexAB-OprM specific efflux pump inhibitors in Pseudomonas aeruginosa. Part 7: Highly soluble and in vivo active quaternary ammonium analogue D13-9001, a potential preclinical candidate. Bioorganic & Medicinal Chemistry *15*, 7087–7097.

Yu, H.B., Croxen, M.A., Marchiando, A.M., Ferreira, R.B.R., Cadwell, K., Foster, L.J., and Finlay, B.B. (2014). Autophagy Facilitates Salmonella Replication in HeLa Cells. MBio *5*, e00865-14.

Zaborowski, M.P., Balaj, L., Breakefield, X.O., and Lai, C.P. (2015). Extracellular Vesicles: Composition, Biological Relevance, and Methods of Study. Bioscience *65*, 783–797.

Zhang, C.-Z., Chen, P.-X., Yang, L., Li, W., Chang, M.-X., and Jiang, H.-X. (2017). Coordinated Expression of acrAB-tolC and Eight Other Functional Efflux Pumps Through Activating ramA and marA in Salmonella enterica serovar Typhimurium. Microbial Drug Resistance *24*, 120–125.

Zhang, J.-H., Chung, T.D.Y., and Oldenburg, K.R. (1999). A simple statistical parameter for use in evaluation and validation of high throughput screening assays. Journal of Biomolecular Screening *4*, 67–72.

Ziha-Zarifi, I., Llanes, C., Kohler, T., Pechere, J.C., and Pleisat, P. (1999). In vivo emergence of multidrug-resistant mutants of Pseudomonas aeruginosa overexpressing the active efflux system MexA-MexB-OprM. Antimicrobial Agents and Chemotherapy *43*, 287–291.

Zoller, E.E., Lykens, J.E., Terrell, C.E., Aliberti, J., Filipovich, A.H., Henson, P.M., and Jordan, M.B. (2011). Hemophagocytosis causes a consumptive anemia of inflammation. Journal of Experimental Medicine *208*, 1203–1214.

Zumla, A., Rao, M., Parida, S.K., Keshavjee, S., Cassell, G., Wallis, R., Axelsson-Robertsson, R., Doherty, M., Andersson, J., and Maeurer, M. (2015). Inflammation and tuberculosis: host-directed therapies. Journal of Internal Medicine *277*, 373–387.

Zumla, A., Rao, M., Wallis, R.S., Kaufmann, S.H.E., Rustomjee, R., Mwaba, P., Vilaplana, C., Yeboah-Manu, D., Chakaya, J., Ippolito, G., et al. (2016). Host-directed therapies for infectious diseases: current status, recent progress, and future prospects. The Lancet Infectious Diseases *16*, e47–e63.

APPENDIX A. SAFIRE PROTOCOL DEVELOPMENT

To arrive at the SAFIRE screening protocol described in **Chapter 2**, I optimized standard aspects of the gentamicin protection assay (Nagy et al., 2013) to maximize the assay window and enable high-throughput screening. Using CFU plating in a 24-well infection format, I first evaluated the contribution of opsonization, centrifugation, infection duration, and medium aspiration toward bacterial uptake (2 h.p.i.) and replication (6-18 h.p.i.). Typically, bacteria are coated with complement from normal mouse serum (NMS) prior to macrophage infection to aid phagocytosis; however, I found that opsonization did not contribute to bacterial uptake or

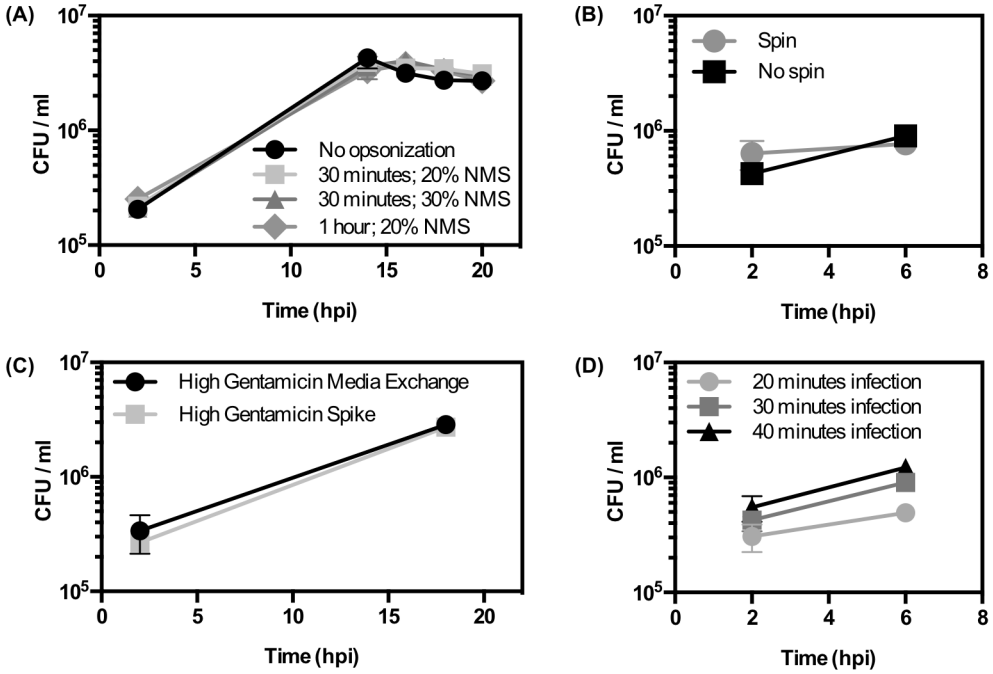

Figure A-1. Opsonization, centrifugation, infection length, gentamicin spike, and infection length have minimal effects on infection of RAW 264.7. One hundred and fifty thousand macrophages were seeded in 24-well plates. After 24 hours, macrophages were infected with opsonized bacteria (30 minutes; 20% NMS) at a multiplicity of infection of 10:1, centrifuged, and incubated for 30 minutes. At indicated timepoints, wells were washed, lysed, and plated to enumerate CFUs. **(A)** Bacteria were opsonized as indicated in the legend. **(B)** After addition of opsonized bacteria, plates were centrifuged for 5 minutes at 500 x *g* or not. **(C)** Opsonized bacteria were added to macrophages and plates were centrifuged; at 30 minutes post infection media was removed and replaced with fresh media containing gentamicin, or gentamicin was spiked into the wells without media exchange. **(D)** Macrophages were infected with non-opsonized bacteria and plates were not spun. Infection proceeded for the indicated time before media was spiked with gentamicin. Data shown are mean + SD of at least duplicate samples from one experiment.

replication in RAW 264.7 (**Figure A-1A**). Many groups also centrifuge plates after bacterial addition to more quickly bring floating bacteria in contact with adherent macrophages. I found that there may be a slight effect of centrifugation on bacterial uptake, but that it appears to be minor (**Figure A-1B**). I also found that a medium exchange could be eliminated by spiking in high gentamicin after the infection stage with no alterations to uptake or replication (**Figure A-1C**). Finally, to compensate for any decrease in uptake due to not spinning, I found that lengthening the infection duration slightly increased bacterial uptake (**Figure A-1D**).

Next, I tested several fluorescent bacterial strains to evaluate their infection and fluorescence. I found that a strain (ALR#003; DET#0829) harboring the pTag-RFP plasmid was defective in RAWs (**Figure A-2**), likely due to very high expression of the fluorescent protein. Of the remaining strains, only those expressing a green fluorophore were viable options, based on the microscopes available in our department. I found that bacteria harboring the pACYC184-GFP plasmid (ALR#002; DET#0014) were too bright and the fluorescence filled the whole macrophage (data not shown). In contrast, bacteria expressing GFP from the *sifB* locus (ALR#004; DET#1021) exhibited bright fluorescence restricted to bacterial rods (data not shown), and I decided to employ the *sifB*::GFP strain for future work.

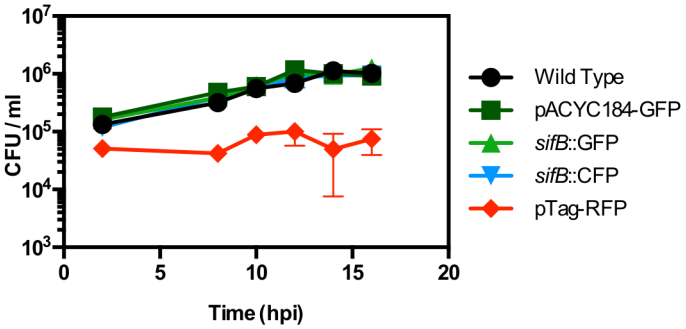

Figure A-2. *sifB*::GFP bacteria colonize RAW 264.7 equally to wild type bacteria. RAW 264.7 were seeded as in Figure A-1 and infected with non-opsonized bacteria at a multiplicity of infection of 10:1; plates were centrifuged and gentamicin was spiked at 30 minutes post infection. At indicated timepoints, wells were washed, lysed, and plated to enumerate CFUs. Data shown are mean + SD of duplicate samples from one experiment.

In order to enhance reproducibility in screening, I used identical frozen aliquots of RAWs for screening. I tested the effect of freezing density and recovery time on infection and macrophage viability. I used CFU plating and microscopy to evaluate infection and macrophage viability

(**Figure A-3**). I found that freezing aliquots at a higher density (1.5 x 10^7 cells vs 5 x 10^6 / ml) led to higher recovered CFUs (**Figure A-3A**). Similarly, I found that thawing macrophages and growing them for 1 day prior to reseeding, rather than thawing and directly seeding into assay plates, led to higher recovered CFUs. Upon microscopic analysis of uninfected and infected macrophages, I found that thawing and directly seeding macrophages led to fewer cells after infection (**Figure A-3B**). Thus, I concluded that decreased recovered CFUs from low-density frozen aliquots and directly seeded samples was likely due to poor macrophage robustness under these conditions. However, high-density frozen aliquots allowed to recover for 1 day prior to reseeding for infection displayed similar infection as a continuous culture of macrophages, suggesting the cells were robust to infection under these conditions. Ultimately, I elected to let macrophages recover for 3 days prior to reseeding for infection to enable more expansion.

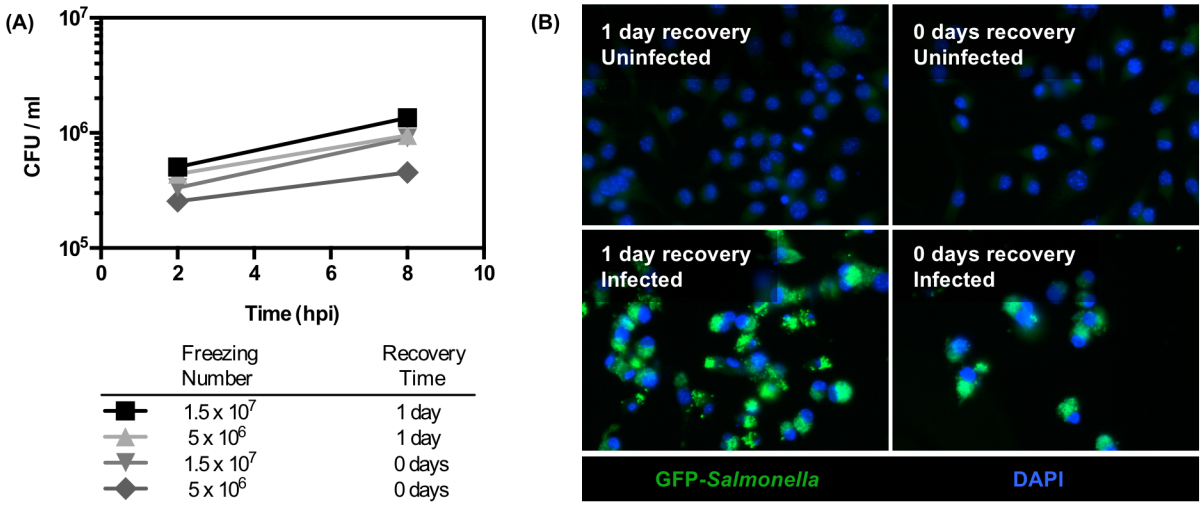

Figure A-3. High density freezing and post-thaw recovery prior to infection increases infection and macrophage survival. Cryovials of macrophages were frozen with the indicated number of macrophages. Macrophages were thawed and cultured for 1 day prior to seeding 24 hours before infection, or thawed and directly seeded 24 hours prior to infection; cells were seeded in 96-well tissue-culture plates and in glass-bottomed plates for imaging. Macrophages were infected with nonopsonized bacteria; plates were centrifuged and gentamicin was spiked at 30 minutes post infection. **(A)** At indicated timepoints, wells were washed, lysed, and harvested for CFUs. Data shown are mean + SD of triplicate samples from one experiment. **(B)** Cryovials frozen at 1.5 x 10^7 cells were thawed and infected as described (or left uninfected). At 18 hours post infection, wells were fixed, stained with DAPI, and imaged. Representative images are shown.

Next, I optimized the number of bacteria used for infection. The above experiments were performed with bacteria at a multiplicity of infection of 10, or 10 bacteria for each macrophage, as is typically utilized in the field. However, I hypothesized that infection *concentration*, rather than relative ratio of bacteria to macrophage, is the main driver of per-macrophage infection. I tested different numbers of macrophages and different infection concentrations of bacteria. I found that the per-macrophage bacterial load was identical when the same infection concentration was used, even though the multiplicity was different (**Figure A-4A**). Thus, I concluded that infection appears to be cell-autonomous and that maintaining infection

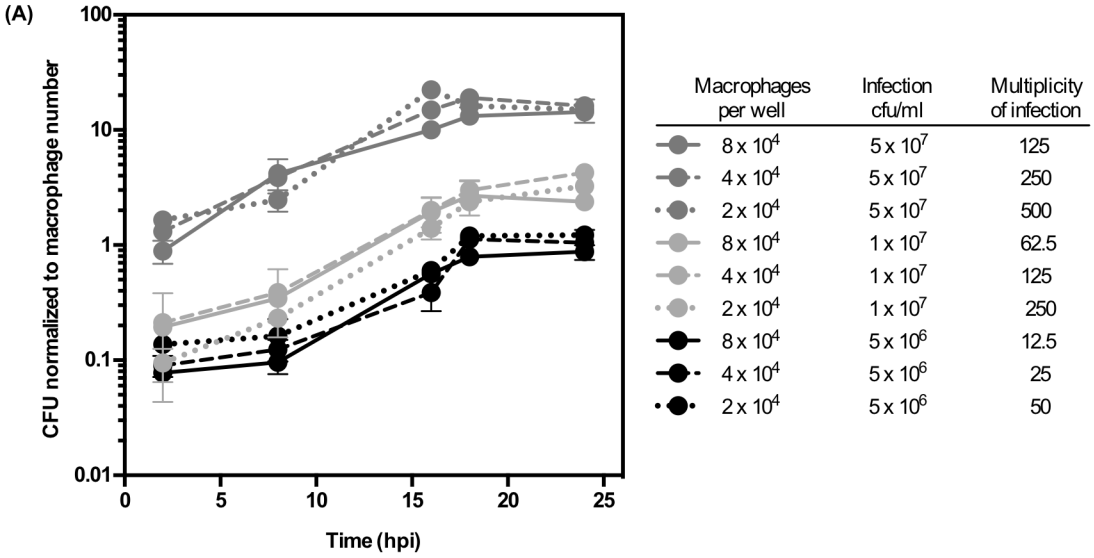

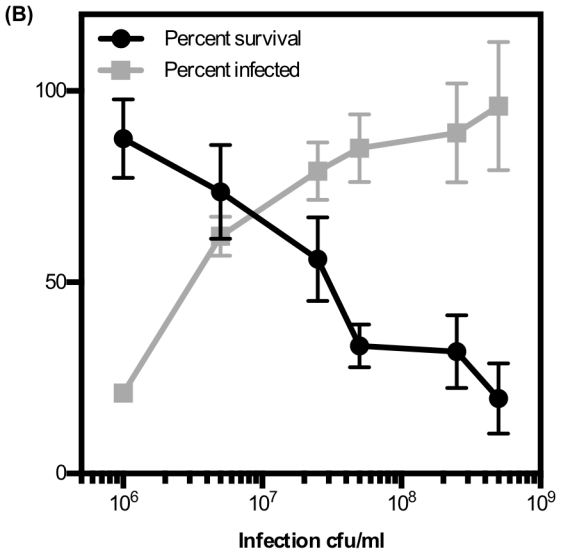

Figure A-4. Infection concentration, not multiplicity of infection, affects macrophage infection and survival. Macrophages were thawed as described in **Chapter 2**. **(A)** The indicated numbers of macrophages were seeded and infected with the indicated concentration of bacteria. At indicated timepoints, wells were washed, lysed, and plated to enumerate CFUs. **(B)** 3 x 10^4 macrophages were seeded and infected with the indicated concentration of bacteria. At 18 hours post infection, wells were processed for fluorescence microscopy. Data shown are mean + SD of duplicate samples from one experiment.

concentration, not multiplicity of infection, is important for consistent results.

High bacterial infection can lead to macrophage death. To identify a balance point between macrophage infection and survival, I established the optimal infection concentration. Using 96-well plates, I tested a range of infection concentrations using microscopic quantification of infection and macrophage numbers as described in **Chapter 2**. I found that the infection concentration affects both the macrophage survival and the percentage of infected macrophages (**Figure A-4B**). To preserve the majority of infected macrophages while also maintaining infection above 70%, I elected to use an infection concentration of 1×10^7 bacteria / ml. Finally, I found that seeding 5×10^4 macrophages per 96-well yielded sufficient cells to image under these infection conditions.

To enable higher throughput screening, the protocol was modified to include addition of 40 μg/ml gentamicin at 45 minutes post infection, then addition of compound using a pin tool at 2 h.p.i. without any further medium exchange. Together with Amy Crooks, I determined the effect of different concentrations of gentamicin on bacteria in the supernatant and within cells, and we investigated any potential effects of bacterial debris from the initial gentamicin treatment remaining in the well due to no medium exchange. These experiments were performed in 96-well plates. We first quantified intracellular and extracellular bacteria by CFU plating of lysed macrophages and supernatant, respectively, using the previous protocol of 1.25 hours treatment with 100 μg/ml gentamicin, followed by 16 hours of 10 μg/ml gentamicin. We found that there was 4 logs killing of extracellular bacteria during the high gentamicin treatment, and that the low gentamicin mostly inhibited extracellular growth of bacteria while allowing intracellular growth from 2-18 h.p.i., as expected (**Figure A-5A; black circles**). We next tested the effect of gentamicin concentration on intracellular growth from 2-16 h.p.i. by treating with 100 μg/ml gentamicin for 1.25 hours, then exchanging medium and treating with different concentrations of gentamicin (**Figure A-5A**). We found that 40 μg/ml gentamicin yielded similar intracellular

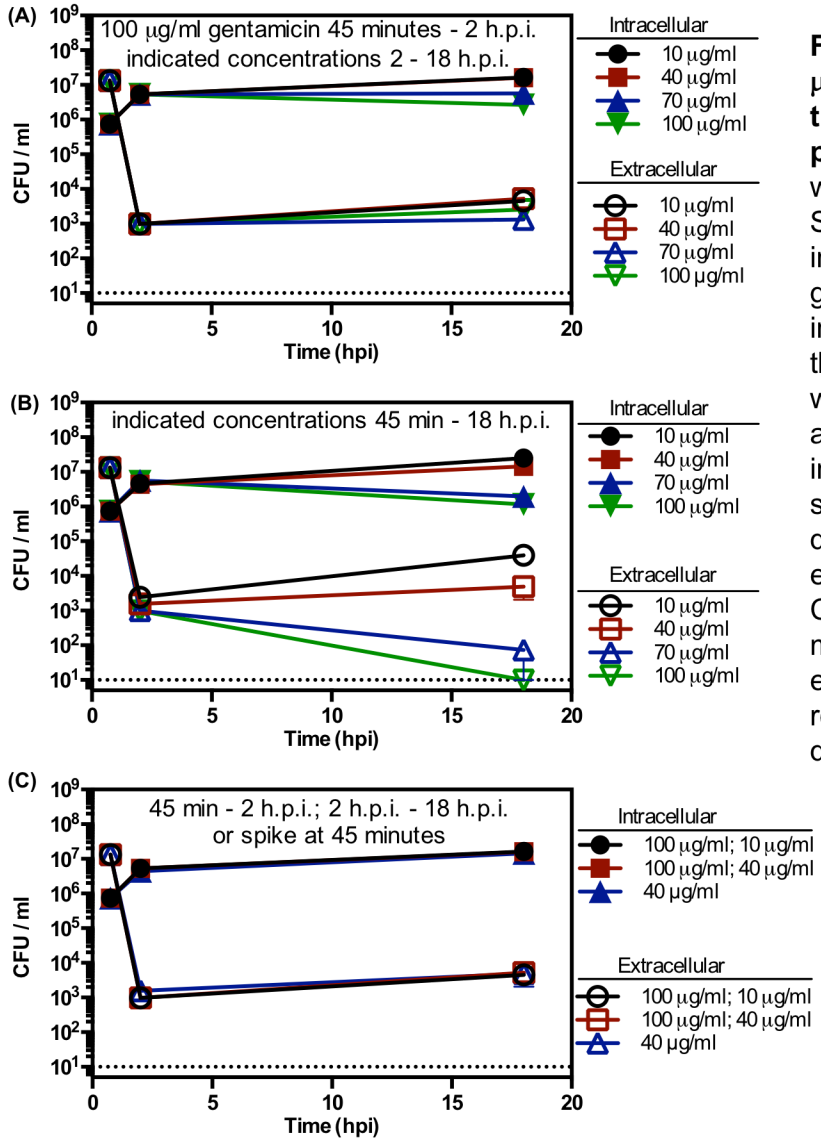

Figure A-5. Spiking 40 μg/ml gentamicin mimics the standard infection protocol. Macrophages were infected following the SAFIRE protocol described in **Chapter 2**, except that gentamicin was added as indicated in the figures. At the indicated timepoints, wells were washed, lysed, and plated to enumerate intracellular CFUs, and supernatant was harvested, diluted, and plated to enumerate extracellular CFUs. Data shown are mean + SD of one experiment. Dotted line represents the limit of detection.

replication as 10 μg/ml, but that 70 and 100 μg/ml appeared to inhibit growth or even reduce bacterial load at 18 h.p.i. All concentrations tested inhibited extracellular bacterial growth similar to the standard protocol, as expected.

Finally, we tested the effect of spiking different concentrations of gentamicin at 45 minutes post infection for the duration of the experiment (**Figure A-5B**). We found that all concentrations tested caused similar drops in extracellular bacteria at 2 h.p.i., though small (~2-fold) increases in recovered extracellular bacteria were observed with lower gentamicin concentration (10 μg/ml

vs 100 μg/ml). In addition, we observed that treatment with 70 or 100 μg/ml gentamicin reduced bacterial load at 18 h.p.i. as observed above. However, we observed very similar CFUs between the standard 100/10 protocol, the 100/40 protocol, and the 40 spike protocol (**replotted in Figure A-5C**). This result suggests that spiking 40 μg/ml gentamicin kills nearly as many extracellular bacteria by 2 h.p.i. as 100 μg/ml but does not affect intracellular bacteria survival or replication, thus mimicking the standard gentamicin protection assay. Thus, we elected to spike 40 μg/ml gentamicin at 45 minutes post infection for future experiments.

APPENDIX B. MATLAB® ANALYSIS SCRIPTS

Image analysis scripts are copied here and deposited on the MATLAB file exchange at https://www.mathworks.com/matlabcentral/fileexchange/ under SAFIRE_CV1000, SAFIRE_Olympus_ix81, and SAFIRE_ArrayScan.

Olympus IX81 Montager

```
%Script to Produce Montages for Visual Analysis using images from Olympus
%IX81 running Slidebook

%Abigail Reens, abigail.reens@colorado.edu

%This script takes in a folder of blue, green, and red images that are
%named Name=Color, in alphabetical order such that blue (DAPI_, green (FITC),
%and red (Texas) are read in that order. It then produces a RGB image in
%16bit display, and combines that with the individual channels to produce
%a montage. The RGB and the montage are saved to appropriate folders as
%tiffs so they can be altered in imagej for presentation.

%select folder and change to that folder
folder_path = uigetdir('.', 'Select Folder to Process');
cd(folder_path);

%make struct of .tiff files in folder
imagelist = dir('*.tiff');

%check to make sure right number of images in folder
%if mod(max(size((imagelist))),3) ~= 0
    %error('You do not have the right number of images to proceed!')
%end

%select folders to save RGB and Montages
rgb_save = uigetdir('.', 'Select Folder to Save RGB Images');
montage_save = uigetdir('.', 'Select Folder to Save Montages');

timeStart = clock;

%make a loop counter so can count how many images processed
montage_counter = 0;

%set pixel width of borders (can make a gui to ask in the future...)
border_pixels = 5;

%set dimensions of montage borders
image = imread([imagelist(1).name]);
[height, width] = size(image);
border_vert = 65535 * ones(height,border_pixels,3);
border_horz = 65535 * ones(border_pixels,(2*width+border_pixels),3);

numberImages = max(size(imagelist))/3;
%iterate through images
for i=1:numberImages

    %read images
    [blue12, green12, red12, name] = readBGR(imagelist,i);

    %adjust 12bit images to 16bit images so that they actually display
    blue = 16*blue12;
    green = 16*green12;
    red = 16*red12;
```

```
    %combine colors into rgb images
    rgb(:,:,1) = red;
    rgb(:,:,2) = green;
    rgb(:,:,3) = blue;

    %save rgb as .tif into rgb folder?, with approp intensity settings...
    imwrite(rgb, fullfile(rgb_save,[name '_RGB.tif']));

    %make b&w images into color but still look black and white
    red_montage = repmat(red,[1,1,3]);
    green_montage = repmat(green,[1,1,3]);
    blue_montage = repmat(blue,[1,1,3]);

    %combine individuals, rgb into montage
    montage = [blue_montage  border_vert red_montage  ; ...
                             border_horz              ; ...
               green_montage border_vert     rgb      ];

    %save montage as .tif into montage folder
    imwrite(montage, fullfile(montage_save, [name '_Montage.tif']));

    %increment montage counter
    montage_counter = montage_counter + 1;
end

timeEnd = clock;
time = etime(timeEnd,timeStart);
sec = mod(time,60);
minhr = (time-sec)/60;
min = mod(minhr,60);
hr = (minhr-min)/60;

beep;

%show message with number of montages made
msgbox({['Runtime = ' int2str(hr) 'hrs, ' int2str(min) 'min, ' int2str(sec) 'sec.']...
    []...
    [int2str(montage_counter) ' montages have been saved to ' montage_save]});
```

OlympusIX81 Analyzer

```
%Script for analyzing bacteria within cells

    %This script processes a folder of red, green, and blue images to determine
    %bacterial load within macrophages. It then applies a two-way median
    %polish to the data to remove row / column effects, and transforms data
    %into B-scores.

%Now we will briefly describe the scheme of the script.

    %User input.
        %the user is asked to select folders for processing and saving data

        %the user is also asked to enter a pixel value between 0-4095.
        %this is the threshold above which a pixel is GFP positive. This
        %number must be determined empirically using uninfected, positive,
        %and negative controls, such that there are very few GFP+ pixels
        %in uninfected controls. Typically, the threshold is determined as
        %the minimum+200

        %The user is asked to input the background GFP value. This is to
        %remove background signal for correct calculation of percent
        %inhibition data.

        %the user also enters how many images were taken per well and how
        %%many columns were images. these numbers facilitates the
        %correct ordering of images for output

    %Reading, naming, segmenting, saving images
        %images are read in order blue green red, according to how they are
        %saved in the folder. short names are extracted and compared to
        %ensure that they match.

        %images are segmented using a watershed algorithm to identify macrophages

        %segmented images are combined with raw data to produce overlays
        %for reference

    %Extracting statistics

        %using the segmented cell boundaries, various statistics are
        %quantified about the area / intensity of GFP within the
        %macrophages.

        %when applicable, statistics are also compiled for infected cells
        %only, using a threshold of >2 GFP+ pixels for a cell to be
        %classified as infected

    %Exporting image data and histograms

        %the struct of all data is saved as a .mat for future manipulation
        %in matlab

        %per-image data for every statistic calculated is exported into a
        %.txt file. this file can be easily imported into prism for
        %graphical analysis.

        %histograms are also produced for every image for every statistic
        %and saved as .jpg

    %Averaging image data to get well data
        %a function iterates through the data and averages images whose
        %names match to get the average data for that well. this data is
        %saved as a .mat for future manipulation in matlab

    %Calculating residuals and B-scores
        %well averaged data is processed using the B-score method (see
        %functions for citations). this method uses a two-way median polish
        %to remove row and column effects, and produces residuals, which
        %essentially describe the true value in a particular well. these
        %residuals enable the calculation of the bscore, which describes
        %the significance of a particular well's difference. note that the
        %median polish does not work when there are <2 rows or columns

    %Exporting well data and heatmaps
        %well data in the format of raw, residuals, or b-scores is saved as
```

```
        %.txt files in a 96-well format. these same data are also processed
        %into heatmaps and saved as .jpg

%% Block for user input
%user input and initializing of stuffs
    %ask for directory and change to that directory
    folder_path = uigetdir('.','Select Folder To Process');
    cd(folder_path);
    disp(folder_path);
    mask_saving = uigetdir('.','Select Folder to Save Masks and Variants');

    %first, make all the files not have spaces because they are EVIL
    %also add 0 in front of everything so that they go in order
    [schloop,schloopy] = system('for name in *\ *; do mv "$name" "${name// /}"; done');
    [schloop,schloopy] = system(['for file in *-??_*; do '...
        'b=${file%-??_*};e=${file#*-??_};wn=${file%$e};wn=${wn#$b};'...
        'mv $file ${b}${wn%??}0${wn#??}${e};done']);

    %location of data file to save
    data_saving = uigetdir('.','Select Folder to Save Numerical Data');
    hist_saving = uigetdir('.','Select Folder to Save Histogram Data');
    heatmap_saving = uigetdir('.','Select Folder to Save Heatmap Data');

    %ask for name for ssaving things
    data_filename = inputdlg({'Enter Filename for Saving Numerical Data'},'Summary Data
Filename',1,{'Filename'});
    data_filename = data_filename{1};
    disp(data_filename);

    %ask user to input threshold for GFP+pixels and convert to number
    %ask user to input GFP background value
    %ask how many images per well, how many columns
    %in future, could potentially automate thresholding
    input = inputdlg({'GFP+ Pixel Threshold Value between 0-4095',...
        'Background GFP Value between 0-4095','Images Per Well','Columns Imaged on Plates'},...
        'Threshold and Image Format',1,{'450','150','2','11'});
    thresh = str2double(input(1));
    disp(thresh);
    bkgdGFP = str2double(input(2));
    disp(bkgdGFP);
    imageDensity = str2double(input(3));
    numcol = str2double(input(4));

    timeStart = clock;
    disp(['start ' num2str(clock)]);

    %a macrophages must have at least 2 GFP+ pixels to be considered infected
    %this value must be in balance with the pixel threshold, such that there
    %are very few GFP+ pixels in uninfected images
    infectedThresh = 2;

    imagelist = dir('*.tiff');

    %make an array of the tiffs in the folder in the correct order
%     imagelist_wrong = dir('*.tiff');
%     imagelist_4D = reshape(imagelist_wrong,3,imageDensity,numcol,[]);
%     imagelist_4D_right = imagelist_4D(:,:,[4:numcol 1:3],:);
%     imagelist = imagelist_4D_right(:);

    %calculate number of images
    numberImages = max(size(imagelist))/3;

    %instantiate allDataStruct
    data = struct;

%% Block for processing images
%iterate through each image, save masks, extract data
for j=1:numberImages
%read images and check that short names match
    [blue, green, red, name] = readBGR(imagelist,j);
    disp(name);
%segment
    cellMask = segmentCells(red,blue);
%combine masks with appropriate images
    save_masks(cellMask,red,green,blue,name,mask_saving);

%extract information and save to the data struct
%save image name to data struct
```

```
data(j).ImageName = name;

%ask matlab to turn each cell into an object of linked pixels
cellInfo = bwconncomp(cellMask);

%get the number of objects, and the object / pixel array
cellNumber = cellInfo.NumObjects;
cellArray = cellInfo.PixelIdxList;

%add number cells to data struct
data(j).NumberMacrophages = cellNumber;

k=0;

%iterate through the cells in the image (the pixel-linked objects)
for i=1:cellNumber

    %turn the pixels for each object into an array
    pixelArray = cellArray{i};

    %number of gfp+ pixels in that macrophage
    %ask whether pixels in green at each pixel in the object are >thresh
    %if so, turn them into 1; if not, turn them 0
    %and then add up all the 1s to get gfpcount
    gfpThreshCount = sum(green(pixelArray)>thresh);
    %store the gfp positive pixel count in the data struct in the
    %appropriate position in the sub-array
    data(j).NumGFPPosPixels(i) = gfpThreshCount;

    %calculate and store the fractional GFP+area in the macrophage
    %find the area of the the macrophage / object
    macNumPixels = length(pixelArray);
    fracGFPPixels = gfpThreshCount / macNumPixels;
    data(j).FractionalGFPArea(i) = fracGFPPixels;

    %sum of intensities of gfp+ pixels in that macrophage, also store
    gfpThreshIntensity = sum(green(green(pixelArray)>thresh));
    data(j).IntensityGFPPosPixels(i) = gfpThreshIntensity;
    data(j).IntensityGFPPosPixelsBKGD(i) = gfpThreshIntensity - bkgdGFP;

    %gfp+ pixel intensity divided by area of mac
    gfpThreshIntensityArea = gfpThreshIntensity / macNumPixels;
    data(j).AreaIntensityGFPPosPixels(i) = gfpThreshIntensityArea;
    data(j).AreaIntensityGFPPosPixelsBKGD(i) = gfpThreshIntensityArea - bkgdGFP;

    %sum of total intensity of gfp in that macrophage
    gfpTotalIntensity = sum(green(pixelArray));
    data(j).IntensityTotal(i) = gfpTotalIntensity;
    data(j).IntensityTotalBKGD(i) = gfpTotalIntensity - bkgdGFP;

    %total gfp divided by mac area
    gfpTotalIntensityArea = gfpTotalIntensity / macNumPixels;
    data(j).AreaIntensityTotal(i) = gfpTotalIntensityArea;
    data(j).AreaIntensityTotalBKGD(i) = gfpTotalIntensityArea - bkgdGFP;

    %now, if mac is infected, add those data to a special category for
    %only infected cells
    if gfpThreshCount > infectedThresh
        k=1+k;
        data(j).InfectedNumGFPPosPixels(k) = gfpThreshCount;
        data(j).InfectedFractionalGFPArea(k) = fracGFPPixels;
        data(j).InfectedIntensityGFPPosPixels(k) = gfpThreshIntensity;
        data(j).InfectedIntensityGFPPosPixelsBKGD(k) = gfpThreshIntensity - bkgdGFP;
        data(j).InfectedAreaIntensityGFPPosPixels(k) = gfpThreshIntensityArea;
        data(j).InfectedAreaIntensityGFPPosPixelsBKGD(k) = gfpThreshIntensityArea - bkgdGFP;
        data(j).InfectedIntensityTotal(k) = gfpTotalIntensity;
        data(j).InfectedIntensityTotalBKGD(k) = gfpTotalIntensity - bkgdGFP;
        data(j).InfectedAreaIntensityTotal(k) = gfpTotalIntensityArea;
        data(j).InfectedAreaIntensityTotalBKGD(k) = gfpTotalIntensityArea - bkgdGFP;
    end
end

%calculate % infected macs
data(j).InfectedMacsCount = k;
numInfectedMacs = k;
percentInfected = 100*(numInfectedMacs / cellNumber);

%calculate and store means for all the things for this image
```

```
data(j).AvgGFPPosPixels = mean(data(j).NumGFPPosPixels);
data(j).AvgFractionalGFPArea = mean(data(j).FractionalGFPArea);
data(j).AvgIntensityGFPPos = mean(data(j).IntensityGFPPosPixels);
data(j).AvgIntensityGFPPosBKGD = mean(data(j).IntensityGFPPosPixelsBKGD);
data(j).AvgAreaIntensityGFPPos = mean(data(j).AreaIntensityGFPPosPixels);
data(j).AvgAreaIntensityGFPPosBKGD = mean(data(j).AreaIntensityGFPPosPixelsBKGD);
data(j).AvgIntensityTotal = mean(data(j).IntensityTotal);
data(j).AvgIntensityTotalBKGD = mean(data(j).IntensityTotalBKGD);
data(j).AvgAreaIntensityTotal = mean(data(j).AreaIntensityTotal);
data(j).AvgAreaIntensityTotalBKGD = mean(data(j).AreaIntensityTotalBKGD);

%%output information for infected macs count, either the numbers or 0
if data(j).InfectedMacsCount ~= 0
    data(j).AvgInfectedGFPPosPixels = mean(data(j).InfectedNumGFPPosPixels);
    data(j).AvgInfectedFractionalGFPArea = mean(data(j).InfectedFractionalGFPArea);
    data(j).AvgInfectedIntensityGFPPos = mean(data(j).InfectedIntensityGFPPosPixels);
    data(j).AvgInfectedIntensityGFPPosBKGD = mean(data(j).InfectedIntensityGFPPosPixelsBKGD);
    data(j).AvgInfectedAreaIntensityGFPPos = mean(data(j).InfectedAreaIntensityGFPPosPixels);
    data(j).AvgInfectedAreaIntensityGFPPosBKGD = mean(data(j).InfectedAreaIntensityGFPPosPixelsBKGD);
    data(j).AvgInfectedIntensityTotal = mean(data(j).InfectedIntensityTotal);
    data(j).AvgInfectedIntensityTotalBKGD = mean(data(j).InfectedIntensityTotalBKGD);
    data(j).AvgInfectedAreaIntensityTotal = mean(data(j).InfectedAreaIntensityTotal);
    data(j).AvgInfectedAreaIntensityTotalBKGD = mean(data(j).InfectedAreaIntensityTotalBKGD);
    data(j).PercentInfectedMacs = percentInfected;
else
    data(j).AvgInfectedGFPPosPixels = 0;
    data(j).AvgInfectedFractionalGFPArea = 0;
    data(j).AvgInfectedIntensityGFPPos = 0;
    data(j).AvgInfectedIntensityGFPPosBKGD = 0;
    data(j).AvgInfectedAreaIntensityGFPPos = 0;
    data(j).AvgInfectedAreaIntensityGFPPosBKGD = 0;
    data(j).AvgInfectedIntensityTotal = 0;
    data(j).AvgInfectedIntensityTotalBKGD = 0;
    data(j).AvgInfectedAreaIntensityTotal = 0;
    data(j).AvgInfectedAreaIntensityTotalBKGD = 0;
    data(j).PercentInfectedMacs = 0;
end
end

%save data struct to file
save(fullfile(data_saving,[data_filename '_imageData']),'data');

%% Block for exporting image data
disp(['output ' num2str(clock)]);
%output the image data to a txt file
    statistics1 = {'ImageName',...
        'AvgGFPPosPixels',...
        'AvgFractionalGFPArea',...
        'AvgIntensityGFPPos',...
        'AvgIntensityGFPPosBKGD',...
        'AvgAreaIntensityGFPPos',...
        'AvgAreaIntensityGFPPosBKGD',...
        'AvgIntensityTotal',...
        'AvgIntensityTotalBKGD',...
        'AvgAreaIntensityTotal',...
        'AvgAreaIntensityTotalBKGD',...
        'AvgInfectedGFPPosPixels'...
        'AvgInfectedFractionalGFPArea',...
        'AvgInfectedIntensityGFPPos',...
        'AvgInfectedIntensityGFPPosBKGD',...
        'AvgInfectedAreaIntensityGFPPos',...
        'AvgInfectedAreaIntensityGFPPosBKGD',...
        'AvgInfectedIntensityTotal',...
        'AvgInfectedIntensityTotalBKGD',...
        'AvgInfectedAreaIntensityTotal',...
        'AvgInfectedAreaIntensityTotalBKGD',...
        'PercentInfectedMacs'};
    style = {'%s ','%d ','%d ','%d ','%d ','%d ','%d ','%d ','%d ','%d ','%d ','%d ','%d ','%d '
','%d ','%d ','%d ','%d ','%d ','%d '};
    filename = fullfile(data_saving,[data_filename '_ImageData.txt']);
    dataFile = fopen(fullfile(filename),'w');
    fprintf(dataFile,'%s',data_filename);
    %iterate through the fields and print names and fields
    for s = 1:length(statistics1)
        fprintf(dataFile,'\n%s ',statistics1{s});
        for m=1:numberImages
            fprintf(dataFile,style{s},getfield(data(m),statistics1{s}));
        end
```

```
    end
    fprintf(dataFile,'\n ');
    fprintf(dataFile,'\n%s ','NumberMacrophages');
    for m=1:numberImages
           fprintf(dataFile,'%d ',data(m).NumberMacrophages);
    end
    fprintf(dataFile,'\n ');
    fclose(dataFile);


%% Block for exporting histograms
disp(['histograms ' num2str(clock)]);
%now output histograms of distributions to jpg
% statistics2 =
{'NumGFPPosPixels','FractionalGFPArea','IntensityGFPPosPixels','IntensityGFPPosPixelsBKGD',...
%     'AreaIntensityGFPPosPixels','IntensityTotal','AreaIntensityTotal',...
%     'AreaIntensityGFPPosPixelsBKGD','IntensityTotalBKGD','AreaIntensityTotalBKGD',...
%     'InfectedNumGFPPosPixels','InfectedFractionalGFPArea','InfectedIntensityGFPPosPixels','InfectedIn
tensityGFPPosPixelsBKGD',...
%     'InfectedAreaIntensityGFPPosPixels','InfectedIntensityTotal','InfectedAreaIntensityTotal',...
%     'InfectedAreaIntensityGFPPosPixelsBKGD','InfectedIntensityTotalBKGD','InfectedAreaIntensityTotalB
KGD'};
statistics2 =
{'FractionalGFPArea','AreaIntensityTotal','AreaIntensityTotalBKGD','PercentInfectedMacs'};
histogram = figure('visible','off');
for s = 1:length(statistics2)
    disp(['statistic ' statistics2{s}]);
    for m=1:numberImages
        hist(getfield(data(m),statistics2{s}));
        fig = findobj(gca,'Type','patch');
        set(fig,'FaceColor',[0 .7 0]);
        ylabel('Number of Cells');
        xlabel(statistics2{s});
        title(data(m).ImageName);
        saveas(histogram,fullfile(hist_saving,[statistics2{s} '_' data(m).ImageName]),'jpg');
    end
end


%% Block for running just the averager part
disp(['averager ' num2str(clock)]);

statistics = {'AvgGFPPosPixels',...
        'AvgFractionalGFPArea',...
        'AvgIntensityGFPPos',...
        'AvgIntensityGFPPosBKGD',...
        'AvgAreaIntensityGFPPos',...
        'AvgAreaIntensityGFPPosBKGD',...
        'AvgIntensityTotal',...
        'AvgIntensityTotalBKGD',...
        'AvgAreaIntensityTotal',...
        'AvgAreaIntensityTotalBKGD',...
        'AvgInfectedGFPPosPixels'...
        'AvgInfectedFractionalGFPArea',...
        'AvgInfectedIntensityGFPPos',...
        'AvgInfectedIntensityGFPPosBKGD',...
        'AvgInfectedAreaIntensityGFPPos',...
        'AvgInfectedAreaIntensityGFPPosBKGD',...
        'AvgInfectedIntensityTotal',...
        'AvgInfectedIntensityTotalBKGD',...
        'AvgInfectedAreaIntensityTotal',...
        'AvgInfectedAreaIntensityTotalBKGD',...
        'PercentInfectedMacs'};

%use averager to make matrices of averages of all data; only averages correct wells
%note that will mess up if missing all data points for a particular well;
%it should catch that error though by checking how many wells it should find
wells = averager(data,numcol);
save(fullfile(data_saving,[data_filename '_wellData']),'wells');

%iterate through averaged data, calculating polished and bscores and saving matrices, lists, and
heatmaps
for s=1:length(statistics)
    raw = getfield(wells,statistics{s});
    %compute zprime for this plate; save control means & zprime to text file
    DMSO = [raw(1,1) raw(3,1) raw(5,1) raw(7,1)];
    RIF = [raw(2,1) raw(4,1) raw(6,1) raw(8,1)];
    avgDMSO = mean(DMSO);
```

```
    stdDMSO = std(DMSO);
    avgRIF = mean(RIF);
    stdRIF = std(RIF);
    zprime = (1-((3*(stdDMSO+stdRIF))/(abs(avgDMSO-avgRIF))));
    plate = [avgDMSO stdDMSO avgRIF stdRIF zprime];
    dlmwrite(fullfile(data_saving,[data_filename '_plateControls_' statistics{s} '.txt']),plate);
    %save text file of raw data in 8x12 and in list
    dlmwrite(fullfile(data_saving,[data_filename '_wellData8x12_' statistics{s} '.txt']),raw);
    save_heatmap(getfield(wells,statistics{s}), statistics{s},'wellData',data_filename,heatmap_saving);
    raw_list = raw';
    raw_list = raw_list(:);
    dlmwrite(fullfile(data_saving,[data_filename '_wellDataList_' statistics{s} '.txt']),raw_list);
    %calculate % of DMSO and save as 8x12 and list
    norm = raw / avgDMSO * 100;
    dlmwrite(fullfile(data_saving,[data_filename '_PercentDMSO-8x12_' statistics{s} '.txt']),norm);
    save_heatmap(norm,statistics{s},'PercentDMSO',data_filename,heatmap_saving);
    norm_list = norm';
    norm_list = norm_list(:);
    dlmwrite(fullfile(data_saving,[data_filename '_PercentDMSO-List_' statistics{s}
'.txt']),norm_list);
    %polish medians for compounds, save residuals as 8x12 and list
    wells_cpd = raw(:,2:11);
    [ge, re, ce, resid] = median_polish(wells_cpd);
    dlmwrite(fullfile(data_saving,[data_filename '_residuals8x12_' statistics{s} '.txt']),resid);
    save_heatmap(resid, statistics{s},'residuals',data_filename,heatmap_saving);
    resid_list = resid';
    resid_list = resid_list(:);
    dlmwrite(fullfile(data_saving,[data_filename '_residualsList_' statistics{s} '.txt']),resid_list);
    %calculate bscores, save as 8x12 and list
    b = bscore(resid);
    dlmwrite(fullfile(data_saving,[data_filename '_bscore8x12_' statistics{s} '.txt']),b);
    save_heatmap(b,statistics{s},'bscore',data_filename,heatmap_saving);
    blist = b';
    blist = blist(:);
    dlmwrite(fullfile(data_saving,[data_filename '_bscoreList_' statistics{s} '.txt']),blist);
end

%calculate and then display time
timeEnd = clock;
time = etime(timeEnd,timeStart);
sec = mod(time,60);
minhr = (time-sec)/60;
min = mod(minhr,60);
hr = (minhr-min)/60;

msgbox({['Runtime = ' int2str(hr) 'hrs, ' int2str(min) 'min, ' int2str(sec) 'sec.']...
    []...
    [int2str(numberImages) ' images have been processed for plate ' data_filename]...
    ['GFP Background: ' num2str(bkgdGFP) '; GFP+ Threshold: ' num2str(thresh)]});
beep;
```

OlympusIX81 Reader

```
%Read files from folder given array of images and the iterator number


function [blue, green, red, short_name] = readBGR(imagelist,iter)

%read images from file
blue = imread([imagelist(3*iter-2).name]);
green = imread([imagelist(3*iter-1).name]);
red = imread([imagelist(3*iter).name]);

%make short names
blue_name = imagelist(3*iter-2).name;
blue_equals = find(blue_name == '=');
blue_trim = blue_equals -1;
blue_short = blue_name(1:blue_trim);

green_name = imagelist(3*iter-1).name;
green_equals = find(green_name == '=');
green_trim = green_equals -1;
green_short = green_name(1:green_trim);

red_name = imagelist(3*iter).name;
red_equals = find(red_name == '=');
red_trim = red_equals -1;
red_short = red_name(1:red_trim);

%check that short names match so know are using same image
if (red_short ~= green_short)
    error('You are trying to combine images that do not match!');
end
if (green_short ~= blue_short)
    error('You are trying to combine images that do not match!');
end
if (red_short ~= blue_short)
    error('You are trying to combine images that do not match!');
end

%set name for image group
short_name = red_short;
end
```

OlympusIX81 Segmenter

```
% This is a segmenter for cells
function mask = segmentCells(red,blue)
    red = imadjust(red,stretchlim(red,0.01));
    cells = im2bw(red,graythresh(red));

    blue = imadjust(blue,stretchlim(blue,0.01));
    nuclei = im2bw(blue,graythresh(blue));

    cells = cells | nuclei;
    cells = imdilate(cells,strel('disk',5,0));

    nuclei = imerode(nuclei,strel('disk',3,0));

    imageC = imcomplement(red/2 + blue/2);
    %imageC = imfilter(imageC,fspecial('gaussian',5,3));
    imageC = imimposemin(imageC,~cells | nuclei);
    L = watershed(imageC);
    mask = bwareaopen(L>0,100);

    % i need a way to go through the cells that are segmented
    % and remove those that don't have a nucleus.
    allcells = bwconncomp(mask);
    for i=1:allcells.NumObjects
        pxs = allcells.PixelIdxList{i};
        if ~any(nuclei(pxs))
            mask(pxs) = false;
        end
    end
end
```

OlympusIX81 Averager

```
%This function averages appropriate images from the same well, based on
%having the core of the images' names match. It saves those averages to a
%new struct in a 96-well format, although it does take in the number of
%columns to help it adapt to having 11 or 12 columns, for example.

function [wells] = averager(data,numcol)

numberImages = max(size(data));

%for purposes of iterating properly, the input struct has one more element added
data(end+1).ImageName = 'Schloop_000';

wells.AvgGFPPosPixels = [];
wells.AvgFractionalGFPArea = [];
wells.AvgIntensityGFPPos = [];
wells.AvgIntensityGFPPosBKGD = [];
wells.AvgAreaIntensityGFPPos = [];
wells.AvgAreaIntensityGFPPosBKGD = [];
wells.AvgIntensityTotal = [];
wells.AvgIntensityTotalBKGD = [];
wells.AvgAreaIntensityTotal = [];
wells.AvgAreaIntensityTotalBKGD = [];
wells.AvgInfectedGFPPosPixels = [];
wells.AvgInfectedFractionalGFPArea = [];
wells.AvgInfectedIntensityGFPPos = [];
wells.AvgInfectedIntensityGFPPosBKGD = [];
wells.AvgInfectedAreaIntensityGFPPos = [];
wells.AvgInfectedAreaIntensityGFPPosBKGD = [];
wells.AvgInfectedIntensityTotal = [];
wells.AvgInfectedIntensityTotalBKGD = [];
wells.AvgInfectedAreaIntensityTotal = [];
wells.AvgInfectedAreaIntensityTotalBKGD = [];
wells.PercentInfectedMacs = [];

statistics = {'AvgGFPPosPixels',...
        'AvgFractionalGFPArea',...
        'AvgIntensityGFPPos',...
        'AvgAreaIntensityGFPPos',...
        'AvgIntensityTotal',...
        'AvgAreaIntensityTotal',...
        'AvgIntensityGFPPosBKGD',...
        'AvgAreaIntensityGFPPosBKGD',...
        'AvgIntensityTotalBKGD',...
        'AvgAreaIntensityTotalBKGD',...
        'AvgInfectedGFPPosPixels'...
        'AvgInfectedFractionalGFPArea',...
        'AvgInfectedIntensityGFPPos',...
        'AvgInfectedAreaIntensityGFPPos',...
        'AvgInfectedIntensityTotal',...
        'AvgInfectedAreaIntensityTotal',...
        'AvgInfectedIntensityGFPPosBKGD',...
        'AvgInfectedAreaIntensityGFPPosBKGD',...
        'AvgInfectedIntensityTotalBKGD',...
        'AvgInfectedAreaIntensityTotalBKGD',...
        'PercentInfectedMacs'};

j=0;
namearray = {};
while j <= (numberImages)
    j=j+1;

    %append newest name to namearray
    namearray = [namearray {data(j).ImageName(1:end-4)} ];

    %if there is only one image, or if the image names match, skip
    %everything below and start at beginning of loop
    if length(namearray)==1 || strcmpi(namearray{end},namearray{end-1})
        continue
    end

    %exclude most recent image
    numImagesThisWell = length(namearray)-1;

    %for all the statistics...
    for s=1:length(statistics)
```

```
        count=0;

        %go through matching images...
        for i=1:numImagesThisWell
            %add up the matching images for each stat
            count = count + getfield(data(j-i),statistics{s});
        end
        %average and store in position in statistics in struct
        value = count / numImagesThisWell;
        wells.(statistics{s}) = [wells.(statistics{s}) value];
    end
    %only keep the last entry in the namearray
    namearray = namearray(end);
end

% now go through all of the final matrices and reshape them to be 96-well format
for s=1:length(statistics)
    wells.(statistics{s}) = reshape(wells.(statistics{s}),numcol,[])';
end

end
```

ArrayScan Montager

```
%Script to Produce Montages for Visual Analysis

%Abigail Reens, abigail.reens@colorado.edu

%This script takes in a folder of blue, green, and red images that are
%named Name=Color, in alphabetical order such that blue (DAPI_, green (FITC),
%and red (Texas) are read in that order. It then produces a RGB image in
%16bit display, and combines that with the individual channels to produce
%a montage. The RGB and the montage are saved to appropriate folders as
%tiffs so they can be altered in imagej for presentation.

%select folder and change to that folder
folder_path = uigetdir('.', 'Select Folder to Process');
cd(folder_path);

%make struct of .tiff files in folder
imagelist = dir('*.DIB');

%check to make sure right number of images in folder
if mod(max(size((imagelist))),4) ~= 0
    error('You do not have the right number of images to proceed!')
end

%select folders to save RGB and Montages
saving_path = uigetdir('.','Select Folder To Save Images');
cd(saving_path);
mkdir('RGB');
rgb_save = fullfile(saving_path,'RGB');
mkdir('Montages');
montage_save = fullfile(saving_path,'Montages');

cd(folder_path);
timeStart = clock;

%make a loop counter so can count how many images processed
montage_counter = 0;

%set pixel width of borders (can make a gui to ask in the future...)
border_pixels = 5;

%set dimensions of montage borders
image = readcdib([imagelist(1).name]);
[height, width] = size(image);
%border_vert = 512 * ones(height,border_pixels,3);
%border_horz = 512 * ones(border_pixels,(2*width+border_pixels),3);
border_vert = 65535 * ones(height,border_pixels,3);
border_horz = 65535 * ones(border_pixels,(2*width+border_pixels),3);

numberImages = max(size(imagelist))/4;
%iterate through images
for i=1:numberImages

    %read images
    %[blue12, green12, red12, name] = readBGR(imagelist,i);
    [red12, green12, blue12, name] = readRGB_ArrayScan(imagelist,i);

    disp(name);
    %%maybe set the intensity settings??

    %adjust 12bit images to 16bit images so that they actually display
    blue = 16*blue12;
    green = 16*green12;
    red = 16*red12;

    %combine colors into rgb images
    rgb(:,:,1) = red;
    rgb(:,:,2) = green;
    rgb(:,:,3) = blue;

    %save rgb as .tif into rgb folder?, with approp intensity settings...
    imwrite(rgb, fullfile(rgb_save,[name '_RGB.tif']));

    %make b&w images into color but still look black and white
    red_montage = repmat(red,[1,1,3]);
    green_montage = repmat(green,[1,1,3]);
```

```
    blue_montage = repmat(blue,[1,1,3]);

    %combine individuals, rgb into montage
    montage = [blue_montage  border_vert red_montage  ; ...
                             border_horz              ; ...
               green_montage border_vert     rgb      ];

    %save montage as .tif into montage folder
    imwrite(montage, fullfile(montage_save, [name '_Montage.tif']));

    %increment montage counter
    montage_counter = montage_counter + 1;
end

timeEnd = clock;
time = etime(timeEnd,timeStart);
sec = mod(time,60);
minhr = (time-sec)/60;
min = mod(minhr,60);
hr = (minhr-min)/60;

beep;
beep;

%show message with number of montages made
msgbox({['Runtime = ' int2str(hr) 'hrs, ' int2str(min) 'min, ' int2str(sec) 'sec.']...
    []...
    [int2str(montage_counter) ' montages have been saved to ' montage_save]});
```

ArrayScan Analyzer

```
 %Script for analyzing bacteria within cells, using images produced from
   %an ArrayScan and exported as dib files; this script exports B-scores
   %suitable for screening normalization

   %Abigail Reens; abigail.reens@colorado.edu

    %This script processes a folder of red, green, and blue images to determine
    %bacterial load within macrophages. It then applies a two-way median
    %polish to the data to remove row / column effects, and transforms data
    %into B-scores. A separate script is used for
    %non-screening purposes, which lacks B-score normalization.

%Now we will briefly describe the scheme of the script.

    %User input.
        %the user is asked to select folders for processing and saving data

        %the user is also asked to enter a pixel value between 0-4095.
        %this is the threshold above which a pixel is GFP positive. This
        %number must be determined empirically using uninfected, positive,
        %and negative controls, such that there are very few GFP+ pixels
        %in uninfected controls.

        %the user also enters how many images were taken per well and how
        %%many columns were imaged. these numbers facilitate the
        %correct ordering of images for output

    %Reading, naming, segmenting, saving images
        %images are read in order red green blue, according to how they are
        %saved in the folder. short names are extracted and compared to
        %ensure that they match.

        %images are segmented using a watershed algorithm to identify macrophages

        %segmented images are combined with raw data to produce overlays
        %for reference

    %Extracting statistics

        %using the segmented cell boundaries, various statistics are
        %quantified about the area / intensity of GFP within the
        %macrophages.


    %Exporting image data and histograms

        %the struct of all data is saved as a .mat for future manipulation
        %in matlab

        %per-image data for every statistic calculated is exported into a
        %.txt file. this file can be easily imported into prism for
        %graphical analysis.

    %Averaging image data to get well data
        %a function iterates through the data and averages images whose
        %names match to get the average data for that well. this data is
        %saved as a .mat for future manipulation in matlab

    %Calculating residuals and B-scores
        %well averaged data is processed using the B-score method (see
        %functions for citations). this method uses a two-way median polish
        %to remove row and column effects, and produces residuals, which
        %essentially describe the true value in a particular well. these
        %residuals enable the calculation of the bscore, which describes
        %the significance of a particular well's difference. note that the
        %median polish does not work when there are <2 rows or columns

    %Exporting well data and heatmaps
        %well data in the format of raw, residuals, or b-scores is saved as
        %.txt files in a 96-well format. these same data are also processed
        %into heatmaps and saved as .jpg

%% Block for user input
%user input and initializing of stuffs
    %ask for directories to process and to save
```

```
    folder_path = uigetdir('.','Select Folder To Process');
    cd(folder_path);
    saving_path = uigetdir('.','Select Folder To Save Data');

    %initialize folders to save data
    cd(saving_path);
    mkdir('Masks');
    mask_saving = fullfile(saving_path,'Masks');
    mkdir('Data');
    data_saving = fullfile(saving_path,'Data');
    mkdir('Heatmaps');
    heatmap_saving = fullfile(saving_path,'Heatmaps');

    %ask for name for saving things
    data_filename = inputdlg({'Enter Filename for Saving Numerical Data'},'Summary Data
Filename',1,{'Filename'});
    data_filename = data_filename{1};
    disp(data_filename);

    %change to folder for processing
    cd(folder_path);
    disp(folder_path);

    %ask user to input threshold for GFP+pixels and convert to number
    %ask user to input GFP background value
    %ask how many images per well, how many columns
    %in future, could potentially automate thresholding
    input = inputdlg({'GFP+ Pixel Threshold Value between 0-4095',...
        'Images Per Well','Number Columns Imaged on Plate'},...
        'Threshold and Image Format',1,{'900','2','22'});
    thresh = str2double(input(1));
    disp(thresh);
    imageDensity = str2double(input(2));
    numcol = str2double(input(3));

    timeStart = clock;
    disp(['start ' num2str(clock)]);

    %a macrophages must have at least 2 GFP+ pixels to be considered infected
    %this value must be in balance with the pixel threshold, such that there
    %are very few GFP+ pixels in uninfected images
    infectedThresh = 2;

    %make array of DIB files: red, green, blue, outlines
    imagelist = dir('*.DIB');

    %calculate number of images; arrayscan exports red, green, blue, and a
    %log file for each position
    numberImages = max(size(imagelist))/4;

    %instantiate allDataStruct
    data = struct;

%% Block for processing images
%iterate through each image, save masks, extract data
for j=1:numberImages
%read images and check that short names match
    [red, green, blue, name] = readRGB_ArrayScan(imagelist,j);
    disp(name);
%segment
    cellMask = segmentCells_ArrayScan(red,blue);
%combine masks with appropriate images
    save_masks(cellMask,red,green,blue,name,mask_saving);

%extract information and save to the data struct
%save image name to data struct
data(j).ImageName = name;

%ask matlab to turn each cell into an object of linked pixels
cellInfo = bwconncomp(cellMask);

%get the number of objects, and the object / pixel array
cellNumber = cellInfo.NumObjects;
cellArray = cellInfo.PixelIdxList;

%add number cells to data struct
data(j).NumberMacrophages = cellNumber;
```

```
k=0;

%iterate through the cells in the image (the pixel-linked objects)
for i=1:cellNumber

    %turn the pixels for each object into an array
    pixelArray = cellArray{i};

    %number of gfp+ pixels in that macrophage
    %ask whether pixels in green at each pixel in the object are >thresh
    %if so, turn them into 1; if not, turn them 0
    %and then add up all the 1s to get gfpcount
    gfpThreshCount = sum(green(pixelArray)>thresh);

    %calculate and store the fractional GFP+area in the macrophage
    %find the area of the the macrophage / object
    macNumPixels = length(pixelArray);
    fracGFPPixels = gfpThreshCount / macNumPixels;
    data(j).FractionalGFPArea(i) = fracGFPPixels;

    %sum of intensities of gfp+ pixels in that macrophage, also store
    gfpThreshIntensity = sum(green(green(pixelArray)>thresh));
    data(j).IntensityGFPPosPixels(i) = gfpThreshIntensity;

    %gfp+ pixel intensity divided by area of mac
    gfpThreshIntensityArea = gfpThreshIntensity / macNumPixels;
    data(j).AreaIntensityGFPPosPixels(i) = gfpThreshIntensityArea;

    %sum of total intensity of gfp in that macrophage
    gfpTotalIntensity = sum(green(pixelArray));
    data(j).IntensityTotal(i) = gfpTotalIntensity;

    %total gfp divided by mac area
    gfpTotalIntensityArea = gfpTotalIntensity / macNumPixels;
    data(j).AreaIntensityTotal(i) = gfpTotalIntensityArea;
    if gfpThreshCount > infectedThresh
        k=1+k;
    end
end

%calculate % infected macs
data(j).InfectedMacsCount = k;
numInfectedMacs = k;
percentInfected = 100*(numInfectedMacs / cellNumber);
data(j).PercentInfectedMacs = percentInfected;

%calculate and store fractional gfp area for this image
data(j).AvgFractionalGFPArea = mean(data(j).FractionalGFPArea);
data(j).AvgIntensityGFPPosPixels = mean(data(j).IntensityGFPPosPixels);
data(j).AvgAreaIntensityGFPPosPixels = mean(data(j).AreaIntensityGFPPosPixels);
data(j).AvgIntensityTotal = mean(data(j).IntensityTotal);
data(j).AvgAreaIntensityTotal = mean(data(j).AreaIntensityTotal);

end

%save data struct to file
save(fullfile(data_saving,[data_filename '_imageData']),'data');

%% Block for exporting image data
disp(['output ' num2str(clock)]);
%output the image data to a txt file
    statistics1 = {'ImageName','PercentInfectedMacs','AvgFractionalGFPArea',...
        'AvgIntensityGFPPosPixels','AvgAreaIntensityGFPPosPixels','AvgIntensityTotal','AvgAreaIntensity
Total'};
    style = {'%s ','%d ','%d ','%d ','%d ','%d ','%d '};
    filename = fullfile(data_saving,[data_filename '_ImageData.txt']);
    dataFile = fopen(fullfile(filename),'w');
    fprintf(dataFile,'%s',data_filename);
    %iterate through the fields and print names and fields
    for s = 1:length(statistics1)
        fprintf(dataFile,'\n%s ',statistics1{s});
        for m=1:numberImages
            fprintf(dataFile,style{s},getfield(data(m),statistics1{s}));
        end
    end
    fprintf(dataFile,'\n ');
    fprintf(dataFile,'\n%s ','NumberMacrophages');
    for m=1:numberImages
```

```
            fprintf(dataFile,'%d ',data(m).NumberMacrophages);
    end
    fprintf(dataFile,'\n ');
    fclose(dataFile);

%% Block for running just the averager part
disp(['averager ' num2str(clock)]);
statistics = {'AvgFractionalGFPArea','AvgIntensityGFPPosPixels','AvgAreaIntensityGFPPosPixels',...
    'AvgIntensityTotal','AvgAreaIntensityTotal','PercentInfectedMacs','NumberMacrophages'};

%use averager to make matrices of averages of all data; only averages correct wells
%note that will mess up if missing all data points for a particular well;
%it should catch that error though by checking how many wells it should find
wells = averagerArrayScanAddtlStat(data,numcol);
save(fullfile(data_saving,[data_filename '_wellData']),'wells');

%iterate through averaged data, calculating polished and bscores and saving matrices, lists, and
heatmaps
for s=1:length(statistics)
    raw = getfield(wells,statistics{s});

    %save text file of raw data in 384 and in list
    dlmwrite(fullfile(data_saving,[data_filename '_wellData384_' statistics{s} '.txt']),raw);
    save_heatmap_raw_ArrayScan(getfield(wells,statistics{s}),
statistics{s},'wellData',data_filename,heatmap_saving);
    raw_list = raw';
    raw_list = raw_list(:);
    dlmwrite(fullfile(data_saving,[data_filename '_wellDataList_' statistics{s}
'.txt']),raw_list);

    %polish medians for compounds, save residuals as 384 and list
    %this is set to have compounds in columns 3-22
    wells_cpd = raw(:,2:21);
    [ge, re, ce, resid] = median_polish(wells_cpd);
    dlmwrite(fullfile(data_saving,[data_filename '_residuals384_' statistics{s} '.txt']),resid);
    save_heatmap_ArrayScan(resid, statistics{s},'residuals',data_filename,heatmap_saving);
    resid_list = resid';
    resid_list = resid_list(:);
    dlmwrite(fullfile(data_saving,[data_filename '_residualsList_' statistics{s} '.txt']),resid_list);

    %calculate bscores, save as 384 and list
    b = bscore(resid);
    dlmwrite(fullfile(data_saving,[data_filename '_bscore384_' statistics{s} '.txt']),b);
    save_heatmap_ArrayScan(b,statistics{s},'bscore',data_filename,heatmap_saving);
    blist = b';
    blist = blist(:);
    dlmwrite(fullfile(data_saving,[data_filename '_bscoreList_' statistics{s} '.txt']),blist);

    %perform t tests to count rows & column effects and output to file
    [rowcount, colcount] = tPosEff_ArrayScan(wells_cpd);
    poseff = [rowcount, colcount];
    dlmwrite(fullfile(data_saving,[data_filename '_PositionalEffect_Rows,Cols' statistics{s}
'.txt']),poseff);

    %compute zprime for this plate; save control means & zprime to text file
    DMSO = [raw(2,1) raw(4,1) raw(6,1) raw(8,1) raw(10,1) raw(12,1) raw(14,1) raw(16,1)];
    RIF = [raw(1,1) raw(3,1) raw(5,1) raw(7,1) raw(9,1) raw(11,1) raw(13,1) raw(15,1)];
    UNINF = raw(:,end);
    avgDMSO = mean(DMSO);
    stdDMSO = std(DMSO);
    avgRIF = mean(RIF);
    stdRIF = std(RIF);
    avgUNINF = mean(UNINF);
    stdUNINF = std(UNINF);
    zprime = (1-((3*(stdDMSO+stdRIF))/(abs(avgDMSO-avgRIF))));
    zprime2 = (1-((3*(stdDMSO+stdUNINF))/(abs(avgDMSO-avgUNINF))));
    plate = [avgDMSO stdDMSO 0 ; avgRIF stdRIF zprime ; avgUNINF stdUNINF zprime2];
    dlmwrite(fullfile(data_saving,[data_filename '_Controls_avg,std,zprime_DMSO,rif,uninf'
statistics{s} '.txt']),plate);
end

%calculate % of mean number of macs for viability cutoffs
raw = getfield(wells,'NumberMacrophages');
meanNumMac = mean(mean(raw));
percentNumMac = raw/meanNumMac;
dlmwrite(fullfile(data_saving,[data_filename '_PercentNumberMacrophages384.txt']),percentNumMac);
save_heatmap_raw_ArrayScan(percentNumMac,'NumberMacrophages','percentNumMacrophages',data_filename,heat
map_saving);
```

```
percentNumMac_list = percentNumMac';
percentNumMac_list = percentNumMac_list(:);
dlmwrite(fullfile(data_saving,[data_filename
'_PercentNumberMacrophagesList.txt']),percentNumMac_list);

%calculate and then display time
timeEnd = clock;
time = etime(timeEnd,timeStart);
sec = mod(time,60);
minhr = (time-sec)/60;
min = mod(minhr,60);
hr = (minhr-min)/60;

msgbox({['Runtime = ' int2str(hr) 'hrs, ' int2str(min) 'min, ' int2str(sec) 'sec.']...
    []...
    [int2str(numberImages) ' images have been processed for plate ' data_filename]...
    ['GFP+ Threshold: ' num2str(thresh)]});
beep;
beep;
```

ArrayScan Pixeler

```
function pixels = readcdib(filename)
%READCDIB Reads DIB image files from Cellomics® devices.
%   READCDIB(FILENAME) reads bitmapped image data from the specified file.
%   Files from Cellomics® High Content Screening systems may omit the file
%   header information. This function ignores the missing header and
%   returns the pixels data.
%
%   Notes: This function uses TYPECAST to parse the files bytes, which
%   means that it requires R14SP3.  This was done because was it easier to
%   prototype, but you could rather easily rework it to use a bunch of
%   smaller FREAD commands.
%
%   Also it's worth mentioning that because these are 16-bit images that
%   don't span the full dynamic range of 16-bit data (0 to 65,355), the
%   images will appear very dark without changing the CLim.  You can do
%   either of these:
%
%     imshow(X, [])
%
%   or
%
%     imagesc(X)
%     colormap(gray)

%   Copyright 2009, The MathWorks, Inc.

% Get the data for the whole DIB.
fid = fopen(filename, 'r');
buffer = fread(fid, inf, 'uint8=>uint8');
fid = fclose(fid);

% Extract the header elements.
biSize = typecast(buffer(1:4), 'uint32');
biWidth = typecast(buffer(5:8), 'uint32');
biHeight = typecast(buffer(9:12), 'uint32');
biPlanes = typecast(buffer(13:14), 'uint16');
biBitCount = typecast(buffer(15:16), 'uint16');
biCompression = typecast(buffer(17:20), 'uint32');
biSizeImage = typecast(buffer(21:24), 'uint32');
biXPelsPerMeter = typecast(buffer(25:28), 'uint32');
biYPelsPerMeter = typecast(buffer(29:32), 'uint32');
biClrUsed = typecast(buffer(33:36), 'uint32');
biClrImportant = typecast(buffer(37:40), 'uint32');

% Convert the pixels.
startIdx = 1;
endIdx = biWidth * biHeight * double(biBitCount) / 8;
pixels = reshape(typecast(buffer(52 + (startIdx:endIdx)), 'uint16'), ...
                 [biWidth biHeight]);
```

ArrayScan Reader

```
%Read files from folder given array of images and the iterator number


function [red, green, blue, short_name] = readRGB_ArrayScan(imagelist,iter)

%read images from file
red = readcdib([imagelist(4*iter-3).name]);
green = readcdib([imagelist(4*iter-2).name]);
blue = readcdib([imagelist(4*iter-1).name]);

%make short names
red_name = imagelist(4*iter-3).name;
red_short = red_name(29:36);
green_name = imagelist(4*iter-2).name;
green_short = green_name(29:36);
blue_name = imagelist(4*iter-1).name;
blue_short = blue_name(29:36);

%check that short names match so know are using same image
if (red_short ~= green_short)
    error('You are trying to combine images that do not match!');
end
if (green_short ~= blue_short)
    error('You are trying to combine images that do not match!');
end
if (red_short ~= blue_short)
    error('You are trying to combine images that do not match!');
end

%set name for image group
short_name = red_short;
end
```

ArrayScan Segmenter

```
% This is a segmenter for cells
function mask = segmentCells_ArrayScan(red,blue)
    % imadjust will make the pixels fill the full 16 bit range
    red = imadjust(red,stretchlim(red,0.01));
    %%imtool(red)

    % get the cells with a simple automatic threshold
    cells = im2bw(red,graythresh(red));
    %%imtool(cells)
    blue = imadjust(blue,stretchlim(blue,0.01));
    %%imtool(blue)

    % I used to get the nuclei with a threshold:
    %   nuclei = im2bw(blue,graythresh(blue));
    % but they're so close to each other I'm going to watershed them
    % independently from the rest of the cells.
    %imtool(blue)
    bluefilt = imfilter(blue,fspecial('gaussian',5,3));
    %imtool(bluefilt)
    threshes = multithresh(blue,2);
    allnuclei = im2bw(blue,double(threshes(1))/2^16);
    %imtool(allnuclei)
    allnucleid = imdilate(allnuclei,strel('disk',1,0));
    %imtool(allnucleid)
    bluecomp = imcomplement(bluefilt);
    %imtool(bluecomp)
    bluecompz = bluecomp;
    bluecompz(~allnucleid) = 0;
    %imtool(bluecompz)
    labelnuc = watershed(bluecompz);
    %imtool(label2rgb(labelnuc))
    nuclei = labelnuc > 0;
    nucleiclean = nuclei;
    %imtool(nuclei)
    allnucdata = bwconncomp(nuclei);
    centroids = regionprops(allnucdata,'Centroid');
    centroidmask = false(size(nuclei));
    for i=1:length(centroids)
        pxs = allnucdata.PixelIdxList{i};
        if sum(sum(allnuclei(pxs)==0)) < length(pxs)/2
            loc = round(centroids(i).Centroid);
            centroidmask(loc(2),loc(1)) = true;
        else
            nucleiclean(pxs) = false;
        end
    end
    %imtool(nucleiclean)
    %imtool(centroidmask)
    centroidmaskd = imdilate(centroidmask,strel('disk',1,0));
    %imtool(centroidmaskd)
    %for i=1:allnucdata.

    cells = cells | allnuclei;
    %imtool(cells)
    %cells = imdilate(cells,strel('disk',2,0));
    cells = imdilate(cells,strel('disk',3,0));
    % Lets try actually

    %nuclei = imerode(nuclei,strel('disk',3,0));
    %nuclei = imerode(nuclei,strel('disk',2,0));

    imageC = imcomplement(red/2 + blue/2);
    %imtool(imageC)
    %imtool(~cells | centroidmaskd)
    %imageC = imfilter(imageC,fspecial('gaussian',5,3));
    imageC = imimposemin(imageC,~cells | centroidmaskd);
    %imtool(imageC)
    L = watershed(imageC);
    %imtool(label2rgb(L))
    %mask = bwareaopen(L>0,100);
    mask = L>0;
    %imtool(mask)

    % i need a way to go through the regions that are segmented
    % and remove those that aren't a cell.
```

```
    allcells = bwconncomp(mask);
    for i=1:allcells.NumObjects
        pxs = allcells.PixelIdxList{i};
        % If more than half the pixels in the region are outside cells,
        % then this region is not a cell, it is between cells.
        if sum(sum(cells(pxs))) < length(pxs)/2
            mask(pxs) = false;
        end
    end
    %imtool(mask)
    montage = zeros([size(mask),3],'uint8');
    montage(:,:,1) = uint8(red/256);
    montage(:,:,2) = 150*mask;
    montage(:,:,3) = 150*allnuclei;
    %imtool(montage)
end
```

ArrayScan Averager

```
%This function averages appropriate images from the same well, based on
%having the core of the images' names match. It saves those averages to a
%new struct in a 96-well format, although it does take in the number of
%columns to help it adapt to having 11 or 12 columns, for example.

function [wells] = averagerArrayScanAddtlStat(data,numcol)

numberImages = max(size(data));

%for purposes of iterating properly, the input struct has one more element added
data(end+1).ImageName = 'Schloop_000';

wells.AvgFractionalGFPArea = [];
wells.PercentInfectedMacs = [];
wells.NumberMacrophages = [];
wells.AvgIntensityGFPPosPixels = [];
wells.AvgAreaIntensityGFPPosPixels = [];
wells.AvgIntensityTotal = [];
wells.AvgAreaIntensityTotal = [];

statistics = {'AvgFractionalGFPArea','PercentInfectedMacs','NumberMacrophages',...
    'AvgIntensityGFPPosPixels','AvgAreaIntensityGFPPosPixels',...
    'AvgIntensityTotal','AvgAreaIntensityTotal'};



j=0;
namearray = {};
while j <= (numberImages)
    j=j+1;

    %append newest name to namearray
    namearray = [namearray {data(j).ImageName(1:end-4)} ];

    %if there is only one image, or if the image names match, skip
    %everything below and start at beginning of loop
    if length(namearray)==1 || strcmpi(namearray{end},namearray{end-1})
        continue
    end

    %exclude most recent image
    numImagesThisWell = length(namearray)-1;

    %for all the statistics...
    for s=1:length(statistics)
        count=0;

        %go through matching images...
        for i=1:numImagesThisWell
            %add up the matching images for each stat
            count = count + getfield(data(j-i),statistics{s});
        end
        %average and store in position in statistics in struct
        value = count / numImagesThisWell;
        wells.(statistics{s}) = [wells.(statistics{s}) value];
    end
    %only keep the last entry in the namearray
    namearray = namearray(end);
end

% now go through all of the final matrices and reshape them to be 96-well format
for s=1:length(statistics)
    wells.(statistics{s}) = reshape(wells.(statistics{s}),numcol,[])';
end

end
```

CV1000 Montager

```
%Script to Produce Montages for Visual Analysis using images from Olympus
%CV1000

%Abigail Reens, abigail.reens@colorado.edu

%This script takes in a folder of blue, green, and red images that are
%named Name=Color, in alphabetical order such that blue (DAPI_, green (FITC),
%and red (Texas) are read in that order. It then produces a RGB image in
%12bit display, and combines that with the individual channels to produce
%a montage. The RGB and the montage are saved to appropriate folders as
%tifs so they can be altered in imagej for presentation.

%select folder and change to that folder
disp('Select Folder to Process'); pause(0.5)
folder_path = uigetdir('.', 'Select Folder to Process');
disp(['Folder to Process',folder_path]);
cd(folder_path);

%check to make sure right number of images in folder
%if mod(max(size((imagelist))),3) ~= 0
    %error('You do not have the right number of images to proceed!')
%end

%select folders to save images
disp('Select Folder to Save Data'); pause(0.5)
data_save = uigetdir('.', 'Select Folder to Save RGB and Montages');
disp(['Folder to Save Data: ', data_save]);
cd(data_save);
mkdir('RGB');
rgb_save = fullfile(data_save,'RGB');
mkdir('Montages');
montage_save = fullfile(data_save,'Montages');

%make struct of folders in folder
cd(folder_path);
folderlist2 = dir('./Well*');
folderlist = folderlist2([folderlist2.isdir]);
numberFolders = max(size(folderlist));

cd(fullfile(folderlist(1).folder, folderlist(1).name));
imagelist = dir('*.tif');

timeStart = clock;

%make a loop counter so can count how many images processed
montage_counter = 0;

%set pixel width of borders (can make a gui to ask in the future...)
border_pixels = 5;

%set dimensions of montage borders
image = imread([imagelist(1).name]);
[height, width] = size(image);
border_vert = 65535 * ones(height,border_pixels,3);
border_horz = 65535 * ones(border_pixels,(2*width+border_pixels),3);

numberImages = max(size(imagelist))/3;
%iterate through images

for j=1:numberFolders

    cd(fullfile(folderlist(j).folder, folderlist(j).name));
    imagelist = dir('*.tif');

for i=1:numberImages

    %read images
    [blue, green, red, name] = readBGR(imagelist,i);
    disp(name);

    %combine colors into rgb images
    rgb(:,:,1) = red;
    rgb(:,:,2) = green;
    rgb(:,:,3) = blue;
```

```
    %save rgb as .tif into rgb folder?, with approp intensity settings...
    imwrite(rgb, fullfile(rgb_save,[name '_RGB.tif']));

    %make b&w images into color but still look black and white
    red_montage = repmat(red,[1,1,3]);
    green_montage = repmat(green,[1,1,3]);
    blue_montage = repmat(blue,[1,1,3]);

    %combine individuals, rgb into montage
    montage = [blue_montage  border_vert red_montage  ; ...
                             border_horz              ; ...
               green_montage border_vert     rgb      ];

    %save montage as .tif into montage folder
    imwrite(montage, fullfile(montage_save, [name '_Montage.tif']));

    %increment montage counter
    montage_counter = montage_counter + 1;
end
end

timeEnd = clock;
time = etime(timeEnd,timeStart);
sec = mod(time,60);
minhr = (time-sec)/60;
min = mod(minhr,60);
hr = (minhr-min)/60;

beep;
cd(folder_path);

%show message with number of montages made
msgbox({['Runtime = ' int2str(hr) 'hrs, ' int2str(min) 'min, ' int2str(sec) 'sec.']...
    []...
    [int2str(montage_counter) ' montages have been saved to ' montage_save]});
```

CV1000 Analyzer

```
%Script for analyzing bacteria within cells, using images from an Olympus
%CV1000

%Abigail Reens, abigail.reen@colorado.edu

    %This script processes a folder of red, green, and blue images to determine
    %bacterial load within macrophages..

%Now we will briefly describe the scheme of the script.

    %User input.
        %the user is asked to select folders for processing and saving data

        %the user is also asked to enter a pixel value between 0-4095.
        %this is the threshold above which a pixel is GFP positive. This
        %number must be determined empirically using uninfected, positive,
        %and negative controls, such that there are very few GFP+ pixels
        %in uninfected controls. Typically, the threshold is determined as
        %the minimum+200

        %The user is asked to input the background GFP value. This is to
        %remove background signal for correct calculation of percent
        %inhibition data.

        %the user also enters how many images were taken per well and how
        %%many columns were images. these numbers facilitates the
        %correct ordering of images for output

    %Reading, naming, segmenting, saving images
        %images are read in order blue green red, according to how they are
        %saved in the folder. short names are extracted and compared to
        %ensure that they match.

        %images are segmented using a watershed algorithm to identify macrophages

        %segmented images are combined with raw data to produce overlays
        %for reference

    %Extracting statistics

        %using the segmented cell boundaries, various statistics are
        %quantified about the area / intensity of GFP within the
        %macrophages.

    %Exporting image data and histograms

        %the struct of all data is saved as a .mat for future manipulation
        %in matlab

        %per-image data for every statistic calculated is exported into a
        %.txt file. this file can be easily imported into prism for
        %graphical analysis.

        %histograms are also produced for every image for every statistic
        %and saved as .jpg

    %Averaging image data to get well data
        %a function iterates through the data and averages images whose
        %names match to get the average data for that well. this data is
        %saved as a .mat for future manipulation in matlab


    %Exporting well data and heatmaps
        %well data in the format of raw is saved as
        %.txt files in a 96-well format. these same data are also processed
        %into heatmaps and saved as .jpg

%% Block for user input
%user input and initializing of stuffs
    %ask for directories to process and to save
    disp('Select Folder to Process'); pause(0.5)
    folder_path = uigetdir('.','Select Folder To Process');
    cd(folder_path);
    disp(['Folder To Process: ',folder_path]);
    disp(folder_path);
```

```
    disp('Select Folder to Save Images and Data'); pause(0.5)
    saving_path = uigetdir('.','Select Folder to Save Masks and Variants');
    disp(['Folder To Save Masks and Variants: ',saving_path]);

    %initialize folders to save data
    cd(saving_path);
    mkdir('Masks');
    mask_saving = fullfile(saving_path,'Masks');
    mkdir('Data');
    data_saving = fullfile(saving_path,'Data');
    mkdir('Heatmaps');
    heatmap_saving = fullfile(saving_path,'Heatmaps');
    mkdir('Histograms');
    hist_saving = fullfile(saving_path,'Histograms');

    %ask for name for saving things
    data_filename = inputdlg({'Enter Filename for Saving Numerical Data'},'Summary Data
Filename',1,{'Filename'});
    data_filename = data_filename{1};
    disp(['Data Filename: ', data_filename]);

    %change to folder for processing
    cd(folder_path);

    %ask user to input threshold for GFP+pixels and convert to number
    %ask user to input GFP background value
    %ask how many images per well, how many columns
    %in future, could potentially automate thresholding
    input = inputdlg({'GFP+ Pixel Threshold Value between 0-65535                                    .',...
        'Images Per Well','Number Columns Imaged on Plate',...
        'Compound Column Left for Screening with B-scores','Compound Column Right for Screening with B-
scores'},...
        'Threshold and Plate Format',1,{'6000','4','11','0','0'},'on');
    thresh = str2double(input(1));
    disp(['GFP Threshold = ', thresh]);
    imageDensity = str2double(input(2));
    numcol = str2double(input(3));
    screenleft = str2double(input(4));
    screenright = str2double(input(5));

    timeStart = clock;
    disp(['start ' num2str(clock)]);

    %a macrophages must have at least 2 GFP+ pixels to be considered infected
    %this value must be in balance with the pixel threshold, such that there
    %are very few GFP+ pixels in uninfected images
    infectedThresh = 2;

    % make a struct of the folders for each well, then go into the first
    % folder and make an imagelist to set the values of the iteration
    cd(folder_path);
    folderlist2 = dir('./Well*');
    folderlist = folderlist2([folderlist2.isdir]);
    numberFolders = max(size(folderlist));

    cd(fullfile(folderlist(1).folder, folderlist(1).name));
    imagelist = dir('*.tif');
    numberImages = max(size(imagelist))/3;

    %make an array of the tiffs in the folder in the correct order
%     imagelist_wrong = dir('*.tiff');
%     imagelist_4D = reshape(imagelist_wrong,3,imageDensity,numcol,[]);
%     imagelist_4D_right = imagelist_4D(:,:,[4:numcol 1:3],:);
%     imagelist = imagelist_4D_right(:);

    %instantiate allDataStruct and counter to put each image in the data
    %struct
    data = struct;
    j = 0;

%% Block for processing images
%iterate through each well folder, then image, save masks, extract data

for y=1:numberFolders

    cd(fullfile(folderlist(y).folder, folderlist(y).name));
    imagelist = dir('*.tif');
    numberImages = max(size(imagelist))/3;
```

```
for p=1:numberImages
%read images and check that short names match
    j=j+1;
    [blue, green, red, name] = readBGR(imagelist,p);
    disp(name);
%segment
    cellMask = segmentCells(red,blue);
%combine masks with appropriate images
    save_masks(cellMask,red,green,blue,name,mask_saving);

%extract information and save to the data struct
%save image name to data struct
data(j).ImageName = name;

%ask matlab to turn each cell into an object of linked pixels
cellInfo = bwconncomp(cellMask);

%get the number of objects, and the object / pixel array
cellNumber = cellInfo.NumObjects;
cellArray = cellInfo.PixelIdxList;

%add number cells to data struct
data(j).NumberMacrophages = cellNumber;

k=0;

%iterate through the cells in the image (the pixel-linked objects)
for i=1:cellNumber

    %turn the pixels for each object into an array
    pixelArray = cellArray{i};

    %number of gfp+ pixels in that macrophage
    %ask whether pixels in green at each pixel in the object are >thresh
    %if so, turn them into 1; if not, turn them 0
    %and then add up all the 1s to get gfpcount
    gfpThreshCount = sum(green(pixelArray)>thresh);
    %store the gfp positive pixel count in the data struct in the
    %appropriate position in the sub-array
    data(j).NumGFPPosPixels(i) = gfpThreshCount;

    %calculate and store the fractional GFP+area in the macrophage
    %find the area of the the macrophage / object
    macNumPixels = length(pixelArray);
    fracGFPPixels = gfpThreshCount / macNumPixels;
    data(j).FractionalGFPArea(i) = fracGFPPixels;

    %sum of intensities of gfp+ pixels in that macrophage, also store
    gfpThreshIntensity = sum(green(green(pixelArray)>thresh));
    data(j).IntensityGFPPosPixels(i) = gfpThreshIntensity;

    %gfp+ pixel intensity divided by area of mac
    gfpThreshIntensityArea = gfpThreshIntensity / macNumPixels;
    data(j).AreaIntensityGFPPosPixels(i) = gfpThreshIntensityArea;

    %sum of total intensity of gfp in that macrophage
    gfpTotalIntensity = sum(green(pixelArray));
    data(j).IntensityTotal(i) = gfpTotalIntensity;

    %total gfp divided by mac area
    gfpTotalIntensityArea = gfpTotalIntensity / macNumPixels;
    data(j).AreaIntensityTotal(i) = gfpTotalIntensityArea;

    %now, if mac is infected, add those data to a special category for
    %only infected cells
    if gfpThreshCount > infectedThresh
        k=1+k;
        data(j).InfectedNumGFPPosPixels(k) = gfpThreshCount;
        data(j).InfectedFractionalGFPArea(k) = fracGFPPixels;
        data(j).InfectedIntensityGFPPosPixels(k) = gfpThreshIntensity;
        data(j).InfectedAreaIntensityGFPPosPixels(k) = gfpThreshIntensityArea;
        data(j).InfectedIntensityTotal(k) = gfpTotalIntensity;
        data(j).InfectedAreaIntensityTotal(k) = gfpTotalIntensityArea;
    end
end

%calculate % infected macs
```

```
data(j).InfectedMacsCount = k;
numInfectedMacs = k;
percentInfected = 100*(numInfectedMacs / cellNumber);

%calculate and store means for all the things for this image
data(j).AvgGFPPosPixels = mean(data(j).NumGFPPosPixels);
data(j).AvgFractionalGFPArea = mean(data(j).FractionalGFPArea);
data(j).AvgIntensityGFPPos = mean(data(j).IntensityGFPPosPixels);
data(j).AvgAreaIntensityGFPPos = mean(data(j).AreaIntensityGFPPosPixels);
data(j).AvgIntensityTotal = mean(data(j).IntensityTotal);
data(j).AvgAreaIntensityTotal = mean(data(j).AreaIntensityTotal);
data(j).CellNumber = cellNumber;

%%output information for infected macs count, either the numbers or 0
if data(j).InfectedMacsCount ~= 0
    data(j).AvgInfectedGFPPosPixels = mean(data(j).InfectedNumGFPPosPixels);
    data(j).AvgInfectedFractionalGFPArea = mean(data(j).InfectedFractionalGFPArea);
    data(j).AvgInfectedIntensityGFPPos = mean(data(j).InfectedIntensityGFPPosPixels);
    data(j).AvgInfectedAreaIntensityGFPPos = mean(data(j).InfectedAreaIntensityGFPPosPixels);
    data(j).AvgInfectedIntensityTotal = mean(data(j).InfectedIntensityTotal);
    data(j).AvgInfectedAreaIntensityTotal = mean(data(j).InfectedAreaIntensityTotal);
    data(j).PercentInfectedMacs = percentInfected;
else
    data(j).AvgInfectedGFPPosPixels = 0;
    data(j).AvgInfectedFractionalGFPArea = 0;
    data(j).AvgInfectedIntensityGFPPos = 0;
    data(j).AvgInfectedAreaIntensityGFPPos = 0;
    data(j).AvgInfectedIntensityTotal = 0;
    data(j).AvgInfectedAreaIntensityTotal = 0;
    data(j).PercentInfectedMacs = 0;
end
end
end

%save data struct to file
save(fullfile(data_saving,[data_filename '_imageData']),'data');

%% Block for exporting image data
disp(['output ' num2str(clock)]);
%output the image data to a txt file
    statistics1 = {'ImageName',...
        'AvgGFPPosPixels',...
        'AvgFractionalGFPArea',...
        'AvgIntensityGFPPos',...
        'AvgAreaIntensityGFPPos',...
        'AvgIntensityTotal',...
        'AvgAreaIntensityTotal',...
        'AvgInfectedGFPPosPixels'...
        'AvgInfectedFractionalGFPArea',...
        'AvgInfectedIntensityGFPPos',...
        'AvgInfectedAreaIntensityGFPPos',...
        'AvgInfectedIntensityTotal',...
        'AvgInfectedAreaIntensityTotal',...
        'PercentInfectedMacs',...
        'CellNumber'};
    style = {'%s ','%d ','%d ','%d ','%d ','%d ','%d ','%d ','%d ','%d ','%d ','%d ','%d ','%d
','%d'};
    filename = fullfile(data_saving,[data_filename '_ImageData.txt']);
    dataFile = fopen(fullfile(filename),'w');
    fprintf(dataFile,'%s',data_filename);
    %iterate through the fields and print names and fields
    for s = 1:length(statistics1)
        fprintf(dataFile,'\n%s ',statistics1{s});
        for m=1:numberImages
            fprintf(dataFile,style{s},getfield(data(m),statistics1{s}));
        end
    end
    fprintf(dataFile,'\n ');
    fprintf(dataFile,'\n%s ','NumberMacrophages');
    for m=1:numberImages
          fprintf(dataFile,'%d ',data(m).NumberMacrophages);
    end
    fprintf(dataFile,'\n ');
    fclose(dataFile);


%% Block for exporting histograms
disp(['histograms ' num2str(clock)]);
```

```
%now output histograms of distributions to jpg
% statistics2 = {'NumGFPPosPixels','FractionalGFPArea','IntensityGFPPosPixels',...
%     'AreaIntensityGFPPosPixels','IntensityTotal','AreaIntensityTotal',...
%     'InfectedNumGFPPosPixels','InfectedFractionalGFPArea','InfectedIntensityGFPPosPixels','InfectedIn
tensityGFPPosPixelsBKGD',...
%     'InfectedAreaIntensityGFPPosPixels','InfectedIntensityTotal','InfectedAreaIntensityTotal'};
statistics2 = {'FractionalGFPArea','AreaIntensityTotal','PercentInfectedMacs'};
histogram = figure('visible','off');
for s = 1:length(statistics2)
    disp(['statistic ' statistics2{s}]);
    for m=1:numberImages
        hist(getfield(data(m),statistics2{s}));
        fig = findobj(gca,'Type','patch');
        set(fig,'FaceColor',[0 .7 0]);
        ylabel('Number of Cells');
        xlabel(statistics2{s});
        title(data(m).ImageName);
        saveas(histogram,fullfile(hist_saving,[statistics2{s} '_' data(m).ImageName]),'jpg');
    end
end


%% Block for running just the averager part
disp(['averager ' num2str(clock)]);

statistics = {'AvgGFPPosPixels',...
        'AvgFractionalGFPArea',...
        'AvgIntensityGFPPos',...
        'AvgAreaIntensityGFPPos',...
        'AvgIntensityTotal',...
        'AvgAreaIntensityTotal',...
        'AvgInfectedGFPPosPixels'...
        'AvgInfectedFractionalGFPArea',...
        'AvgInfectedIntensityGFPPos',...
        'AvgInfectedAreaIntensityGFPPos',...
        'AvgInfectedIntensityTotal',...
        'AvgInfectedAreaIntensityTotal',...
        'PercentInfectedMacs',...
        'CellNumber'};

%use averager to make matrices of averages of all data; only averages correct wells
%note that will mess up if missing all data points for a particular well;
%it should catch that error though by checking how many wells it should find
wells = averager(data,numcol);
save(fullfile(data_saving,[data_filename '_wellData']),'wells');

%iterate through averaged data, exporting raw, and saving matrices, lists, and heatmaps
for s=1:length(statistics)
    raw = getfield(wells,statistics{s});

    dlmwrite(fullfile(data_saving,[data_filename '_wellData8x12_' statistics{s} '.txt']),raw);
    save_heatmap(getfield(wells,statistics{s}), statistics{s},'wellData',data_filename,heatmap_saving);
    raw_list = raw';
    raw_list = raw_list(:);
    dlmwrite(fullfile(data_saving,[data_filename '_wellDataList_' statistics{s} '.txt']),raw_list);

    if screenleft ~= 0

    %polish medians for compounds, save residuals as 384 and list
    %this is set to have compounds in columns 3-22
    wells_cpd = raw(:,screenleft:screenright);
    [ge, re, ce, resid] = median_polish(wells_cpd);
    dlmwrite(fullfile(data_saving,[data_filename '_residuals384_' statistics{s} '.txt']),resid);
    save_heatmap(resid, statistics{s},'residuals',data_filename,heatmap_saving);
    resid_list = resid';
    resid_list = resid_list(:);
    dlmwrite(fullfile(data_saving,[data_filename '_residualsList_' statistics{s} '.txt']),resid_list);

    %calculate bscores, save as 384 and list
    b = bscore(resid);
    dlmwrite(fullfile(data_saving,[data_filename '_bscore96_' statistics{s} '.txt']),b);
    save_heatmap(b,statistics{s},'bscore',data_filename,heatmap_saving);
    blist = b';
    blist = blist(:);
    dlmwrite(fullfile(data_saving,[data_filename '_bscoreList_' statistics{s} '.txt']),blist);

    %perform t tests to count rows & column effects and output to file
    [rowcount, colcount] = tPosEff(wells_cpd);
```

```
    poseff = [rowcount, colcount];
    dlmwrite(fullfile(data_saving,[data_filename '_PositionalEffect_Rows,Cols' statistics{s}
'.txt']),poseff);

    else end

end

%calculate and then display time
timeEnd = clock;
time = etime(timeEnd,timeStart);
sec = mod(time,60);
minhr = (time-sec)/60;
min = mod(minhr,60);
hr = (minhr-min)/60;

num = numberImages * numberFolders;

msgbox({['Runtime = ' int2str(hr) 'hrs, ' int2str(min) 'min, ' int2str(sec) 'sec.']...
    []...
    [int2str(num) ' images have been processed for plate ' data_filename]...
    ['GFP+ Threshold: ' num2str(thresh)]});
cd(folder_path);
beep;
```

CV1000 Reader

```
%Read files from folder given array of images and the iterator number


function [blue, green, red, short_name] = readBGR(imagelist,iter)

%read images from file
blue = imread([imagelist(3*iter-2).name]);
green = imread([imagelist(3*iter-1).name]);
red = imread([imagelist(3*iter).name]);

%make short names
blue_name = imagelist(3*iter-2).name;
blue_equals = find(blue_name == 'C');
blue_trim = blue_equals -1;
blue_short = blue_name(1:blue_trim);

green_name = imagelist(3*iter-1).name;
green_equals = find(green_name == 'C');
green_trim = green_equals -1;
green_short = green_name(1:green_trim);

red_name = imagelist(3*iter).name;
red_equals = find(red_name == 'C');
red_trim = red_equals -1;
red_short = red_name(1:red_trim);

%check that short names match so know are using same image
if (red_short ~= green_short)
    error('You are trying to combine images that do not match!');
end
if (green_short ~= blue_short)
    error('You are trying to combine images that do not match!');
end
if (red_short ~= blue_short)
    error('You are trying to combine images that do not match!');
end

%set name for image group
short_name = red_short;
end
```

CV1000 Segmenter

```
% This is a segmenter for cells
function mask = segmentCells(red,blue)
    red = imadjust(red,stretchlim(red,0.01));
    cells = im2bw(red,graythresh(red));

    blue = imadjust(blue,stretchlim(blue,0.01));
    nuclei = im2bw(blue,graythresh(blue));

    cells = cells | nuclei;
    cells = imdilate(cells,strel('disk',5,0));

    nuclei = imerode(nuclei,strel('disk',3,0));

    imageC = imcomplement(red/2 + blue/2);
    %imageC = imfilter(imageC,fspecial('gaussian',5,3));
    imageC = imimposemin(imageC,~cells | nuclei);
    L = watershed(imageC);
    mask = bwareaopen(L>0,100);

    % i need a way to go through the cells that are segmented
    % and remove those that don't have a nucleus.
    allcells = bwconncomp(mask);
    for i=1:allcells.NumObjects
        pxs = allcells.PixelIdxList{i};
        if ~any(nuclei(pxs))
            mask(pxs) = false;
        end
    end
end
```

CV1000 Averager

```
%This function averages appropriate images from the same well, based on
%having the core of the images' names match. It saves those averages to a
%new struct in a 96-well format, although it does take in the number of
%columns to help it adapt to having 11 or 12 columns, for example.

function [wells] = averager(data,numcol)

numberImages = max(size(data));

%for purposes of iterating properly, the input struct has one more element added
data(end+1).ImageName = 'Schloop_000';

wells.AvgGFPPosPixels = [];
wells.AvgFractionalGFPArea = [];
wells.AvgIntensityGFPPos = [];
wells.AvgAreaIntensityGFPPos = [];
wells.AvgIntensityTotal = [];
wells.AvgAreaIntensityTotal = [];
wells.AvgInfectedGFPPosPixels = [];
wells.AvgInfectedFractionalGFPArea = [];
wells.AvgInfectedIntensityGFPPos = [];
wells.AvgInfectedAreaIntensityGFPPos = [];
wells.AvgInfectedIntensityTotal = [];
wells.AvgInfectedAreaIntensityTotal = [];
wells.PercentInfectedMacs = [];
wells.CellNumber = [];

statistics = {'AvgGFPPosPixels',...
        'AvgFractionalGFPArea',...
        'AvgIntensityGFPPos',...
        'AvgAreaIntensityGFPPos',...
        'AvgIntensityTotal',...
        'AvgAreaIntensityTotal',...
        'AvgInfectedGFPPosPixels'...
        'AvgInfectedFractionalGFPArea',...
        'AvgInfectedIntensityGFPPos',...
        'AvgInfectedAreaIntensityGFPPos',...
        'AvgInfectedIntensityTotal',...
        'AvgInfectedAreaIntensityTotal',...
        'PercentInfectedMacs',...
        'CellNumber'};

j=0;
namearray = {};
while j <= (numberImages)
    j=j+1;

    %append newest name to namearray
    namearray = [namearray {data(j).ImageName(1:end-12)} ];

    %if there is only one image, or if the image names match, skip
    %everything below and start at beginning of loop
    if length(namearray)==1 || strcmpi(namearray{end},namearray{end-1})
        continue
    end

    %exclude most recent image
    numImagesThisWell = length(namearray)-1;

    %for all the statistics...
    for s=1:length(statistics)
        count=0;

        %go through matching images...
        for i=1:numImagesThisWell
            %add up the matching images for each stat
            count = count + getfield(data(j-i),statistics{s});
        end
        %average and store in position in statistics in struct
        value = count / numImagesThisWell;
        wells.(statistics{s}) = [wells.(statistics{s}) value];
    end
    %only keep the last entry in the namearray
    namearray = namearray(end);
end
```

```
% now go through all of the final matrices and reshape them to be 96-well format
for s=1:length(statistics)
    wells.(statistics{s}) = reshape(wells.(statistics{s}),numcol,[])';
end

end
```

DataExport MaskSaver

```
%This function takes in various images and a location and makes combos of
%appropriate images for saving.

%inputs: mask, various colors, and location for saving
function save_masks(cellMask,red,green,blue,name,mask_saving)

%find edges of mask so overlay has only edges
edgeMask = edge(cellMask);

%turn all images into 16bit for display
edgeMask16 = uint16(65535*edgeMask);
green16 = green;
red16 = red;
blue16 = blue;

%make the images white at the edges
greenmasked = green16;
greenmasked(edgeMask) = 65535;
redmasked = red16;
redmasked(edgeMask) = 65535;
bluemasked = blue16;
bluemasked(edgeMask) = 65535;

%combine appropriately so we get the right images
greenMask(:,:,1) = edgeMask16;
greenMask(:,:,2) = greenmasked;
greenMask(:,:,3) = edgeMask16;
redblueMask(:,:,1) = redmasked;
redblueMask(:,:,2) = edgeMask16;
redblueMask(:,:,3) = bluemasked;

%save mask and overlays to folder
imwrite(cellMask, fullfile(mask_saving,[name '_Mask.tif']));
imwrite(redblueMask, fullfile(mask_saving,[name '_RedBlueMask.tif']));
imwrite(greenMask, fullfile(mask_saving,[name '_GreenMask.tif']));
end
```

DataExport RawHeatmapSaver

```
%This function takes in a matrix, various descriptors, and a saving
%location and creates a heatmap with appropriates axes titles and colors.

%inputs: x = matrix, stat=classifer1, type=classifer2,
%date_filename=classifier3, loc=saving location
function save_heatmap_raw_ArrayScan(x,stat,type,data_filename,loc)

fig = figure('visible','off');
colormap([[63:-1:0]' [0:63]' [0:31 31:-1:0]']/63);
imagesc(x);
colorbar;
title([data_filename stat type]);
axis equal;

yticks = [1 2 3 4 5 6 7 8 9 10 11 12 13 14 15 16];
set(gca,'YTick',yticks);
ylabels = ['A';'B';'C';'D';'E';'F';'G';'H';'I';'J';'K';'L';'M';'N';'O';'P'];
set(gca,'YTickLabel',ylabels);

xticks = [1 2 3 4 5 6 7 8 9 10 11 12 13 14 15 16 17 18 19 20 21 22];
set(gca,'XTick',xticks);
xlabels = [2 3 4 5 6 7 8 9 10 11 12 13 14 15 16 17 18 19 20 21 22 23];
set(gca,'XTickLabel',xlabels);

saveas(fig,fullfile(loc,[data_filename 'heatmap_' stat '_' type '.jpg']));
end
```

DataExport HeatmapSaver

```
%This function takes in a matrix, various descriptors, and a saving
%location and creates a heatmap with appropriates axes titles and colors.

%inputs: x = matrix, stat=classifer1, type=classifer2,
%date_filename=classifier3, loc=saving location
function save_heatmap(x,stat,type,data_filename,loc)

fig = figure('visible','off');
colormap([[63:-1:0]' [0:63]' [0:31 31:-1:0]']/63);
imagesc(x);
colorbar;
title([data_filename stat type]);
axis equal;

yticks = [1 2 3 4 5 6 7 8];
set(gca,'YTick',yticks);
ylabels = ['A';'B';'C';'D';'E';'F';'G';'H'];
set(gca,'YTickLabel',ylabels);

xticks = [1 2 3 4 5 6 7 8 9 10 11 12];
set(gca,'XTick',xticks);
xlabels = [1 2 3 4 5 6 7 8 9 10 11 12];
set(gca,'XTickLabel',xlabels);

saveas(fig,fullfile(loc,[data_filename 'heatmap_' stat '_' type '.jpg']));
end
```

ScreenAnalysis MedianPolisher

```
%Function for Tukey's two-way median polish

%This function is useful for accounting for row and column effects within
%physically organized data. This approach is based on Tukey's 2-way
%additive median polish, and decomposes a 2D matrix into the overall
%effect, a 1D matrix of row effects, a 1D matrix of column effects, and a
%2D matrix of residuals. These residuals represent the value of the
%measurement, ignoring row and column effects. Alternating rows and
%columns, the function takes of the median of each row (rm). It then takes the
%median of those medians (rmm), and subtracts it from the rm vector to
%determine the change in row effect (dre). The change is then added to the
%row effect (re). The rmm is also added to the grand effect (ge). Finally,
%the row medians are subtracted from the appropriate rows. Columns are then
%treated similarly.

%Relevant citations:

%Brideau C, Gunter B, Pikounis B, Liaw A (2003) Improved Statistical
%methods for hit selection in high-throughput screening. J Biomol Screen
%8:634.

%Dragiev P, Nadon R, Makarenkov V (2011) Systematic error etection in
%experimental high-throughput screening. BMC Bioinformatics 12:25.

%Malo N, Hanley JA, Cerquozzi S, Pelletier J, Nadon R (2006) Statistical
%practice in high-throughput screening data analysis. Nature Biotech 24:2.

function [ge, re, ce, x] = median_polish(x,maxiter)

Narg = nargin;
if (Narg < 2)
    maxiter = 100;
end

%set effects to zero
ge = 0;
re = zeros(size(x,1),1);
ce = zeros(1,size(x,2));

for i=1:maxiter

    %save the most recent x to compare to determine endpoint
    x_temp = x;

    %polish row medians
    rm = nanmedian(x,2);
    rmm = nanmedian(rm);
    dre = bsxfun(@minus,rm,rmm);
    re = re+dre;
    ge = ge+rmm;
    x = bsxfun(@minus,x,rm);

    %polish column medians
    cm = nanmedian(x,1);
    cmm = nanmedian(cm);
    dce = bsxfun(@minus,cm,cmm);
    ce = ce+dce;
    ge = ge+cmm;
    x = bsxfun(@minus,x,cm);

    %if residuals have not changed, end program
    if x_temp == x
        break;
    end

end
end
```

Screening Analysis Fitter

```
function [aa, bb] = fitAB(arrayOfVariances)

%%this function takes in an array of variances, calculated as the square of
%%the standard deviation of replicates, and outputs correction factors, a &
%%b, which can be used to correct the variances based on an inverse gamma
%%distribution. this overall enables refinement of the variances and
%%enhanced statistical power.

%fit to inverse gamma / f distribution and output a, b values
[f x] = ecdf(arrayOfVariances);
ft = fittype(@(a,b,x) fcdf(x*a*b,1,2*a));
out = fit(x,f,ft,'Lower',[0 0],'Startpoint',[1 1]);
aa = out.a;
bb = out.b;
```

Screening Analysis Bscorer

```
%Bscore calculator

%This function takes a matrix of residuals (typically produced by the
%median_polish function) and converts the data into B-scores, a robust
%metric for determining the true value of a measurement.

%The function first calculates the Gaussian adjusted median absolute
%deviation, which is median{|rij - median(rij)|}. Then, the bscore is
%calculated by dividing each residuals by the mad. And magic ensues!

%Relevant citations:

%Brideau C, Gunter B, Pikounis B, Liaw A (2003) Improved Statistical
%methods for hit selection in high-throughput screening. J Biomol Screen
%8:634.

%Dragiev P, Nadon R, Makarenkov V (2011) Systematic error etection in
%experimental high-throughput screening. BMC Bioinformatics 12:25.

%Malo N, Hanley JA, Cerquozzi S, Pelletier J, Nadon R (2006) Statistical
%practice in high-throughput screening data analysis. Nature Biotech 24:2.

function [bscore] = bscore(resid)

med = nanmedian(nanmedian(resid));
diff = abs(bsxfun(@minus,resid,med));
mad = nanmedian(nanmedian(diff));

bscore = resid / mad;

end
```

APPENDIX C. SAFIRE PILOT SCREEN OF 3,200 COMPOUNDS

PrioR to the full screen of 14,400 compounds from the Maybridge HitFinder™ v11 library, I performed a pilot screen of the first 3,200 compounds in a 96-well format. The assay was performed essentially as described in **Chapter 2**, except that compounds were pinned into a transfer plate containing media, which was then transferred into infected assay plates after removing the infection media. In this screen, I used both the percent infected statistic, which counts infected macrophages within an image based on number of GFP+ pixels, and the fractional GFP area statistic, which quantifies the number of GFP+ pixels within a macrophage divided by the total pixels in that macrophage and averages across all macrophages in the image, which yielded a Z'-factor of 0.66. I performed B-score normalization to remove positional effects and calculated *p*-values using a modified t-test assuming an inverse gamma distribution of variations, as described.

To call hits, I used a dual threshold of B-score at least 2 standard deviations away from the mean, and a *p*-value of less than 0.01. These cutoffs were more stringent than those that we used in the full screen due to less variability in 96-well plates. I identified 48 positives using the Percent Infected statistic, and 55 positives using the Area statistic (**Figure C-1**). Of these, 33 were identified by both statistics; 25 reduced bacterial load and 8 increase bacterial load. Forty-one additional compounds were called as hits by one of the statistics. I next triaged the 74 hits by examining the microscopy images to eliminate toxic or autofluorescent compounds and selected 26 consistent hits for further characerization.

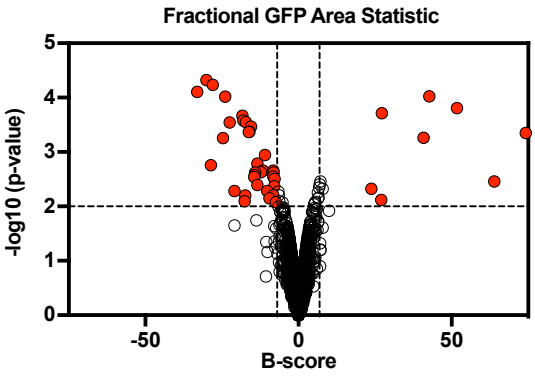

Figure C-1. Volcano plot showing assay results from pilot screen.

I determined IC50s for the 26 hits in the SAFIRE assay and by conventional CFU plating assays (**Figure C-2**). The IC50s ranged from 2-1000 μM, although there was generally good

correlation between the two assays (Pearson correlation coefficient = 0.47, *p*-value 0.0124). Finally, I identified the structures of the hits. I identified chloramphenicol and 4 additional chloramphenicol-family antibiotics, which served as internal controls. I also identified the FDA-approved tricyclic antidepressant clomipramine. The remainder of the hits were unknown structures.

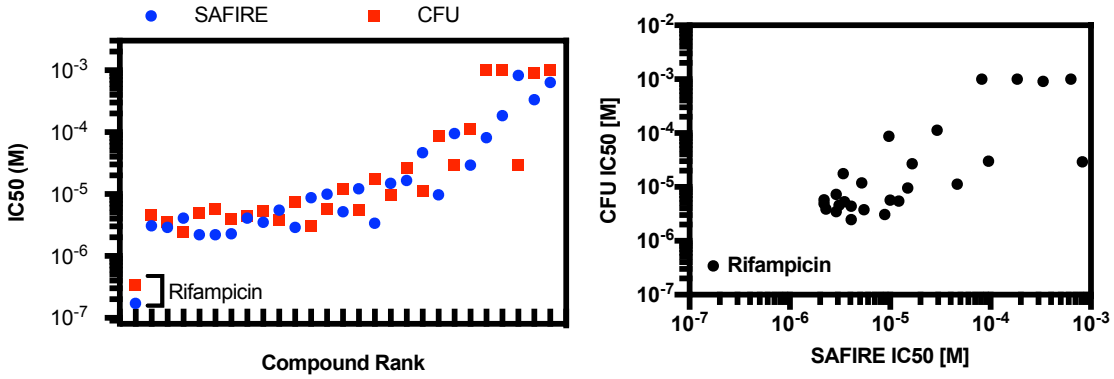

Figure C-2. IC50s for 26 compounds and rifampicin were determined against intracellular *Salmonella* using SAFIRE or CFU assays. IC50s were calculated using nonlinear curve fit, and correlation analysis was performed (Graphpad Prism).

APPENDIX D. SAFIRE SCREEN OF 562 COMPOUNDS FROM THE HERGENROTHER GROUP

In collaboration with the Hergenrother group at the University of Illinois, I screened a library of 562 natural-product derived molecules at a concentration of 10 μM in 96-well plates in duplicate (**Figure D-1**). I used a threshold of 2 standard deviations above the mean for both percent infected and fractional GFP area. This threshold identified 28 positives, all of which has *p*-values less than 0.05. I next visually examined the images and eliminated 8 positives based on toxicity or focus issues. Of the remaining 20, 13 exhibited moderate to high activity without observable toxicity. Two were known to have antibacterial activity: lovastatin, an anticholesterol, and lycorine, a toxin. The remaining molecules were derivatives of abietic acid and quinine. The Hergenrother group next searched the compounds we had screened for structurally related molecules to enable an impromptu structure-activity relationship analysis.

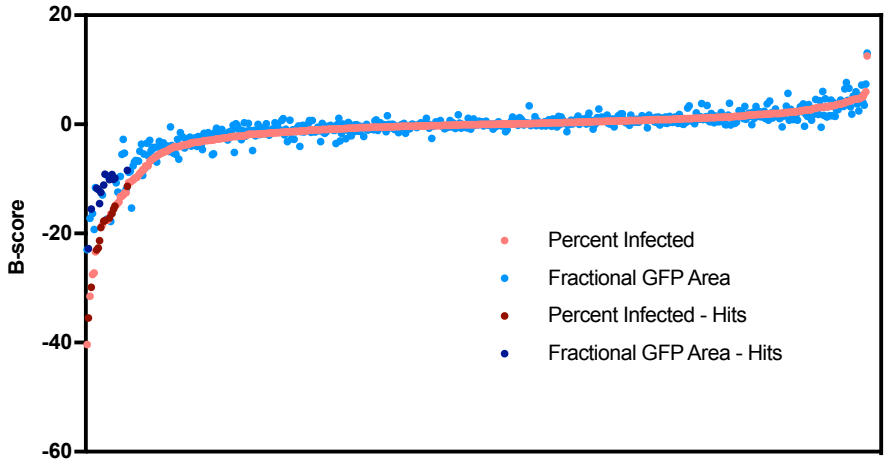

Figure D-1. B-score activity distribution by percent infected and fractional GFP area of 562 compounds from the Hergenrother group. The same compound is plotted for both statistics. Dark dots met the activity cutoff for that statistic.

I identified 4 derivatives of abietic acid as hits in the screen. One demonstrated excellent antibacterial activity and no toxicity. Two others exhibited excellent antibacterial activity and some toxicity. The fourth was moderately antibacterial and somewhat toxic. There were 8 structurally related compounds in the library; 3 exhibited slight antibacterial activity and all were nontoxic. The active compounds appeared to share an amine on the bottom ring, as replacing the amine with a carboxylic acid or large steric groups eliminated activity. We selected the 4 hit

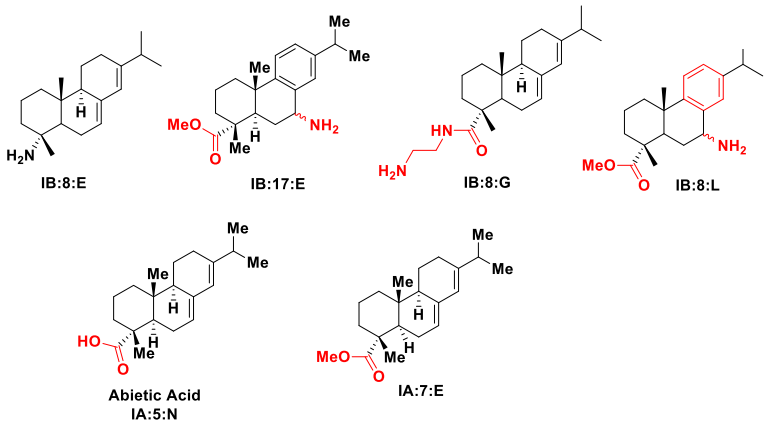

Figure D-2. Abietic acid derivatives selected for further study. Top: active compounds. Bottom: inactive compounds.

compounds and 2 representative inactive compounds to study further (**Figure D-2**).

The library contained a large selection of quinine-derived molecules. A subgroup containing a diphenyl ether with quinoline core had 2 excellent hits with a positively charged nitrogen / amino at the same position relative to the core at physiological pH. Inactive compounds had a different core or bulky groups. We selected the 2 hit compounds, 2 representative inactive compounds, and quinine to study further (**Figure D-3**). A second subgroup of 3 highly active quinines contained a fused ring with different side chains (**Figure D-4**). Finally, we selected an additional highly active nontoxic heterocyclic compound for study; 2 similar compounds with bulkier groups were inactive (**Figure D-5**). Future studies for all these compounds will involve validation in SAFIRE, broth activity assays, and cytological profiling to identify the mechanism of action.

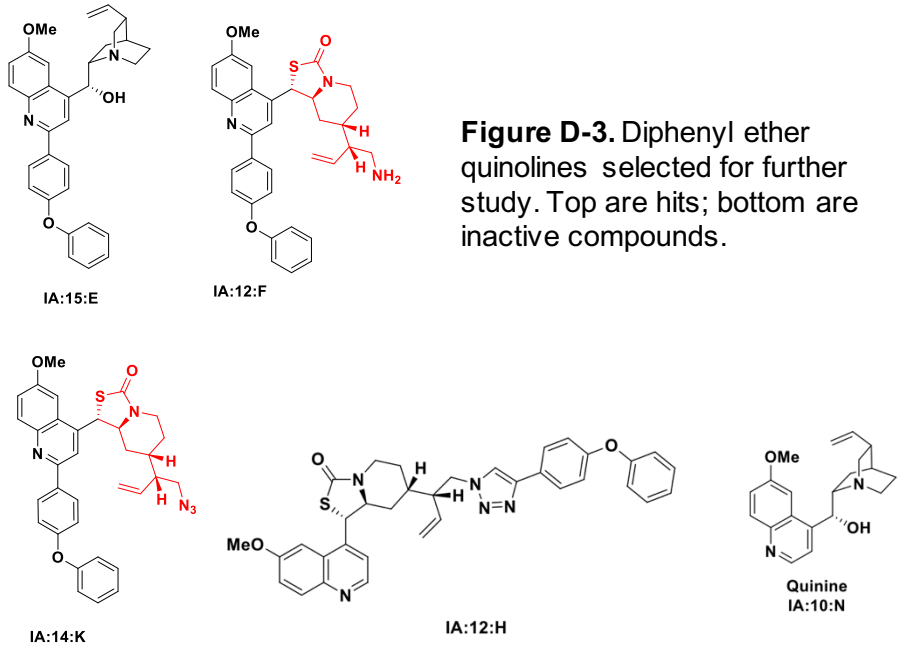

Figure D-3. Diphenyl ether quinolines selected for further study. Top are hits; bottom are inactive compounds.

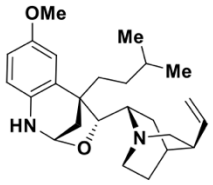

IA:11:F

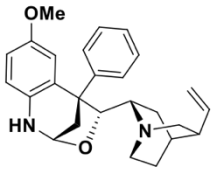

IA:11:N

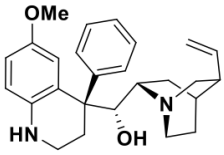

IA:11:I

Figure D-4. Fused ring quinine derivatives.

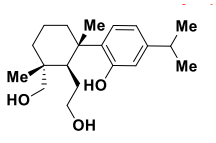

AA7
IA:5:M

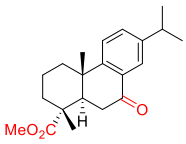

IA:16:F

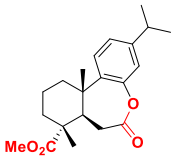

IA:16:H

Figure D-5. Heterocycle derivatives. Top compound is active; bottom are inactive.

APPENDIX E. FLUORESCENCE DILUTION STRAIN OPTIMIZATION

The published fluorescence dilution system for measuring *Salmonella* replication within macrophages employs the pDiGc plasmid constitutively expressing GFP and arabinose-inducible dsRed (Helaine et al., 2010). To adapt the system for use in my experiments, I first validated growth kinetics of wild-type bacteria harboring pDiGc. In rich media, I found a slight lag for the pDiGc strain with and without arabinose (**Figure E-1A**), suggesting the plasmid compromises growth. I next tested growth in the MgMES-based minimal medium that is optimized for dsRed induction (Helaine et al., 2010). I found that the medium significantly

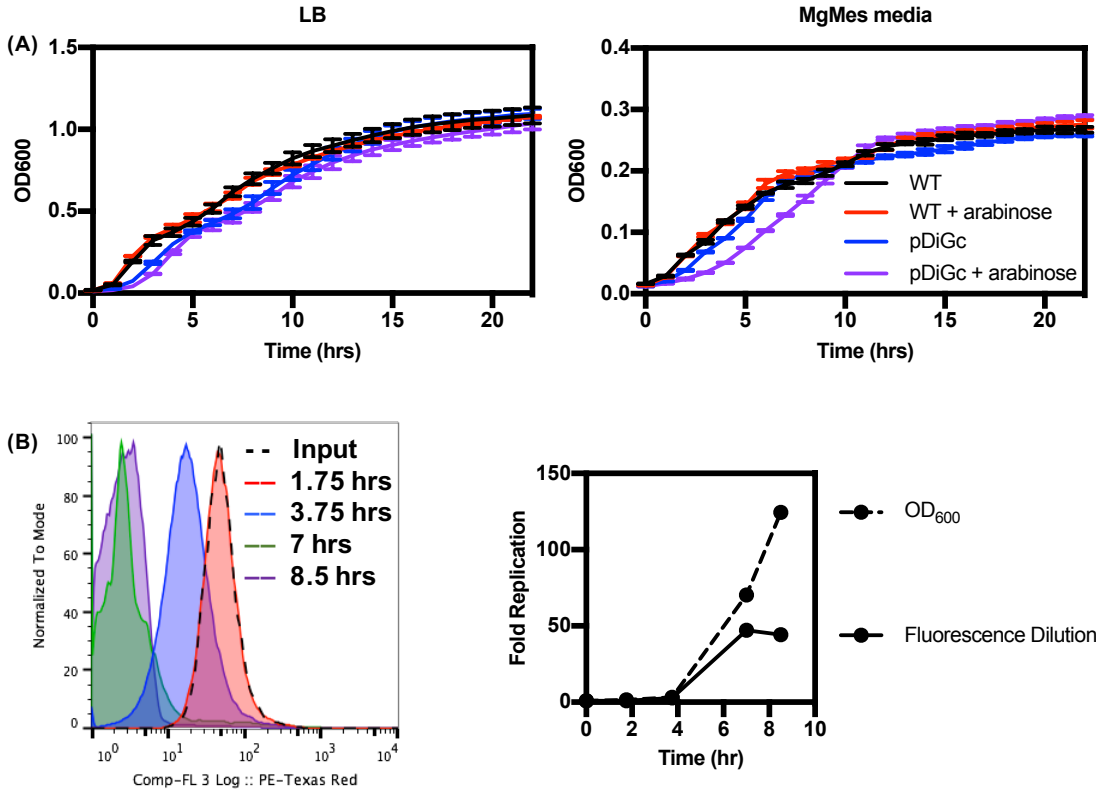

Figure E-1. Fluorescence dilution system enables measurement of replication. (A) The indicated strains were grown in LB (left) or MgMES inducing media with or without arabinose to induce dsRed expression (right). Data are mean + SD of one experiment conducted in triplicates. **(B)** Bacteria were grown in MgMES inducing media with arabinose and transferred to LB media without arabinose. At the indicated timepoints, dsRed fluorescence was analyzed using flow cytometry and optical density. Left: flow cytometry plots. Right: quantification of fold replication calculated by fluorescence dilution or OD_{600}. Data are from one experiment.

reduced growth for wild-type bacteria with and without the plasmid (**Figure E-1A**). Addition of arabinose to induce dsRed also conferred a growth lag on the pDiGc strain, though it reached a similar final OD_{600}.

I next induced dsRed production during overnight growth of pDiGc strain, and transferred bacteria into LB medium without arabinose to confirm dilution of dsRed fluorescence (**Figure E-1B**). Although I measured dsRed fluorescence with the wrong channel on the flow cytometry (PE-Texas instead of PE), I did observe dilution of dsRed over time, roughly corresponding to bacterial replication measured by OD_{600}.

I next infected RAW 264.7 macrophages with bacteria harboring pDiGc, and analyzed GFP and dsRed fluroescence using flow cytometry. pDiGc bacteria exhibited extremely bright fluorescence, and were easily distinguishable from uninfected macrophage lysates (**Figure E-2A**). However, I observed modest replication by fluorescence dilution (2-fold), in contrast to the higher ranges that I usually observe using CFU (10-fold, data not shown). Through other experiments, it became clear that the high GFP signal of the strain complicated compensation, and thus it was impossible to obtain accurate dsRed measurements (data not shown).

While optimizing the infection protocol, I also found that a low percentage of collected events from macrophage lysates were bacteria (2-3%). As a result, data was calculated based on less than 30,000 bacteria, which was the recommendation (Helaine et al., 2010). Thus, I hypothesized that the pDiGc strain could have poor infection of macrophages, either due to the plasmid or dsRed induction or both. To test this possibility, I added the same concentration (1 x 10^7 cfu/ml) of wild-type or pDiGc bacteria grown in LB or MgMEM-arabinose-inducing medium and measured the proportion of bacteria internalized at 2 h.p.i. and the growth from 2-18 h.p.i (**Figure E-2C**). I found that 10 times fewer wild-type bacteria were internalized when grown in MgMES-arabinose rather than LB, but that growth was essentially unchanged (black vs. red). I also found that 10 times fewer pDiGc bacteria were internalized relative to wild type when both were grown in LB medium (black vs. blue), though growth was again unchanged.

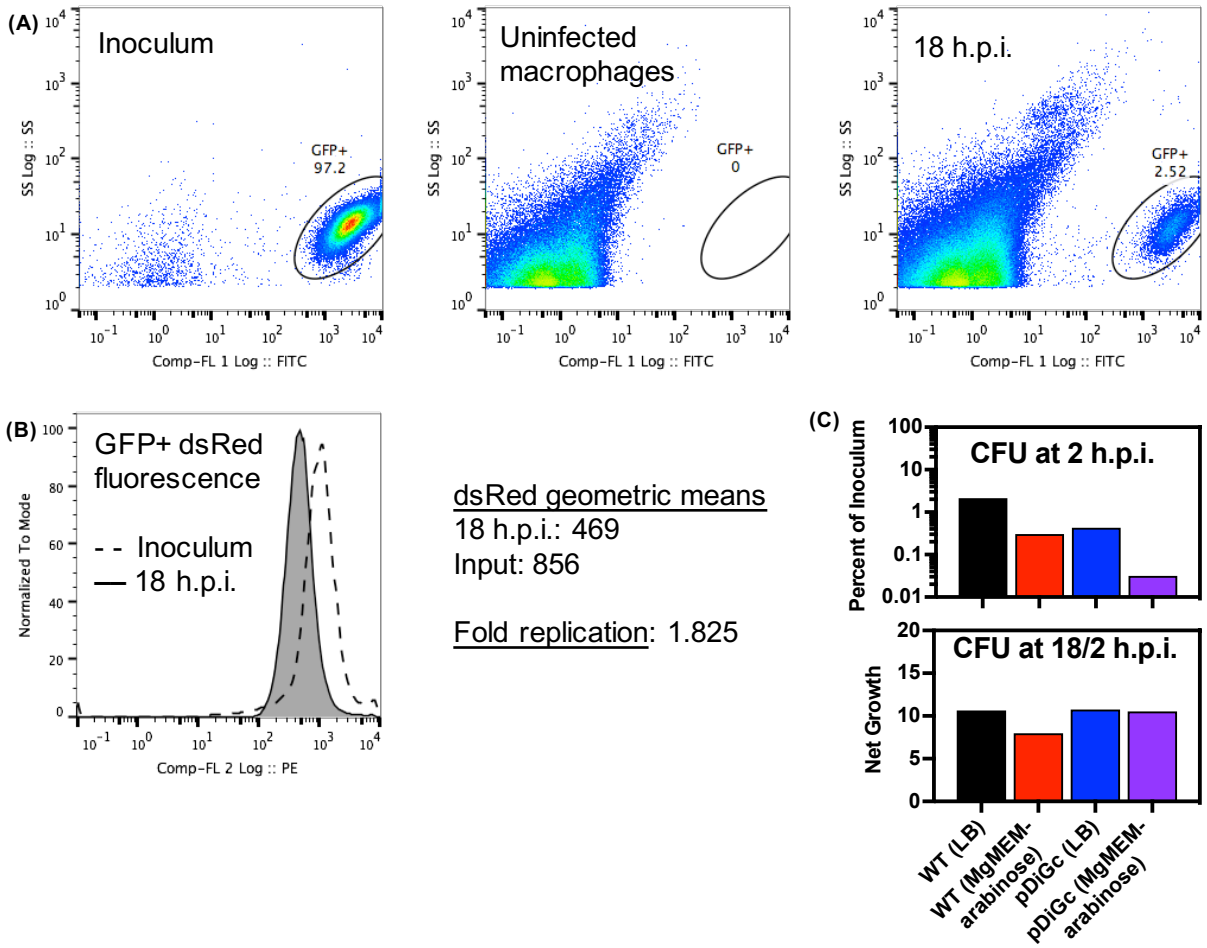

Figure E-2. pDiGc has extremely bright GFP fluorescence. RAW 264.7 macrophages were infected with wild type bacteria harboring pDiGc. **(A)** Flow cytometry plots of the indicated samples. **(B)** The geometric mean of dsRed fluorescence from the inoculum and 18 h.p.i. samples were used to calculated fold replication. **(C)** CFU data for RAW 264.7 macrophages infected with the indicated strains pregrown in the indicated media. Top: 2 h.p.i. data for intracellular bacteria were normalized to the number of bacteria added to the well. Bottom: 18 h.p.i. data were normalized to 2 h.p.i. data to calculate net growth. Data are from one experiment.

These effects were compounded for the pDiGc strain grown in inducing media, as 100 times fewer bacteria were taken up (black vs purple). The observed defects could be due to differences in bacterial invasion, macrophage uptake, or survival during early infection. Importantly, growth remained essentially unchanged between the four conditions.

Given that high expression of fluorescent proteins can compromise bacterial integrity and that our cytometer did not have a large enough range to ensure accurate compensation of GFP

from pDiGc as discussed above, I developed an alternate fluorescent dilution system using a different plasmid, pDiGi, which encodes arabinose-inducible dsRed and IPTG-inducible GFP. To identify a different constitutive GFP marker, I tested the fluroescence of two different chromosomal GFP markers. I found that a strain harboring *sifB*::GFP exhibited biphasic GFP expression, but that a strain harboring *rpsM*::GFP had consistent moderate GFP expression (**Figure E-3**).. In contrast, pDiGc bacteria were extremely bright, as expected. I constructed new strains for fluorescence dilution which harboring pDiGi and had the *rpsM*::GFP marker.

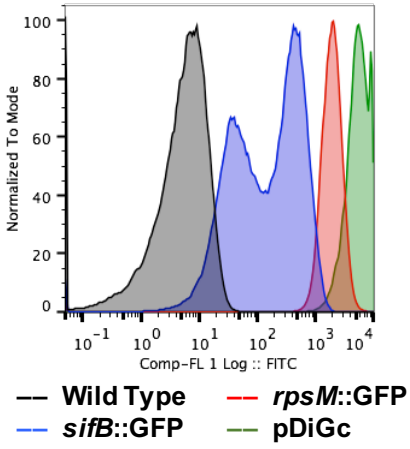

Figure E-3. Flow cytometry profiling of different GFP-expressing strains. The indicated strains were grown in LB and GFP fluroescence was measured using flow cytometry. Data are from one experiment.

I also found that the new strain was still distinguishable from macrophage lysates, despite the lower GFP expression (**Figure E-4A**). Using the GFP+ gated population, I found a bimodal distribution of dsRed fluorescence, indicating that many bacteria had replicated. Indeed, I calculated fold replication using the whole GFP+ gate to be approximately 10-fold, similar to data acquired by CFU (data not shown).

I next compared infection by the new FD (fluorescence dilution) strain and wild-type using CFU plating (**Figure E-4B**). As in the previous experiment, I found that wild-type bacteria had reduced uptake after growth in the inducing medium (black vs red). However, I found the new FD strain infected macrophages similarly to wild type, suggesting that this strain did not have toxic GFP expression (black vs blue). However, I found that culturing the FD strain in inducing medium prior to infection reduced uptake (black vs purple), as before. To address this problem, I infected with higher concentrations of bacteria, and found a dose-dependent effect of inoculum concentration with uptake at 2 h.p.i. I decided to use an infection concentration of 3 x 10^7 cfu/ml,

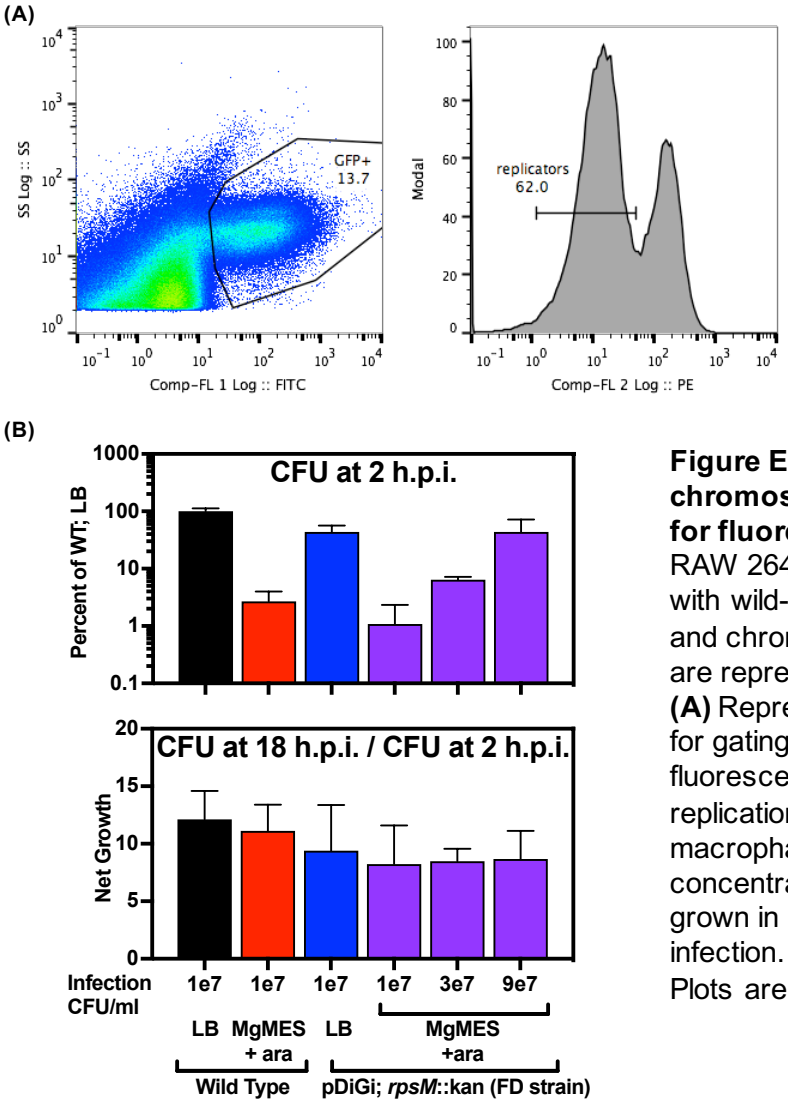

dsRed geometric means
18 h.p.i.: 18.9
Input: 177

Fold replication: 9.365

Figure E-4. pDiGi combined with chromosomal *rpsM*::GFP is suitable for fluorescence dilution experiments. RAW 264.7 macrophages were infected with wild-type bacteria harboring pDiGi and chromosomally encoded GFP. Data are representative of many experiments. **(A)** Representative flow cytometry plots for gating on GFP and dsRed fluorescence to determine fold replication. **(B)** CFU data for RAW 264.7 macrophages infected with the indicated concentration of the indicated strain grown in the indicated media prior to infection. Data are from one experiment. Plots are as in **Figure E-2C.**

which typically yielded high enough infection to acquire 30,000 bacteria by flow cytometry.

In later experiments, I needed to quantify the replication of one strain during co-infection with a second strain. To evaluate the best competitor, I co-infected the standard wild-type FD strain with wild-type bacteria harboring pDiGc or pDiGi with or without arabinose induction (competitors lacked *rpsM*::GFP). I found that the FD strain replicated similarly with any of the competitors as it did as a single infection (**Figure E-5A**). I also found no large differences by CFU between 2 and 18 h.p.i. (**Figure E-5B**), though there was a trend toward the FD strain outcompeting pDiGc + arabinose (dark red bar). Similar results were observed whether I

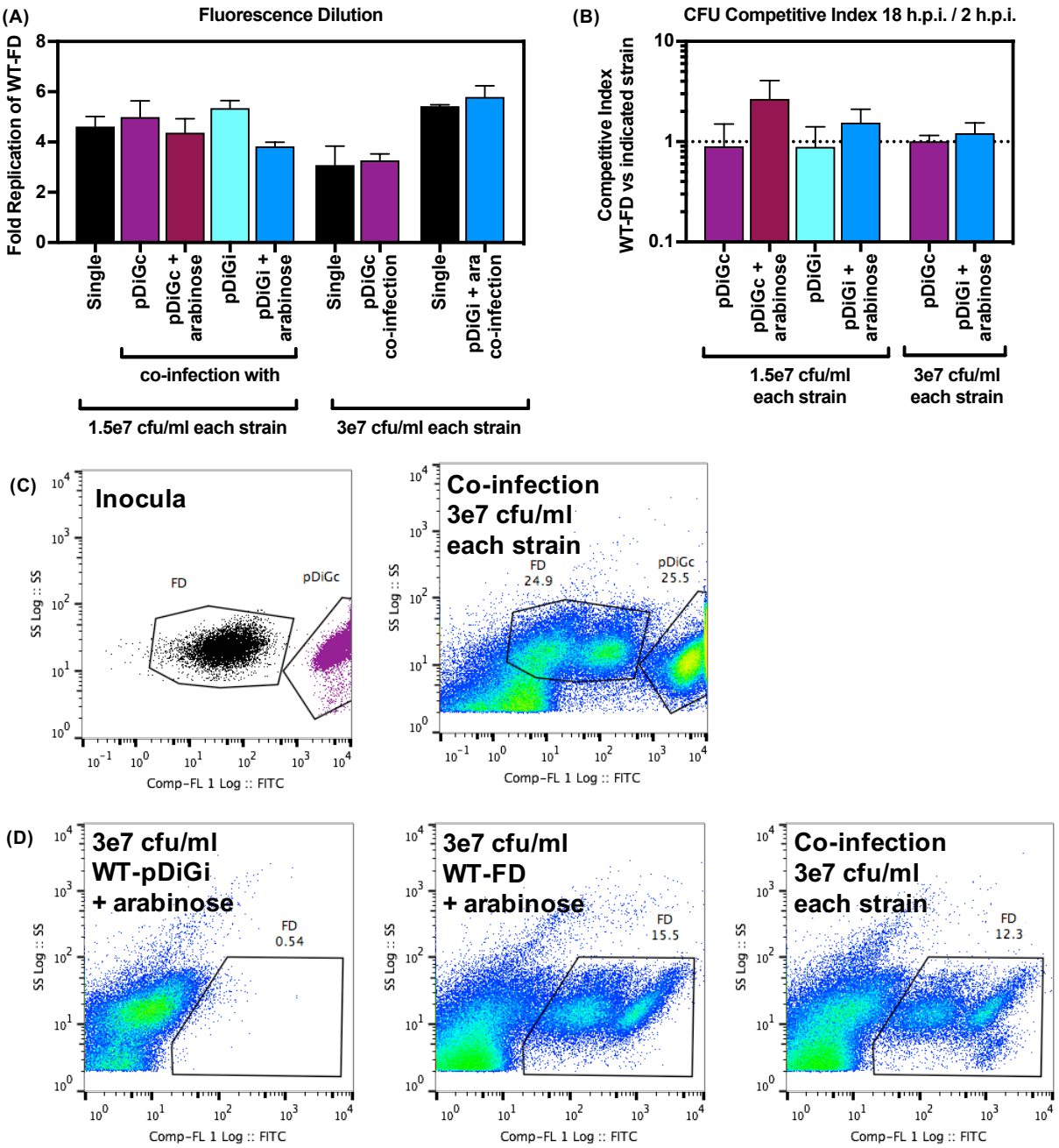

Figure E-5. FD strain (pDiGi; *rpsM*::GFP) and pDiGi, both expressing dsRed, compete equally in bone marrow macrophages. BMDMs were infected with equal concentrations of the standard FD strain induced to express dsRed and the indicated competitor, with both strains at 3e7 or 6e7 cfu/ml, as indicated. **(A)** Fold replication of the FD strain was measured using flow cytometry. **(B)** The competitive index between the standard FD strain and the indicated competitor was calculated as the ratio of the two strains at 18 h.p.i. normalized to the ratio at 2 h.p.i. Values above the dotted line indicate higher numbers of the standard FD strain. **(C)** Representative flow cytometry plots for inocula and 18 h.p.i. infected lysates from macrophages infected with the standard FD strain and pDiGc or **(D)** the standard FD strain and pDiGi + arabinose.

infected with 1.5 x 10^7 cfu/ml each strain (3 x 10^7 cfu/ml total) or 3 x 10^7 cfu/ml each strain (6 x 10^7 cfu/ml total). Thus, any of these strains were tenable competitors for co-infections with the FD strain.

I also compared the ease of gating the FD strain when competitors were present in macrophage lysates. I found that the FD strain and pDiGc (without arabinose) were easily distinguishable by flow cytometry (**Figure E-5C**). I also found that the FD strain was distinguishable from the arabinose-induced pDiGi strain (**Figure E-5D**). I utilized both combinations for experiments testing the requirement for the *Salmonella* gene *feoB*, but ultimately I used the FD strain vs pDiGi-arabinose for the data shown in **Figure 6-4**. Functionally, this combination yielded more consistent results, and scientifically, the presence or absence of *rpsM*::GFP was a simpler variable than possible toxicities introduced by the presence of pDiGc.

APPENDIX F. DATA FILES DEPOSITED IN THE DETWEILER LAB ARCHIVE

Associated data and figure files are organized in folders corresponding to the appropriate chapter and are available on the department server (collie.int.colorado.edu/DetweilerLab/PreviousLabMembers/AbigailReens/Thesis as of publication). Laboratory notebooks are filed on the Detweiler Lab lab notebook shelf with corresponding names.

Figure/Table	Relevant Filename(s)	Dates	Lab Notebook Pages
Figure 2-1B	ScreenN1Plate21WellF03F00 (folder)	2015.06.23	SCREEN/EPM 49-51 (A. Crooks)
Figure 2-1C	Volcano.pzfx Maybridge2015_FullAnalysis.xlsx	2015.06.09 2015.06.15 2015.06.23 2015.07.23 2015.07.28 2015.09.04 2015.09.22 2015.09.29 2015.10.01 2015.10.28 2015.11.03	SCREEN/EPM 42-45 SCREEN/EPM 46-48 SCREEN/EPM 49-51 SCREEN/EPM 52-54 SCREEN/EPM 55-57 SCREEN/EPM 65-67 SCREEN/EPM 68-70 SCREEN/EPM 71-73 SCREEN/EPM 74-76 SCREEN/EPM 82-89 SCREEN/EPM 90-96 (A. Crooks)
Figure 2-2B	RAW_EPM (folder)	2016.06.22	SCREEN/EPM 358
Figure 2-2C	Broth.pzfx Broth.xlsx	2016.02.02 2016.02.10 2016.03.03 2016.03.10	MADDIE SCREEN ETC (M. Edwards)
Table 2-1	Downs.xlsx		
Table 2-2	Known Substances.xlsx		
Figure 2-3	Nalidixic Acid.pzfx	2016.06.22 2016.07.05 2016.07.13	SCREEN/EPM 358 SCREEN/EPM 364 SCREEN/EPM 365-366
Figure 2-4	Microscopy vs CFU.pzfx Raw CFU.xlsx	2015.10.28 2015.11.03	SCREEN/EPM 83-89 SCREEN/EPM 90-96 (A. Crooks)
Figure 3-2	Hoechst.pzfx	2016.11.15 2016.11.22 2016.12.13	SCREEN/EPM 391-392 SCREEN/EPM 396 SCREEN/EPM 416-417
Figure 3-3	RAW IC50s.pzfx	2018.04.25 2018.04.30 2018.05.03	SCREEN/EPM 494 SCREEN/EPM 483,494 SCREEN/EPM 483,494
Figure 3-4	RAM Nitrocefin.pzfx	2018.05.10 2018.05.11 2018.05.11	SCREEN/EPM 501-502 SCREEN/EPM 503-505 SCREEN/EPM 503-505
Figures 3-5, 3-6	Nile Red Kinetics.pzfx Nile Red Timepoint.pzfx		Amy Crooks

Figure/Table	Relevant Filename(s)	Dates	Lab Notebook Pages
Figure 3-7	Nile Red Kinetics.pzfx	2016.11.29	SCREEN/EPM 397-398
Figure 3-8	TMRM.pzfx	2017.06.27 2017.07.04 2017.07.05	SCREEN/EPM 461-463 SCREEN/EPM 464-465
Figure 3-8	Swimming.pzfx	2016.12.06 2016.12.19	SCREEN/EPM 407-408 SCREEN/EPM 423-424
Figure 3-10	Salmonella Nitrocefin.pzfx	2016.10.26 2016.11.20 2016.11.21	SCREEN/EPM 474 SCREEN/EPM 477-479
Figure 3-11	AMP Growth Curves.pzfx	2016.06.25	SCREEN/EPM 359-360 Additional ns from Jessy Podoll
Figure 3-12	Mutant CFU.pzfx	2016.12.12 2016.12.19 2017.09.14	SCREEN/EPM 413-415 SCREEN/EPM 425-429 SCREEN/EPM 467-469
Figure 3-13	H2O2.pzfx		From Jessy Podoll
Figure 3-14	Salmonella Nitrocefin.pzfx	2016.10.26 2016.11.20 2016.11.21	SCREEN/EPM 474 SCREEN/EPM 477-479
Figure 3-15	Hoechst EPM PB.pzfx	2017.10.27 2017.11.20 2017.11.21	SCREEN/EPM 476 SCREEN/EPM 477-479
Figure 3-16	Nile Red EPM PB.pzfx		Data from Amy Crooks
Figure 3-17 A,B	DRB CHX.pzfx		Data from Toni Nagy
Figure 3-17C	DRB CHX.pzfx	2017.02.16	SCREEN/EPM 449-450
Figure 3-18A	HeLa.pzfx	2017.01.13 2017.02.02	SCREEN/EPM 438-442 SCREEN/EPM 447-448
Figure 3-18B	HeLa.pzfx	2016.01.21 2016.02.02 2016.06.22	SCREEN/EPM 341-342 SCREEN/EPM 343-344 SCREEN/EPM 358
Figure 3-18C	HeLa images (folder)	2016.06.22	SCREEN/EPM 358
Figure 3-19	Mutant CFU.pzfx	2016.12.12 2016.12.19 2017.09.14	SCREEN/EPM 413-415 SCREEN/EPM 425-429 SCREEN/EPM 467-469
Table 3-1	Broth Checkerboards.docx	2017.11	SCREEN/EPM 483
Figure 3-20	Macrophage Checkerboards.pzfx	2018.04.21 2018.04.30 2018.05.03	SCREEN/EPM 483-494
Figure 3-21	Tet 35 Mice.pzfx	2016.12.17	SCREEN/EPM 443-446
Figure 4-1 (Microscopy)	CMP Imaging (folder)	2015.08.18	CMP 52-56
Figure 4-1 (CFU)	Activity.pzfx RAW CFU.xlsx (Chapter 2)	2015.10.28 2015.11.03	SCREEN/EPM 83-89 SCREEN/EPM 90-96 (A. Crooks)

Figure/Table	Relevant Filename(s)	Dates	Lab Notebook Pages
Figure 4-2	Requirements.pzfx	2015.12.15 2015.12.22 2015.12.30	CMP 88-92 CMP 96-100 CMP 101-104
Figure 4-3	Requirements.pzfx	2015.12.08 2015.12.11 2015.12.15 2015.12.22	CMP 81-85 CMP 86-87, 111 CMP 88-92 CMP 96-100
Figure 4-5	Analogs IC50s.pzfx	2015.06.02 2015.07.03 2015.08.18	CMP 41-46 CMP 47-51 CMP 52-56
Figure 4-6	Analogs IC50s.pzfx	2016.03.05 2016.03.06 2016.04.01 2016.04.02 2016.04.03 2016.04.14 2016.05.18	MADDIE SCREEN ETC (M. Edwards)
Figure 4-7	Analogs IC50s.pzfx	2017.09.05 2017.09.07 2017.09.08	CMP 131-132 CMP 133 CMP 134-135
Figure 4-8	Polymixin B.pzfx	2016 (x4)	MADDIE SCREEN ETC (M. Edwards)
Figure 4-9	Requirements.pzfx	2015.12.08 2015.12.15 2015.12.22 2015.12.30	CMP 81-85 CMP 88-92 CMP 96-100 CMP 101-104
Figure 4-10	Requirements.pzfx	2015.12.15 2015.12.22 2015.12.30	CMP 88-92 CMP 96-100 CMP 101-104
Figure 4-11	Requirements.pzfx	2015.06.02 2015.07.03 2015.08.18 2015.12.15 2015.12.22 2015.12.30	CMP 41-46 CMP 47-51 CMP 52-56 CMP 88-92 CMP 96-100 CMP 101-104
Figure 4-12	CMP autophagy (folder)		Toni Nagy
Figure 4-13	Mice.pzfx	2016.11.21 2016.12.19	CMP 127-128 CMP 129-130
Figure 5-2	Broth.pzfx	2014.05.14 2014.10.05 2014.10.13 2014.10.20 2014.10.27 2014.11.03 2014.11.10 2014.11.17 2014.11.24 2014.11.28 2014.12.01	GLYSHUNT 177-178 GLYSHUNT 312-317 GLYSHUNT 312-317 GLYSHUNT 312-317 GLYSHUNT 312-317 GLYSHUNT 312-317 GLYSHUNT 312-317 GLYSHUNT 312-317 GLYSHUNT 312-317 GLYSHUNT 312-317 GLYSHUNT 312-317

Figure/Table	Relevant Filename(s)	Dates	Lab Notebook Pages
Figure 5-2 (continued)	Broth.pzfx	2014.12.12 2014.12.15 2018.01.30 2018.02.01 2018.02.02 2018.02.06	GLYSHUNT 312-317 GLYSHUNT 312-317 GLYSHUNT 649* GLYSHUNT 649* GLYSHUNT 649* GLYSHUNT 649*
Figure 5-3	Broth.pzfx	2018.01.12 2018.01.26 2018.01.30 2018.02.01 2018.02.02 2018.02.06 2018.11.20 2018.12.04	GLYSHUNT 648 GLYSHUNT 649 GLYSHUNT 649* GLYSHUNT 649* GLYSHUNT 649* GLYSHUNT 649* GLYSHUNT 698 GLYSHUNT 698
Table 5-1		2017.09	GLYSHUNT 671 GLYSHUNT 673-674
Figure 5-4	Oleate Growth (folder)	2018.03.06	GLYSHUNT 671
Figure 5-5	Mice.pzfx	2016.05.31 2016.07.16 2016.07.27 2016.09.09 2016.09.26 2017.05.11 2017.07.06 2017.09.04 2018.01.19	GLYSHUNT 472-473 GLYSHUNT 496-499 GLYSHUNT 496,500-502 GLYSHUNT 518-521 GLYSHUNT 518,522-524 GLYSHUNT 582-584 GLYSHUNT 605-606 GLYSHUNT 623-627 GLYSHUNT 650-651
Figure 5-6	Mice.pzfx	2015.07.14 2016.08.12 2016.09.09 2016.09.26 2017.07.06 2017.09.04 2017.09.18	GLYSHUNT 412-417 GLYSHUNT 503-505 GLYSHUNT 518-521 GLYSHUNT 518,522-524 GLYSHUNT 605-606 GLYSHUNT 623-627 GLYSHUNT 629-633
Figure 5-7	Mice.pzfx	2013.10.22 2015.07.14 2018.02.25 2018.05.18 2018.05.21 2018.12.18	GLYSHUNT 72-79 GLYSHUNT 412-417 GLYSHUNT 732 GLYSHUNT 680 GLYSHUNT 681 GLYSHUNT 704
Figure 5-8	Mice.pzfx	2017.07.03 2017.08.21	GLYSHUNT 605-606 GLYSHUNT 619-621
Figure 5-9	Macrophages nonNEAA.pzfx	2015.06.04 2015.06.09 2015.12.01 2015.12.16 2016.01.08	GLYSHUNT 377-379 GLYSHUNT 380-382 GLYSHUNT 442-443 GLYSHUNT 444-445 GLYSHUNT 446-449

Figure/Table	Relevant Filename(s)	Dates	Lab Notebook Pages
Figure 5-9 (continued)	Macrophages nonNEAA.pzfx	2017.03.20 2017.04.24	GLYSHUNT 553-558 GLYSHUNT 574-577
Figure 5-11	Macrophages WT.pzfx	2015.06.04 2015.06.09 2015.12.01 2015.12.16 2016.01.08 2017.03.20 2017.04.24 2017.08.14 2017.08.21 2017.08.28 2017.09.11 2017.10.10 2017.10.18 2017.11.02	GLYSHUNT 377-379 GLYSHUNT 380-382 GLYSHUNT 442-443 GLYSHUNT 444-445 GLYSHUNT 446-449 GLYSHUNT 553-558 GLYSHUNT 574-577 GLYSHUNT 610-612 GLYSHUNT 614-615 GLYSHUNT 616-618 GLYSHUNT 643-646 GLYSHUNT 643-646 GLYSHUNT 643-646 GLYSHUNT 643-646
Figure 5-12	Lipid Loading (folder)	2018.11.12	GLYSHUNT 692-696
Figures 5-13, 5-14, 5-17, 5-18	Macrophages.pzfx	2017.08.14 2017.08.21 2017.08.28 2017.09.11 2017.10.10 2017.10.18 2017.11.02	GLYSHUNT 610-612 GLYSHUNT 614-615 GLYSHUNT 616-618 GLYSHUNT 643-646 GLYSHUNT 643-646 GLYSHUNT 643-646 GLYSHUNT 643-646
Figure 5-15	Lipid User Calculations.pzfx	2015.06.04 2015.06.09 2015.12.01 2015.12.16 2016.01.08 2017.03.20 2017.04.24 2017.08.14 2017.08.21 2017.08.28 2017.09.11 2017.10.10 2017.10.18 2017.11.02	GLYSHUNT 377-379 GLYSHUNT 380-382 GLYSHUNT 442-443 GLYSHUNT 444-445 GLYSHUNT 446-449 GLYSHUNT 553-558 GLYSHUNT 574-577 GLYSHUNT 610-612 GLYSHUNT 614-615 GLYSHUNT 616-618 GLYSHUNT 643-646 GLYSHUNT 643-646 GLYSHUNT 643-646 GLYSHUNT 643-646
Figure 5-16	Macrophages CFU.pzfx	2017.08.14 2017.08.21 2017.08.28 2017.09.11 2017.10.10 2017.10.18 2017.11.02	GLYSHUNT 610-612 GLYSHUNT 614-615 GLYSHUNT 616-618 GLYSHUNT 643-646 GLYSHUNT 643-646 GLYSHUNT 643-646 GLYSHUNT 643-646
Figure 6-1	Titrations.pzfx	2015.05.06 2015.05.21 2015.05.28 2015.06.09	GLYSHUNT 356-360 GLYSHUNT 370-372 GLYSHUNT 373-375 GLYSHUNT 380-382

Figure/Table	Relevant Filename(s)	Dates	Lab Notebook Pages
Figure 6-2	Transwells.pzfx	2019.02.06 2019.03.12 2019.03.18	GLYSHUNT 726-728 GLYSHUNT 734-736 GLYSHUNT 737-739
Figure 6-3	Conditioned Medium.pzfx	2015.04.15 2015.04.22 2015.05.28 2015.06.04 2015.06.09 2015.06.17	GLYSHUNT 342-343 GLYSHUNT 347-351 GLYSHUNT 373-375 GLYSHUNT 377-379 GLYSHUNT 380-382 GLYSHUNT 388-392
Figure 6-4	FeoB FD and CFU.pzfx FeoB CI.pzfx	2016.07.13 2016.08.31	GLYSHUNT 484-492 GLYSHUNT 507-510
Figure 6-5	RBC iron mutant.pzfx	2018.12.17 2019.01.08 2019.01.22	GLYSHUNT 700-703 GLYSHUNT 709-712 GLYSHUNT 715-717
Figure 6-6	RBC iron.pzfx	2017.04.03 2017.04.10 2017.04.17 2017.05.01	GLYSHUNT 564-567 GLYSHUNT 568-570 GLYSHUNT 571-573 GLYSHUNT 578-579
Figure 6-7	qPCR bacteria.pzfx qPCR plex mac.pzfx	2017.03.20 2017.05.22 2017.06.13 2017.06.26 2017.07.03 2018.04.13 2018.05.01 2019.03.05	GLYSHUNT 553-558 GLYSHUNT 585-589 GLYSHUNT 592-594 GLYSHUNT 598-599 GLYSHUNT 601-604 GLYSHUNT 672 GLYSHUNT 679 GLYSHUNT 733
Figure 6-8	Lipid mutants.pzfx	2015.12.01 2015.12.16 2015.01.21	GLYSHUNT 442-443 GLYSHUNT 444-445 GLYSHUNT 446-449
Figure 6-9	Bodipy.wsp	2019.01.22	GLYSHUNT 715-717
Figure 6-10	qPCR bacteria.pzfx	2017.06.26 2017.07.03 2018.05.01	GLYSHUNT 598-599 GLYSHUNT 601-604 GLYSHUNT 679
Figure 6-11	RBC hmpA.pzfx	2018.06.26 2018.07.02	GLYSHUNT 684-686 GLYSHUNT 687-691
Figure 6-12	Nitric oxide.pzfx	2017.03.20 2017.03.27 2017.04.03 2017.04.10 2017.04.17 2017.05.01 2017.05.22	GLYSHUNT 553-558 GLYSHUNT 559-563 GLYSHUNT 564-567 GLYSHUNT 568-570 GLYSHUNT 571-573 GLYSHUNT 578-579 GLYSHUNT 585-589
Figure 6-13	Neutral Griess.pzfx	2019.01.22 2019.01.29 2019.02.06	GLYSHUNT 713-714 GLYSHUNT 720 GLYSHUNT 726-728
Figure 6-14	Ghosts.pzfx	2017.03.27 2017.04.03 2017.05.22	GLYSHUNT 559-563 GLYSHUNT 564-567 GLYSHUNT 585-589

Figure/Table	Relevant Filename(s)	Dates	Lab Notebook Pages
Figure 6-15	RBC sorting.pzfx	2015.04.08 2015.04.15 2015.05.13	GLYSHUNT 335-339 GLYSHUNT 340-341 GLYSHUNT 361-362
Figure 6-16	RBC cytoD.pzfx	2015.06.04 2015.06.09 2015.06.17	GLYSHUNT 377-379 GLYSHUNT 380-382 GLYSHUNT 388-392
Figure 6-17	PS exposure.pzfx	2016.06.22 2016.10.06 2016.10.17 2017.04.10 2018.06.26 2018.07.02	GLYSHUNT 477-478 GLYSHUNT 527-531 GLYSHUNT 532-539 GLYSHUNT 568-570 GLYSHUNT 684-686 GLYSHUNT 687-691
Figure 6-18	RBC ligands.pzfx Ter119 Western.pzfx Western (folder)	2015.06.17 2015.07.09 2015.07.15 2015.07.22 2015.08.05 2016.06.07 2016.06.22 2016.09.14 2017.04.10 2018.06.26 2018.07.02 2019.01.08 2019.02.25	GLYSHUNT 388-392 GLYSHUNT 397-399 GLYSHUNT 401-410 GLYSHUNT 418-422 GLYSHUNT 426-429 GLYSHUNT 470-471 GLYSHUNT 477-478 GLYSHUNT 514-517 GLYSHUNT 568-570 GLYSHUNT 684-686 GLYSHUNT 687-691 GLYSHUNT 709-712 GLYSHUNT 730-731
Figure 6-19	Signaling inhibitors	2016.09.07 2016.09.14 2016.10.17 2017.03.27	GLYSHUNT 511-513 GLYSHUNT 514-517 GLYSHUNT 532-539 GLYSHUNT 559-563
Figure 6-20	qPCR plex mac.pzfx	2017.03.20 2017.05.22 2017.06.13 2018.04.13 2019.03.05	GLYSHUNT 553-558 GLYSHUNT 585-589 GLYSHUNT 592-594 GLYSHUNT 672 GLYSHUNT 733
Figure 6-21A	Titrations.pzfx J PS Griess.pzfx	2015.05.21 2015.05.28 2015.06.09 2018.12.17 2019.01.08 2019.01.22 2019.02.06 2019.03.12 2019.03.18 2019.03.26	GLYSHUNT 370-372 GLYSHUNT 373-375 GLYSHUNT 380-382 GLYSHUNT 700-702 GLYSHUNT 709-712 GLYSHUNT 715-717 GLYSHUNT 722-725 GLYSHUNT 734-736 GLYSHUNT 737-739 GLYSHUNT 740-741
Figure 6-21B	J PS Requirements.pzfx	2018.12.17 2019.01.08 2019.01.22 2019.02.06	GLYSHUNT 700-703 GLYSHUNT 709-712 GLYSHUNT 715-717 GLYSHUNT 726-728

Figure/Table	Relevant Filename(s)	Dates	Lab Notebook Pages
Figure 6-21 C,D	J PS Rescues.pzfx	2019.02.06 2019.03.12 2019.03.18	GLYSHUNT 726-728 GLYSHUNT 734-736 GLYSHUNT 737-739
Figure 6-21E	Neutral Griess.pzfx	2019.01.22 2019.01.29 2019.02.06	GLYSHUNT 713-714 GLYSHUNT 720 GLYSHUNT 726-728
Figure 6-22 A,D	J PS Requirements.pzfx	2018.12.17 2019.01.08 2019.01.22 2019.02.06 2019.03.26 2019.04.11	GLYSHUNT 700-703 GLYSHUNT 709-712 GLYSHUNT 715-717 GLYSHUNT 726-728 GLYSHUNT 740-741 GLYSHUNT 742-743
Figure 6-22 B,C	J PS Rescues.pzfx	2019.02.06 2019.03.12 2019.03.18	GLYSHUNT 726-728 GLYSHUNT 734-736 GLYSHUNT 737-739
Figure 6-23	J PS qPCR.pzfx qPCR plex mac.pzfx	2018.11.12 2018.12.17 2019.01.08 2019.01.22 2019.03.05	GLYSHUNT 692-696 GLYSHUNT 700-703 GLYSHUNT 709-712 GLYSHUNT 715-717 GLYSHUNT 733
Figure 6-24 A,B	Transwells.pzfx	2019.02.06 2019.03.12 2019.03.18	GLYSHUNT 726-728 GLYSHUNT 734-736 GLYSHUNT 737-739
Figure 6-24C	J PS Requirements.pzfx	2018.12.17 2019.01.08 2019.01.22 2019.02.06 2019.03.12 2019.03.18	GLYSHUNT 700-703 GLYSHUNT 709-712 GLYSHUNT 715-717 GLYSHUNT 726-728 GLYSHUNT 734-736 GLYSHUNT 737-739
Figure 6-24 D,E	J PS Sorting Supe.pzfx Sorting.wsp	2019.03.18 2019.03.26 2019.04.11	GLYSHUNT 737-739 GLYSHUNT 740-741 GLYSHUNT 742-743
Figure A-1A	SAFIRE Development.pzfx	2013.07.08	SCREEN/EPM 53-66
Figure A-1 B,D	SAFIRE Development.pzfx	2013.08.05	SCREEN/EPM 95-97
Figure A-1C	SAFIRE Development.pzfx	2013.07.03	SCREEN/EPM 45-51
Figure A-2	SAFIRE Development.pzfx	2013.07.24	SCREEN/EPM 88-94
Figure A-3	SAFIRE Development.pzfx	2013.08.26	SCREEN/EPM 102-107
Figure A-4A	SAFIRE Development.pzfx	2014.07.08	SCREEN/EPM 147-181
Figure A-4B	SAFIRE Development.pzfx	2014.08.04	SCREEN/EPM 182-202
Figure A-5	SAFIRE Development.pzfx	2015.03.03	SCREEN/EPM 315
Figure C-1	Pilot Screen.pzfx Pilot Screen.xlsx	2014.08.27 2014.09.05 2014.09.10 2014.09.17	SCREEN/EPM 255-257 SCREEN/EPM 258-260 SCREEN/EPM 261-263 SCREEN/EPM 264-266 SCREEN/EPM 267-278
Figure C-2	Pilot Screen.pzfx Pilot Screen.xlsx	2014.10.09	SCREEN/EPM 300-306

Figure/Table	Relevant Filename(s)	Dates	Lab Notebook Pages
Figure D-1	Hergenrother Screen.pzfx Hergenrother Screen.xlsx	2017.04.21 2017.04.24	SCREEN/EPM 456-457 SCREEN/EPM 470-473
Figure E-1A	FD optimization.pzfx	2014.10.22	GLYSHUNT 235
Figure E-1 B,C	FD optimization.pzfx Broth dilution.wsp	2014.10.06	GLYSHUNT 225-229
Figure E-2	pDiGc macrophages.wsp FD optimization.pzfx	2014.10.23	GLYSHUNT 236-241
Figure E-3	GFP strains.wsp	2014.11.06	GLYSHUNT 247
Figure E-4A	pDiGi macrophages.wsp	2014.11.17	GLYSHUNT 253-263
Figure E-4B	FD optimization.pzfx	2014.10.29	GLYSHUNT 242-245
Figure E-5	FD optimization.pzfx FD pDiGc competitive.wsp FD pDiGi competitive.wsp	2016.01.05 2016.01.21 2016.07.13	GLYSHUNT 446-449 GLYSHUNT 484-492

APPENDIX G. BACTERIAL STRAINS USED IN THIS WORK

ALR#	DET#	Name	Background	Genotype	Plasmid	Resistances	Source / Notes
001	0001	Wild Type	*S*.Tm SL1344	Wild Type	-	Str	Also ALR #445, #446, #447, #448
002	0014	pGFP	*S*.Tm SL1344	Wild Type	pACYC184-rpsM::GFP, cmR	Str Cm	
003	0829	pRFP	*S*.Tm SL1344	Wild Type	pTag-RFP-rpsM::RFP, AmpR	Str Amp	Very hIgh expression
004	1021	SDFR3	*S*.Tm SL1344	*sifB*::GFP/kan	-	Str Kan	(Rollenhagen et al., 2004); screening was with ALR#109
005	1022	SRU2	*S*.Tm SL1344	*sifB*::GFP/kan	-	Str Kan	Bumann
006	1023	SRU5	*S*.Tm SL1344	*sifB*::CFP/kan	-	Str Kan	Bumann (Urbani Thesis 2009)
009	0983	*aceB*::kan	*S*.Tm SL1344	*aceB*::kan		Str, Cm	Wanner method transduced into #001
015	0982	*aceA*::kan	*S*.Tm SL1344	*aceA*::kan	-	Str Kan	Wanner method transduced into #001
025	0215	pKD3	*E.* coli DH5α		pKD3	Amp Cm	Template plasmid for Wanner
026	0216	pKD4	*E.* coli DH5α		pKD4	Amp Kan	Template plasmid for Wanner
027	0213	pCP20	*E.* coli DH5α		pCP20, FLPase	Amp 30C	FLPase for Wanner cassette removal
028	0221	Wanner λ-Red	*S*.Tm 14028		pKD46: λ-Red recombinase (arabinose inducible)	Amp 30C	Recombineering strain for Wanner
034		Δ*aceB*	*S*.Tm SL1344	Δ*aceB*		Str	FLPed out from #009
038		Δ*aceA*	*S*.Tm SL1344	Δ*aceA*		Str	FLPed out from #015
077		*yafH*::kan	*S*.Tm SL1344	*yafH*::kan		Str, Kan	Wanner method transduced into #001
081		*fadBA*::kan	*S*.Tm SL1344	*fadBA*::kan		Str, Kan	Wanner method transduced into #001
085		*fadL*::kan	*S*.Tm SL1344	*fadL*::kan		Str, Kan	Wanner method transduced into #001
089		*fadD*::kan	*S*.Tm SL1344	*fadD*::kan		Str, Kan	Wanner method transduced into #001
097		*fadR*::kan	*S*.Tm SL1344	*fadR*::kan		Str, Kan	Wanner method transduced into #001
109	1270	*sifB*::GFP	*S*.Tm SL1344	*sifB*::GFP,kan	-	Str Kan	ALR#004 transduced into ALR#001
171		Δ*yafH*	*S*.Tm SL1344	Δ*yafH*		Str	FLPed out from #077
175		Δ*fadBA*	*S*.Tm SL1344	Δ*fadBA*		Str	FLPed out from #081
179		Δ*fadL*	*S*.Tm SL1344	Δ*fadL*		Str	FLPed out from #085
183		Δ*fadD*	*S*.Tm SL1344	Δ*fadD*		Str	FLPed out from #089
218	222	*rpsM*::GFP	*S*.Tm SL1344	*rpsM*::GFP,kan	-	Str Kan	(Vazquez-Torres et al., 1999)
228		WT-pDiGi	*S*.Tm SL1344	-	pDiGi	Str, Amp	Transformed into #001

ALR#	DET#	Name	Background	Genotype	Plasmid	Resistances	Source / Notes
234	1271	WT-BFP	*S*.Tm SL1344	-	pACYC-amp/rpsM-Tag2BFP	Str Amp	For nitrocefin permeability assay, TMRM
258		WT-FD	*S*.Tm SL1344	*rpsM*::GFP	pDiGi	Str, Kan, Amp	pDiGi transformed and #218 transduced into #001
259		Δ*aceA*-FD	*S*.Tm SL1344	Δ*aceA*; *rpsM*::GFP/kan	pDiGi	Str, Kan, Amp	pDiGi transformed and #218 transduced into #038
260		Δ*fadL*-FD	*S*.Tm SL1344	Δ*fadL*; *rpsM*::GFP/kan	pDiGi	Str, Kan, Amp	pDiGi transformed and #218 transduced into #179
261		Δ*fadD*-FD	*S*.Tm SL1344	Δ*fadD*; *rpsM*::GFP/kan	pDiGi	Str, Kan, Amp	pDiGi transformed and #218 transduced into #183
262		Δ*yafH*-FD	*S*.Tm SL1344	Δ*yafH*; *rpsM*::GFP/kan	pDiGi	Str, Kan, Amp	pDiGi transformed and #218 transduced into #171
282		Δ*aceB*-FD	*S*.Tm SL1344	Δ*aceB*; *rpsM*::GFP/kan	pDiGi	Str, Kan, Amp	pDiGi transformed and #218 transduced into #034
286		Δ*fadBA*-FD	*S*.Tm SL1344	Δ*fadBA*; *rpsM*::GFP/kan	pDiGi	Str, Kan, Amp	pDiGi transformed and #218 transduced into #175
298		*ydiD*::kan	*S*.Tm SL1344	*ydiD*::kan		Str, Kan	Wanner method transduced into #001
334	1238	pSLTS	*S*.Tm	-	pSLTS	Str Amp 30C	Recombineering strain for Juhan method
363		*feoB*::cm	*S*.Tm SL1344	*feoB*::cm		Str, Cm	Juhan method transduced into #334 and cured
383		*feoB*::cm-pDiGi	*S*.Tm SL1344	*feoB*::cm	pDiGi	Str, Cm, Amp	pDiGi transformed into #363
385		WT-pDiGc	*S*.Tm SL1344	Wild Type	pDiGc	Str, Amp	pDiGc transformed into #001
387		*feoB*::cm-pDiGc	*S*.Tm SL1344	*feoB*::cm	pDiGc	Str, Cm, Amp	pDiGc transformed into #363
391		*feoB*::cm-FD	*S*.Tm SL1344	*feoB*::cm; *rpsM*::GFP/kan	pDiGi	Str, Cm, Amp	pDiGi transformed and #218 transduced into #363
393	1248	S10801	*S*.Tm	-		Str Amp Tet	BEI Resources NR22067
400	1258	*macAB*::kan	*S*.Tm SL1344	*macAB*::kan	pSLTS	Str Kan	Juhan method transduced into #334
401	1269	*tolC*::cm	*S*.Tm SL1344	*tolC*::cm	pSLTS	Str Cm	Juhan method transduced into #334
411	1257	*acrAB*::kan	*S*.Tm SL1344	*acrAB*::kan	pSLTS	Str Kan	Juhan method transduced into #334
412		*hmpA*::kan	*S*.Tm SL1344	*hmpA*::kan		Str, Kan	Vazquez-Torres
419		Δ*hmpA*	*S*.Tm SL1344	Δ*hmpA*		Str	FLPed out from #412
438		Δ*fadD*; *ydiD*::kan	*S*.Tm SL1344	Δ*fadD*; *ydiD*::kan		Str, Kan	#298 transduced into #183

ALR#	DET#	Name	Background	Genotype	Plasmid	Resistances	Source / Notes
439		*yfcYX*::kan	*S*.Tm SL1344	*yfcYX*::kan		Str, Kan	Juhan method transduced into #334 and cured
441		Δ*fadBA*; *yfcYX*::kan	*S*.Tm SL1344	Δ*fadBA*; *yfcYX*::kan		Str, Kan	#439 transduced into #175
451		Δ*yafH*; *ydiO*::cm	*S*.Tm SL1344	Δ*yafH*; *ydiO*::kan		Str, Cm	#461 transduced into #171
461		*ydiO*::cm	*S*.Tm SL1344	*ydiO*::cm		Str, Cm	Wanner method transduced into #001
493		Δ*fadL*-pRB3_*fadL*	*S*.Tm SL1344	Δ*fadL*	pRB3_*fadL*	Str, Amp	Plasmid transformed into #179
495		*fadL*::kan-pRB3_*fadL*	*S*.Tm SL1344	*fadL*::kan	pRB3_*fadL*	Str, Kan, Amp	Plasmid transformed into #085
497		Δ*fadD*-pRB3_*fadD*	*S*.Tm SL1344	Δ*fadD*	pRB3_*fadD*	Str, Amp	Plasmid transformed into #183
499		*fadD*::kan-pRB3_*fadD*	*S*.Tm SL1344	*fadD*::kan	pRB3_*fadD*	Str, Kan, Amp	Plasmid transformed into #089
510		Δ*aceA*-pRB3_*aceA*	*S*.Tm SL1344	Δ*aceA*	pRB3_*aceA*	Str, Amp	Plasmid transformed into #038
512		*aceA*::kan-pRB3_*aceA*	*S*.Tm SL1344	*aceA*::kan	pRB3_*aceA*	Str, Kan, Amp	Plasmid transformed into #038
522	1258	RAM121	*E.coli*	ompC mutation to increase pore size		-	For nitrocefin efflux assay
526		*aceB*::cm	*S*.Tm SL1344	*aceB*::cm		Str, Cm	Juhan method transduced into #001
584		Δ*hmpA*-FD	*S*.Tm SL1344	Δ*hmpA*; *rpsM*::GFP/kan	pDiGi	Str, Kan, Amp	pDiGi transformed and #218 transduced into #419
585		Δ*iroN*; Δ*fepA*	*S*.Tm SL1344	Δ*iroN*; Δ*fepA*		Str	Toni Nagy
591		*aceB*::cm-pRB3_*aceB*	*S*.Tm SL1344	*aceB*::cm	pRB3_*aceB*	Str, Cm, Amp	Plasmid transformed into #526
601		*feoB*::cm; Δ*iroN*; Δ*fepA*-FD	*S*.Tm SL1344	*feoB*::cm; Δ*iroN*; Δ*fepA*; *rpsM*::GFP/kan	pDiGi	Str, Kan, Cm, Amp	pDiGi transformed and #363, #218 transduced into #585
603		Δ*aceB*-pRB3_*aceB*	*S*.Tm SL1344	Δ*aceB*	pRB3_*aceB*	Str, Amp	Plasmid transformed into #034

APPENDIX H. GENERAL PROTOCOLS USED IN THIS WORK

MEDIA RECIPES

LB per 1L:
10 g tryptone
5 g yeast extract
5 g sodium chloride
autoclave

5X M9 salts per 1L:
30g Na_2HPO_4
15g KH_2PO_4
2.5g NaCl
5g NH_4Cl

5X No Carbon E (NCE) salts per 1L:
19.7 g KH_2PO_4
32.3 g $K_2HPO_4 \bullet 3H_2O$ or 24.66g K_2HPO_4
17.5 $NaNH_4HPO_4 \bullet H_2O$

M9 or E minimal media:
1X M9 or NCE salts
1 mM magnesium sulfate
0.004% histidine
0.4% carbon source
100 μM calcium chloride (optional)
0.1% casamino acids (optional)

Oleate M9 media:
Add 1% igepal CA-630 and 0.1% sodium oleate to M9 media

MgMes minimal medium for fluorescence dilution induction from Helaine 2011
170mM MES pH 5.0
5mM KCl
7.5mM $(NH_4)_2SO_4$
500uM K_2SO_4
1mM KH_2PO_4
10mM $MgCl_2$
0.3% glycerol
0.1% casamino acids
dsRed induction: add 10mM arabinose
GFP induction: add 0.5mM IPTG

SPI2-inducing medium (or control) from Coombes 2004
80mM MES pH 5.0 (or 7.0 for non-SPI2 control)
5mM KCl
7.5mM $(NH_4)_2SO_4$
500uM K_2SO_4
337uM KH_2PO_4
8uM $MgCl_2$
0.3% glycerol
0.1% casamino acids

BASIC *SALMONELLA* TECHNIQUES

Thaw from frozen stock:
Scrape sterile loop around cryovial
Streak loop onto LB-antibiotic plate
Using fresh loops, dilute streak across remainder of plate
Incubate overnight 37 °C

Streak plate:
*Restreak plates every 2-3 weeks
Touch a single colony with sterile loop
Streak loop onto fresh LB-antibiotic plate
Using fresh loops, dilute streak across remainder of plate
Incubate overnight 37 °C

Liquid culture from frozen stock:
Scrape sterile loop around cryovial
Swirl in 5mL LB-antibiotic
Incubate 37 °C roller (less than 12 hours generally to reach saturation)

Liquid culture from plate:
Touch a single colony with sterile loop
Immerse loop in 5mL LB-antibiotic
Incubate 37 °C roller (less than 12 hours generally to reach saturation)

Liquid culture from liquid culture (subculture):
Add 10uL of previous culture to 5mL fresh LB-antibiotic
Incubate 37 °C roller (less than 8 hours generally)

Freeze stock from liquid culture:
Coming 750uL bacterial overnight with 250uL 80% glycerol (20% glycerol final)
Place in -80 °C

Freeze and thaw reproducible bacterial aliquots from liquid culture:
Take OD600; dilute bacteria to OD = 1
Dilute 1000X (in 6 ml final volume)
Add 2 ml 80% glycerol; mix well
Aliquot 100 μl; freeze at -80 °C
Thaw into 5 ml LB-antibiotic
Incubate 37 °C for 18 hours rolling
Store at 4 °C until ready to use (< 8 hours)

96-WELL PLATE READER GROWTH CURVE

Day 0:
Start overnight of strain in LB-antibiotic

Day 1:
Wash 150 μl culture 3X PBS; resuspend in 1.5 ml PBS
Take OD600; dilute culture to OD = 0.1
Dilute 10X (100 + 900 μl media) into appropriate medium (gives OD600 = 0.01)
Aliquot 300 μl 1X culture in triplicate
Aliquot 300 μl blank (100 μl PBS + 900 μl media**)**
Aliquot 300 μl water into edge wells
Read on plate reader at 37 °C shaking continuously; read every 20 minutes at 600 nm
Can run for 2.5 days

Analysis:
Subtract appropriate blank
Average triplicates

POLYMERASE CHAIN REACTION

Per 25 μL reaction:
12.5 μL 2X Taq Master Mix (Thermo)
2.5 μL primer 1 (5 μM stock)
2.5 μL primer 2 (5 μM stock)
1-3 μL template
Water to 25 μL

PCR program
95 °C for 3 minutes
* 95 °C for 30 seconds
52 °C for 30 seconds
72 °C for 1 minutes / kb template
repeat from * 35 times
72 °C for 7 minutes

Modification for colony PCR
Resuspend colony (very small) into 30 μL water; use 3 μL as template
Change initial denaturation to 7 minutes

GENOMIC RECOMBINEERING

Two shocks per insert: 2uL and 5uL of purified PCR product
1 shock = 50uL competent cells = 10mL culture @ OD 0.5-0.6

Start 5mL overnight of strain 14028S-pKD46 in LB-amp at 30C (Wanner)
strain SL1344-pSLTS in LB-str-amp at 30C (Juhan)

Inoculate 55mL LB-amp with 200uL overnight; shake 15-30minutes
Add arabinose to final concentration 10mM
Shake at 30C until OD = 0.5-0.6 (3.5-4.5hrs)
Chill in ice-water shaking 15min
Spin in 50mL conical @ maximum speed 8min (4C)
Resuspend in 50mL cold water; pellet again
Resuspend in 1mL water; pellet in microcentrifuge (4C)
Wash additional 2x1mL water and 3x1mL 10% glycerol
Resuspend in 250uL 10% glycerol (50uL per 10mL initial culture)
Combine 50uL cells with 2 or 5uL DNA / 10-100ng DNA; add to cuvette on ice; incubate 15min
Electroporate at 1.8kV; immediately add 1mL prewarmed LB; transfer to culture tube
Rinse cuvette with additional 1mL LB; transfer to culture tube
Let cells recover 1-3hrs rolling at 30C
Centrifuge culture and resuspend in 200uL LB
Plate on appropriate media; grow 1-2 days at 30C

Patch putative colonies onto fresh plates; incubate 37 or 30C
Confirm recombination by PCR

P22 PHAGE LYSATES AND TRANSDUCTION

Phage lysate
Use with strain SL1290 to produce empty phage lysate
Use with strain of interest to transduce mutations

Day 1
Start 5ml overnight of donor strain
Add chloroform to existing empty P22 stock if old

Day 2
Combine 4ml LB, 1ml saturated overnight, 100ul P22 stock
Incubate rolling 37 °C overnight

Day 3
Add 100-200ul chloroform to lysate; vortex vigorously
Incubate at 37°C rolling exactly 5 minutes
Transfer to conical and spin 20 minutes maximum speed
Transfer supernatant to fresh 15ml conical; add chloroform
Spin if using immediately
Parafilm lid and store at 4 °C

Transduction

Day 1
Inoculate 5ml overnight of recipient strain
If P22 stock is old, add chloroform

Day 2
Spread 200ul 0.25 M EDTA pH 7.4 onto plates
Mix 100 ul recipient and 100 ul phage lysate
Incubate exactly 30 minutes at 37 °C rolling
Plate 50-150 ul onto EGTA-plates
Incubate overnight 37 °C

Day 3
Patch colonies onto fresh EGTA plate (confirms tranduction, dilutes phage)
Incubate overnight 37 °C

PLASMID ENGINEERING FOR COMPLEMENTATION

Find sequence(s) of interest: http://microbesonline.org/

Check sequences for existing restriction sites: http://nc2.neb.com/NEBcutter2/

Design primers using NCBI Primer-Blast (https://www.ncbi.nlm.nih.gov/tools/primer-blast/) to amplify region of interest (300bp upstream of start site, 50bp downstream of stop codon to be safe); append restriction digest recognition sites to 5' end of primers; apend 6bp spacer sequences to 5' end of primers

PCR amplify region of interest using high-fidelity polymerase (100-200ul total reaction)

Agarose gel check PCR product

PCR purify inserts using Qiagen pcr purification kit

Set up restriction digest of inserts and vector (make excess vector and save)
50ul reation: 1ug DNA, 5ul 10x buffer, water, 1ul enzyme(s) – typically 1 hr 37C
PCR purify digested inserts
Gel purify linearized plasmid using Qiagen gel purification kit; may need to PCR purify to increase concentration

Set up T4 ligation
20ul reaction, 2ul 10X buffer, 1ul enzyme, 1hr 25C then 10 minutes 65C
50ng linearized vector; 3:1 vector:insert molar ratio
calculate molarity using Promega BioMath Calculator
https://www.promega.com/a/apps/biomath/index.html?calc=molarity)

Transform 5ul into 50ul NEB 5alpha high efficiency competent cells; incubate on ice 30 minutes; heat shock 42C 30 sec, ice 5 minutes; add 950ul SOC; recover warm room shaking 1 hour; plate 200ul on LB-amp

Miniprep; send for sequencing at Macrogen (500ng plasmid and 25pmol primer)
Align sequencing reads to target sequence using ClustalOmega
(https://www.ebi.ac.uk/Tools/msa/clustalo/)

BASIC TISSUE AND CELL CULTURE TECHNIQUES

Macrophage, HeLa media:
DMEM high glucose
10% fetal bovine serum
2 mM L-gluatmine
1 mM sodium pyruvate
10 mM HEPES pH 7.0
50 μM β-mercaptoethanol
1X non-essential amino acids (optional)
Include 1X penicillin/streptomycin for routine maintenance

Jurkat media:
RPMI 1640
10% fetal bovine serum

Incubation conditions:
37 °C; 5% CO_2

Vessel volume guidelines:
96-well: 200 μl
24-well: 500 μl
6-well: 3 ml
T25: 8 ml
T75: 15 ml
T175: 35 ml

Bone marrow derived macrophages generation:
Humanely euthanize mouse; dissect femurs and tibias and scrape free of tissue
Cut bones in half with razor blade; flush with PBS using 27 ½ needle (5 ml per bone)
Layer 5 ml suspension over 5 ml Histopaque 1083; centrifuge 25 minutes 2500 x *g* (slow brake)
Aspirate to 1 ml above interface; remove interface, wash in complete medium 10 minutes 500 x *g*
Seed at 1-2 x 10^5 cells / ml; feed with equal volume at 3 days; activate 6-7 days
Seeding and feeding media: 35% conditioned medium from 3T3-MCSF cells

RAW / nRAW passaging:
Aspirate medium from cell culture flask; add fresh media
Scrape surface to gently dislodge cells
Pipette and rinse surface to collect cells
Subculture 1:5 – 1:10
nRAW only: select with 3ug/mL on mostly confluent T75 for 2-3 days at thaw and P15

HeLa passaging:
Aspirate; rinse with PBS; add 0.25% trypsin-EDTA to cover surface; incubate 5-10 minutes 37
Add complete medium and rinse surface; split 1:5 – 1:10

Jurkat passaging:
Centrifuge 5 minutes at 500 x *g* to remove dead cells
Resuspend and split 1:2 or 1:3; feed or split every 2-3 days

Frozen stocks:
Thaw cells in 37 °C water bath until thawed (~2min)
Pipette into ~8 mL media
Centrifuge 500 x *g* 5min; aspirate supernatant
Resuspend in 8 ml media; transfer to T25 flask
Next day passage entire volume into T75 with 15 mL final volume
Harvest cells, count, and freeze 1 x 10^7 cells in 900 μL medium + 100 μL DMSO (10%)
Slow-freeze in -80 °C in isopropanol bath (must be room temperature before use)
Frozen stocks are viable ~ 1 year at -80 °C; indefinitely in liquid nitrogen

Generating shRNA-expressing cell lines in RAW
Day 0: Seed 400,000 cells in 6 wells
Day 1: Add 1ml virus, 1ml fresh medium, 2ul polybrene (10ug/ml final)
Spin 2500xg in centrifuge 1 hr 33C; incubate ~16 hrs
Day 2: replace with 2ml fresh media
Day 3: replace with 2ml fresh medium + 6ug/ml puro
Day 5: replace with 2ml fresh medium + 6ug/ml puro
Uninfected controls should be dead; expand and freeze cells

Blood harvest:
Prepare 27 ½ needle with 100-200 μl heparin sulfate (1000 U/ml) and 1 ml syringe
Euthanize mouse and immediately cardiostick:
Place left thumb and forefinger at base of rib cage
Insert needle with bevel up between fingers parallel to mouse body
Slowly retract plunger; massage chest and rotate needle to aid flow
If needed, open ribcage with scissors to expose heart

Preparation of erythrocyte ghosts:
Start with at least 20-fold excess
Wash at ~2e8/ml (>10X volume original blood)
Wash 2-3 times (until supernatant and pellet clear of Hgb by absorbance / color)
5 mM $NaPO_4$ pH 8.0; centrifuge 2500 x *g* for 10 minutes cold
Monitor supernatant hemoglobin with absorbance spectrum; peak at 404 nm
To count – need to use high magnification phase without trypan blue; very difficult to see

COMPLEXING FATTY ACIDS TO BOVINE SERUM ALBUMIN

Materials
Sodium salt of fatty acid
Fatty-acid free BSA
Water baths at 37 °C and 55 °C
Use glassware: fatty acids stick to plastic
0.1 M sodium carbonate (Na_2CO_3)

Final fatty acid concentration: 3 mM
Final molar ratio BSA:FA: 6:1
Final BSA concentration: 18 mM

Prepare concentrated BSA (6/5X)
Dissolve BSA in PBS; stir in water bath at 37 °C
Split in half for vehicle control

Prepare concentrated fatty acids (6X)
Dissolve in 1/3 volume 0.1 M sodium carbonate
Stir in water bath 55 °C until dissolved
Bring up to full volume with PBS; continue stirring at 55 °C

Prepare vehicle control
Combine 1 part sodium carbonate, 2 parts PBS for vehicle control
Add to BSA for vehicle control

Complex fatty acids to BSA
While stirring BSA at 37 °C, slowly add concentrated fatty acid, ~ 5ml at a time
Stir 1 hour at 37 °C

Storage
Check pH and adjust to 7.4 if necessary
Filter-sterilize
Aliquot and store at -20 °C (recommended to use glass)
Thaw at 37 °C for ~10 minutes prior to use

SALMONELLA INFECTION OF TISSUE CULTURE CELLS

Day 0:
Seed cells about 24 hours prior to infection
BMDM: already seeded in wells; typically about 4 x 10^5 per 24-well; 2 x 10^6 per 6-well
RAW/nRAW: seed 1.5 x 10^5 per 24-well; 5 x 10^4 per 96-well; 7 x 10^3 per 384-well
HeLa: seed 1 x 10^4 per 96-well
Activate cells about 18 hours prior to infection by spiking in cytokine
2 ng/ml IFN-γ 20 ng/ml IL-4 20 ng/ml LPS
Start overnight(s) of bacteria in appropriate media

Day 1:
Count BMDM (6-well): wash 1X PBS; add 1 ml Gibco ion-free PBS + 2.5 mM EDTA; incubate fridge ~10 minutes; scrape gently; add 1ml medium and mix well; count

Prepare bacteria
Dilute culture in PBS and take OD600
Calculate CFU/mL using conversion factor
Typically 8 x 10^8 CFU / ml for OD600 = 1 for LB-grown bacteria
Typically 6 x 10^8 CFU / ml for OD600 = 1 for FD-induced bacteria
Dilute in medium to infect with 1 x 10^7 cfu/mL (standard) or 3 x 10^7 cfu/ml (FD)
*Can also spike in concentrated bacteria though less reproducible

Infect macrophages
Aspirate or dump medium and replace with infection cocktail (or spike); incubate 45 minutes
Aspirate or dump medium and replace with 100 μg/ml gentamicin for 75 minutes
Aspirate or dump medium and replace with 10 μg/ml gentamicin
** To minimize medium changes, can replace with 40 μg/ml gentamicin at 45 minutes and no change at 2 hours

FD/CFU Timepoint
Collect conditioned medium for secondary assays
Wash wells 3 x PBS; add 0.1% filter-steril Triton X-100 in water; incubate 10 minutes room temp
Add PBS; serially dilute and plate to determine CFUs
For FD: centrifuge lysate 2500 x *g* 20 minutes 4 °C; fix 1.6% PFA; wash PBS
Run flow: SSC threshold 0.02

See following pages for additional timepoint protocols:
Macrophage Flow RNA isolation SAFIRE processing

Treatment variations:
Most treatments were initiated at 2 hours post addition, concurrently with low gentamicin: erythrocytes, small molecules for screening, LNIL
Macrophage signaling inhibitors: typically added 1 hour post infection to end of experiment
Cytochalasin D to prevent erythrocyte uptake: treatment with 20 μM from 1.5-2 hr
Media variations: typically introduced 18-24 hours prior to infection

Old protocol variants:
Historically infect at MOI 10:1 Infect for 30 minutes, then high gentamicin for 1.5 hours
Opsonize bacteria with 20% NMS 30 minutes

HEMOPHAGOCYTIC MACROPHAGE FLOW CYTOMETRY

Materials

Red Blood Cell Lysis Buffer (10X) – dilute to 1X in water
Gibco ion-free PBS
Scraping Buffer = Gibco PBS with 2.5mM EDTA
Live/Dead Near-IR Stain from Invitrogen (use at 1:3000)
FACS Buffer = 1% FBS, 0.02% sodium azide in PBS
Perm Buffer = 0.1% saponin in FACS Buffer
FC Block from BD Pharminogen (use at 1:50)
Fixative = 1.6% PFA, 1.6% sucrose in PBS
Ter119-APC from eBioscience (use at 1:200)

ACK RBC lysis 10X:
8.3g ammonium chloride (NH_4Cl)
1g potassium bicarbonate ($KHCO_3$)
0.037g EDTA (or 200mL 0.5M EDTA, pH7.3)
all in 100mL H_2O pH adjusted to 7.3.

Scraping

Aspirate media; add 400µL room-temp RBC Lysis Buffer for 30s – 1min; quench with 4mL PBS
Aspirate; wash with 5mL Gibco PBS; aspirate; add 1mL cold scraping buffer
Incubate 10-15 minutes fridge; gently scrape cells
Pipette into cold Falcon tube; rinse well 1x2mL cold PBS; centrifuge 500xg 5min 4C
Aspirate supernatant; resuspend in 500 µL; aliquot 3x100 and 1x200 in 96-well plate

Live/Dead

Centrifuge 500xg 5min 4C; blot plate
Resuspend in 80 or 160uL PBS or live/dead stain (1:3000 in PBS); incubate on ice 20min

FC Block

Add 200 µL cold PBS; centrifuge 500xg 5min 4C; blot plate
Resuspend in 40 or 80µL FB or FC Block (1:50 in FB); incubate on ice 20min

Fixative

Add 200 µL cold FB; centrifuge 500xg 5min 4C; blot plate
Resupend in 100 µL fixative; incubate room temp 10 minutes or 4C 2-24 hours

Ter119 Staining

Add 200uL FB; centrifuge 500xg 5min RT; blot plate
Resuspend 300 µL PB; incubate 20min RT; centrifuge 500xg 5min RT; blot plate
Resuspend 40 or 80 µL PB or Ter119-APC (1:200 in PB); incubate 20min RT
Add 200 µL PB; centrifuge 500xg 5min RT [twice]
Resuspend in 200 or 400 µL FB into FACS tube; store at 4C until analysis

Flow Cytometry

Set voltages (starting FSC = 3, SSC = 350, APC = 750, APC/Cy7 = 900)
Collect 20,000 cells (FSC/SSC gate) for staining controls
Collect 50,000 live (APC/Cy7 low) for fully stained sample

Analysis Using FlowJo

Gate on cells (FSC/SSC)
Compensate using single color controls (get MFI of negative == MFI of single)
Gate on live (APC-Cy7/SSC)
Gate on HM (APC/SSC)
Quantify % live, and % HM

RNA ISOLATION, REVERSE TRANSCRIPTION, qPCR

Bacterial harvest (no more than 1e9 bugs)
Collect bugs into pellet
Lyse with 100ul 400ug/ml lysozyme in TE (10mM Tris-Cl, 1mM EDTA pH 8.0)
Vortex and incubate 3-4 minutes RT

RNA lysis using Rneasy
Lyse with Buffer RLT + 1% Bme (stable ~ 1 month)
2ml (T75), 600uL (6-well macrophage), or 350ul (enzymed-bugs)
Transfer to 3, 1, or, 1 Qiashredder columns; spin 2min microcentrifuge to homogenize
Can store at -80 if needed up to 6 months
Add 1 volume 70% EtOH; cap and shake vigorously to mix

Mammalian RNA prep using Rneasy
Load into spin column; spin 5 min in RNA swinging centrifuge or 30sec in microcentrifuge
Wash 2mL or 700uL Buffer RW1; spin again
Prepare Dnase (25uL aliquot + 175uL RDD buffer); add 200uL or 80uL to column; incubate 15m
Add 2mL or 400uL Buffer RW1; incubate 5min; spin 2min or 30s
Wash 2X 2.5ml or 500uL Buffer RPE; spin
Elute 150uL or 50uL water, stand 1min, spin; repeat elution with same eluate

Bacterial RNA prep using PureLink
Load into spin cartridge; spin 30 sec in microcentrifuge
Wash 700ul Wash Buffer I; spin 30 seconds; place cartridge in new tube
Wash 500ul wash buffer II; spin 30 seconds; discard
Wash 500ul wash buffer II; spin 30 seconds; discard; spin 1 minute to dry column
Elute with 50ul water; incubate 1 minute; spin 1 minute
Pass eluate over column again; incubate 1 minute; spin 1 minute
Prepare Qiagen DNase: add 175ul Buffer RDD to 25ul DNase aliquot
Add 50ul prepared DNase to 50ul eluate; incubate 30 minutes room temperature
Add EDTA to 2.5mM; heat at 65C for 10 minutes to inactive DNase; Freeze at -80

Reverse Transcription using iScript 1708891
Combine 1000ng RNA, 1uL RT enzyme, 4uL 5X buffer
Bring to 20uL total volume with water
** Include no template control (1) and noRT control for each sample
Cycle 5 minutes at 25C, 30 minutes at 42C, 5min at 85C, hold at 4C; Store cDNA in -20

qPCR reaction with SYBR Green (triplicates)
Combine 8uL template cDNA of appropriate dilution for each replicate
10uL 2X SYBR Green mix
200nM primer (usually 0.8uL from 5uM stock, so dilute with water to have 20uL total volume)
Cycle using SYBR green, 40 cycles, follow with melt curve analysis
**For new experiments, perform 10fold dilutions (or 2fold of low-abundance targets) to determine appropriate dilution and efficiency (plot Ct vs log(dilution), E = -1+10^(-1/slope)

Analysis of qPCR on Eppendorf machine
1. Examine melt curve analysis to ensure single peak
2. Fix baseline for entire assay
Switch off log view (checkbox) Adjust baseline to manual

Alter max cycle range so have all traces looking even (i.e. not dipping below axis)

3. Adjust threshold manually for each target

Turn log view back on Select wells with target

Set threshold to be in linear range and so that replicates agree

Record Ct values for that gene from list; also record threshold value

Analysis of qPCR Ct values

Average the replicates for target and references ΔCt: Normalize target to reference (subtract)

ΔΔCt: Normalize treated sample to control sample(s) (subtract)

Calculate fold change (2^-ΔΔCt) Average fold change across biological replicates

PROTEIN PREP AND WESTERN BLOTTING

RIPA buffer: Toni: 50ml RIPA Buffer: 150mM NaCl (0.435g), 1% NP-40, 50mM Tris Hcl pH 8.0 (0.30285g)

Alternative: 10mM Tris-HCl pH 8.0, 1mM EDTA, 1% Triton X-100, 0.1% sodium deoxycholate, 0.1% SDS, 140mM NaCl

Add 1mM PMSF or protease inhibitors (Sigma); if doing phospho proteins, add phosphatase inhibitor cocktails 1+2 (Sigma)

10ml 5X loading dye: 2.5ml 1M Tris, 1ml 10% SDS, 5ml glycerol, 1ml 0.5M EDTA, 0.5ml bromophenol blue. Combine 900ul dye with 100ul Bme prior to use

Other solutions:
1L 10X Running Buffer (dilute to 1X for use): 30g Tris base, 144g glycine, 10g SDS per 1L
1L 10X Transfer Buffer: 58.2g Tris, 29.3g glycine, 37.5ml 10% SDS
1L 1X Transfer Buffer: 100ml 10X transfer buffer, 200ml MeOH, 700ml water
1L 10X TBS: 200mM Tris base (24g), 1.5M NaCl (88g)
TBS-T: TBS with 0.1% Tween-20

Protein prep
Wash with cold PBS
Lyse cells on ice using 300 (6-well) or 100uL (24-well) RIPA buffer with protease inhibitor added (can decrease volumes to increase concentration if needed)
Scrape into Eppendorf and incubate on ice 15min total
Spin samples in microcentrifuge maximum speed 4C 10 minutes
Transfer supernatant to new tube, reserve 30ul for BCA/Bradford
Add 5X loading buffer to remainder; boil at 100C for 5 minutes
Freeze at -20 for storage; thaw and directly load into gel based on BCA assay (20-30ug usually)

BCA assay
Prepare working reagent (dilute colored reagent 50x in buffered reagent)
Dispense 10-25uL BSA standards and samples (may need to dilute samples)
Add 200uL working reagent; mix briefly on shaker
Incubate 30 minutes at 37C; cool to room temperature
Read on plate reader at 562nm
Construct standard curve and determine protein concentration

Bradford Assay
Dispense 5ul standards and samples
Add 250ul dye reagent; incubate 5-60 minutes at room temperature
Read on plate reader at 595nm
Construct standard curve and determine protein concentration

Casting Gels
Wash plates with ethanol; assemble into casting frame (test with water for leakage!)
Test comb and mark plates with line for resolving gel height
Combine buffer, water, SDS, APS, TEMED, mix briefly and immediately pipette into frame
Let polymerize; repeat for stacking gel (be sure to insert comb!)
Store in a wet paper towel wrapped in saran wrap in fridge if needed

Running Gels
Insert gel(s) into electrode assembly; ensure chamber does not leak; rinse wells with pipette
Load samples into wells; run gel 80V until samples through stacking gel, then 100V (~2.5 hrs)

Transfer to PVDF membrane
Cut membrane and filter paper
Activate membrane in 100% MeOH
Soak membrane, gel, filter paper, pads in transfer buffer
Make stack: pad, filter paper, membrane, gel (get rid of bubbles!), filter paper, pad
Load stack so gel is closer to negative electrode, membrane is closer to positive electrode
Fill chamber with transfer buffer, add ice pack and stir bar to spin while running
Transfer 1hr at 100mA, ensure ladder transferred

Staining
Rinse membrane briefly in TBST
Block with TBST + 5% BSA or milk, depending on antibody, 1 hr room temperature rocking
Cut membrane if needed using scissors or razor blade
Stain overnight 4C with primary antibody in block in dish, packet, or parafilm bubble
    Dish: 10 ml full membrane
    Packet: 5ml full membrane
    Bubble: 3ml full membrane
Wash 3x10min TBST
Stain secondary room temp 1hr in block
Wash 3x10min TBST

Detection
Combine 1 part each reagent for HRP reaction; add to membrane; incubate 5 minutes
** Need about 4-5 ml for full membrane
Blot membrane on kimwipe and stick inside plastic sleeve in radiography cassette
In dark room, expose film and develop (half or full sheets only in developer!)
Note orientation and exposure time
Push button near loading slot on developer if it's off
Scan or take a picture

Densitometry
Invert image in imagej and use the measure feature to get the intensity mean value of each band (measure the same area for each band)
Normalize protein of interest to loading control

Stripping
If needed rinse blot in TBS briefly
Immerse in stripping buffer (Thermo Restore) shaking for 15 minutes RT
Dump and rinse briefly in TBS
Restain and develop as above

SAFIRE PROCESSING AND MICROSCOPY

SAFIRE processing
At 17.5 hours, spike MitoTracker Red CMXRos: final 100 nM for 96-well; 300 nM for 384-well
At 18 hours, spike 16% PFA to get 1-4% final concentrations; incubate 15 minutes room temp
Wash 1X PBS (store in PBS in fridge if needed)
Blot; add 1 mM DAPI; incubate 20 minutes room temperature
Wash 2X PBS; add 90% glycerol in 1X PBS; spin briefly to remove bubbles
Store in fridge until ready to image

ArrayScan imaging
Turn on microscope and computer; open acquisition software
Hit middle pane to calibrate scope; load plate; load protocol
Find sample: pick random well; set channel to DAPI; click autofocus to find focal plane
Set exposures so brightest pixel is indicated percent of camera:
    DAPI 25% of signal (~25 ms); GFP 65% (~300 ms), MitoTracker 40% (~50 ms)
Select wells, field order, and enter Plate ID and Plate Name
Start run; change names between plates
Export to DIBs: open vHCS View, select plate, file → Export Plate / Images
    Export type is 8 bit tiff; uncheck export data

Olympus IX-81 imaging
Turn on microscope, computer, stage, lamp; put plate in holder
Open Slidebook; open “Focus” and “Capture” windows; change to 10X objective
Set exposures: FITC 300 ms gain 10; DAPI 100 ms gain 0; Texas 300 ms gain 0
Click on “Slide” window; select “Special Capture” → “Capture MultiWell”
Set plate to Abby-Matrical96
Change filter to Texas Red; set exposure to 10 ms; open fluor
Move to well B2; get the crosshairs centered over the top of the well; set upper left
Move to well B11; get the crosshairs centered over the top of the well; set upper right
Move to well G11; get the crosshairs centered on the right of the well; set lower right
Close fluor; select wells you want to image and hit “export points”
Change “Focus” tab to XY-position; manually go through positions and set z position
Snap to confirm exposures; in “Capture,” “XY location capture” pane set to “multiwell capture”
In “Capture” click Advanced; Focus tab, check Autofocus, set to 60 um search using Texas
In “Image Info” pane set plate name; hit start

CV1000 imaging
Turn on scope, load incubator chamber to prewarm microscope to 33C and cool camera to -55C
Prewarm plate at 37C; load into plate holder
On “Sample” tab, select “Brooks 96 well”
On “Experiment” tab, set save path for data
On “Measurement” tab, set starting exposures. Hit “Detail” and change pinhole to through
In “Fixed Position” Pane, hit dotted square button and select wells; set “Fixed Position” number
In “Z-stack” pane, set autofocus options: dropdown menu, every field AF, every field SF
In “Z-stack” pane, set slices to 1
Find sample: select well, blue channel, hit search button in “Z-stack” pane; hit “<<” to set Z
Confirm exposures: hit the red dot to image all three channels. Alter exposures until brightest
    pixel is around 40,000 (~2/3 of the maximum pixel intensity)
Hit record

MOUSE INFECTION

Orogastric:

Day 0:
Starve 7 weeks old mice ~ 12 hours prior to infection
Start overnight(s) of strain(s): 1 overnight for each animal

Day 1:
Wash overnights 3X PBS
Resuspend in 100 μl per 5 ml culture
Take OD of 1:100 dilution
Dilute to 1 x 10^{10} cfu / ml
Wash gavage needle 3X 70% ethanol; 3X PBS
Scruff animals and gently insert needle; inject 100 μl (gives 1 x 10^9 cfu / mouse)
Dilute and plate inoculum to verify MOI

Intraperitoneal:

Day 0:
Start overnight of strain(s)

Day 1:
Take OD600 of overnight
Dilute to 1 x 10^4 cfu/ml (SV129 chronic model) or 1 x 10^5 cfu/ml (C57/Bl6 acute model)
Scruff animals; insert 25 5/8 needle bevel up, center of side of belly, parallel with knee joint
Needle enters at about 45° angle; inject 100 μl

Sacrifice and harvest:
Prepare tubes with 1 ml PBS; preweigh
Euthanize; weigh animal
Cut skin and rip to expose peritoneum; carefully cut peritoneum to expose organs
Remove spleen
Gently remove intestines without pulling apart; mesenteric lymph nodes are central
Use fine forceps to pinch Peyer's patches and collect with razor blade
Use scissors to cut cecum and liver
Weigh tubes to determine organ weight
Homogenize PP, MLN, S, L, C; wash H_2O, EtOH, EtOH, H_2O, PBS between organs
Plate to determine CFU

$$\text{Bacterial load in cfu/g} = \frac{([\text{count}] \times [\text{dilution}] / [\text{volume}]) \times (1\text{mL} + [\text{organ weight}])}{\text{Organ weight (g)}}$$

Organ weight ~ organ vol

$$\text{Competitive index} = \frac{\text{output (WT CFU / mutant CFU)}}{\text{Input (WT CFU / mutant CFU)}}$$

convert to log10 for graphing